Ising model in three dimensions with long-range power-law correlated site disorder: a Monte Carlo study

D I S S E R T A T I O N

ZUR ERLANGUNG DES AKADEMISCHEN GRADES

doctor retum naturalium
Dr. ret. nat.,

VORGELEGT VON

M. Sc. Stanislav Kazmin

GEBOREN AM 20.03.1988 IN VORONEZH (RUSSLAND)

Gutachter:
Prof. Dr. Wolfhard Janke
Dr. Christophe Chatelain

Bibliographic description

Stanislav Kazmin

Ising model in three dimensions with long-range power-law correlated site disorder: a Monte Carlo study

Universität Leipzig, Dissertation
197 Seiten, 141 Literaturverweise, 0 Abbildungen, 0 Tabellen, 4 Anlagen

Folgende Arbeit beschäftigt sich mit dem Ising-Modell in drei Dimensionen auf einem Gitter mit einer langreichweitigen, potenzförmig korrelierten ($\propto r^{-a}$) Unordnung mithilfe von Monte Carlo Simulationstechniken. Der Hauptteil der Arbeit ist die Bestimmung der kritischen Exponenten des Ising-Modells in Abhängigkeit von der Korrelationsstärke a. Dies wird durch die Anwendung der Finite-Size-Scaling Analyse und der Temperatur-Scaling Analyse umgesetzt. Dabei wird insbesondere die Vorhersage von Weinrib und Halperin ($\nu = 2/a$) überprüft. Weiterführend, werden die kritischen Temperaturen in Abhängigkeit vom Korrelationsexponenten a und der Defektkonzentration ermittelt und die Hyperscaling-Relation studiert. Ergänzend werden vielfältige Aspekte, wie die Autokorrelation der Observablen, die Anwendung der Histogram-Reweighting-Methode und Messung der Korrelationsstärken a auf Gittern erläutert.

In this thesis the three-dimensional Ising model on a lattice with long-range power-law correlated ($\propto r^{-a}$) site disorder is studied with the help of Monte Carlo simulation techniques. The key part of the work is the estimation of the critical exponents of the Ising model in dependence of the correlation strength a. This is done by applying finite-size scaling analysis and the temperature scaling analysis. In particular, the conjecture by Weinrib and Halperin ($\nu = 2/a$) is reviewed. Additionally, the critical temperatures in dependence of the correlation exponent a and the concentration of defects are provided and the hyperscaling relation is checked. Supplementary, various aspects such as autocorrelation times of the observables, applicability of the histogram reweighting technique and the measured correlation exponents a on the lattices are provided.

Zusammenfassung der Dissertation

Ising model in three dimensions with long-range power-law correlated site disorder: a Monte Carlo study

der Fakultät für Physik und Geowissenschaften der Universität Leipzig
eingereicht von

M. Sc. Stanislav Kazmin

angefertigt am

Max-Planck-Institut für Mathematik in den Naturwissenschaften (Leipzig) und
Institut für Theoretische Physik/Computational Quantum Field Theory Group
Universität Leipzig

Mai 2021

Introduction

In this work we investigated one specific variant of the Ising model with the help of Monte Carlo simulation techniques. We introduced a quenched site disorder (empty sites or defects η) on the lattice and studied the influence of such structural changes on the critical behavior of the Ising model. Motivated by the nature, we distinguished between two different disorder classes. The first class is the random (or uncorrelated) disorder with randomly placed defects. The second class is called long-range correlated disorder, which imposes the condition of a certain spacial correlation relation between the defects. In the present work a power-law decay was chosen, i.e., the correlation function between the defects had the form $\langle \eta_x \eta_y \rangle \propto r^{-a}$, with r being the distance between the sites x and y. In both cases, an additional parameter of the system was crucial — the concentration of defects p_d. The critical exponents of the model in the thermodynamic limit are expected to be independent of p_d. However, for finite-size lattices the concentration was an additional degree of freedom which had to be considered.

Both disorder classes were already studied with the help of Monte Carlo techniques and Renormalization Group techniques in the literature, e.g., in Refs. [1–4] for the uncorrelated case and Refs. [5–9] for the correlated case. In particular, for the uncorrelated disorder case a new universality class was observed and confirmed multiple times. This is in accordance with the Harris criterion [10] which predicts a change in the universality class for disordered systems if the critical exponent of the specific heat α is greater than zero in the pure system (the same system without disorder). The critical exponents in the uncorrelated disorder case were also investigated several times. In the case of the correlated disorder, yet another universality class is expected according to the extended Harris criterion for strong-enough correlations with $a < d$. From Renormalization Group calculations, there exists the conjecture by Weinrib and Halperin [5] that the correlation exponent of the correlation length will have the form $\nu = 2/a$ in that case.

Motivation

The main goal of this work was the observation of the critical exponents of the Ising model on a lattice with site disorder. We intentionally used many correlation exponents a to obtain a comprehensive picture of the dependence of the critical exponents on a. Such a study was not considered before and the results for the case of $a = 2.0$ found in the literature are quite contradictory [5–9]. Therefore, our aim was to compare the known results with each other and also extend the known results to other a which were not covered before. Additionally, we used numerous concentrations of defects p_d in order to provide consistent p_d-independent estimates of the critical exponents. The uncorrelated case was an important case to study as well for two reasons. First, in order to verify the analysis techniques and compare the obtained results to the known results from literature, e.g., to Refs. [1–4]. Second, to study the dependence on a and to compare to the uncorrelated case, we needed results for both cases which were obtained with exactly the same techniques. Accompanying, we wanted to provide a full and dedicated analysis of the underlying disorder configurations. The long-range correlated disorder was generated by using a modified variant of the Fourier Filter Method from Ref. [11], which was originally introduced in Ref. [12]. In particular, the true measurable correlation exponents $\overline{a}$ were of great interest. In our opinion, only by providing the real correlation exponents $\overline{a}$, the obtained critical exponents can be put into a context with each other and a global picture can be achieved.

Most important results

- Estimation of the critical exponents ν, γ and β, and of the confluent correction exponent ω in dependence of the correlation exponent a for five correlated cases and the uncorrelated case with $a = \infty$. These results are obtained through a finite-size scaling analysis and verified for ν and γ with the temperature scaling analysis.
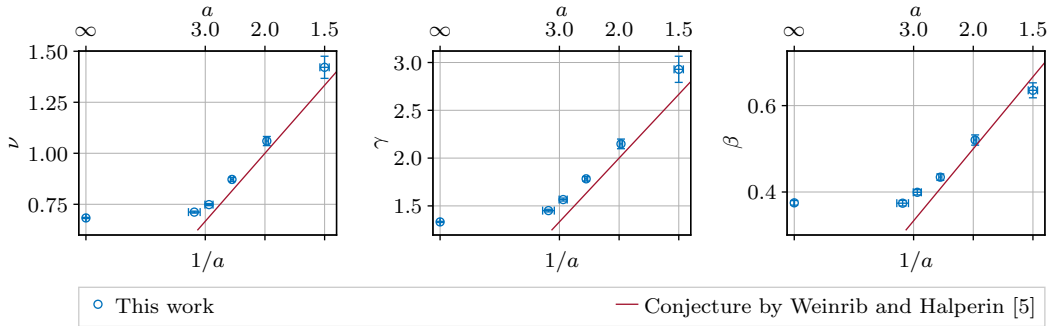
- Qualitative verification of the Weinrib and Halperin prediction of $\nu \propto 1/a$. Quantitatively, our values lie $\approx 10\,\%$ above the prediction of $\nu = 2/a$.
- Observation of the crossover regime between the correlated and the (effectively) uncorrelated cases at $a \approx 3.0 = d$. From our analyses we can conclude that this region diverges from the Weinrib and Halperin prediction the most.
- We see an indication that the hyperscaling relation may be violated in the crossover region around $a \approx 3.0$. For stronger correlations (smaller a) the hyperscaling relation becomes valid again, as it is in the uncorrelated case.
- Derivation of the critical temperatures in dependence of the correlation exponent a and the concentration of defects p_d. Contrarily to the critical exponents, the critical temperatures depend on the concentration of defects p_d and even on the type of the disorder and its generation process.

- Dedicated analysis of the generated long-range correlated disorder lattices yielded a deviation of the imposed parameters a and the truly measured $\overline{a}$. The underlying generation method was the Fourier Filter Method [11, 12]. The deviations were mostly pronounced for weaker correlation exponents (larger a). The observation of such deviations has emphasized the necessity of a full disorder configurations analysis prior to the final analyses of the Ising model itself.
- Study of the autocorrelation times of observables in dependence of the parameters a, p_d and L. It was shown that the autocorrelation times can be neglected during the analyses presented in this work.

Own publications

[KJ20] S. Kazmin and W. Janke, Phys. Rev. B **102**, 174206 (2020).

[KJ22] S. Kazmin and W. Janke, Phys. Rev. B **105**, 214111 (2022).

References

[1]   H. G. Ballesteros et al., Phys. Rev. B **58**, 2740–2747 (1998).

[2]   P. Calabrese et al., Phys. Rev. E **68**, 036136 (2003).

[3]   P. E. Berche et al., Eur. Phys. J. B **38**, 463–474 (2004).

[4]   M. Hasenbusch et al., J. Stat. Mech. **2007**, P02016 (2007).

[5]   A. Weinrib and B. I. Halperin, Phys. Rev. B **27**, 413–427 (1983).

[6]   H. G. Ballesteros and G. Parisi, Phys. Rev. B **60**, 12912–12917 (1999).

[7]   V. V. Prudnikov et al., Phys. Rev. B **62**, 8777–8786 (2000).

[8]   V. V. Prudnikov et al., Condens. Matter Phys. **8**, 213–224 (2005).

[9]   D. Ivaneyko et al., Physica A **387**, 4497–4512 (2008).

[10]   A. B. Harris, J. Phys. C: Solid State Phys. **7**, 1671–1692 (1974).

[11]   J. Zierenberg et al., Phys. Rev. E **96**, 062125 (2017).

[12]   H. Makse et al., Chaos, Solitons & Fractals **6**, 295–303 (1995).

This thesis contains partially the results published in Ref. [KJ20] and Ref. [KJ22] (published after the thesis defense) together with my supervisor Prof. Dr. Wolfhard Janke. In particular, Ref. [KJ20] contains the study of the underlying disorder configurations, the measurement of the correlation exponents a and the estimation of the critical exponent ν and the confluent correction exponent ω. Also, the estimates of the critical temperatures are part of Ref. [KJ20]. However, after the reference was published, we included more data to the analyses and improved the numerical results. Hence, the estimates in the present work slightly deviate from that in Ref. [KJ20]. Ref. [KJ20] was mainly prepared and written by Stanislav Kazmin, while Prof. Dr. Wolfhard Janke had the consulting, correcting and guiding functions. The improved results together with the estimates of the critical exponents β and γ and with more precise critical temperature estimates were published in Ref. [KJ22]. Finally, a third publication is planned for the American Journal of Physics with the focus on the julia implementation of the Ising model.

This thesis was mostly written at the Max Planck Institute for Mathematics in the Sciences located in Leipzig and at the Institute for Theoretical Physics of the Universität Leipzig. The supervisor was Prof. Dr. Wolfhard Janke from the Universität Leipzig. Parts of the work were done during a two-week stay at the Laboratoire de Physique et Chimie Théoriques at the University of Lorraine, France. Here, I had intensive discussions with Dr. Christophe Chatelain and Prof. Dr. Malte Henkel. The simulations were performed on the local cluster of the Max Planck Institute for Mathematics in the Sciences and at the Max Planck Computing and Data Facility located in Garching.

Contents

List of Figures

List of Tables

Acknowledgments

Preface

Before we dive in into the physical topics of this thesis, would like to introduce some conventions which will be used throughout the whole work. They will hold unless stated otherwise.

- We plot curves obtained by using fits to the data as solid lines and with shaded areas which show confidence intervals of the fitted curves. Often, the shaded areas are hard to see due to their small extent, but they are still plotted for consistency.
- Contrarily, dashed or dotted lines are used to guide the eyes between the measured data points or mark specific values.
- In the legend, the errorbars are left out for clarity.
- We use the symbol $\sigma(x)$ for denoting the standard deviation of x and $\epsilon(x)$ to denote the standard error of x, i.e., the standard deviation of its mean, $\epsilon(x) = \sigma(\overline{x})$. We often skip the notion of the mean, so $x = \overline{x}$ hold whenever the context is clear.
- After each section (excluding the "Introduction" and the "Conclusions" chapters) we present a box with a short *Summary* of the section to keep the reader on track.
- Important equations are highlighted with a surrounding box.
- The normal distribution is denoted by $\mathcal{N}$ and its parameters are the mean μ and the variance σ^2, i.e., $\mathcal{N}(\mu, \sigma^2)$.
- We switch between the vector notation with bold and normal letters depending on the context of the current section. This is done in order to simplify the notation as much as possible.
- We use the alphanumeric style for our references since we would like to improve the recognition of already mentioned references during the reading process. Due to the structure of this work we will come to the same references over and over again. The reference labels are organized as follows: for one author the first three letters of the name are used (e.g., [May21]), for two and three authors, their first letters are used (e.g., [AB21] or [ABC21]), for more than three authors the first three letters of the first author are used followed by a plus sign (e.g., [May+21]). The year is then appended at the end (the "21" in the examples above). In case of duplicates, a lowercase unique letter is appended to the year starting with "a" (e.g., [May21a]). All web references start with an "@" and are listed separately. We hope that the reading experience will benefit from these referencing decisions.

Imagination is more important than
knowledge. Knowledge is limited.
Imagination encircles the world.

Albert Einstein [EV29]

Introduction

<div style="text-align: right; font-size: 3em;">**1**</div>

We would like to start by introducing the three main ingredients of the model which was investigated in the present work and which are contained in its title: the Ising model, the Monte Carlo simulation technique and the disorder. We will be quite brief in the introduction, because each of these subjects will be addressed in a separate section in much greater detail. Instead, we would like to show the red thread which led us to the final setup for this thesis.

Let us begin with the most essential ingredient — the Ising model. Last year, in 2020, the Ising model celebrated its 100th birthday. Back in the year 1920, it was Wilhelm Lenz, who gave his student, Ernst Ising, this spin model with next-neighbor interactions as a problem for his thesis [Len20]. Five years later Ising solved in the one-dimensional case [Isi25]. However, the lack of a phase transition for a non-zero temperature surly bore no huge potential for further studies. It took almost twenty years to solve the problem in two dimensions. This was done by Lars Onsager with the help of the transfer matrix method [Ons44]. The existence of a phase transition at a non-zero temperature was crucial for the Ising model to evolve to one of the most common models in statistical physics. By now, the original paper by Ising, Ref. [Isi25] counts more than 1900 citations [@Spr] and ScienceDirect gives approximately 16 000 results containing the keyword "Ising model" [@Sci]. Since then, the Ising model quickly became a well-established theoretical model for studying phase transitions and critical phenomena. Not least, this process was powered by the ever-increasing possibilities in computational analysis. Its simplicity in the formulation in combination with the existence of a second-order phase transition make it so unique. However, due to the lack of an analytic solution in tree dimensions, the Monte Carlo simulation techniques, e.g., Refs. [FXL18; Has10a; Has10b], the Renormalization Group techniques, e.g., Refs. [GZ98; PS08], their variations and combinations, e.g., Monte Carlo Renormalization Group in Refs. [Blö+96; Paw+84] and recently also Bootstrap methods, e.g., Refs. [CMO19; El+12; El+14; Kos+16] currently remain the only possibilities to investigate the model quantitatively.

The second ingredient for the studied model is the notion of disorder. In nature, we rarely can observe an ideal material without any distortions or impurities. We can observe disorder in practically any realistic scenario and the natural question arises — how does disorder influence the behavior of the system? To introduce the quenched disorder (a disorder which does not changes over time) on the lattice, which is the building block of the Ising model, we can proceed in several ways. The most simple way is to introduce random disorder, i.e., fill some sites on the lattice with defects. Such disorder would correspond to a doped semiconductor, e.g., silicon doped with phosphorus or a doped ferromagnetic material, e.g., zinc-oxide doped with magnesium [Mit+86]. A naturally introduced additional degree of freedom for disordered systems is the concentration of defects p_d.

However, such random disorder is not the only possibility. In fact, in nature the disorder often comes with a certain spacial structure, e.g., extended lines, clumps, clusters and so on. To mimic such a spacial extension, we introduced a spatial correlation between the defects. The form of the correlation can be chosen in different ways. However, for a scale-invariant model, a power-law for $\propto r^{-a}$ was an appropriate choice. The concentration of defects p_d remains a parameter of the system but now additionally we also have the correlation strength described by the correlation exponent a. Throughout the whole thesis, these two parameters will be of great importance.

Finally, the Monte Carlo simulation technique is the last ingredient. It is an incredibly useful tool which allows to us to study comparably large systems (systems with many degrees of freedom) by using computational resources and concepts of the statistical physics. Having its own right for being an interesting approach to study, it becomes particularly handy when the model under consideration does not have an analytic solution, as it is the case for the three-dimensional Ising model (even without disorder). The steady advancement in computational capabilities is a boon and a bane. On the one hand, larger and larger systems can be investigated and more complex systems can be studied in a reasonable amount of time. But simultaneously, the results achieved decades ago quickly become imprecise or can be overrun by newer works. Partially, this problem was present in the topic which was studied in this thesis. The Ising model with long-range correlated disorder was already studied in several works [BP99; Iva+08; PPF00; Pru+05; WH83]. However, with currently available computational capabilities, we were able to extend the study substantially. In particular, an important question was whether the critical exponent of the correlation length ν will follow the conjecture by Weinrib and Halperin [WH83] which states that in the correlated disorder case $\nu = 2/a$ is valid. In order to check this conjecture, we used many a values which was not done before. To summarize, we visualized the three main ingredients and how they glue together and build the title of this thesis in Figure 1.1. We will address each of the building blocks separately in the course of this thesis starting in the next section.
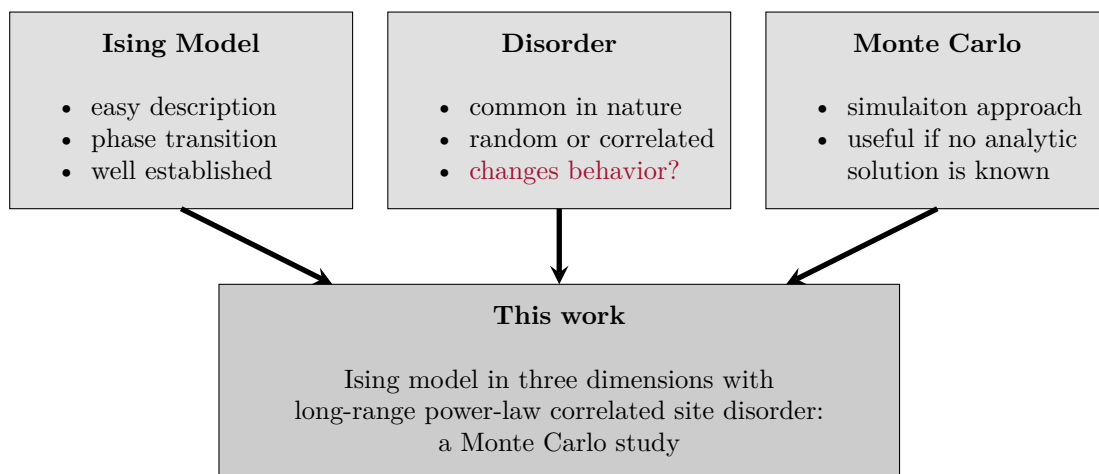
Figure 1.1: Building blocks for the topic of the present work. The question in red "changes behavior?" relates to the main question of this thesis: how does the (correlated) disorder changes the behavior of the system.

The thesis is organized as follows. In the second Chapter, "Theory", we will introduce the theoretic background which is essential to understand later parts of the work. We will introduce the canonical ensemble, define the Ising model and derive essential observables, explain the concept behind the phase transition and briefly introduce the Renormalization Group theory. The presented concepts will be closely connected with each other while being quite general in their formulation. One exception will be the section on the disordered Ising model predictions which will contain the theoretical (Renormalization Group) predictions as well as the simulation results of other groups. In the third chapter, "Methods", we will summarize the tools needed for later analyses. The sections within this chapter will be only loosely connected and each will cover one particular tool. We will present the finite-size scaling technique, introduce the Monte Carlo simulation technique, resampling methods for calculating errors, the histogram reweighting technique and the Fourier Filter Method for the generation of the long-range correlated disorder. In the main fourth chapter, "Results", we will present all our analyses. We will start with the details of our simulations, show the analysis of the disorder configurations, cover the autocorrelation times of the observables and the estimation of various observables. Then, we will present the key part of the thesis which is the estimation of the critical exponents through the finite-size scaling analysis. We will also compare these results to the temperature scaling approach. In the fifth chapter, "Conclusions", we will summarize all the results and give an outlook for further possible research directions.

In addition to the topics covered in the main sections of the thesis, we will present some results which were obtained during the research but which do not fit into the main red thread of the work in Appendices. This will include the comparison of the global fit ansatz with the weighted mean over individual fits and the occurrence of negative spectral density values in the generation process of the long-range correlated disorder. Finally, the appendix contains the implementation.

Theory

2

2.1 Canonical ensemble

We briefly recall the main aspects of the canonical ensemble and the corresponding aspects which will be of importance for further understanding of the present work. This section is not a complete introduction to this very broad topic. For further and more complete presentation we refer to any book on statistical physics, e.g., Refs. [Gar95; Nol14; Sch02].

The canonical ensemble describes a small subsystem S which is embedded into a much larger system S_{hb}, called the **heat bath**. The total system is isolated from the surrounding environment. Systems S and S_{hb} can exchange energy but are not allowed to exchange particles. They are supposed to be in equilibrium. The situation is schematically shown in Figure 2.1. The system of interest is the subsystem S. It is characterized by the volume V, the number of particles N and the temperature T. The Hamiltonian of the total system is given by [Sch02, p. 50]

$$\mathscr{H}_{\mathrm{tot}} = \mathscr{H}_1 + \mathscr{H}_2 + \mathscr{W} \approx \mathscr{H}_1 + \mathscr{H}_2 \,, \tag{2.1}$$

where we need the interaction term $\mathscr{W}$ to allow the subsystems to reach equilibrium but as it is assumed that $\mathscr{W} \ll \mathscr{H}_{1,2}$ we can neglect it.
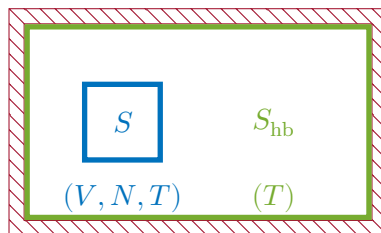
Figure 2.1: The basic setup for the canonical ensemble. The subsystem S is embedded into a larger system S_{hb}. The total system is isolated from the surrounding environment. All characterizing values are listed in brackets. We left out the volume and the number of particles of the large system S_{hb} because they are of no importance for the system of interest S in the framework of the canonical ensemble. Adapted from Ref. [Sch02, Fig. 2.11].

2.1.1 Partition function and important observables

The crucial quantity which contains the whole information about the system is the **partition function** of the canonical ensemble. It is given by [LB05, p. 7]

$$\mathscr{Z} = \mathrm{Tr}\, e^{-\mathscr{H}/(k_B T)} = \sum_{\mu} e^{-E_{\mu}/(k_B T)} \,, \tag{2.2}$$

with the Hamiltonian $\mathscr{H}$ which represents the energy of the system at state μ,

$$E_\mu = \mathscr{H}(\mu) \,. \tag{2.3}$$

In Equation (2.2) the sum runs over all possible states μ of the system with the corresponding energy E_μ and k_B is the Boltzmann constant. From the partition function $\mathscr{Z}$ we can derive all thermodynamic quantities and study the statistical properties of the system.

In the canonical ensemble the probability p_μ to find the system in a state μ follows the **Boltzmann distribution** and is given by [NB99, p. 8]

$$p_\mu = \frac{1}{\mathscr{Z}} e^{-E_\mu/(k_B T)} \,. \tag{2.4}$$

The next important quantity is the canonical density matrix or the **density of states** which is defined by

$$\rho = \sum_\mu p_\mu |\mu\rangle\langle\mu| \,. \tag{2.5}$$

With the help of Equations (2.2) and (2.4) we can rewrite Equation (2.5) to

$$\rho = \frac{1}{\mathscr{Z}} \sum_\mu e^{-E_\mu/(k_B T)} = \frac{1}{\mathscr{Z}} e^{-\mathscr{H}/(k_B T)} \,. \tag{2.6}$$

This form of the density of states allows us to calculate the expectation value of any observable $\mathscr{O}$ in the canonical ensemble through [Sch02, p. 51]

$$\langle \mathscr{O} \rangle = \mathrm{Tr}\left(\rho\, \mathscr{O}\right) = \sum_\mu p_\mu \mathscr{O}_\mu = \frac{1}{\mathscr{Z}} \sum_\mu \mathscr{O}_\mu e^{-E_\mu/(k_B T)} \,. \tag{2.7}$$

The Equations (2.6) and (2.7) play an important role in Monte Carlo simulations, in particular when it comes to the importance sampling. We will discuss it in more detail in Section 3.1.

The thermodynamic potential which corresponds to the canonical ensemble is the **free energy** $\mathscr{F}$. It is related to the partition function by [Sch02, p. 58]

$$\mathscr{F} = -k_B T \ln \mathscr{Z} \,. \tag{2.8}$$

Derivatives of the free energy lead us to all thermodynamic quantities. One of the most important observables is the internal energy. We will denote the internal energy by E and not by U since it turns out that in thermodynamic limit the total energy of the system (relative to its center of mass) is equal to the internal energy of the system [Nol14, p. 77]. In other words: the internal energy of the system is the mean energy in the thermodynamic limit $N \to \infty$ (see Section 2.1.2 for the definition). We will therefore refer to the internal energy simply by energy from now on. The energy can be derived from the free energy by taking the derivative with respect to the temperature,

$$E = -T^2 \frac{\partial(\mathscr{F}/T)}{\partial T} \,. \tag{2.9}$$

Using Equation (2.8) and performing some simple algebraic transformations we arrive at

$$E = -T^2 \frac{\partial}{\partial T} \left(\frac{-k_B T}{T} \ln \mathscr{Z} \right) \tag{2.10a}$$

$$= -T^2 \frac{\partial}{\partial T} \left(k_B \ln \left(\sum_\mu e^{-E_\mu/(k_B T)} \right) \right) \tag{2.10b}$$

$$= \frac{1}{\mathscr{Z}} \sum_\mu E_\mu e^{-E_\mu/(k_B T)} \tag{2.10c}$$

$$E = \langle E \rangle = \langle \mathscr{H} \rangle \,, \tag{2.10d}$$

where in the last step we used Equation (2.3) and identified the expectation value of $\mathscr{H}$ calculated with the definition from Equation (2.7).

The next important quantity is the entropy. It describes the disorder of the system. In statistical mechanics the entropy is given by the negative average of the logarithm of the density matrix [Sch02, p. 51],

$$S = -k_B \langle \ln \rho \rangle \,. \tag{2.11}$$

Equation (2.11) is known as **Gibbs entropy** [Sad12, p. 34]. Using Equation (2.7) we can rewrite Equation (2.11) to

$$S = -k_B \operatorname{Tr} \rho \ln \rho \tag{2.12a}$$

$$= -k_B \delta_{\mu\nu} \left(\frac{1}{\mathscr{Z}} \sum_\mu e^{-E_\mu/(k_B T)} \ln \left(\sum_\nu e^{-E_\nu/(k_B T)} \right) \right) \tag{2.12b}$$

$$S = -k_B \sum_\mu p_\mu \ln p_\mu \,. \tag{2.12c}$$

On the other hand, in thermodynamics the entropy is defined by [LB05, p. 9]

$$S = -\left(\frac{\partial \mathscr{F}}{\partial T} \right) \,. \tag{2.13}$$

Inserting Equation (2.8) into Equation (2.13) and using some algebra we derive the entropy expression of the canonical ensemble [Sch02, p. 58],

$$S = -\frac{\partial}{\partial T} \left(-k_B T \ln \mathscr{Z} \right) \tag{2.14a}$$

$$= k_B \left(\ln \mathscr{Z} + \frac{T}{\mathscr{Z}} \left(\frac{1}{k_B T^2} \right) e^{-\mathscr{H}/(k_B T)} \right) \tag{2.14b}$$

$$= k_B \left(\ln \mathscr{Z} + \frac{1}{k_B T} \langle \mathscr{H} \rangle \right) \tag{2.14c}$$

$$S = \frac{1}{T} \left(E + k_B T \ln \mathscr{Z} \right) \,. \tag{2.14d}$$

Note, that Equation (2.14d) can also be derived from Equation (2.11) by inserting Equation (2.4) into it.

Further, we want to write down some important observables which do not have a specific form in the frame of a canonical ensemble but rather are standard thermodynamic quantities. We will assume a magnetic system as this is the type of systems we studied in this work. For a magnetic system the natural variables of the Hamiltonian are the external magnetic field h and the temperature T,

$$\mathscr{H} = \mathscr{H}(T, h) \,. \tag{2.15}$$

Let us denote the volume of the system by V. The **heat capacity** at constant magnetic field h is defined though the derivative of the internal energy [Sch02, p. 269]

$$C = -T\left(\frac{\partial^2 \mathscr{F}}{\partial T^2}\right)_h = \left(\frac{\partial E}{\partial T}\right)_h = \left(\frac{\partial \langle \mathscr{H} \rangle}{\partial T}\right)_h . \tag{2.16}$$

Normalized by the volume of the system we get the **specific heat**

$$c = \frac{C}{V} . \tag{2.17}$$

The **magnetic moment** of the system is defined as [Sch02, p. 268]

$$M = -\left(\frac{\partial \mathscr{F}}{\partial h}\right)_T . \tag{2.18}$$

Normalized by the volume we get the **magnetization**

$$m = \frac{M}{V} . \tag{2.19}$$

The derivative of the magnetic moment defines the (isothermal) **magnetic susceptibility** [Sch02, p. 269]

$$\chi = -\frac{1}{V}\left(\frac{\partial^2 \mathscr{F}}{\partial h^2}\right)_T = \left(\frac{\partial M}{\partial h}\right)_T . \tag{2.20}$$

Note, that for c, χ and other observables we will skip the index indicating the constant parameter ($T = $ const. or $h = $ const.) as we will not cover other variants like adiabatic susceptibility ($S = $ const.).

Finally, we would like to introduce the **inverse temperature**,

$$\beta = \frac{1}{k_B T} . \tag{2.21}$$

This definition of temperature is very common in Monte Carlo simulations, and we will use it most of the time instead of the temperature T and call it simply temperature.

With the definition in Equation (2.21), we define the derivative with respect to β of a general observable $\mathscr{O}$ given through Equation (2.7),

$$\partial_\beta \mathscr{O} = \frac{\partial}{\partial \beta} \langle \mathscr{O} \rangle \tag{2.22a}$$

$$= \frac{\partial}{\partial \beta} \frac{1}{\mathscr{Z}} \sum_\mu \mathscr{O}_\mu e^{-\beta E_\mu} \tag{2.22b}$$

$$= \frac{\partial}{\partial \beta} \frac{\sum_\mu \mathscr{O}_\mu e^{-\beta E_\mu}}{\sum_\mu e^{-\beta E_\mu}} \tag{2.22c}$$

$$= \frac{\sum_\mu -E_\mu \mathscr{O}_\mu e^{-\beta E_\mu} \sum_\mu e^{-\beta E_\mu} - \sum_\mu \mathscr{O}_\mu e^{-\beta E_\mu} \sum_\mu -E_\mu e^{-\beta E_\mu}}{\left(\sum_\mu e^{-\beta E_\mu}\right)^2} \tag{2.22d}$$

$$= \frac{\sum_\mu -E_\mu \mathscr{O}_\mu e^{-\beta E_\mu}}{\mathscr{Z}} - \frac{\sum_\mu \mathscr{O}_\mu e^{-\beta E_\mu}}{\mathscr{Z}} \frac{\sum_\mu -E_\mu e^{-\beta E_\mu}}{\mathscr{Z}} , \tag{2.22e}$$

which finally leads to a very general representation of the derivative in terms of expectation values,

$$\boxed{\partial_\beta \mathscr{O} = \langle \mathscr{O} \rangle \langle E \rangle - \langle \mathscr{O} E \rangle .} \tag{2.23}$$

Equation (2.23) will be of great use later, since it will allow us to calculate derivatives of observables from measured time series and disorder realizations.

2.1.2 Thermodynamic limit

We introduced the system S and characterized it by its volume V, the number of particles N and the temperature T. The volume already appeared in some of the observables which were introduced. However, in many cases we want to extrapolate to the infinite system in the following way [Nol14, p. 388]:

$$V \to \infty \quad \text{and} \quad N \to \infty \quad \text{with} \quad \frac{N}{V} = \text{const.}, \tag{2.24}$$

i.e., the number of particles and the volume are taken to infinity while keeping the particle density N/V constant. The limit procedure in Equation (2.24) is called the **thermodynamic limit**. Only in the thermodynamic limit all different ensembles, i.e., the canonical ensemble (constant T) introduced here, as well as the micro-canonical ensemble (constant E) and the grand-canonical ensemble (constant chemical potential μ), yield the same results. Study the thermodynamic limit is extremely important in the case of simulations since any simulation is constrained by a finite volume and finite number of particles. In the case of Monte Carlo simulations performed in this work, we studied the influence of the finite size by applying the finite-size scaling techniques which will be discussed in Section 3.2.

Summary. We introduced the canonical ensemble as one of possibilities to describe a system with constant number of particles and at a constant temperature T. Its partition function allow us to derive all other thermodynamic observables and by taking the thermodynamic limit we can compare the results obtained by using a canonical ensemble to results from all other ensembles.

2.2 Ising model

In this section we will give a brief introduction to the pure Ising model. For more detailed introduction we refer to, e.g., Ref. [FV17] for a mathematical description or Ref. [LB05] for a description from the point of view of computational physics.

The Ising model is a simplified ferromagnetic model which was introduced in 1920 by Wilhelm Lenz [Len20] and first solved by Ernst Ising in 1925 [Isi25] in one dimension. Its basic formulation consists of a lattice where each site of the lattice contains a spin variable. Each of these discrete variables represent a dipole moment of an atomic spin in the system and is restricted to only two different states, "up" and "down", typically represented by ± 1. Further, only next-neighboring spins interact with each other and all other interactions are neglected.

Despite its simplicity, the model and its variations are still widely used to analyze different aspects of phase transitions in statistical physics and study the behavior of magnetic systems in general. In two dimensions the model was analytically solved by Lars Onsager in 1944 [Ons44]. He used the transfer matrix method and was able to show the existence of a phase transition as well as to derive the analytic solution for the critical temperature. It is exactly the combination of the very simple description in terms of next-neighbor interacting spins and the existence of a phase transition at a finite temperature $T > 0$ which makes the Ising model so outstanding and widely studied model.

Various modified versions of the original Ising model on a hyper-cubic lattice have been studied since it was first introduced. Examples are Ising model on triangular lattices [Bug96; Zhi+09], Ising model on graphs and trees [DM10; SNH17] or long-range interacting Ising model [Chr+20]. We also studied a modified version of the Ising model — Ising model on a site disordered lattice. We will first give some more precise description of the standard Ising model and afterwards introduce its modified form used in this work.

2.2.1 Pure Ising model

We define a lattice Λ which consists of sites on which the spins s are placed, and bonds which are the connections between the sites. In principle, a general graph can be used as a lattice, but we will focus on quadratic or cubic lattices with equal linear extension L in each direction. An example of a three-dimensional Ising model lattice with next neighbor interactions is schematically shown in Figure 2.2.
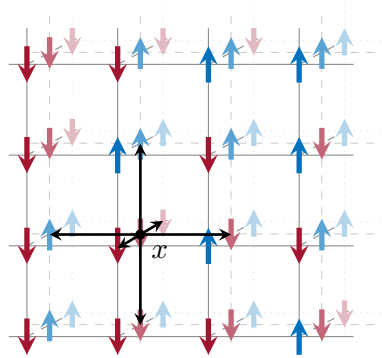
Figure 2.2: A three-dimensional Ising model lattice. The next-neighbor interactions of the spin at site x are shown as black arrows. The spin states ± 1 are shown as blue (up) and red (down) arrows.

The Hamiltonian of the Ising model is [LB05, p. 68]

$$\mathscr{H} = -J \sum_{\langle xy \rangle} s_x s_y - h \sum_x s_x \,, \tag{2.25}$$

where $s_x = \pm 1$ is the spin at site x of the lattice Λ, J denotes the coupling between two spins, h is the external magnetic field and $\langle xy \rangle$ denotes all next-neighbor site pairs. In this work we used the natural units and set the coupling constant as well as the Boltzmann constant to unity, i.e., $J = 1$ and $k_B = 1$, respectively. Further, we had no external magnetic field, i.e., $h = 0$. This will simplify the Hamiltonian in Equation (2.25). However, the magnetic term with h is needed in order to be able to perform derivatives with respect to it, e.g., for the susceptibility defined in Equation (2.20). In such cases, $h = 0$ is set after the derivative was taken. For the general treatment of the Ising model we will use the canonical ensemble which we have introduced in Section 2.1.

This brief introduction of the Ising model may occur surprising, since it is the basic Model for the whole work presented here. However, we will return to the Ising model in many of the following sections and will discuss different aspects of the model. More precisely, most of the time we will discuss the site disordered Ising model which will be presented next.

2.2.2 Site disordered Ising model

In the pure Ising model a spin is present on each site of the lattice. When we start to remove some of these spins from the lattice we arrive at the site disordered Ising model. In contrast to the site disorder there exists also the bond disorder where the connections (bonds) between two neighboring sites are removed while spins are still present on each site. We will work with the site disorder. In the literature the word "dilution" is often used as a synonym for disorder, as it is the case in, e.g., Refs. [BF83; Boc83; BP99; SFN09; Tim97]. Sometimes disorder in the literature also stands for disordered couplings, $J_{xy} \neq$ const. Such models were studied in, e.g., Refs. [Cha17; FM13; FT10; TF11; Wan+19]. Unless stated otherwise, in this work "disorder" will always describe the quenched site disorder on the lattice. However, in theory all different disorder cases, i.e., the site disorder, the bond disorder and the disordered coupling should fall into the same universality classes (see Section 2.3.3 for the definition) [FHY03].

In this work we will work with the **quenched site disorder**, i.e., the disorder is fixed while the dynamics of the Ising model happens on this disordered lattice. One such realization of the disorder will be called **disorder configuration** or realization. The concentration of defects on the lattice will be denoted by p_d while the concentration of the spins on the lattice will be $p = 1 - p_d$. It is important to notice that the spin concentration must be below the percolation threshold, $p < \hat{p}$, in order to ensure the existence of an infinite cluster of spins in the thermodynamic limit. Consequently, also the concentration of defects is limited by this threshold $p_d < 1 - \hat{p}$. We will address this a little more in Section 2.4.3. A schematic lattice for different concentrations of defects is shown in Figure 2.3. In this work we take the **grand canonical approach** [Zie+17] and p_d and p are mean values taken over all disorder configurations, the so-called **disorder ensemble**. The concentration of defects can therefore vary significantly from one configuration to another.

$p_d = 0.$ $p_d \approx 0.2.$ $p_d \approx 0.25.$ $p_d \approx 0.35.$
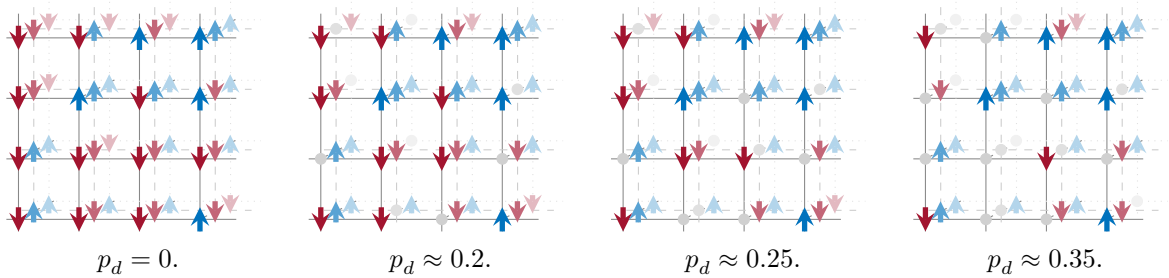
Figure 2.3: Three-dimensional disordered Ising model lattices with different concentrations of defects p_d. The gray points represent the defects (vacant sites). The spin states ± 1 are shown as blue (up) and red (down) arrows. The left most figure is the pure Ising model with $p_d = 0$.

To describe the defects in our model we introduce the **defect variables** η_x at each site of the lattice Λ. These variables can take the value 1 when it is an occupied site or 0 when the site is vacant (a defect). With these new variables we write down the Hamiltonian of the disordered Ising model

$$\mathcal{H} = -J \sum_{\langle xy \rangle} \eta_x \eta_y s_x s_y - h \sum_x \eta_x s_x \,, \tag{2.26}$$

We distinguish between two different disorder types. The first type is the **uncorrelated disorder** or random disorder. In this case the defects are chosen randomly according to the probability density

$$\not{p}\,(\eta) = p\delta(\eta) + p_d\delta(\eta - 1)\,. \tag{2.27}$$

The second type is the **correlated disorder**. In this case the probability density for the defects is again given by Equation (2.27), however, additionally the spacial correlation between the defects obeys a power-law decay

$$\langle\eta_x\eta_y\rangle \propto \frac{1}{r(x,y)^a} = C(r(x,y))\,, \tag{2.28}$$

where $r(x,y)$ is the distance between sites x and y, C denotes the correlation function and $a > 0$ is the **correlation exponent**. In Figure 2.4 we show slices of a three-dimensional Ising model lattice with different concentrations of defects and different correlation exponents near the critical temperature. One can see that correlated defects tend to form clusters.

| $a = \infty$, $p_d = 0$. | $a = \infty$, $p_d = 0.2$. | $a = \infty$, $p_d = 0.4$. |

| $a = 1.5$, $p_d = 0.2$. | $a = 1.5$, $p_d = 0.4$. |
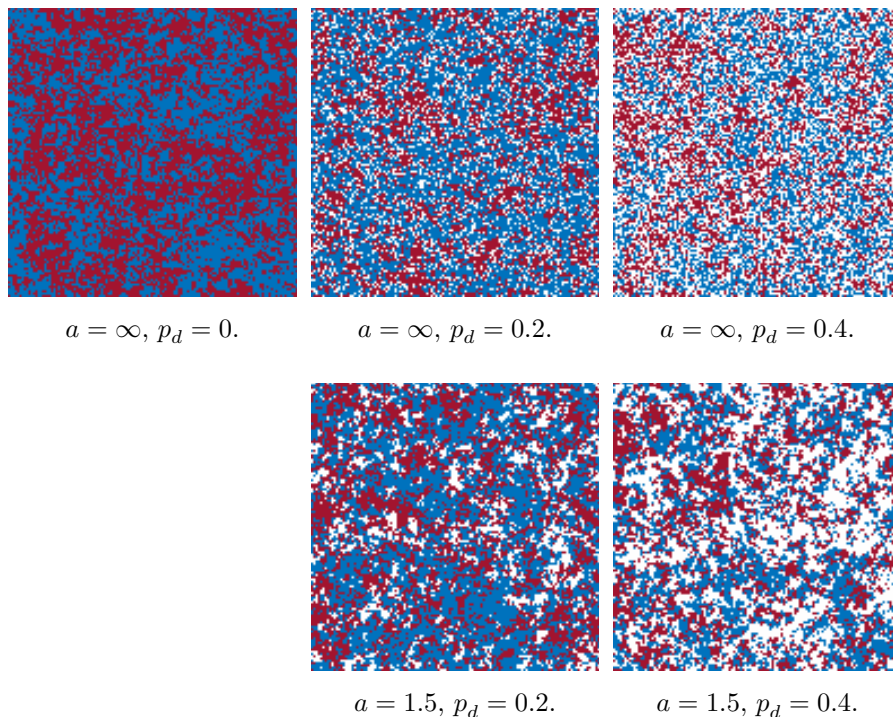
Figure 2.4: Slices of a three-dimensional Ising model lattice with $L = 128$ simulated near the critical temperature for different concentrations of defects p_d and correlation exponents a. Red and blue points represent the spin states $s_x = \pm 1$ and white points represent the defects $\eta_x = 0$.

This correlated disorder in one approach to mimic the structured disorder found in nature. We can imagine, that it can be useful to model, e.g., magnetic aerogels (a rigid foam) which probably have a similar "clustered" form, as e.g., the studied material in Ref. [Kis+04]. Magnetic aerogels were already studied in e.g., Refs. [Mar09; MBM96; PV06], but until now, the long-range correlated disorder fixed point was not found to be the dominant behavior. However, a more detailed study, in particular the comparison between experimental and theoretical data would be of great interest. The main problem with the experimental approach however, would probably be the measurement of the correlation strength a. An ongoing

research on magnetic foams in two dimensions is announced by Klimenkova and Shchur in Ref. [KS21]. They use a very different model with line of spins which are randomly placed on the plane.

A much more similar approach to ours was used in Refs. [BP99; Iva+08; Pru+05][1]. Here, lines of defects were placed on a lattice. It is argued that in tree dimensions, the defect lines correspond to a correlation exponent of $a = 2.0$. Although it may be exact for the infinite system, we are skeptical about the validity of this assumption of a finite lattice. At least, we were not able to measure a proper correlation function on such lattices. A visual comparison between the lattices with clustered defects and lines of defect is shown in Figure 2.5.
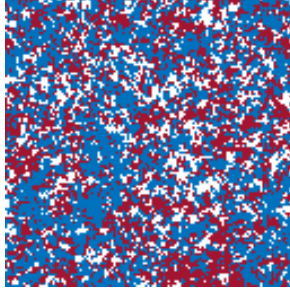
(a) Clustered defects generated with Fourier Filter Method.
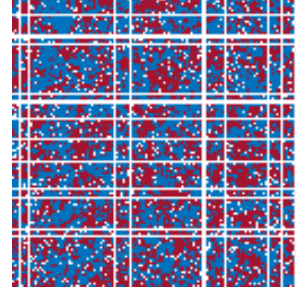
(b) Lines of defects. White dots are lines pointing upwards.

Figure 2.5: Slices of a three-dimensional Ising model lattice for $a = 2.0$ and $p_d = 0.2$ obtained with the fourier Filter Method used in this work (see Section 3.5) and lines of defects used in Refs. [BP99; Iva+08; Pru+05]. The lattice size is $L = 128$ and the temperautre was near to the critical temperature with $\beta_c = 0.25071$. Red and blue points represent the spin states $s_x = \pm 1$ and white points represent the defects $\eta_x = 0$.

2.2.3 Observables of the Ising model

In this Section we want to summarize the observables of the Ising model which will be needed to understand later parts of this work. As we will work with the disordered Ising model and with finite lattices most of the time, we will use the Hamiltonian defined in Equation (2.26) on a d-dimensional hypercubic lattice Λ with spatial extensions L_i for $i = 1, \dots, d$. Let us start with the two simplest observables, namely the energy of the system,

$$E_\mu = -J \sum_{\substack{\langle xy \rangle \\ x,y \in \Lambda}} \eta_x \eta_y s_x s_y \,, \tag{2.29}$$

and the magnetization of the system,

$$M_\mu = \sum_{x \in \Lambda} \eta_x s_x \,. \tag{2.30}$$

---

[1]   In Ref. [BP99] also the clustered defects were studied, similar to our work.

These two observables are defined for any state μ of the system. For the disordered Ising model a state μ is uniquely identified by all spin values s_x and all defect variables η_x for $x \in \Lambda$. Using Equation (2.7), we easily obtain the expectation values,

$$E = [\![\langle E \rangle]\!] \, , \tag{2.31}$$

$$M = [\![\langle M \rangle]\!] \, . \tag{2.32}$$

Because we will work with the disordered Ising model, we need two types of averages in Equations (2.31) and (2.32), the **thermal average** $\langle \cdot \rangle$, and the **disorder average** $[\![\cdot]\!]$. Often, the volume normalized variables,

$$e = E/V, \tag{2.33}$$

$$m = M/V, \tag{2.34}$$

will be used where V is the system volume

$$V = \prod_{i=1}^{d} L_i \, , \tag{2.35}$$

with d being the dimensionality of the system and L_i the linear extent in i-th direction. Note, that for the magnetization M (and m), we will usually take the absolute value in order to overcome the problem of averaging-to-zero of the magnetization throughout the whole temperature range because of the finite lattice size,

$$M = [\![\langle |M| \rangle]\!] \, , \quad m = [\![\langle |m| \rangle]\!] \, . \tag{2.36}$$

This is a common step in data analysis of spin model simulations [Jan08, p. 114].

Next observable which can be naturally measured on the lattice of an Ising model and which is in fact an important observable for the later understanding of phase transitions, critical exponents and finite-size scaling, is the **spin correlation function** (or more precise, two-point spin correlation function) [NB99, p. 14],

$$C_s(r) = C_s(s_x, s_y) = \langle s_x s_y \rangle - \langle s_x \rangle \langle s_y \rangle \, , \tag{2.37}$$

where r is the distance between the sites x and y (assuming translational invariance) [Jan08, p. 82],

$$r = |y - x| \, . \tag{2.38}$$

We will address this quantity im more detail shortly, when we will discuss the phase transitions of the Ising model, Section 2.2.2.

Further observables of interest are composed of averages of the energy and the magnetization and thus provide one value from all the simulation data. Their definition can be found in almost all text books on Monte Carlo simulations, e.g., Refs. [Jan12; LB05; NB99]. The first important observable is the susceptibility χ which was introduced in Equation (2.20) and which, in the case of disordered Ising model, reads

$$\chi = \beta V \left([\![\langle m^2 \rangle]\!] - [\![\langle |m| \rangle^2]\!] \right) \, . \tag{2.39}$$

Please note the position of the thermal and disorder averages. The definition follows directly from taking the disorder average of χ over several realizations,

$$\chi = [\![\chi^c]\!] = [\![\beta V(\langle m^2 \rangle - \langle |m| \rangle^2)]\!] \; , \tag{2.40}$$

where χ^c is the susceptibility calculated for one disorder realization c. Due to the linearity of the disorder average, Equation (2.40) can be brought to the form given in Equation (2.39). In the high temperature phase the expectation value of the magnetization vanishes by definition, $\langle m \rangle = 0$, and we can define a modified susceptibility estimator,

$$\tilde{\chi} = \beta V [\![\langle m^2 \rangle]\!] \; . \tag{2.41}$$

This definition will be useful for temperature scaling as it does not need the "inexact" usage of the absolute values $|m|$ instead of m.

In the same way as for the susceptibility, one gets the specific heat, Equation (2.17),

$$c = \beta^2 V([\![\langle e^2 \rangle]\!] - [\![\langle e \rangle^2]\!]) \; . \tag{2.42}$$

Next two useful observables which we would like to present are the derivative with respect to β of the magnetization,

$$\partial_\beta(|m|) = \frac{\partial}{\partial \beta} [\![\langle |m| \rangle]\!] = V([\![\langle |m| \rangle]\!] \, [\![\langle e \rangle]\!] - [\![\langle |m| \, e \rangle]\!]) \; , \tag{2.43}$$

and the derivative with respect to β of the logarithm of the magnetization,

$$\partial_\beta(\ln|m|) = \frac{\partial}{\partial \beta} \ln([\![\langle |m| \rangle]\!]) = V\left([\![\langle e \rangle]\!] - \frac{[\![\langle |m| \, e \rangle]\!]}{[\![\langle |m| \rangle]\!]}\right) \; , \tag{2.44}$$

In Equations (2.43) and (2.44) we used the derivative defined in Equation (2.23). Applying Equation (2.23) on $\ln([\![\langle |m| \rangle]\!])$ naturally explains why we do not use the disorder average on the whole equation, like

$$V\left[\!\!\left[\langle e \rangle - \frac{\langle |m| \, e \rangle}{\langle |m| \rangle}\right]\!\!\right] \; . \tag{2.45}$$

In contrast to the susceptibility and the specific heat, due to the quotient in the expression, Equation (2.44) and Equation (2.45) are not equal. Finally, we would like to define the Binder cumulant, which is a common observable used to obtain the critical temperature of the Ising model and comparable models,

$$U_2 = 1 - \frac{[\![\langle m^2 \rangle]\!]}{3 \, [\![\langle |m| \rangle^2]\!]} \; . \tag{2.46}$$

Since the Binder cumulant is a constructed observable and cannot be derived directly from another physical observable, we have the choice to place the disorder average like it is done in Equation (2.46) or outside the quotient. Both ways are used in literature. Our definition is used in, e.g., Refs. [Bal+98a; BP99; Cha02; Cha14; Cha17; Iva+08; Pru+05] whereas the version of the disorder average around the quotient is used in, e.g., Refs. [Has+07; Vas+15; Wan+19].

Finally, let us introduce one observable of the system which is closely related to the correlation function defined in Equation (2.37) — the correlation length ξ. It describes how fast the correlation length decays when the system is not at the critical temperature (see Equation (2.52) for the definition of the correlation length). At this point, we would like to explain how it can be measured on the lattice during the simulation. We will use the so-called **second-moment correlation length** [AM05, p. 472]. It is suitable for a finite lattice case and was successfully used in many works, e.g., in Refs. [Bal+98a; Cal+03; FM16; FXL18; PV02]. Its definition is [FM16]

$$\xi = \frac{1}{2\sin(\pi/L)}\sqrt{\frac{\tilde{C}_s(\mathbf{0})}{\tilde{C}_s(\mathbf{1})} - 1}\,, \tag{2.47}$$

where $\tilde{C}_s$ are the discrete Fourier transforms of the spin correlation function C_s [Jan08, p. 127],

$$\tilde{C}_s(\mathbf{k}) = \mathrm{DFT}(C_s(\mathbf{r})) = \sum_{\mathbf{r}} C_s(\mathbf{r})e^{-\mathrm{i}\mathbf{k}\mathbf{r}}\,, \tag{2.48}$$

calculated at two different k-space vectors $\mathbf{0} = (0,0,0)^T$ and $\mathbf{1} = (\frac{2\pi}{L},0,0)^T$. For the zero vector it turns out, that [Jan08, p. 127]

$$\tilde{C}_s(\mathbf{0}) = \frac{\tilde{\chi}}{\beta}\,, \tag{2.49}$$

where $\tilde{\chi}$ is the high temperature susceptibility defined in Equation (2.41). We know, that this is essentially the average over squared magnetization. The remaining task is to calculate the value of $\tilde{C}_s(\mathbf{1})$. One can show that [Jan08, p. 127]

$$\tilde{C}_s(\mathbf{k}) = \frac{1}{V}\left\langle \left|\sum_{\mathbf{r}} s(\mathbf{r})e^{\mathrm{i}\mathbf{k}\mathbf{r}}\right|^2 \right\rangle\,. \tag{2.50}$$

Equation (2.50) gives us an easy way of calculating ξ. We have to store the values $\sum_{\mathbf{r}} s(\mathbf{r})e^{\mathrm{i}\mathbf{k}\mathbf{r}}$ for a chosen $\mathbf{k} = \mathbf{1}$ at each measurement step of our simulation and afterwards take the thermal average to obtain $\tilde{C}_s(\mathbf{1})$. Finally, using Equation (2.47) gives the estimate of the correlation length ξ for one disorder realization. Taking the disorder average yields the final estimate

$$\xi = [\![\xi^c]\!]\,. \tag{2.51}$$

Please note, that Equation (2.47) by definition is valid only on the high temperature phase since the used $\tilde{\chi}$ is defined only in this phase.

This completes our presentation of the observables for the (disordered) Ising model. We will go into some more detail on the calculation of these observables from data obtained in our simulations in Section 4.3.

Summary. We introduced the pure and the site disordered Ising model. The definitions of the uncorrelated and long-range correlated site disorder cases were given, and we introduced the concentration of defects p_d and the correlation exponent a. All important observables of the Ising model used in this work were presented. The thermal and disorder averages were introduced for the disordered Ising model, and we explained how exactly the disorder averages were used in our work.

2.3 Phase transitions and critical exponents

In this section we briefly discuss the concepts of phases and phase transitions. In physical sense a **phase** is a possible state of a matter or system at equilibrium [Nol14, p. 279]. It is characterized by a set of (a few) observables which are uniform on a macroscopic level [NO10, p. 1]. It is further characterized by a thermodynamic potential (we will usually take the free energy $\mathscr{F}$) which is a function of these uniformly distributed observables. Typical examples of phases are the phases of water: ice, liquid water and vapor water. By changing the parameter of the thermodynamic potential one can go from one phase to another. This is called a **phase transition**. A phase transition is usually supplied by a dramatic change in the system through a relatively small change in its parameters.

We will not cover the **Ginzburg-Landau theory** [Sch02, p. 357] which is a continuous description of phase transitions and the **Mean-Field approximation** [NO10, p. 17] which is a procedure of reducing the number of degrees of freedom by using averages and allows one to study phase transitions analytically as well. Our analyses do not rely on these concepts and introducing them here would go beyond the scope of this work.

2.3.1 Classification of phase transitions

The phase transitions can be divided into two main categories: first-order and second-order phase transitions. Originally this classification was introduced by Ehrenfest in 1933 [Sau17]. In the original formulation it classified the phase transitions into first-order, and various higher orders. However, after a while criticism on the classification starting with the second-order led to basically only two classes [Nol14, p. 283], first-order and second-order. From modern perspective one sometimes refers to the first-order phase transitions as discontinuous and to all higher order phase transitions as continuous phase transitions.

In the case of a first-order phase transition the thermodynamic potential has a discontinuity during the transformation. This implies that at least one of the derivatives of the thermodynamic potential has a finite jump as the transition happens. Taking the common example of water, the melting of ice is a first-order phase transition with a finite jump in the entropy of the system which is the first derivative of the free energy, Equation (2.13). A typical observed phenomenon of a first-order phase transition is the coexistence of different phases, e.g., undercooled water [Nol14, p. 282]. We will not discuss the first-order phase transitions in detail as they are not relevant for this work.

For the second-order phase transitions, the thermodynamic potential is continuous at the transition point but has a discontinuity in at least one of its derivatives. Schematically, the comparison between the behavior of different quantities for a first-order and a second-order

phase transition is shown in Figure 2.6. In the following we will concentrate on magnetic systems and especially on the Ising model introduced in Section 2.2. However, most of the concepts presented here are valid for second-order phase transitions in general.

(a) First-order phase transition.

(b) Second-order phase transition.
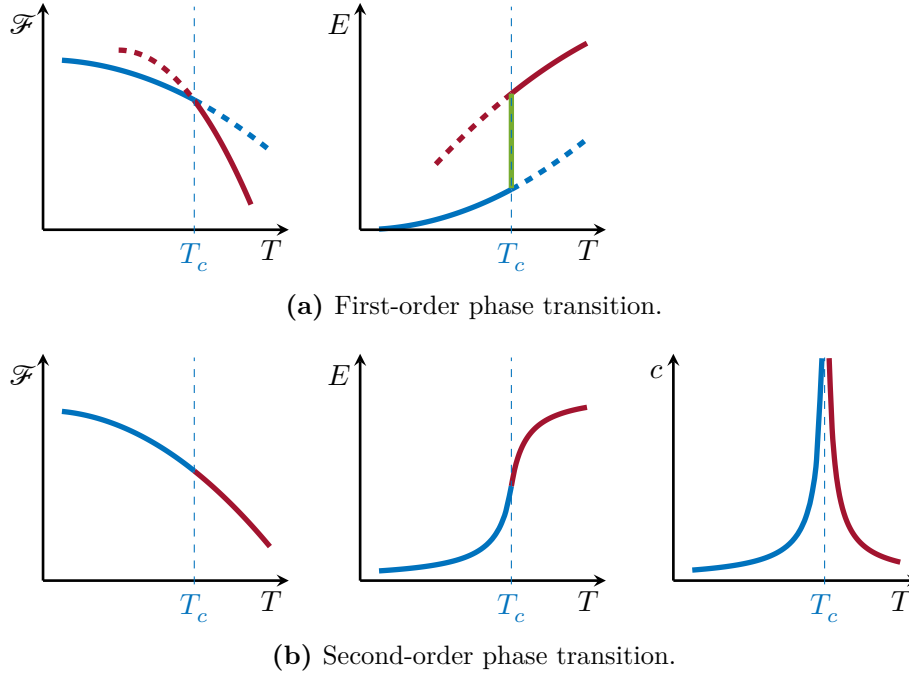
Figure 2.6: The qualitative behavior of the free energy $\mathscr{F}$, the internal energy E and the specific heat c for a first-order and a second-order phase transitions. The red and blue colors represent the two different phases. The dashed regions in the first-order plots are regions of possibly metastable states. The green line in the energy plot for the first-order transition is the finite jump in energy [NO10, p. 4] Adapted from Ref. [LB05, Fig. 2.3].

2.3.2 Phase transitions of the Ising model

Let us now take our concrete case and analyze the Ising model defined by the Hamiltonian from Equation (2.25) and the magnetization per spin m. The phase diagram in the T-h-space is presented in Figure 2.7a. Let T_c denote the critical temperature below which the system is in the ferromagnetic state. When $T < T_c$, we can apply a negative h. In this case the magnetization is in the region $-1 \leq m < 0$. By increasing the h to positive values we observe a change in the magnetization sign which now will be in the region $0 < m \leq +1$. This transition is a first-order transition with a finite jump in the magnetization and is shown schematically in Figure 2.7b. However, if we start at $T > T_c$, set the external field to zero $h = 0$ and decrease the temperature, we will observe a second-order phase transition from the paramagnetic to the ferromagnetic phase [Gar95]. This transition is shown schematically in Figure 2.7c. The appearance of the lattice of the three-dimensional Ising model in the different phases is shown in Figure 2.8.

The transition happens at a critical temperature T_c (inverse temperature β_c). In the **ferromagnetic phase** (also called **ordered phase** or **low temperature phase**), $T < T_c$, the majority of the spins have the same value. In the **paramagnetic phase** (also called **disordered phase** or **high temperature phase**), $T > T_c$, one sees randomly fluctuating spins. Thus, the magnetization takes a nonzero value in the ferromagnetic case, and is zero

(a) T-h-phase diagram of a magnetic system.

(b) First-order phase transition below T_c when changing the external field h.

(c) Second-order phase transition for $h = 0$ when changing the temperature from $T > T_c$ to $T < T_c$.
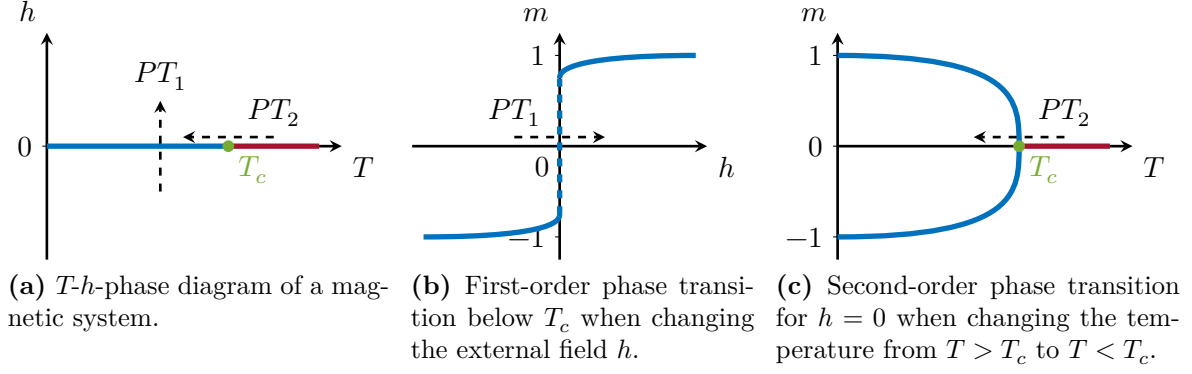
Figure 2.7: The T-h-phase diagram of a magnetic system and the two different phase transitions it can have. Dashed arrows show the direction of the parameter change for the phase transition. PT_1 is the first-order phase transition and PT_2 the second-order phase transition. Blue represents the ferromagnetic (low temperature) and green the paramagnetic (high temperature) regions. Adapted from Ref. [NO10, Fig. 1.3].

(a) $\beta = 0.4 > \beta_c$, $(T < T_c)$.

(b) $\beta = 0.221654 \approx \beta_c$, $(T \approx T_c)$.

(c) $\beta = 0.001 < \beta_c$, $(T > T_c)$.
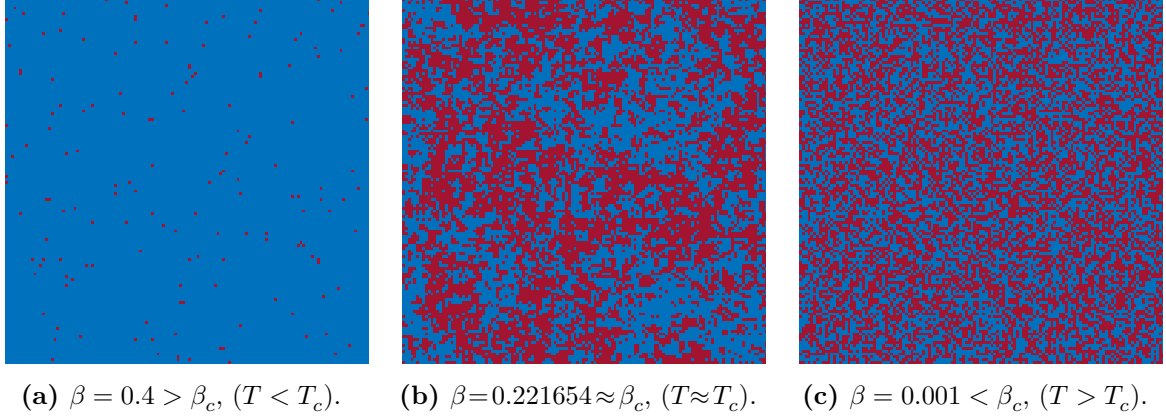
Figure 2.8: Pure three-dimensional Ising model lattice slices at different temperatures. Red and blue points represent the spin states $s_x = \pm 1$. The model is in the ferromagnetic phase in (a), at the critical temperature in (b) and in the paramagnetic phase in (c).

in the paramagnetic case. The magnetization m is called the **order parameter** of the phase transition. Generally, an order parameter is an observable of the system which has a finite nonzero value in one phase but is zero in the other phase [LB05, p. 13].

When we study the correlation function of the spins defined in Equation (2.37), we obtain the following results. Away from the critical temperature the spacial correlation $C_s(r)$ decays exponentially (for $r \gg 1$) and eventually becomes zero at infinite distance [Jan08, p. 82],

$$C_s(r) \propto r^{\kappa} \, e^{-r/\xi} \quad \text{with } T \neq T_c. \tag{2.52}$$

where exponent κ is dependent on the dimension of the system and the phase which is studied (ordered or disordered), e.g., $\kappa = -(d-1)/2$ for the Ising model in disordered phase [LB05, p. 16]. Equation (2.52) defines a further quantity, the **correlation length** ξ. It describes how fast the spins become spatially uncorrelated when the system is not at T_c. For a second-order phase transition a crucial feature is that the correlation length ξ diverges as the system

approaches the critical temperature [Jan08, p. 82],

$$\xi \to \infty \quad \text{for } T \to T_c. \tag{2.53}$$

Practically, it means that despite the fact that only next-neighbor interactions are present in the Ising model, the spins "feel" each other on any length scale. On the other hand, exactly at the critical temperature, the correlation function behaves like a power-law [LB05, p. 17],

$$C_s(r) \propto r^{-d+2-\eta} \quad \text{with } T = T_c. \tag{2.54}$$

The exponent η measures the deviation from a purely Gaussian behavior [VFB10, p. 559]. The exponent η is called a **critical exponent**. We will introduce the general concept of the critical exponents next.

2.3.3 Critical exponents

Roughly speaking, a critical exponent describes how a certain observable $\mathcal{O}$ behaves during a phase transition. The formal definition of a critical exponent $x_{\mathcal{O}}^{\pm}$ for an observable $\mathcal{O}$ is [Hen99, p. 5]

$$x_{\mathcal{O}}^{\pm} = \lim_{t \to \pm 0} \frac{\ln \mathcal{O}(t)}{\ln |t|} < \infty, \tag{2.55}$$

where, for convenient notation, we introduced the **reduced temperature**,

$$t = 1 - \frac{T}{T_c}. \tag{2.56}$$

It is clear from Equation (2.55), that the critical exponent for a certain observable exists only if the corresponding limit is finite. In Equation (2.55) we introduced the index $\pm$ to differentiate between the limit directions $t \to +0$ and $t \to -0$, respectively. However, in almost all cases, this direction does not matter and the critical exponents are equal, i.e., $x_{\mathcal{O}}^{+} = x_{\mathcal{O}}^{-}$. For the rest or this work we will therefore not distinguish between the limit direction.

Now, we can define the critical exponents for various observables [Jan08, p. 83],

$$c = c_{\text{reg}} + c_0^{\pm} |t|^{-\alpha} + \dots, \tag{2.57}$$

$$m = m_0^{\pm} |t|^{\beta} + \dots \quad (T < T_c), \tag{2.58}$$

$$\chi = \chi_{\text{reg}} + \chi_0^{\pm} |t|^{-\gamma} + \dots, \tag{2.59}$$

$$\xi = \xi_0^{\pm} |t|^{-\nu} + \dots. \tag{2.60}$$

The dots in the equations above represent the analytic and confluent corrections which become more and more important as t increases. The amplitudes $\mathcal{O}_0^{+}$ and $\mathcal{O}_0^{-}$ are valid for the high temperature and low temperature phases, respectively. In general, they are not equal. Contrarily, their ratios of the form $\mathcal{O}_0^{+}/\mathcal{O}_0^{-}$ are universal and can be studied, see e.g., Ref. [PV02, p. 561] for complete set of different ratios. The $\mathcal{O}_{\text{reg}}$ are regular background terms. Usually, this term is neglected for the susceptibility, $\chi_{\text{reg}} \approx 0$, but not for c because usually $\gamma \gg \alpha$ [Jan12, p. 143]. Last critical exponent δ is related to the magnetization along the isotherm $T = T_c$ and along the h-direction [Hen99, p. 6],

$$m \propto \left| \frac{h}{k_B T} \right|^{1/\delta}. \tag{2.61}$$

The set of critical exponents α, β, γ, δ, η and ν completely describe a phase transition of the system of interest. Systems with the same critical exponents belong to a common **universality class** [Lav15, p. 96]. In general, systems are divided into universality classes according to [Lav15, p. 96]

1. the dimension of the system d,
2. the symmetry group of the order parameter,
3. possibly some other criteria.

For one particular universality class the critical exponents should be equal or at worst be a continuous function of a few parameters of the system.

A set of six independent exponents would suggest that pretty much any system would belong to its own unique universality class. However, the critical exponents presented above are not independent. In fact, fixing two of them already fixes all the remaining exponents as well. The relations are named after the four researchers, (the corresponding references are Refs. [Fis69; Gri65; Jos67a; Jos67b; Rus63]), who have originally shown them (first, as inequalities, though) [Jan08, p. 83],

$$d\nu = 2 - \alpha \qquad \text{Josephson's law}, \tag{2.62}$$

$$2\beta + \gamma = 2 - \alpha \qquad \text{Rushbrooke's law}, \tag{2.63}$$

$$\beta(\delta - 1) = \gamma \qquad \text{Griffiths's law}, \tag{2.64}$$

$$\nu(2 - \eta) = \gamma \qquad \text{Fisher's law}. \tag{2.65}$$

Equations (2.63) to (2.65) are commonly called **scaling relations** while the Equation (2.62) is called **hyperscaling relation** because is contains the dimension of the system [Hen99, p. 10]. We will use the scaling and hyperscaling relations in Section 4.5.6 to check our results for consistency.

The above relations can be rigorously derived from the Renormalization Group theory which we will briefly describe in the next section.

2.3.4 Renormalization Group theory

As already mentioned, all the presented scaling relations can be derived by using the machinery of the Renormalization Group theory (RG). In fact, the RG goes alongside the simulation approach and is the second widely used technique to study critical phenomena and phase transitions. As we will see in Section 2.4, the theoretical predictions for the disordered Ising model will be in fact RG calculations. For this work we have not used the RG but in order to give a complete and consistent picture of the underlying concepts, we will give a very brief overview on RG here. In particular, we will derive the scaling relations by following Ref. [NO10, pp. 52 ff.]. For much more detailed introduction to RG we refer to, e.g., Refs. [AM05; Gar95; Hol07].

The key idea of the RG is to transform the system by tracing out a number of degrees of freedom while keeping the partition function invariant under the transformation. As an example, one would construct block spins out of individual spins of the lattice and thereby reducing the lattice by a (a priori arbitrary) factor $b > 1$. We will not explain the concrete procedure here, see Ref. [NO10, p. 52] for more information. Let us write down the

transformation of the Hamiltonian of the system,

$$\mathcal{H}' = R_b \mathcal{H}, \tag{2.66}$$

where R_b is a (in general non-trivial) transformation which scales the length r and the number of particles (spins) N accordingly,

$$r' = b^{-1} r, \tag{2.67}$$

$$N' = b^{-d} N. \tag{2.68}$$

We impose that the partition function remains invariant under R_b, i.e.,

$$\mathcal{Z}(\mathcal{H}') = \mathcal{Z}(\mathcal{H}). \tag{2.69}$$

Now, before going further, let us remark that the set of all R_b transformations forms a semigroup (in contrast to its imprecise name "Renormalization Group theory"). It has two group properties,

1. the existence of an identity element,

$$\mathcal{H} = R_1 \mathcal{H}, \tag{2.70}$$

2. and the associativity,

$$R_{b_2} R_{b_1} \mathcal{H} = R_{b_2 b_1} \mathcal{H}, \tag{2.71}$$

but lacks an inverse element R_b^{-1}. This is clear since we remove degrees of freedom by applying R_b and hence cannot simply recover them back. Now, if we start exactly at the critical point of the system, where it is scale-invariant due to the divergence of the correlation length ξ, subsequently applying the transformation R_b on $\mathcal{H}$ will drive the system to a fixed point,

$$\mathcal{H}^* = \lim_{n \to \infty} R_b^n \mathcal{H}, \tag{2.72}$$

with the fixed condition

$$\mathcal{H}^* = R_b \mathcal{H}^*. \tag{2.73}$$

Contrary, if the system was not exactly at the critical point, it will drift away from the fixed point towards one of the phases, depending on where the starting point was. This driving towards or away from the fixed point is called the **Renormalization Group flow**, and it is schematically depicted in Figure 2.9. Starting from this point, one can study the Renormalization Group flow towards the fixed point by using path integral formalism and loop expansions, see e.g., Ref. [AM05] for a detailed explanation. This will usually result in, e.g., critical exponents in an n-order loop approximation. But we will stop at this point and instead just derive the scaling relations through appliance of the RG.

Let us take a look at the free energy and its scaling under R_b which is governed by its definition in Equation (2.8) and the Equation (2.69),

$$\mathcal{F}(\mathcal{H}') = b^d \mathcal{F}(\mathcal{H}). \tag{2.74}$$
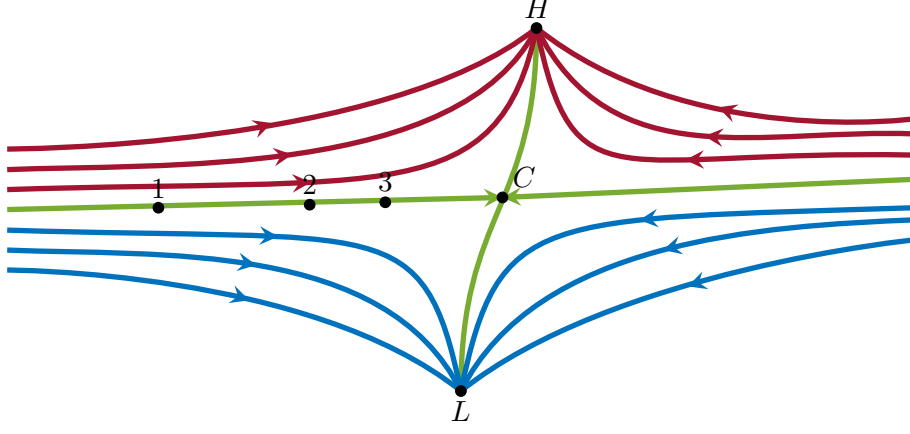
Figure 2.9: Schematic representation of the Renormalization Group flow. The critical point C is reached by successively applying the transformation R_b along the critical path (green), denoted as black numbered points. Starting at any other point other than one on the green lines, the Renormalization Group flow will drive the system away from the critical point towards the high temperature fixed point H or the low temperature fixed point L. Adapted from Ref. [LB05, Fig. 9.2].

Applying the transformation R_b n times and writing out the dependence of the free energy on the (reduced) temperature t and the magnetic field h, we get

$$\mathcal{F}(t, h) = b^{-nd}\mathcal{F}(b^{ny_t}t, b^{ny_h}h) \,, \tag{2.75}$$

where y_t and y_h are some unknown exponents for the scaling behavior of t and h, respectively. The next step is a crucial idea for the derivation. Away from critical temperature, i.e., $t \neq 0$, we can set

$$b^{ny_t}t = 1 \,. \tag{2.76}$$

This is the case for $T > T_c$, otherwise we use $|t|$ and -1 in Equation (2.76). Physically, Equation (2.76) means that by applying R_b n times we drive the system away from the critical temperature and by this replace the condition $|t| \ll 1$. By solving it for b^n and inserting into Equation (2.75), we finally get

$$\mathcal{F}(t, h) = t^{d/y_t}\mathcal{F}(1, t^{-y_h/y_t}h) = t^{d/y_t}\mathcal{F}_0(t^{-y_h/y_t}h) \,. \tag{2.77}$$

This is the key equation for all the scaling relations, and it is called the **scaling law**. Note, that on the right-hand side of Equation (2.77) we introduced the **scaling function $\mathcal{F}_0$**, which, in contrast to $\mathcal{F}$, has only one parameter. The free energy (or more precise, its singular part) is therefore a generalized homogeneous function in mathematical sense [NO10, p. 63].

As we have seen in Section 2.1, all further quantities can be derived from the free energy. Let us take the susceptibility χ and derive it from Equation (2.77) through Equation (2.20),

$$\chi(t, 0) \propto \left.\frac{\partial^2 \mathcal{F}(t, h)}{\partial h^2}\right|_{h=0} \propto t^{(d-2y_h)/y_t} \,, \tag{2.78}$$

Comparing the exponents in Equation (2.78) with Equation (2.59), we immediately see, that

$$\gamma = \frac{2y_h - d}{y_t} \,. \tag{2.79}$$

Analogously, one derives relations for other observables and get

$$\alpha = 2 - \frac{d}{y_t}\,, \tag{2.80}$$

$$\beta = \frac{d - y_h}{y_t}\,, \tag{2.81}$$

$$\delta = \frac{y_h}{d - y_t}\,. \tag{2.82}$$

For the correlation length exponent ν one derives the scaling relation first, analogously to the derivation of Equation (2.77), which reads [NO10, p. 66]

$$C_s(r, t) \propto t^{2(d - y_h)/y_t}\,, \quad (T \neq T_c)\,, \tag{2.83}$$

$$C_s(r) \propto r^{-2d + 2y_h}\,, \quad (T = T_c)\,, \tag{2.84}$$

Again, comparing the exponents leads to

$$\nu = \frac{1}{y_t}\,, \tag{2.85}$$

$$\eta = d - 2y_h + 2\,. \tag{2.86}$$

Equations (2.79) to (2.82), (2.85) and (2.86) finally can be combined to provide the scaling relations presented in Equations (2.62) to (2.65). During the presented derivation we have implicitly shown, why only two critical exponents can be chosen independently and all others are then related by the scaling relations. It is the fact, that the free energy depends on two variables, t and h which together can have only two scaling exponents, i.e., y_t and y_h, respectively.

Summary. We introduced the notion of a phase transition and classified our studied Ising model phase transition as second-order. We explained how the transition can be described in terms of power-law decaying observables and their corresponding critical exponents. By looking into the basics of the Renormalization Group theory, we showed how the relations between the critical exponents can be derived.

2.4 Predictions of universality classes for the disordered Ising model

Contrarily to the previous sections which provided us with exact analytic formulas, this section will be a summary of results obtained for the disordered Ising model with the help of Renormalization Group (RG) calculations and the Monte Carlo (MC) simulations. This is a consequence of the lack of an analytic solution of the Ising model in three dimensions even for the pure case. Therefore, we would like to summarize the known results for referencing them later in this work.

2.4.1 Uncorrelated disorder

For the uncorrelated disorder case, there exists a so-called **Harris criterion** which was introduced by Harris [Har74]. It is a result obtained through resummation of perturbation theory and couples the influence of the disorder on the system to the critical exponent of the specific heat. The condition is that introducing disorder to the system leads to a change in the universality class if

$$d\nu_{\text{pure}} - 2 = -\alpha_{\text{pure}} < 0\,, \tag{2.87}$$

where α_pure and ν_pure are critical exponents of the system without disorder. Although this result is not a rigorous calculation, it has been tested and confirmed various times since it was first introduced in 1974. If $\alpha_\text{pure} < 0$ the prediction tells the opposite — the disorder becomes irrelevant and the system stays in its universality class. However, no prediction for the case $\alpha_\text{pure} = 0$ can be given. This is the reason why the Ising model in two dimensions (which happens to have $\alpha_\text{pure} = 0$) is a difficult edge problem. Various studies of the uncorrelated disordered Ising model in two dimensions [Bal+97; BP18; Cha14; Cha17; DD83; KP94; KR08; MK99; MP07; Rui97; SFN09; Sha87; Sha94] suggest the view that the universality class remains the same but additional logarithmic corrections have to be considered. Using simulations, such logarithmic corrections are almost always a big problem since the largest lattice sizes one can study are usually not large enough to distinguish logarithmic behavior from other forms like power-laws. This was one of the main reasons which motivated us to investigate the three-dimensional case.

In three dimensions, the disordered Ising model was also studied in various works with the help of the RG techniques [HY98; PS00; PV02; Var00; Xio+10] and MC simulations [Bal+98a; Ber+04; Cal+03; Has+07; Heu93; MKB04; WD98]. A comprehensive list of further works before 2003 can be found in Ref. [FHY03]. A comparison between the different approaches and the difficulties on the agreement between the experiments, the RG calculations and the simulation results is discussed in Ref. [Ber+05]. A very recent RG work is Ref. [KKS21] which also have a very good summary of different works. We added their values in Table 2.3 but since they have quite large errors, we will exclude them in the comparison plots later. Some experimental results for Ising-like materials with disorder are summarized in Table 2.1, although we will not go into a detailed comparison with this data. It may be noticed however, that the critical exponent ν usually lies above the values from RG calculations and MC simulations. Nevertheless, due to the large errors, the experimental values typically cover the theoretical ones fully or at least to a great extent.

Table 2.1: Experimental results of the critical exponents of three-dimensional Ising-like models. Most of the results were obtained through neutron scattering.

Reference	Material	p	ν	α	β	γ
Birgeneau et al. [Bir+83]	$Fe_pZn_{1-p}F_2$	0.6, 0.5	0.73(3)	$-0.09(3)$		1.44(6)
Belanger et al. [Bel+95]	$Fe_pZn_{1-p}F_2$	0.5			0.35	
Mitchell et al. [Mit+86]	$Mn_pZn_{1-p}F_2$	0.7	0.715(35)			1.364(76)
Slanič et al. [SB98; SBF98]	$Fe_pZn_{1-p}F_2$	0.9	0.71(1)	$-0.10(2)$		1.35(1)

In Table 2.3 we summarize results from RG calculations and MC simulations for the uncorrelated and also for the correlated disorder cases, which will be covered in the next section. Due to the large number of works dealing with the uncorrelated case, we restrict ourselves to the most recent results and results with comparably small errors. Also note, that we exclude the critical exponent δ in Table 2.3 as it was not measured directly in any of the known work and also not in this work. The results from the literature are not completely identical but all of them support the Harris prediction that the Ising model with disorder changes its universality class. Moreover, the numerical results (in particular for the critical exponent ν)

are quite close together and more or less coincide within their errorbars. Altogether, the uncorrelated disorder case is well-established and can be used as a solid background to compare newer results to.

2.4.2 Correlated disorder

Let us turn to the correlated disorder case. The literature base for this case is much sparser than for the uncorrelated case. An important work was done by Weinrib and Halperin [WH83] where the authors used the RG ε-δ-expnasion to deal with long-range correlated disorder in models with different dimensions of the order parameter. Here, the expansion happens in two directions, i.e., $\varepsilon = 4 - d$ and $\delta = 4 - a$. The authors have worked out the **extended Harris criterion** which can be summarized in the following form: the system with long-range correlated disorder with a correlation which decays as $\propto r^{-a}$ will change to a new universality class when the correlation is strong enough, i.e., $a < d$. We can combine the extended Harris criterion with the original one into one expression: adding disorder to the system leads to a change in the universality class if

$$
\begin{cases}
d\nu_{\mathrm{pure}} - 2 = -\alpha_{\mathrm{pure}} < 0 & \text{for } a \geq d \\
a\nu_{\mathrm{pure}} - 2 < 0 & \text{for } a < d
\end{cases}.
\tag{2.88}
$$

Note, that the standard Harris criterion is recovered in case of $a \geq d$. We would like to pay attention to a statement in Ref. [WH83] which we found is often overseen: the above expression Equation (2.88) is valid for $a \approx 4$. There is no evident criterion on how far away the correlation exponent a can go from that without introducing noticeable deviations. Also, in case of a three-dimensional model, the two statements $a < 3$ and $a \approx 4$ are quite contradictory. There is one further prediction in Ref. [WH83] which we will call the Weinrib and Halperin (WH) prediction. Its states that the critical exponent of the correlation length ν will take the form

$$
\nu = \frac{2}{a},
\tag{2.89}
$$

if the long-range correlated disorder is relevant, i.e., $a < d$. The WH prediction is supposed to be exact in the case of the Ising model as suggested by the authors. However, no rigorous proof is given. There exists a work by Honkonen and Nalimov [HN89] where the authors claim to provide a rigor proof of Equation (2.89) by showing that it is valid up to any expansion order. However, it remains unclear to us, whether both expansion variables can be taken arbitrarily far away from 4, i.e., ε **and** δ or only one of them. We therefore leave the WH prediction as a conjecture and will compare our results to it in order to further support or reject it.

For the case of a system with an order parameter larger than one, the authors in Ref. [WH83] also provide expressions for other exponents,

$$
\alpha = \frac{2\,(a - d)}{a},
\tag{2.90}
$$

$$
\beta = \frac{2 - \varepsilon}{a},
\tag{2.91}
$$

$$
\gamma = \frac{4}{a},
\tag{2.92}
$$

where we have left out the notion of further corrections of order $O(\varepsilon^2)$. Equations (2.90) to (2.92) are sad to be derived from scaling relations. By using scaling relations from Equations (2.62) and (2.63) and Equations (2.89) and (2.92), we get a second expression for β,

$$\beta = \frac{d-2}{a} \, . \tag{2.93}$$

Also it is not clear from the text whether these expressions are valid in the case of the Ising model, we included those expressions (with Equation (2.93) for β) into Table 2.3 and will compare our estimates to these predictions as well.

There exist a contradicting work by Prudnikov et al. [PPF00] where the authors also study the correlated case with the help of RG calculations but get completely different estimates for the exponent ν and consequently the other exponents. The reason for such extreme deviations remains unclear to us. This work and also the accompanying MC results from Ref. [Pru+05] are provided in Table 2.3 for completeness. Further works with MC simulations dealing with the three-dimensional Ising model with correlated disorder are Refs. [BP99; Iva+08]. Their estimates are summarized in Table 2.3 as well. All works with MC simulations used only one correlation exponent $a = 2.0$ and a limited number of concentrations of defects p_d. This fact and also the discrepancy between the results by Prudnikov et al. [PPF00] and Weinrib and Halperin [WH83] were a big motivation for us to attack the problem once again.

2.4.3 Concentration threshold

Last aspect in connection to the site disordered Ising model we would like to discuss is the concentration threshold for the defects on the lattice. It is natural to insist that an infinite connected spin cluster has to be present below T_c for $L \to \infty$. Hence, the concentration of spins has to be equal or above the site-percolation threshold in three dimensions. This concentration in three dimensions is known to be [Wan+13]

$$\widehat{p}^\infty = 0.311\,607\,7(2) \, , \tag{2.94a}$$

$$\widehat{p}_d^\infty = 1 - \widehat{p}^\infty = 0.688\,392\,3(2) \, , \tag{2.94b}$$

where the threshold for the concentration of defects $p_d \leq \widehat{p}_d$ was introduced and the index ∞ indicates that this is the percolation threshold for the uncorrelated case with $a = \infty$. As one can see, in the uncorrelated case about two thirds of the lattice can be turned into disorder without destroying the infinite spin cluster.

For the correlated cases, there was a work by Zierenberg et al. [Zie+17] where the dependence of the percolation concentration on the correlation exponent a was studied. The results from Ref. [Zie+17] are presented in Table 2.2. The main outcome is somewhat counterintuitive at the first glance: for stronger correlations, the percolation threshold decreases. This means that even more defects can be put onto the lattice without destroying the spin cluster. Although one might expect the opposite, the qualitative explanation of this behavior exists. If the defects tend to form clusters on the lattice, it is more likely that even a larger concentration of them will still not be sufficient to split the largest spin cluster apart. Consider the edge case of $a \to 0$. In this case all defects effectively are one big defect cluster. Independent of the ratio between the occupied sites and the defects, the occupied sites they will also form

one connected cluster. This is a natural consequence of the fact that the correlation between the defect sites and the spin sites follows the same law, e.g., the power-law in our case. Hence, spatially correlated defects go hand in hand with spatially correlated occupied sites.

Finally, we would like to note that the largest concentration of defects $p_d = 0.4$ considered in this work is way below the threshold concentration $\hat{p}_d$ and hence we do not expect any problems with regard to a proper Ising mode on the lattices. However, this does not exclude the possibility for smaller (almost) fully separated regions of spins to exist. Such regions are called **rare regions**. They can lead to significant changes in the behavior of the total system, i.e., to so-called Griffiths singularities and Griffiths phases. However, in the case of the Ising model, the influence of the rare regions decay exponentially [Voj06], and therefore we do not expect any difficulties in our analyses. We will not cover the topic of Griffiths phases here.

Table 2.2: Dependence of the percolation threshold $\hat{p}$ on the correlation exponent a taken from Ref. [Zie+17]. Additionally, the concentration of defects $\hat{p}_d$ is shown for convenience.

a	$\hat{p}$	$\hat{p}_d = 1 - \hat{p}$
∞	0.311 610(2)	0.688 390(2)
4.0	0.238 778(4)	0.761 222(4)
3.0	0.208 438(5)	0.791 562(5)
2.5	0.188 289(7)	0.811 711(7)
2.0	0.163 02(2)	0.836 98(2)
1.5	0.130 22(5)	0.869 78(5)
1.0	0.0863(3)	0.9137(3)
0.5	0.025(3)	0.975(3)

Summary. For the three-dimensional Ising model we expect three different universality classes: the pure case without disorder, the (effectively) uncorrelated case when $a \geq d$ and the correlated case when $a < d$. These cases are schematically depicted in Figure 2.10. In the correlated case the Weinrib and Halperin prediction for $\nu = 2/a$ is a conjecture which we would like to support or reject at the end of this work.
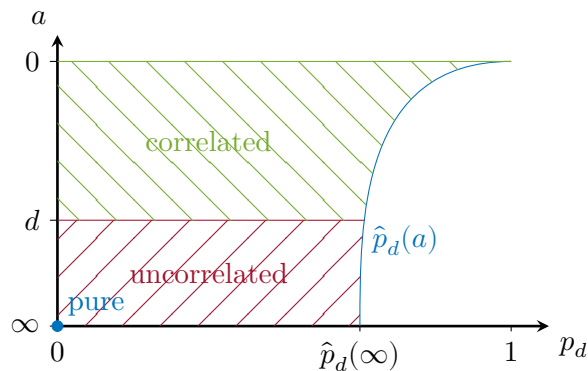
Figure 2.10: Universality classes of the three-dimensional Ising model in dependence of the concentration of defects p_d and the correlation exponent a. The threshold for p_d is shown qualitatively according to the results from Ref. [Zie+17].

Table 2.3: Summary of the critical exponents and some background information from various works dealing with the uncorrelated and long-range correlated disordered Ising model in three dimensions. For comparison, recent high-precision estimates for the pure Ising model are also provided. The critical exponent δ is left out because none of the present works (including this work) estimated it directly. Legend: † — calculated from other exponents through scaling relations in the original work, ‡ — calculated from other exponents through scaling relations by us, * — averaged over various p_d by us (weighted mean), • — not measured (fixed value or the one which gives best fits), ? — stated in the paper as an expression for the case where the dimension of the order parameter is $m > 1$, FSS — data analyzed with finite-size scaling, TS — data analyzed with temperature scaling, MC — Monte Carlo simulations, RG — Renormalization Group calculations, FFM — long-range correlated disorder generated with Fourier Filter Method, DL — long-range correlated disorder reached by using lines of disorder.

Type	Reference	a	ν	η	α	β	γ	ω	p_d	#p_d	max L	#L	N	N_c	Notes
					Pure Ising model										
MC	Ferrenberg et al. [FXL18]	∞	0.629 912(86)	0.036 10(45)‡	0.110 26(26)‡	0.326 30(22)	1.237 08(33)	0.83•			1024	17	$5\cdot 10^6$	$\leq 12\,000$	FSS
					Uncorrelated disorder										
	Ballesteros et al. [Bal+98a]	∞	0.6837(53)	0.0374(45)	$-0.051(16)$†	0.3546(28)†	1.342(10)†	0.37(6)	0.1–0.6	5	128	5	200	20 000	FSS
	Calabrese et al. [Cal+03]	∞	0.683(3)	0.035(2)	$-0.049(9)$†	0.3535(17)†	1.342(6)†	−	0.2	1	256	5	2000	$\approx 15\,000$	TS
MC	Berche et al. [Ber+04]	∞	0.68(2)	0.029(60)‡	$-0.04(6)$‡	0.35(1)	1.34(1)	−	0.3–0.6	3	96	14	2500	≤ 5000	FSS, TS
	Murtazaev et al. [MKB04]	∞	0.678(6)*	0.045(19)*,‡	$-0.0216(70)$*	0.3178(40)*	1.3258(40)*	−	0.05–0.4	4	60	11	$\approx 2\cdot 10^6$	≤ 80	FSS
	Hasenbusch et al. [Has+07]	∞	0.683(2)	0.036(1)	$-0.049(6)$†	0.354(1)†	1.341(4)†	0.33(3)	0.2, 0.35	2	192	10	≈ 500	$\approx 10^5$	FSS
	Pakhnin et al. [PS00]	∞	0.671(5)	0.025(10)	$-0.0125(80)$†	0.344(6)†	1.325(3)†	0.32(6)							5-loop ε-expansion
RG	Pelissetto et al. [PV00]	∞	0.678(10)	0.030(3)	$-0.034(30)$†	0.349(5)†	1.330(17)	0.25(10)							6-loop ε-expansion
	Kompaniets et al. [KKS21]	∞	0.675(19)	0.024(79)†	$-0.025(58)$†	0.346(34)†	1.334(38)	0.15(10)							6-loop $\sqrt{\varepsilon}$-expansion
					Correlated disorder										
	Ballesteros et al. [BP99]	2.0	1.012(16)	0.043(4)	$-1.036(48)$‡	0.528(34)‡	1.980(33)‡	1.01(13)	0.2, 0.35	2	128	5	100	$\leq 20\,000$	FSS, FFM, DL
MC	Prudnikov et al. [Pru+05]	2.0	0.71(1)	$-0.030(36)$‡	$-0.078(30)$	0.362(20)	1.441(15)	0.76(5)•	0.2	1	128	4	$\leq 10^5$	$\leq 15\,000$	FSS, DL
	Ivaneyko et al. [Iva+08]	2.0	0.958(4)	0.191(18)‡	$-0.789(3)$‡	0.528(3)	1.733(11)	0.8•	0.2	1	128	12	50 000	$\leq 10\,000$	FSS, FFM
RG	Weinrib et al. [WH83]	$a < d$	$2/a$	0?	$2(a-d)/a$?	$(d-2)/a$?,‡	$4/a$?	−							2-loop ε-δ-expansion
	Prudnikov et al. [PPF00]	3.0	0.6715	0.0327	-0.014‡	0.347‡	1.321‡	−							
		2.5	0.7046	0.0118	-0.114‡	0.3565†	1.4008†	−							
		2.0	0.715	-0.0205	-0.147‡	0.34‡	1.4456‡	−							scaling functions in 2-loop approximation

Methods

3

3.1 Monte Carlo method

The main part of this work is related to simulations of a physical system, e.g., the tree-dimensional Ising model in our case. Consider any statistical system with a Hamiltonian $\mathcal{H}$. For simplicity, we restrict ourselves to a calculation in the framework of the canonical ensemble introduced in Section 2.1. The main goal is to perform some sort of computations on a computer and calculate observables $\mathcal{O}$ of interest for the studied system at a temperature T. As was shown in Equation (2.7), we can calculate the expectation value of any observable $\mathcal{O}$ by summing over all possible states of the system,

$$\langle \mathcal{O} \rangle = \frac{1}{\mathcal{Z}} \sum_{\mu} \mathcal{O}_{\mu} e^{-E_{\mu}/(k_B T)} \,. \tag{3.1}$$

If one would have an infinite-power supercomputer, the only thing one would need to do would be to generate all possible states and apply Equation (3.1). Unfortunately, this fails due to the scaling of the number of possible states. As an example, the Ising model with only two possible states per site in three dimensions and on a small $10 \times 10 \times 10$ lattice has $2^{1000} \approx 10^{300}$ states. Just sampling through all possible states on the current largest supercomputer in the world, the Fungaku supercomputer [@Fun21], with 442 petaflops would need $\approx 10^{275}$ years.

The next approach would be to randomly pick some states i and stop after a certain number N of pickups. This approach is called random sampling. The approximation of the expectation value of the chosen observable $\mathcal{O}$ would then follow from Equation (3.1) and the definition of the partition function in Equation (2.2),

$$\langle \mathcal{O} \rangle \approx \frac{\sum_i^N \mathcal{O}_i e^{-E_i/(k_B T)}}{\sum_i^N e^{-E_i/(k_B T)}} \,. \tag{3.2}$$

In Equation (3.2), we have replaced the summation over all possible states with a summation over a sequence of observed (simulated) states. The random sampling is essentially equivalent to simulating at infinite temperature $T = \infty$ [Jan08, p. 97]. To hit a state which is typical at $T \ll \infty$ while being at $T = \infty$ is physically possible but practically it will never happen in real simulation runs. The random sampling will instead usually result in a tiny fraction of all possible states and will not be representative for the system at the desired temperature T. For the small Ising system with $10 \times 10 \times 10$ lattice we could go for one year on Fungaku and would reach $\approx 10^{25}$ samples. This is still a $1/10^{250}$ fraction. Therefore, the estimate through Equation (3.2) will hardly have any meaning at all since probably we will not hit any of the substantially contributing states for the given temperature T. This problem clearly calls for better ways.

In the following we will present one very common way to attack this problem, the **Monte Carlo method**. The Mote Carlo method tries to replicate an experimental approach on a computer and to go from one state of the system to the next as in a time direction [NB99, p. 21]. But instead of using random states, we will follow a specific prescription and try to mostly travel through states which contribute most to the sum in Equation (3.2) at the given temperature T. The process of moving from one state to the next can be described by a **Markov chain** and the prescription on how to select the next state will be the **importance sampling** in our case. We will address these two aspects below.

3.1.1 Markov chain and importance sampling

The Markov chain is a very broad topic and was applied and studied in many branches. For a very mathematical and detailed description we can recommend Refs. [Dou+18; Str14] while the basics also presented here are covered in, e.g., Refs. [LB05; NB99; Sad12; Sch02]. In this work we will stick to the needs of using a Markov chain to perform Monte Carlo simulations.

Consider a physical system at state μ_i and assume that it is an equilibrium state at a certain temperature T. Further, let p_μ denote the (equilibrium) probability density function of the states μ of the current system. This can be the Boltzmann distribution for the canonical ensemble, as introduced in Equation (2.4), but generally also any other choice. The goal is to transit to the next state μ_{i+1} with a certain probability $w_i = w(\mu_i \to \mu_{i+1})$. A condition which is imposed on the transition probability w_i is that it depends only on the previous state μ_i and the possible new state μ_{i+1} but not on the whole series of previous states. This makes the process very local in time. This process is then repeated many times producing a Markov chain,

$$... \xrightarrow{w_{i-1}} \mu_i \xrightarrow{w_i} \mu_{i+1} \xrightarrow{w_{i+1}} \mu_{i+2} \xrightarrow{w_{i+2}} ... \, , \tag{3.3}$$

So far, we have no relation between the probability density p_μ and the transition probabilities w. To ensure, that the sequence of the states indeed follows p_μ, the transition probabilities between two states μ and ν, $w(\mu \to \nu)$, have to fulfill three conditions [Jan08, p. 98]:

$$w(\mu \to \nu) \geq 0 \quad \text{for all } \mu, \nu, \tag{3.4}$$

$$\sum_\nu w(\mu \to \nu) = 1 \quad \text{for all } \mu, \tag{3.5}$$

$$\sum_\mu w(\mu \to \nu) p_\mu = p_\nu \quad \text{for all } \nu. \tag{3.6}$$

Equation (3.4) is a trivial restriction to positive or zero probabilities for each transition. Equation (3.5) ensures that the total probability of going from state μ to any other state is normalized to one. The most interesting condition is given in Equation (3.6). It implies that the probability distribution p_μ is an eigenvector of w [Jan08, p. 98]. It can be interpreted as a general balancing condition on w. However, in praxis, often the stricter **detailed balance** is imposed,

$$w(\mu \to \nu) p_\mu = w(\nu \to \mu) p_\nu \quad \text{for all } \mu, \nu. \tag{3.7}$$

Reading it as ratios [NB99, p. 39],

$$\frac{w(\mu \to \nu)}{w(\nu \to \mu)} = \frac{p_\nu}{p_\mu} \quad \text{for all } \mu, \nu, \tag{3.8}$$

immediately reveals the interpretation: transitioning from μ to ν in relation to the back-transition from ν to μ should reflect the ratio of the corresponding probabilities of the states ν and μ, respectively.

An additional requirement is that of **ergodicity**. We have to ensure that starting at any state μ we can reach any other state ν in a finite time [Jan08, p. 98],

$$\sum_{\eta_i, \eta_2, \dots \eta_n} w(\mu \to \eta_1) w(\eta_1 \to \eta_2) \cdot \dots \cdot w(\eta_n \to \nu) > 0 \quad \text{for} \ \ n < \infty \quad \text{for all} \ \ \mu, \nu, \quad (3.9)$$

i.e., there exists a finite realizable path from μ to ν for all possible starting states μ and final states ν. Assuming that all the above conditions are fulfilled for a certain system and the chosen p_μ, we can approximate the expectation values with a modified version of Equation (3.2) [NB99, p. 32],

$$\langle \mathscr{O} \rangle \approx \frac{\sum_i^N \mathscr{O}_i p_{\mu_i}^{-1} e^{-E_i/(k_B T)}}{\sum_i^N p_{\mu_i}^{-1} e^{-E_i/(k_B T)}} \ , \quad (3.10)$$

where we now have the probability densities at each state μ_i as inverse factors. By setting the probability to the Boltzmann distribution, $p_\mu = e^{-E_\mu/(k_B T)}$, Equation (3.10) simplifies to a simple average over the time series produced by going along a Markov chain of states of length N,

$$\boxed{\langle \mathscr{O} \rangle = \sum_\mu p_\mu \mathscr{O}_\mu \approx \overline{\mathscr{O}} = \frac{1}{N} \sum_i \mathscr{O}_i \ ,} \quad (3.11)$$

where $\mathscr{O}_i$ are the observables measured at the state μ_i in the chain. This process of selecting subsequent states which follow the distribution p_μ is called **importance sampling**. In opposite to the previously mentioned random sampling, a considerably smaller number of states is needed to have a sufficient representation of a system at a given temperature T. An important condition however, which we would like to repeat once again at this point is that the system has to be in equilibrium before we can apply Equation (3.11). This implies that any simulation starts with a certain equlibration procedure before the actual measurements can take place.

Equipped with a general prescription for the generation of relevant states and the corresponding estimator for the expectation values of observables, Equation (3.11), we can introduce different update algorithms for concrete systems. In the following, we will present two different update algorithms applied to the Ising model, which was introduced in Section 2.2.

3.1.2 Metropolis update

We begin with the famous and widely used Metropolis algorithm. It was first introduced by Metropolis et al. [Met+53] already about 70 years ago and became a fundament for many other algorithms. We have not used it in our work (because, as we will see later, there exists a much more efficient algorithm for the Ising Model), but it is an important step in understanding the simulation process and therefore we will briefly present it here. Probably the most important reason for the Metropolis algorithm being so popular is its generality. It can be applied to almost any system, including discrete or continuous time, short-range or long-range interactions, lattice or off-lattice models [Jan08, p. 99]. The trick around the

Metropolis algorithm is hidden in the detailed balance condition in Equation (3.8). This condition leaves a lot of freedom in choosing the transition probabilities as only their ratio has to be fulfilled. The general idea is to split the simulation into two steps. First, propose a change to the current system in the state μ to a new state ν. Second, accept this change with a certain probability or reject it and keep the system in the state μ. The procedure of derivation is simple but quite lengthy, and we refer to Ref. [NB99, pp. 46 ff.], where it is presented in great detail. Instead, we present the final algorithm applied to the Ising model [LB05, p. 71]:

Metropolis algorithm for the Ising model
1. intialize a lattice Λ with an equilibrium state
2. choose a random spin at site $x \in \Lambda$ and flip it

$$s_x \to -s_x \tag{3.12}$$

3. accept this change with probability p

$$p = \min\left(1, e^{-J\beta(E_\nu - E_\mu)}\right) \tag{3.13}$$

   if not accepted, undo the flip from step 2
4. go to step 2

In the algorithm description above we have left out the details of implementation and only presented the most important steps. An efficient algorithm can be written in such a way that neither the spin has to be physically flipped (changing it on the lattice Λ) before accepting or rejecting the flip nor has one to repeatedly calculate the exponential function in Equation (3.13). However, the presented formulation reflects the concept of a Metropolis updated in the best way. Equation (3.13) essentially means the following: accept the change when the energy of the new state ν is lower than that of the current state μ, otherwise accept the change with probability $e^{-\beta J(E_\nu - E_\mu)}$. This choice is what is the essential part of the Metropolis update introduced in Ref. [Met+53]. The choice of a site x where the spin is flipped in step 2 in the algorithm has not to be a random decision a priori. It is possible and in fact sometimes even better to do it systematically, like going through each site $x \in \Lambda$ sequentially. At this point two important definitions have to be made which will also be needed in the next algorithm. The proposal to flip one spin at site x in the Metropolis algorithm is called a **swap**. Performing V swaps, where V is the volume of the system, is called a **sweep**. If one tries to flip the spins sequentially, a sweep corresponds to trying to flip each spin of the lattice once.

As already mentioned, the Metropolis update can be used for very different systems due to its generality. However, it does have an important weakness coming from the locality of the update. As discussed in Section 2.3, close to the critical temperature the correlation length of the system diverges. This implies that any local updating algorithm will suffer from a phenomenon called **critical slowing down** [Jan08, p. 106]. This slowing down means that one has to perform many updates in order to get two uncorrelated states. Or in other

words, the correlation time of observables becomes very large. The general dependence has the form [Jan08, p. 107]

$$\tau_{\mathrm{exp}} \propto L^z \,, \tag{3.14}$$

where typically $z \approx 2$ and τ_{exp} is the exponential autocorrelation time. The value z is called **dynamical critical exponent**. The critical slowing down is the main reason why cluster updates are of such a big importance. One such cluster update algorithm will be presented next.

3.1.3 Swendesen-Wang multiple-cluster update

Let us present the multiple-cluster update scheme which was used in this work. It was introduced by Swendsen and Wang [SW87] in 1987 and is applicable to different spin models, e.g., Ising model, XY-model and Heisenberg model. The general idea consists of two steps. First, divide the whole lattice Λ into clusters. A cluster is a set of connected sites on the lattice. Second, randomly set all sites belonging to the same cluster to a new spin value for each cluster. The main difficulty in creating a cluster update scheme is to satisfy the detailed balance, Equation (3.8).

The naive approach is to combine all sites which have the same spin orientation and which are connected, i.e., are direct neighbors on the lattice. Such clusters are called **geometric clusters**. The process is best described in terms of bonds between sites. A bond B_{xy} is the connection between two next-neighboring sites x and y. We first go through all sites x of the lattice Λ and check each bond B_{xy} where y are next-neighbors of x, denoted by $y \in \langle xy \rangle$, and we check each bond only once, which we symbolically denote with $x < y$ for simplicity[1]. So, the prescription reads

$$B_{xy} = \begin{cases} 1 & \text{if } s_x = s_y \\ 0 & \text{otherwise} \end{cases} \quad \text{for all } x \in \Lambda, y \in \langle xy \rangle \text{ and } x < y \,. \tag{3.15}$$

Now, we identify all clusters C_i on the lattice Λ as sites connected by active bonds, $B_{xy} = 1$. See Figure 3.1 for a visual representation. This can be done, e.g., with an efficient cluster-search algorithm called **Hoshen-Kopelman algorithm** [HK76]. We will not discuss this algorithm here, but our implementation can be found in Appendix A.4. However, it turns out that such clusters do not satisfy detailed balance and hence cannot be used in a cluster update algorithm.

The trick of Swendsen and Wang was to introduce a probability according to which two sites which are next to each and share the same orientation really belong to the same cluster. The clusters which are build with this rule are called **stochastic clusters**. Let us write down the multiple-cluster update algorithm [LB05, p. 139]:

---

[1]   More precise, we have to check each component of the coordinates of x and y: $x_i < y_i$ for all $i \in 1, \ldots, d$ and afterwards also apply the boundary conditions properly, e.g., in case of periodic boundary conditions, we have to transform $y_i \to 1$ if $y_i = L + 1$ after the comparison was done.

Swendensen-Wang multiple-cluster update algorithm

1. intialize a lattice Λ
2. generate bonds B_{xy} for all sites of the lattice, $x \in \Lambda$, $y \in \langle xy \rangle$ and $x < y$

$$B_{xy} = \begin{cases} 1 & \text{if } s_x = s_y \\ 0 & \text{otherwise} \end{cases} \quad \text{with } \wp = 1 - e^{-2\beta J} \tag{3.16}$$

   where $\wp$ is the **activation probability**
3. identify all clusters C_i
4. chose a new random spin state S_i for each cluster C_i
5. apply this new state to each site of each cluster

$$s_x = S_i \quad \text{for all } s_x \in C_i \quad \text{for all } i \tag{3.17}$$

6. go to step 2

The identification of the clusters can again be done with the Hoshen-Kopelman algorithm. From the comparison between Equation (3.16) and Equation (3.15) we immediately see that the stochastic clusters are smaller than the geometric ones. Only for the limit of $\beta \to \infty$ both definitions coincide. This is visually shown in Figure 3.1. The form of the probability $\wp$ in Equation (3.16) is derived by rewriting the partition function of the Ising model. Lest us start with Equation (2.2) applied to the Ising model without an external magnetic field ($h = 0$), Equation (2.25) [Jan08, p. 108],

$$\mathscr{Z} = \sum_\mu e^{-\beta E_\mu} \tag{3.18a}$$

$$= \sum_\mu e^{\beta J \sum_{\langle xy \rangle} s_x s_y} \tag{3.18b}$$

$$= \sum_\mu \prod_{\langle xy \rangle} e^{\beta J} \left((1 - \wp) + \wp \delta(s_x, s_y) \right) \tag{3.18c}$$

$$= \sum_\mu \sum_{B_{xy}} \prod_{\langle xy \rangle} e^{\beta J} \left((1 - \wp)\delta(B_{xy}, 0) + \wp \delta(s_x, s_y)\delta(B_{xy}, 1) \right) , \tag{3.18d}$$

where we used the fact that the spins s_x can only have values ± 1 and δ is the Kronecker delta. From Equation (3.18), we can solve for $\wp$ and arrive at the probability used in Equation (3.16).

The next observation is that in the Swendesen-Wang multiple-cluster update algorithm all spins of the lattice are touched on each iteration step. Therefore, one iteration directly corresponds to a Metropolis sweep defined previously. This makes it very easy to compare the effectiveness in terms of sweeps between these two algorithms. When considering the previously mentioned critical slowing-down of the system, it is known that the dynamical critical exponent drops to $z = 0$ for the two-dimensional Ising model [LB05, p. 138] and has a value $z \approx 0.5$ for the tree-dimensional Ising model [Wan90]. Thus, this algorithm reaches uncorrelated states much faster than the Metropolis algorithm. Our implementation of the Swendsen-Wang algorithm for the Ising model can be found in Appendix A.4.

Finally, we would like to mention, that there is another widely used cluster update algorithm for the Ising model: the Wolff single-cluster update algorithm [Wol89]. It uses the same definition of bonds activation as in Equation (3.16), but instead of dividing the whole lattice into clusters at each iteration step, only one stochastic cluster starting at a random

(a) Spin configuration.   (b) Geometric clusters.

(c) $\beta = 0.1$.   (d) $\beta = 0.3$.   (e) $\beta = \beta_c$.   (f) $\beta = 0.5$.   (g) $\beta = 1.0$.
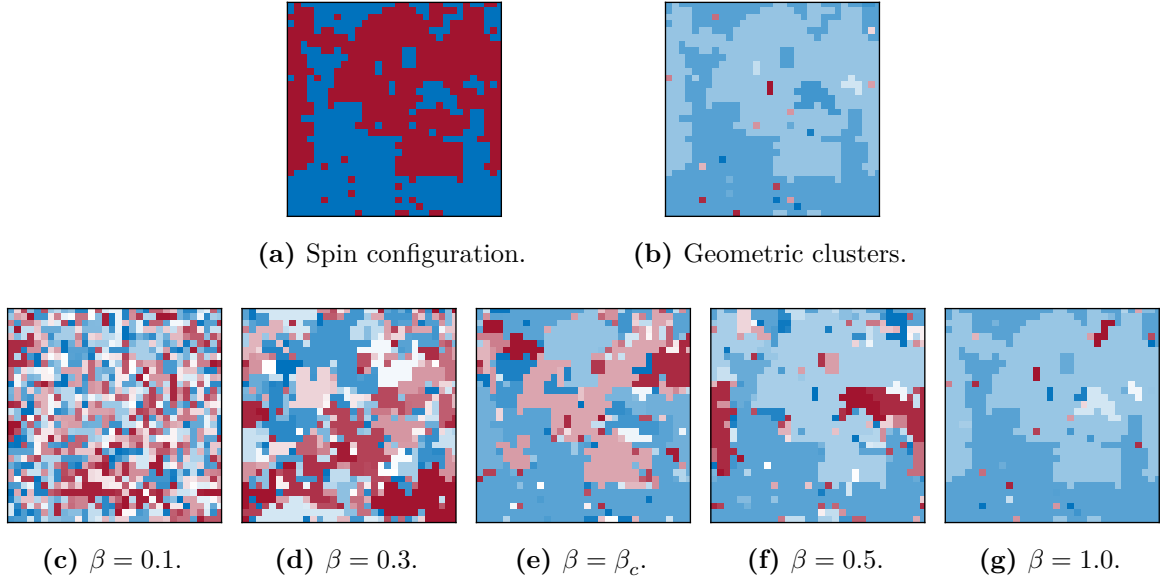
Figure 3.1: Comparison between geometric and stochastic clusters at different temperatures for a two-dimensional Ising model with $L = 32$. The bottom row shows the stochastic clusters as they are identified at different temperatures β. The initial spin configuration is taken from a simulation at $\beta = \beta_c$. Different colors represent different clusters. However, there is no direct interpretation of the color itself. One can see, that for larger β values the stochastic clusters approach the geometric clusters.

site is generated in each step. Therefore, the algorithm is a single-cluster update algorithm. It is known that it works even more efficiently in the case of the tree-dimensional pure Ising model. However, since our model is a disordered Ising model, we expect the multiple-cluster update variant to be more efficient. We expect, that the size of an average stochastic cluster is smaller due to the present disorder on the lattice. Therefore, updating one cluster at a time will generally be a slower update than in the pure case. On the other hand, dividing the whole lattice into individual clusters and update all of them at once does not depend on the disorder because the whole lattice is considered at each step anyway.

Summary. We introduced the Monte Carlo method for effectively simulating physical systems with importance sampling. Applied to the Ising model, we discussed the Metropolis algorithm and explained the Swendsen-Wang multiple-cluster update algorithm which was used in this work.

3.2 Finite-size scaling

In Section 2.3.4 we derived the scaling law, Equation (2.77), for an infinite system which allowed us to establish the scaling relations between different critical exponents. However, as already mentioned several times, in a simulation we are restricted to finite systems. To obtain similar results as in Section 2.3.4 but for the case of a finite lattice size, we will basically repeat the steps for the derivation of the scaling law in the infinite case but for a hypercubic lattice Λ with linear extension $L < \infty$ and dimension d and follow Ref. [NO10, pp. 76 ff.]. In order to be at the critical point, the system has to be at $t = h = 0$ for $L \to \infty$. But now additionally, we have $L < \infty$ and hence we impose that the condition $L^{-1} \to 0$ has to be

fulfilled as well. We take the L^{-1} as a third argument into the definition of the free energy and write the relation between the original free energy and the free energy after applying a Renormalization Group transformation R_b,

$$\mathscr{F}(t, h, L^{-1}) = b^{-d}\mathscr{F}(b^{y_t}t, b^{y_h}h, bL^{-1}). \tag{3.19}$$

From Equation (3.19) we see that the scaling exponent of the lattice size L is $y_L = 1$. This is an analogue equation to the scaling law in Equation (2.77) for the finite lattice. We can calculate the observables by calculating the derivate of the free energy. Let us do this for the susceptibility χ. The susceptibility is the second derivative of the free energy $\mathscr{F}$ with respect to the magnetic field, Equation (3.21), so we get

$$\chi(t, 0, L^{-1}) = b^{2y_h - d} \left.\frac{\partial^2 \mathscr{F}(b^{y_t}t, b^{y_h}h, bL^{-1})}{\partial h^2}\right|_{h=0}. \tag{3.20}$$

We can choose $b = L$ and get

$$\chi(t, 0, L^{-1}) = L^{2y_h - d} \left.\frac{\partial^2 \mathscr{F}(b^{y_t}t, b^{y_h}h, 1)}{\partial h^2}\right|_{h=0}. \tag{3.21}$$

Finally, after using $y_t = 1/\nu$, Equation (2.85), and $2y_h - d = \gamma/\nu$, Equation (2.79), we get

$$\chi(t, L^{-1}) = L^{\gamma/\nu}\chi_0(tL^{1/\nu}), \tag{3.22}$$

where χ_0 is the scaling function (analytic for finite L). The very first observation which we can make by studying Equation (3.22) is that the susceptibility $\chi(L)$ remains finite for finite L. Further, the height of the peak of $\chi(L)$ is proportional to $L^{\gamma/\nu}$. The position of the peak is the same as of the scaling function χ_0. It will be different from $t = 0$ if it is not zero for χ_0. If the position of the peak of χ_0 is at $t = t_c \neq 0$, then the peak position of the peak of χ will be $t = t_c L^{-1/\nu}$. Schematically, the behavior of the susceptibility in dependence of the temperature and the lattice size L is shown in Figure 3.2.
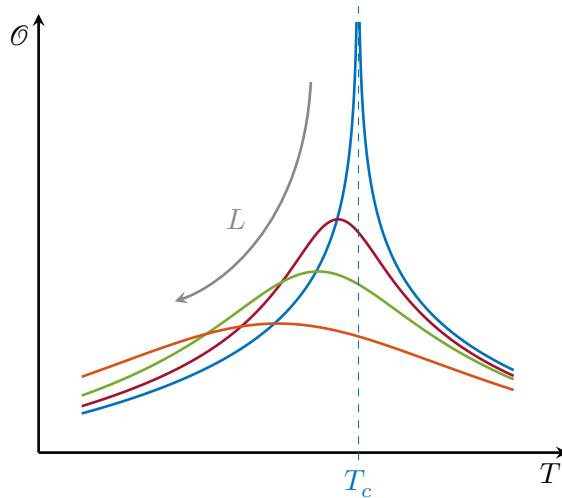
Figure 3.2: Schematic representation of the finite-size scaling behavior of the susceptibility χ, which diverges at critical temperature in the thermodynamic limit. For finite lattice sizes L the divergence becomes finite, its peak is shifted along the temperature axis and the height increases with increasing L.

Equation (3.22) provides a very convenient method of obtaining the critical exponents and critical temperature from observables measured on finite systems. Consider that $\hat{\chi}(L)$ in the maximum of the susceptibility $\chi(\beta, L)$ for a given lattice size L and $\hat{\beta}$ is the corresponding temperature at which this peak occurs. By using Taylor expansion of the scaling function around $t = 0$ in Equation (3.22), we can write the scaling relation for the susceptibility as [Jan08, p. 115]

$$\hat{\chi}(L) = AL^{\gamma/\nu} \left(1 + BL^{-\omega} + ...\right) , \tag{3.23}$$

where A and B are constant factors and ω is the so-called **confluent correction exponent**. The dots represent higher order correction terms with exponents -2ω, -3ω, and so on. Similarly, we can derive relations for other observables of interest, namely,

$$\hat{c}(L) = c_{\text{reg}} + AL^{\alpha/\nu} \left(1 + BL^{-\omega} + ...\right) , \tag{3.24}$$

$$\widehat{\partial_\beta(|m|)}(L) = AL^{(1-\beta)/\nu} \left(1 + BL^{-\omega} + ...\right) , \tag{3.25}$$

$$\widehat{\partial_\beta(\ln|m|)}(L) = AL^{1/\nu} \left(1 + BL^{-\omega} + ...\right) . \tag{3.26}$$

Note, that the factors A and B will be different for each observable, but we left out an additional index to improve readability. Additionally, it can be shown that the temperatures $\hat{\beta}$ at which the various observables $\mathcal{O}$ have their peaks can be used to calculate the critical temperature β_c at $L \to \infty$. Their scaling relation reads [LB05, p. 80]

$$\hat{\beta}(L) = \beta_c + AL^{-1/\nu} \left(1 + BL^{-\omega} + ...\right) . \tag{3.27}$$

Again, the factors A and B will be different for each $\mathcal{O}$. Two important practical conclusions can be drawn from the Equations (3.23) to (3.27):

1. the peaks of observables $\mathcal{O}(\beta, L)$ have to be found to successively apply finite-size scaling ansatz,

2. the critical exponent of the correlation length ν is crucial in order to get the other exponents and not only the ratios, e.g., γ/ν.

These two aspects were essential guides for planing and performing simulations for the present work. We would like to note that one can get the finite-size scaling relations, Equations (3.23) to (3.27), by going through another derivation. On a finite lattice, the correlation length ξ can only grow up to the size of L. Hence, at critical temperature, we can formally "replace" the diverging correlation length by L and set [Jan08, p. 84]

$$t \propto \xi^{-1/\nu} \to L^{-1/\nu} . \tag{3.28}$$

By inserting Equation (3.28) into the free energy and performing derivations in order to obtain the different observables, the very same scaling relations can be recovered. This approach is a good way to understand how the finite size of the system influences the behavior of the system and why the critical exponent of the correlation length ν enters the scaling relations.

Summary. We introduced the main analysis concept which was used in this work, i.e., the finite-size scaling method. The finite-size scaling method derives the scaling relations for different observables in dependence of the system size L. By finding the peaks of different observables for various L, one can get the critical exponents of the system.

3.3 Histogram reweighting technique

One of the key tools used in our analyses of the simulated data was the single histogram reweighting technique. In the form which we have used and which we present here, it was first used by Ferrenberg and Swendsen [FS88]. The idea of the method is quite simple. Recall the fundamental formula for calculating observables from time series measured in a Monte Carlo simulation, Equation (3.10),

$$\overline{\mathcal{O}} = \frac{\sum_i^N \mathcal{O}_i \, \mathcal{p}_{\mu_i}^{-1} e^{-\beta E_i}}{\sum_i^N \mathcal{p}_{\mu_i}^{-1} e^{-\beta E_i}} \, , \tag{3.29}$$

Where $\overline{\mathcal{O}}$ is the estimator of the expectation value $\langle \mathcal{O} \rangle$. Our previous choice was to set the probability distribution $\mathcal{p}_\mu$ to be the Boltzmann distribution at β. However, we can also use any other distribution. Let us take the Boltzmann distribution at another temperature β_0, $\mathcal{p}_\mu = e^{-\beta_0 E_\mu}$. Inserting this into Equation (3.29), we get the fundamental equation for the histogram reweighting technique,

$$\overline{\mathcal{O}}(\beta) = \frac{\sum_i^N \mathcal{O}_i e^{-(\beta-\beta_0)E_i}}{\sum_i^N e^{-(\beta-\beta_0)E_i}} \, . \tag{3.30}$$

Reading Equation (3.30) carefully, we immediately see that we are now able to measure a series of an observable $\mathcal{O}$ at a certain temperature β_0 and then get an estimate of $\mathcal{O}$ at another temperature β. Let us define the function $\mathrm{Rew}(\mathcal{O})(\beta)$, which we will use later in our analyses,

$$\overline{\mathcal{O}}(\beta) = \mathrm{Rew}(\mathcal{O})(\beta) = \frac{\sum_i^N \mathcal{O}_i(\beta_0) e^{-(\beta-\beta_0)E(\beta_0)_i}}{\sum_i^N e^{-(\beta-\beta_0)E(\beta_0)_i}} \, , \tag{3.31}$$

where we have explicitly written down the dependence of the energies $E(\beta_0)_i$ and the observable $\mathcal{O}(\beta_0)_i$ on the simulated temperature β_0. We can use Equation (3.31) for all observables which are directly measurable as time series during the simulation, e.g., moments of the form $\langle E^k M^l \rangle$. Given an infinite series $N \to \infty$, we are done by now. Simulation at one temperature β_0 would provide us estimates for any other temperature β. However, as the series are rather small, the question arises, how far from β_0 can the temperature β be chosen in order to still provide meaningful results without the errors becoming too large.

To derive the estimation for the range where the histogram reweighting technique works, let us first take the energy as our observable, $\mathcal{O} = E$. The Equation (3.31) can then be rewritten as [NB99, p. 213]

$$\mathrm{Rew}(E)(\beta) = \frac{\sum_E E \mathscr{P}_{\beta_0}(E) e^{-(\beta-\beta_0)E}}{\sum_E \mathscr{P}_{\beta_0}(E) e^{-(\beta-\beta_0)E}} \, , \tag{3.32}$$

where we replaced the summation over the time series with a summation over all occurring energies E and $\mathscr{P}_{\beta_0}(E)$ is the number of occurrences of each energy E, i.e., the energy histogram. Here the name "histogram reweighting technique" gets its origin. We take the energy histogram at one temperature β_0 and shift it with exponential factors to another temperature β. This was the formulation originally used in Ref. [FS88]. But beside being the reason for the name, the formulation in Equation (3.32) also reveals another useful insight. We get a

feeling of how far we can go from original temperature by analyzing the original histogram $\mathscr{P}_{\beta_0}$ and the reweighted histogram $\mathscr{P}_\beta$, which is given by

$$\mathscr{P}_\beta(E) = \frac{\mathscr{P}_{\beta_0}(E)e^{-(\beta-\beta_0)E}}{\sum_E \mathscr{P}_{\beta_0}(E)e^{-(\beta-\beta_0)E}}\,, \tag{3.33}$$

and which can be used to rewrite Equation (3.32) as a weighted average [NB99, p. 214],

$$\mathrm{Rew}(E)(\beta) = \sum_E E\mathscr{P}_\beta(E)\,. \tag{3.34}$$

We impose the condition that the peak of the reweighted histogram should lie within the width of the original histogram $\sigma(\mathscr{P}_{\beta_0})$ [Jan08, p. 110],

$$|\mathrm{Rew}(E)(\beta) - \langle E\rangle(\beta_0)| \le \sigma(\mathscr{P}_{\beta_0})\,. \tag{3.35}$$

In Equation (3.35) we assumed that for a not too asymmetrical histograms $\mathscr{P}_{\beta_0}(E)$ and $\mathscr{P}_\beta(E)$ the peaks of the histograms coincide with the corresponding expectation values of the energy, i.e., $\langle E\rangle(\beta_0) \approx \hat{E}$ with $\mathscr{P}_{\beta_0}(\hat{E}) = \max_E \mathscr{P}_{\beta_0}(E)$ and $\mathrm{Rew}(E)(\beta) \approx \hat{E}'$ with $\mathscr{P}_\beta(\hat{E}') = \max_E \mathscr{P}_\beta(E)$, respectively. The histogram width is the standard deviation of the energy at β_0 and reads

$$\sigma(\mathscr{P}_{\beta_0}) = \sqrt{\langle E^2\rangle - \langle E\rangle^2}\,. \tag{3.36}$$

Further, the energy expectation at β, $\mathrm{Rew}(E)(\beta)$ on the left-hand side of Equation (3.35), can be expressed by a Taylor expansion as

$$\mathrm{Rew}(E)(\beta) = \langle E\rangle(\beta_0) + \left.\frac{\partial\langle E\rangle(\beta)}{\partial\beta}\right|_{\beta_0}(\beta-\beta_0) + \ldots\,. \tag{3.37}$$

Finally, using the derivative with respect to β defined in Equation (2.23), and inserting Equations (3.36) and (3.37) into Equation (3.35), we arrive at

$$\boxed{\Delta\beta_{\mathrm{rew}} = |\beta-\beta_0| \le \frac{1}{\sqrt{\langle E^2\rangle - \langle E\rangle^2}}\,,} \tag{3.38}$$

where we defined the reweighting range quantity $\Delta\beta_{\mathrm{rew}}$. The derivation used the histogram of the energy $\mathscr{P}_{\beta_0}(E)$ but is a general result for reweighting different observables with Equation (3.31). Additionally, the histogram was needed for the derivation but is not used in the actual calculation of $\mathrm{Rew}(\mathscr{O})(\beta)$ and $\Delta\beta_{\mathrm{rew}}$. This estimate in Equation (3.38) is a rather conservative estimate for the range where the histogram reweighting works [NB99, p. 216]. It is not unusual to get good results in the range $\pm 2\Delta\beta_{\mathrm{rew}}$ or even larger. In particular, the reweighting quantity naturally depends on the length of the series N which is not taken into account in $\Delta\beta_{\mathrm{rew}}$. Anyway, it is advisable to visually check the reweighting curves $\mathrm{Rew}(\mathscr{O})(\beta)$ to make sure nothing unexpected happens.

Finally, we would like to mention an advanced method, called **multiple histogram reweighting technique** [NB99, pp. 219 ff.]. As the name suggests, this approach combines data from various simulated temperatures β_i and then reweight them to another temperature β. Although, the idea is very similar, the actual technical realization is much more involved. First, one has to reweight the data from each temperature β_i to a common temperature

β_0 and then reweight once again to β. Moreover, as we have seen in the derivation of the reweighting range $\Delta\beta_{\mathrm{rew}}$, we cannot simply use any β_i equally because they will have different distance to β and hence will provide different qualities of the reweighting procedure. One needs a sophisticated ansatz to weight the data from different temperatures in the final estimate which is done by a recursive search of free energies at different temperatures β_i. Also, a large enough overlapping of the histograms at different β_i has to be ensured. Contrary, the ansatz in Equation (3.31) does work without any additional calculations and without errors coming from approximations of the weights. Therefore, although we have simulated at many temperatures, we only used th single histogram reweighting technique in this work.

Summary. We have shown how to apply the single histogram reweighting technique to get estimates of observables at a temperature β by using data from a simulation at another temperature β_0. By using this technique, we can estimate peaks of observables very precise in our later analyses.

3.4 Resampling techniques

We introduced many observables in Section 2.2.3. Some direct observables, e.g., energy and magnetization are measured as a time series during the simulation process. One easily calculates their mean and also the corresponding errors from these series. At least in case that each measurement is uncorrelated from the previous one. However, many observables are composed of means of the energy and magnetization, e.g., the susceptibility χ and the specific heat c. For this kind of observables, we still can calculate the means straight forward but estimating the errors is a more difficult task. The simplest solution is of course use the error propagation rules, e.g., for the specific heat one would get

$$c = \frac{\beta^2}{V}\left(\langle E^2\rangle - \langle E\rangle^2\right), \tag{3.39}$$

$$\sigma^2(c) = \frac{\beta^2}{V}\left(\sigma^2(E^2) + 2\langle E\rangle\sigma^2(E)\right), \tag{3.40}$$

$$\epsilon(c) = \sqrt{\frac{\sigma^2(c)}{N}}. \tag{3.41}$$

In Equation (3.41) we use the available variances of $\langle E^2\rangle$ and $\langle E\rangle$. However, since these two observables are correlated in general, this ansatz will produce errors which will be way too large. This will be the case for practically any composed observable, and so we have to find a better way of getting the error estimates from the available data. The simplest solution is to repeat the simulation many times, calculate an observable of interest each time and finally take the average over all calculated means and calculate the corresponding error. In a world with infinite computation time this would be the final solution. Until this happens, let us discuss more efficient ways.

An easy approach is to take the whole data series with N measurements and split this series into several smaller blocks. This approach is called the **binning analysis** [Jan08, p. 106]. It allows us to calculate a mean of an observable for each block and finally obtain the average value and its error. The main problem with this approach is that each block will have a much smaller length and thus the estimates for each block will fluctuate a lot. This may not

be a problem for simple cases, but, e.g., in the case of applying the histogram reweighting techniques to these subsets would be difficult. We will not discuss the details here, since we have not used this approach in our work.

3.4.1 Jackknife resampling technique

A similar but much more common approach is the **jackknife resampling**. Instead of considering one block at a time, on instead leaves out one block at a time while keeping the majority of the data. This produces much larger individual data blocks at each step and thus leads to more stable calculations. A very detailed mathematical description of the jackknife method can be found in Ref. [ST95]. We will follow a more basic one, presented in Ref. [ET93, pp. 141 ff.].

Assume we have a vector $\boldsymbol{x}$ with a series of measurements x_i. Our goal is to calculate an estimate $y = f(\boldsymbol{x})$ and its error $\epsilon(y)$ where f takes a vector $\boldsymbol{x}$ and returns a scalar value. This can be, e.g., the averaging function,

$$f(\boldsymbol{x}) = \frac{1}{N}\sum_i x_i \,, \tag{3.42}$$

but also a more involved function, e.g., the second moment

$$f(\boldsymbol{x}) = \frac{1}{N}\sum_i x_i^2 \,. \tag{3.43}$$

where the total length of $\boldsymbol{x}$ is N. In the next step we split the vector $\boldsymbol{x}$ into jackknife blocks $\boldsymbol{x}^j$ with $j = 1, \dots, B$ by sequentially leaving out a portion of the data. The length of the removed block should be N_B and the number of the totally considered jackknife blocks will be denoted by B. Ideally, we have $N = BN_B$, otherwise one has to reject a few measurements and reduce N such that the B blocks of length N_B fit perfectly into the new total length. The exact form of a jackknife block $\boldsymbol{x}^j$ is

$$\boldsymbol{x}^j = \{x_i \quad \text{for all } i \in \{1, \dots, N\} \text{ with } i \notin \{(j-1)N_B + 1, \dots, jN_B\}\}\,. \tag{3.44}$$

Please note the difference between the lower index in x_i which is the i-th component of the vector and $\boldsymbol{x}^j$ which is the j-th jackknife block, i.e., a vector where a portion of the data was removed. Schematically, such blocks are shown in Figure 3.3.
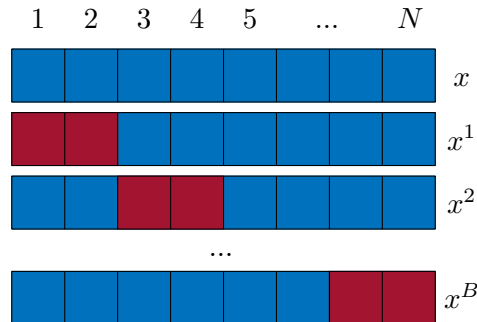
Figure 3.3: Graphical representation of the jackknife blocks $\boldsymbol{x}^j$. Each removed block (red) has the same length N_B and there are B blocks.

We now calculate the function f for each jackknife block $\boldsymbol{x}^j$,

$$y^j = f(\boldsymbol{x}^j) \quad \text{with } j = 1, \dots, B\,. \tag{3.45}$$

Finally, we are interested in the mean and the error of y. The mean is simply the mean over y^j,

$$y^J = \frac{1}{B} \sum_j^B y^j \,, \tag{3.46}$$

where for the moment we have added the index J to distinguish between the jackknifed mean and the value calculated from the whole vector directly, i.e., $y = f(\boldsymbol{x})$. We define the bias between y and y^J [ET93, p. 141]

$$\mathrm{bias}(y) = (B-1)\left(y^J - y\right) \,, \tag{3.47}$$

At this point we want to stress out that for a general f, the bias(y) does not vanish and by applying the jackknife resampling technique one gets an estimator of this bias. However, for the simple case of an average, Equation (3.42), the bias is zero. Last but not least, the error of the estimate y^J can be calculated by using [ET93, p. 141]

$$\epsilon(y^J) = \sqrt{\frac{B-1}{B}\left(\sum_j^B (y^j - y^J)^2\right)} \,. \tag{3.48}$$

In Equations (3.47) and (3.48) the factor $B-1$ reflect the fact that we reuse each data point x_i exactly this many times. Note, that Equation (3.48) is already the error of the mean and not the standard deviation.

3.4.2 Bootstrap resampling technique

As it turns out, the jackknife resampling technique is an approximation of another, more general resampling approach, the **bootstrap resampling technique** [ET93, p. 145]. The main idea of the bootstrap resampling is the same: take subsamples out of the available data and calculate the desired quantity for these subsamples. However, in this case we draw N data points with possible repetitions at each resampling iteration. This process is repeated many times and then the means and errors are estimated from this statistic similarly as in the previous jackknife resampling case. We will not discuss the whole procedure here, since we have not used the bootstrap resampling technique in this work in this form. For more information, we can recommend Ref. [ET93] which is a complete book on bootstrap with a chapter on jackknife resampling as well. Still, we wanted to at least mention this technique in this work for two reasons. First, it is more general than the jackknife resampling. Second, in this work we used a similar approach at one instance in Section 4.5.5. But instead drawing from a vector of data points, we drew from a normal distribution and repeated the fit procedure many times for these normally distributed random values. We will refer to this technique as bootstrap as well, so please do not be confused. Further, at the appropriate place we will give some more detailed information on how exactly we proceeded in this case.

Summary. We explained how the jackknife resampling technique can be used to obtain means and errors of observables which cannot be directly measured at each simulation step but rather are means over the whole simulation which makes error estimation without resampling very difficult.

3.5 Generation of the correlated disorder with Fourier Filter Method

In this section we will present the method used for the generation of the long-range correlated site disorder on the lattice. The method is called **Fourier Filter Method** and was originally introduced by Makse et al. [Mak+95; Mak+96]. The main idea of the method is simple: we start with uncorrelated random variables in k-space and modify them in such a way that after transforming them to back x-space, they have a certain spatial correlation. We used a slightly modified version of the original method as described in [Zie+17], and we will follow this work in the description below. We also note that the implementation code published in [Zie+17] was used for this work. The whole process can be split into following steps [KJ20]:

1. Generate uncorrelated complex random variables in k-space where the real and imaginary parts are each drawn from a normal distribution.
2. Introduce the desired correlations in x-space by multiplying these variables with the square root of the spectral density of the chosen correlation function C (adapted to lattice periodicity).
3. Fourier-transform the variables in k-space back to x-space. The real and imaginary parts of these continuous variables are two independent sets of spatially correlated Gaussian variables with correlation function C.
4. Map each set of the continuous correlated variables to $\{0, 1\}$ by using a threshold which ensures the correct average concentration of defects (zeros). The resulting discrete variables are approximately correlated with C.

Let us discuss the individual steps in more detail. We start with the description of the continuous random variables generation (steps 1–3).

3.5.1 Generating long-range correlated continuous random variables

Let $C(r)$ be an (almost) arbitrary correlation function. The only important condition is that we have to avoid a singularity at $r = 0$. We will work on a hyper-cubic lattice Λ of dimension d with linear extension L in each direction and with periodic boundary conditions. The goal is to provide random variables $\tau(\boldsymbol{x})$ for all lattice coordinates $\boldsymbol{x}$ such that

$$\langle \tau(\boldsymbol{x})\tau(\boldsymbol{x}+\boldsymbol{r}) \rangle = C(d_{\mathrm{bc}}(\boldsymbol{x}, \boldsymbol{x}+\boldsymbol{r})) = C(r) \,, \tag{3.49}$$

where $r = |\boldsymbol{r}| = d_{\mathrm{bc}}(\boldsymbol{x}, \boldsymbol{x}+\boldsymbol{r})$ and $d_{\mathrm{bc}}(\boldsymbol{x}, \boldsymbol{x}+\boldsymbol{r})$ is the Euclidean distance between sites $\boldsymbol{x}$ and $\boldsymbol{x}+\boldsymbol{r}$ on a lattice with periodic boundary conditions. The distance is defined by

$$d_{\mathrm{bc}}(\boldsymbol{x}, \boldsymbol{y}) = \left(\sum_{i=1}^{d} \min\left(|y_i - x_i|, L - |y_i - x_i| - 1\right)^2 \right)^{\frac{1}{2}} \,, \tag{3.50}$$

where we assume that all components of $\boldsymbol{x}$ and $\boldsymbol{y}$ lie in the ranges $0 \leq x_i \leq L - 1$ and $0 \leq y_i \leq L - 1$, respectively.

We start by defining $C(\boldsymbol{r})$ for $\boldsymbol{r} \in \Lambda$,

$$C(\boldsymbol{r}) = C(d_{\mathrm{bc}}(\boldsymbol{x}_0, \boldsymbol{x}_0 + \boldsymbol{r})) \,, \tag{3.51}$$

where we chose an arbitrary reference site $\boldsymbol{x}_0$. We will set $\boldsymbol{x}_0 = (0, 0, \dots, 0)^T$. Through the definition of d_{bc} in Equation (3.50), we see that $C(\boldsymbol{r})$ will be symmetric around $\boldsymbol{x}_0$.

In the next step we calculate the spectral density of $C(\boldsymbol{r})$ by performing a discrete Fourier transform. We use the following definitions of the transform and its inverse adopted to a lattice with linear extension L,

$$z(\boldsymbol{k}) = \mathrm{DFT}(z(\boldsymbol{x})) = \sum_{\boldsymbol{x}} z(\boldsymbol{x}) e^{-2\pi \mathrm{i}\, \boldsymbol{x}\boldsymbol{k}/L} \,, \tag{3.52}$$

$$z(\boldsymbol{x}) = \mathrm{DFT}^{-1}(z(\boldsymbol{k})) = \frac{1}{V} \sum_{\boldsymbol{k}} z(\boldsymbol{k}) e^{2\pi \mathrm{i}\, \boldsymbol{x}\boldsymbol{k}/L} \,, \tag{3.53}$$

where $V = L^d$ and the sum $\sum_{\boldsymbol{y}}$ with $\boldsymbol{y} = \boldsymbol{x}$ or $\boldsymbol{y} = \boldsymbol{k}$ runs over all possible $\boldsymbol{y}$ with $0 \leq y_i \leq L-1$. We calculate the spectral density $S(\boldsymbol{k})$ of $C(\boldsymbol{r})$,

$$S(\boldsymbol{k}) = \mathrm{DFT}(C(\boldsymbol{r})) = \sum_{\boldsymbol{x}} C(\boldsymbol{x}) e^{-2\pi \mathrm{i}\, \boldsymbol{x}\boldsymbol{k}/L} \,. \tag{3.54}$$

Equipped with $S(\boldsymbol{k})$, we produce a set of continuous complex variables

$$\varphi(\boldsymbol{k}) = \sqrt{S(\boldsymbol{k})}\,(R_1(\boldsymbol{k}) + \mathrm{i}R_2(\boldsymbol{k})) \,, \tag{3.55}$$

where R_i are normally distributed real random numbers with

$$R_i \sim \mathcal{N}\!\left(0, \sigma_R^2\right) \,. \tag{3.56}$$

Transforming the variables $\varphi(\boldsymbol{k})$ back to x-space by performing the inverse Fourier transform yields

$$\boxed{\varphi(\boldsymbol{x}) = \mathrm{DFT}^{-1}(\varphi(\boldsymbol{k}))\,.} \tag{3.57}$$

This is the key equation for the generation of the long-range correlated variables $\tau(\boldsymbol{x})$. The real and imaginary parts of $\varphi(\boldsymbol{x})$ have following properties.

1. The $\mathrm{Re}\,\varphi(\boldsymbol{x})$ and $\mathrm{Im}\,\varphi(\boldsymbol{x})$ are normally distributed with

$$\mathrm{Re}\,\varphi(\boldsymbol{x}) \sim \mathrm{Im}\,\varphi(\boldsymbol{x}) \sim \mathcal{N}\!\left(0, \sigma_R^2/V\right) \,. \tag{3.58}$$

2. The $\mathrm{Re}\,\varphi(\boldsymbol{x})$ and $\mathrm{Im}\,\varphi(\boldsymbol{x})$ are spatially correlated with $C(\boldsymbol{r})$ if $\sigma_R^2 = V$

$$[\![\mathrm{Re}\,\varphi(\boldsymbol{x})\,\mathrm{Re}\,\varphi(\boldsymbol{x}+\boldsymbol{r})]\!] = [\![\mathrm{Im}\,\varphi(\boldsymbol{x})\,\mathrm{Im}\,\varphi(\boldsymbol{x}+\boldsymbol{r})]\!] = C(\boldsymbol{r})\,, \tag{3.59}$$

3. The $\mathrm{Re}\,\varphi(\boldsymbol{x})$ and $\mathrm{Im}\,\varphi(\boldsymbol{x})$ are independent

$$[\![\mathrm{Re}\,\varphi(\boldsymbol{x})\,\mathrm{Im}\,\varphi(\boldsymbol{y})]\!] = [\![\mathrm{Im}\,\varphi(\boldsymbol{x})\,\mathrm{Re}\,\varphi(\boldsymbol{y})]\!] = 0\,, \tag{3.60}$$

Note, that we use the disorder average brackets $[\![\cdot]\!]$ here and in the following derivations to emphasize that the average is taken over disorder realizations.

We will start by showing Equation (3.58). By inserting the definition of $\varphi(\boldsymbol{k})$ from Equation (3.55) into Equation (3.57) we get

$$\varphi(\boldsymbol{x}) = \frac{1}{V} \sum_{\boldsymbol{k}} \sqrt{S(\boldsymbol{k})}\,(R_1(\boldsymbol{k}) + \mathrm{i}R_2(\boldsymbol{k}))\, e^{2\pi \mathrm{i}\, \boldsymbol{x}\boldsymbol{k}/L} \,. \tag{3.61}$$

We will show the calculation for the real part of $\varphi(\boldsymbol{x})$. The imaginary part calculation can be done in the same way. Let us first introduce some notation,

$$c_{\boldsymbol{x}\boldsymbol{k}} = \cos(2\pi \boldsymbol{x}\boldsymbol{k}/L)\,, \tag{3.62}$$

$$s_{\boldsymbol{x}\boldsymbol{k}} = \sin(2\pi \boldsymbol{x}\boldsymbol{k}/L)\,, \tag{3.63}$$

and write down the real part of $\varphi(\boldsymbol{x})$,

$$\operatorname{Re}\varphi(\boldsymbol{x}) = \frac{1}{V}\sum_{\boldsymbol{k}}\sqrt{S(\boldsymbol{k})}\left(R_1(\boldsymbol{k})c_{\boldsymbol{x}\boldsymbol{k}} - R_2(\boldsymbol{k})s_{\boldsymbol{x}\boldsymbol{k}}\right). \tag{3.64}$$

Let us concentrate on the first term of Equation (3.64),

$$\operatorname{Re}^1\varphi(\boldsymbol{x}) = \frac{1}{V}\sum_{\boldsymbol{k}}\sqrt{S(\boldsymbol{k})}R_1(\boldsymbol{k})c_{\boldsymbol{x}\boldsymbol{k}}. \tag{3.65}$$

Recall the distribution of R_i from Equation (3.56), $R_i \sim \mathcal{N}(0, \sigma_R^2)$. By using simple properties of the normal distribution we see that

$$\operatorname{Re}^1\varphi(\boldsymbol{x}) \sim \frac{1}{V}\sum_{\boldsymbol{k}}\sqrt{S(\boldsymbol{k})}c_{\boldsymbol{x}\boldsymbol{k}}\mathcal{N}(0, \sigma_R^2) = \mathcal{N}\left(0, \frac{\sigma_R^2}{V^2}\sum_{\boldsymbol{k}}S(\boldsymbol{k})c_{\boldsymbol{x}\boldsymbol{k}}^2\right), \tag{3.66}$$

and analogously for the second term of Equation (3.64),

$$\operatorname{Re}^2\varphi(\boldsymbol{x}) \sim -\frac{1}{V}\sum_{\boldsymbol{k}}\sqrt{S(\boldsymbol{k})}s_{\boldsymbol{x}\boldsymbol{k}}\mathcal{N}(0, \sigma_R^2) = \mathcal{N}\left(0, \frac{\sigma_R^2}{V^2}\sum_{\boldsymbol{k}}S(\boldsymbol{k})s_{\boldsymbol{x}\boldsymbol{k}}^2\right). \tag{3.67}$$

We use the fact that the distribution of the sum of two independent normally distributed random variables is again a normal distribution with the sum of the means and sum of the variances as new parameters [LL02, p. 34] and write down the distribution of $\operatorname{Re}\varphi(\boldsymbol{x})$,

$$\begin{aligned}\operatorname{Re}\varphi(\boldsymbol{x}) &\sim \mathcal{N}\left(0, \frac{\sigma_R^2}{V^2}\sum_{\boldsymbol{k}}S(\boldsymbol{k})c_{\boldsymbol{x}\boldsymbol{k}}^2 + \frac{\sigma_R^2}{V^2}\sum_{\boldsymbol{k}}S(\boldsymbol{k})s_{\boldsymbol{x}\boldsymbol{k}}^2\right)\\ &= \mathcal{N}\left(0, \frac{\sigma_R^2}{V^2}\sum_{\boldsymbol{k}}S(\boldsymbol{k})\left(c_{\boldsymbol{x}\boldsymbol{k}}^2 + s_{\boldsymbol{x}\boldsymbol{k}}^2\right)\right).\end{aligned} \tag{3.68}$$

Noting that $c_{\boldsymbol{x}\boldsymbol{k}}^2 + s_{\boldsymbol{x}\boldsymbol{k}}^2 = 1$ for all $\boldsymbol{x}$ and $\boldsymbol{k}$ and $\sum_{\boldsymbol{k}}S(\boldsymbol{k}) = V$, we finally read the Equation (3.58).

Let us now show Equation (3.59). We first calculate the autocorrelation of $\varphi(\boldsymbol{x})$ for one particular disorder realization,

$$\begin{aligned}\frac{1}{V}\sum_{\boldsymbol{x}}\varphi^*(\boldsymbol{x})\varphi(\boldsymbol{x}+\boldsymbol{r}) &= \frac{1}{V}\sum_{\boldsymbol{x}}\left(\mathrm{DFT}^{-1}(\varphi^*(\boldsymbol{k}))\mathrm{DFT}^{-1}(\varphi(\boldsymbol{k}))\right)\\ &= \frac{1}{V}\sum_{\boldsymbol{x}}\left(\frac{1}{V}\sum_{\boldsymbol{k}}\left(\varphi(\boldsymbol{k})e^{2\pi\mathrm{i}\,\boldsymbol{x}\boldsymbol{k}/L}\right)^*\right)\left(\frac{1}{V}\sum_{\boldsymbol{l}}\varphi(\boldsymbol{l})e^{2\pi\mathrm{i}\,\boldsymbol{x}\boldsymbol{l}/L}\right)\\ &= \frac{1}{V}\sum_{\boldsymbol{x}}\left(\frac{1}{V}\sum_{\boldsymbol{k}}\varphi^*(\boldsymbol{k})e^{-2\pi\mathrm{i}\,\boldsymbol{x}\boldsymbol{k}/L}\right)\left(\frac{1}{V}\sum_{\boldsymbol{l}}\varphi(\boldsymbol{l})e^{2\pi\mathrm{i}\,\boldsymbol{x}\boldsymbol{l}/L}\right)\\ &= \frac{1}{V^2}\sum_{\boldsymbol{k}}\varphi^*(\boldsymbol{k})\sum_{\boldsymbol{l}}\varphi(\boldsymbol{l})e^{2\pi\mathrm{i}\,\boldsymbol{x}\boldsymbol{l}/L}\left(\frac{1}{V}\sum_{\boldsymbol{x}}e^{-2\pi\mathrm{i}\,\boldsymbol{x}(\boldsymbol{l}-\boldsymbol{k})/L}\right).\end{aligned} \tag{3.69}$$

Noting that

$$\frac{1}{V}\sum_{\boldsymbol{x}}e^{-2\pi\mathrm{i}\,\boldsymbol{x}(\boldsymbol{l}-\boldsymbol{k})/L} = \delta(\boldsymbol{k}, \boldsymbol{l}), \tag{3.70}$$

where $\delta(\boldsymbol{k}, \boldsymbol{l})$ is the multidimensional Dirac delta, we can simplify Equation (3.69) further to

$$\frac{1}{V}\sum_{\boldsymbol{x}}\varphi^*(\boldsymbol{x})\varphi(\boldsymbol{x}+\boldsymbol{r}) = \frac{1}{V^2}\sum_{\boldsymbol{k}}\varphi^*(\boldsymbol{k})\varphi(\boldsymbol{k})e^{2\pi\mathrm{i}\,\boldsymbol{x}\boldsymbol{k}/L}. \tag{3.71}$$

We now insert Equation (3.55) into Equation (3.71),

$$\frac{1}{V}\sum_{\boldsymbol{x}}\varphi^*(\boldsymbol{x})\varphi(\boldsymbol{x}+\boldsymbol{r})$$

$$= \frac{1}{V^2}\sum_{\boldsymbol{k}}\left(\sqrt{S(\boldsymbol{k})}\left(R_1(\boldsymbol{k})+\mathrm{i}R_2(\boldsymbol{k})\right)\right)^*\left(\sqrt{S(\boldsymbol{k})}\left(R_1(\boldsymbol{k})+\mathrm{i}R_2(\boldsymbol{k})\right)\right)e^{2\pi\mathrm{i}\,\boldsymbol{x}\boldsymbol{k}/L}, \qquad (3.72)$$

and since $S(\boldsymbol{k})\in\mathbb{R}$, we get

$$\frac{1}{V}\sum_{\boldsymbol{x}}\varphi^*(\boldsymbol{x})\varphi(\boldsymbol{x}+\boldsymbol{r}) = \frac{1}{V^2}\sum_{\boldsymbol{k}}S(\boldsymbol{k})\left(R_1^2(\boldsymbol{k})+R_2^2(\boldsymbol{k})\right)e^{2\pi\mathrm{i}\,\boldsymbol{x}\boldsymbol{k}/L}. \qquad (3.73)$$

Further, we assume translational invariance,

$$\sum_{\boldsymbol{x}}\varphi^*(\boldsymbol{x})\varphi(\boldsymbol{x}+\boldsymbol{r}) = V\varphi^*(\boldsymbol{x}_0)\varphi(\boldsymbol{x}_0+\boldsymbol{r}), \qquad (3.74)$$

where $\boldsymbol{x}_0$ is an arbitrary reference point. Using Equation (3.74) and taking the disorder average we can rewrite Equation (3.73) to

$$[\![\varphi^*(\boldsymbol{x})\varphi(\boldsymbol{x}+\boldsymbol{r})]\!] = \frac{1}{V^2}\sum_{\boldsymbol{k}}S(\boldsymbol{k})\left([\![R_1^2(\boldsymbol{k})]\!]+[\![R_2^2(\boldsymbol{k})]\!]\right)e^{2\pi\mathrm{i}\,\boldsymbol{x}\boldsymbol{k}/L}. \qquad (3.75)$$

The variance of the random numbers R_i can be calculated from $\sigma_R^2 = [\![R_i^2]\!] - [\![R_i]\!]^2$ but since from Equation (3.57) we know that $[\![R_i]\!]^2 = 0$, we have $\sigma_R^2 = [\![R_i^2]\!]$. Finally, with the help of the definition of $S(\boldsymbol{k})$ from Equation (3.54) the Equation (3.75) becomes

$$\boxed{[\![\varphi^*(\boldsymbol{x})\varphi(\boldsymbol{x}+\boldsymbol{r})]\!] = \frac{2\sigma_R^2}{V^2}\sum_{\boldsymbol{k}}S(\boldsymbol{k})e^{2\pi\mathrm{i}\,\boldsymbol{x}\boldsymbol{k}/L} = \frac{2\sigma_R^2}{V}C(\boldsymbol{r}).} \qquad (3.76)$$

Similarly, we can show that

$$\boxed{[\![\varphi(\boldsymbol{x})\varphi(\boldsymbol{x}+\boldsymbol{r})]\!] = 0.} \qquad (3.77)$$

Now, let us analyze different combinations of real and imaginary parts to show Equations (3.59) and (3.60). Using properties of complex numbers we can write

$$[\![\mathrm{Re}\,\varphi(\boldsymbol{x})\,\mathrm{Re}\,\varphi(\boldsymbol{x}+\boldsymbol{r})]\!] = \left[\!\!\left[\left(\frac{\varphi(\boldsymbol{x})+\varphi^*(\boldsymbol{x})}{2}\right)\left(\frac{\varphi(\boldsymbol{x}+\boldsymbol{r})+\varphi^*(\boldsymbol{x}+\boldsymbol{r})}{2}\right)\right]\!\!\right]$$

$$= \frac{1}{4}[\![(\varphi(\boldsymbol{x})+\varphi^*(\boldsymbol{x}))(\varphi(\boldsymbol{x}+\boldsymbol{r})+\varphi^*(\boldsymbol{x}+\boldsymbol{r}))]\!]$$

$$= \frac{1}{4}\Big([\![\varphi(\boldsymbol{x})\varphi(\boldsymbol{x}+\boldsymbol{r})]\!]+[\![\varphi(\boldsymbol{x})\varphi^*(\boldsymbol{x}+\boldsymbol{r})]\!]$$

$$+ [\![\varphi^*(\boldsymbol{x})\varphi(\boldsymbol{x}+\boldsymbol{r})]\!]+[\![\varphi^*(\boldsymbol{x})\varphi^*(\boldsymbol{x}+\boldsymbol{r})]\!]\Big)$$

$$= \frac{1}{4}\Big([\![\varphi(\boldsymbol{x})\varphi(\boldsymbol{x}+\boldsymbol{r})]\!]+[\![\varphi^*(\boldsymbol{x})\varphi(\boldsymbol{x}+\boldsymbol{r})]\!]^*$$

$$+ [\![\varphi^*(\boldsymbol{x})\varphi(\boldsymbol{x}+\boldsymbol{r})]\!]+[\![\varphi(\boldsymbol{x})\varphi(\boldsymbol{x}+\boldsymbol{r})]\!]^*\Big). \qquad (3.78)$$

Using Equations (3.76) and (3.77) and setting $\sigma_R^2 = V$ we finally have

$$[\![\mathrm{Re}\,\varphi(\boldsymbol{x})\,\mathrm{Re}\,\varphi(\boldsymbol{x}+\boldsymbol{r})]\!] = C(\boldsymbol{r}). \qquad (3.79)$$

The same result can be obtained for $[\![\operatorname{Im}\varphi(\boldsymbol{x})\operatorname{Im}\varphi(\boldsymbol{x}+\boldsymbol{r})]\!]$. On the other hand mixing the real and imaginary parts leads to

$$
\begin{aligned}
[\![\operatorname{Re}\varphi(\boldsymbol{x})\operatorname{Im}\varphi(\boldsymbol{x}+\boldsymbol{r})]\!] &= \left[\!\left[\left(\frac{\varphi(\boldsymbol{x})+\varphi^*(\boldsymbol{x})}{2}\right)\left(\frac{\varphi(\boldsymbol{x}+\boldsymbol{r})-\varphi^*(\boldsymbol{x}+\boldsymbol{r})}{2\mathrm{i}}\right)\right]\!\right] \\
&= \frac{1}{4\mathrm{i}}\Big([\![\varphi(\boldsymbol{x})\varphi(\boldsymbol{x}+\boldsymbol{r})]\!] - [\![\varphi(\boldsymbol{x})\varphi^*(\boldsymbol{x}+\boldsymbol{r})]\!] \\
&\quad + [\![\varphi^*(\boldsymbol{x})\varphi(\boldsymbol{x}+\boldsymbol{r})]\!] - [\![\varphi^*(\boldsymbol{x})\varphi^*(\boldsymbol{x}+\boldsymbol{r})]\!] \Big) \\
&= \frac{1}{4\mathrm{i}}\Big([\![\varphi(\boldsymbol{x})\varphi(\boldsymbol{x}+\boldsymbol{r})]\!] - [\![\varphi^*(\boldsymbol{x})\varphi(\boldsymbol{x}+\boldsymbol{r})]\!]^* \\
&\quad + [\![\varphi^*(\boldsymbol{x})\varphi(\boldsymbol{x}+\boldsymbol{r})]\!] - [\![\varphi(\boldsymbol{x})\varphi(\boldsymbol{x}+\boldsymbol{r})]\!]^* \Big) \\
&= 0\,,
\end{aligned}
\tag{3.80}
$$

and analogue for $[\![\operatorname{Im}\varphi(\boldsymbol{x})\operatorname{Re}\varphi(\boldsymbol{x}+\boldsymbol{r})]\!]$. This completes the proof of the properties in Equations (3.58) to (3.60).

A careful reader has probably observed, that in Equation (3.55) we implicitly assumed that the spectral density is non-negative,

$$
S(\boldsymbol{k}) \geq 0 \quad \text{for all } \boldsymbol{k}\,,
\tag{3.81}
$$

in order to take the square root of $S(\boldsymbol{k})$. This is needed as we know from the symmetry of the chosen correlation function $C(\boldsymbol{r})$ that $S(\boldsymbol{k}) \in \mathbb{R}$ for all $\boldsymbol{k}$. Although it is probably expected that Equation (3.81) is true in continuum for (at least) a certain class of correlation functions, working on a discrete lattice and using our desired correlation function we had negative values in certain cases. We followed Ref. [Zie+17] and used a modified spectral density $\tilde{S}(\boldsymbol{k})$ with a zero-cutoff,

$$
\tilde{S}(\boldsymbol{k}) = \begin{cases} S(\boldsymbol{k}) & \text{if } S(\boldsymbol{k}) \geq 0 \\ 0 & \text{else} \end{cases}.
\tag{3.82}
$$

We checked for which cases the negative $S(\boldsymbol{k})$ occur and analyzed the effect of this cutoff on the final disorder. We will discuss the details in Appendix A.1. Let us just remark that in our simulations this problem occurred only at very small lattice sizes and only for the largest used long-range correlation strength.

3.5.2 Generating long-range correlated discrete disorder

After the previous continuous random variables generation process, we are equipped with variables $\tau(\boldsymbol{x}) = \operatorname{Re}\varphi(\boldsymbol{x})$, or alternatively $\tau(\boldsymbol{x}) = \operatorname{Im}\varphi(\boldsymbol{x})$, satisfying the correlation relation

$$
[\![\tau(\boldsymbol{x})\tau(\boldsymbol{x}+\boldsymbol{r})]\!] = C(\boldsymbol{r})\,,
\tag{3.83}
$$

and drawn from a normal distribution

$$
\tau(\boldsymbol{x}) \sim \mathcal{N}(0,1)\,.
\tag{3.84}
$$

In the following we want to map $\tau(\boldsymbol{x}) \to \eta(\boldsymbol{x}) \in \{0,1\}$ in order to identify occupied and empty sites on the lattice. The goal is to produce a desired concentration of defects p_d. We will again follow Ref. [Zie+17] and use the grand canonical approach, i.e., the concentration of defects p_d may vary for each individual realization but equals p_d after averaging over many disorder realizations. The mapping process is quite straight forward. We define a threshold θ and set

$$\eta(\boldsymbol{x}) = \begin{cases} 1 & \text{if } \tau(\boldsymbol{x}) \leq \theta \\ 0 & \text{if } \tau(\boldsymbol{x}) > \theta \end{cases}. \tag{3.85}$$

The threshold itself is connected to the desired concentration of defects through the integration of the probability density of τ

$$p_d(\theta) = \int_{-\infty}^{\theta} \mathrm{d}\tau \, p(\tau) = \frac{1}{2}\left(1 + \mathrm{erf}\left(\frac{\theta}{\sqrt{2}}\right)\right), \tag{3.86}$$

where erf is the standard error function. Note, that in Equation (3.86) we left out the variance of τ since it equals to 1. Equation (3.86) can be solved implicitly to obtain θ for a given p_d.

Summary. The generation of continuous and discrete random variables with a spatial long-range correlation by using the Fourier Filter Method was discussed. A detailed calculation proofed that the method produces correlated sets with a given correlation function C. We presented the threshold definition for mapping the continuous variables to the discrete ones.

Results

<div style="text-align:right; font-size:3em; font-weight:bold">4</div>

4.1 Simulation details

Before going into the actual analyses and presenting the results of this work, let us first present some details of the simulation process. The code used for the simulation in this work can be found in Appendix A.4 and in Ref. [@Git21]. A few general settings were already mentioned at different paces before. Throughout the whole work we used the Swendesen-Wang multiple-cluster [SW87] update and the Hoshen-Kopelman cluster search algorithm [HK76]. Before starting the measurements we always performed 500–1000 thermalization sweeps from a randomly disordered (high temperature) state. A unique seed was used for each parameter tuple (a, p_d, L) for the Mersenne-Twister random number generator which is the standard random number generator in julia [@Rng21] and internally uses the library from Refs. [@MT06; SM09]. Due to our quite short simulation runs we do not expect any problems with the pseudo-randomness in our data.

We produced simulation data for five correlated cases with $a = 1.5, 2.0, 2.5, 3.0, 3.5$ as well as for the uncorrelated case $a = \infty$. For each of these correlation exponents a we used eight different concentrations of defects $p_d = 0.05, 0.1, 0.15, 0.2, 0.25, 0.3, 0.35, 0.4$. We performed our simulations on 19 lattice sizes $L = 8, 12, 16, 20, 24, 28, 32, 40, 48, 56, 64, 80, 96, 112, 128, 160, 192, 224, 256$. Concerning the simulation temperature, we started with simulation of lattices up to $L = 48$ which we performed in a very large β-range but with relatively large spacing of $\Delta\beta = 0.0005$. These simulations provided us with the first estimation on where the peaks of the different observables will approximately lie for each correlation exponent a and concentration of defects p_d. After this first step, we narrowed the range and performed simulations for the lattices $48 < L \leq 112$. The spacing was kept the same. After that, in a third step we simulated the largest lattices with $112 < L \leq 256$. Here, a reduced lattice spacing was used with $\Delta\beta = 0.00025$. For individual combinations of a and p_d we added some more points in between for the largest lattice sizes when the histogram reweighting method failed to find a peak near to the one of already used temperatures. Finally, for the temperature scaling analysis we added some more temperatures on the high temperature side for the largest considered lattice size of $L = 256$. The set of all simulated temperatures can be found in Figure A.11 in the Appendix A.4. The minimum number of different simulation temperatures was 7.

After the thermalization sweeps were performed, we measured the following observables at each sweep: the total energy E, the total magnetization M, the size of the largest stochastic spin cluster $\hat{C}$ and the average size of the stochastic clusters $\overline{C}$, and the Fourier-transposed correlation function $\tilde{C}_s(\mathbf{1})$ defined in Equation (2.50). We performed $N = 10\,000$ sweeps and used $N_c = 1000$ disorder realizations for each parameter tuple $(a, p_d, L, \beta_{\mathrm{sim}})$. The

total amount of stored data was 6.6 TB and 1800 CPU-years on a 2.4 GHz were needed for the simulations. In Appendix A.4 we give some more data about the simulations and the implementation. Additionally, we present the measured data $\overline{C}$ and $\hat{C}$ in Appendix A.3 since we have not used this data in the actual analyses for this work.

4.2 Analysis of the correlated disorder

The first analysis which we performed was the analysis of the underlying disorder configurations which were used for later Ising model simulations. We studied the correct distribution of the concentrations of defects p_d and measured the correlation exponents a. In our opinion, it is an important step in order to provide consistent results for the critical exponents in dependence of a later. In this section we will closely follow the description of this analysis in Ref. [KJ20]. However, the discussion presented here, is a more detailed one.

4.2.1 Disorder concentration

As described in Section 3.5 we used the Fourier Filter Method [Mak+95; Zie+17] for the generation of the long-range correlated disorder. After the generation process was finished, we studied the disorder ensembles before doing the simulations. In the first step we checked that the measured mean concentration of defects $\overline{p}_d$ matches the chosen values for each parameter tuple (a, p_d, L). This was important, since we used the grand canonical approach where the concentration of defects p_d was a mean value over all disorder realizations. Therefore, we checked the mean values $\overline{p}_d$ and tested their distributions for normality.

In Figure 4.1 we present the histograms of the concentrations p_d of defects for different L, $a = 2.0$ and $p_d = 0.2$ as examples. For small lattice sizes we see a slight skewness of the distribution while for larger lattice sizes the distribution looks symmetric and normal. We verified the normality with the Anderson-Darling test [AD52; Tho02, p. 104]. The results of these tests are summarized in Figure 4.2. We clearly see that for the majority of parameter constellations the test suggests a normally distributed p_d with the confidence of 95 %. This is true for all $a \geq 2.0$ and $L \geq 24$. Only for $a = 1.5$ and $L \leq 96$ the test rejects the normality of the distribution for small concentrations $p_d \leq 0.15$. On the other hand, for all parameter tuples with $L \geq 24$ the mean values $\overline{p}_d$ were in perfect agreement with the imposed values p_d.

4.2.2 Disorder correlation

Once we verified that the imposed concentration of defects is correct for all ensembles, we went further and checked the measured correlation exponents a. We measured the correlation function on the lattice Λ with

$$C_\eta(r) = \left[\!\!\left[\frac{\mathscr{C}}{N_r} \sum_{\substack{\boldsymbol{x},\boldsymbol{y} \\ d_{\mathrm{bc}}(\boldsymbol{x},\boldsymbol{y})=r}} (\eta(\boldsymbol{x}) - \overline{p}_d)(\eta(\boldsymbol{y}) - \overline{p}_d) \right]\!\!\right], \tag{4.1}$$

where $\boldsymbol{x}, \boldsymbol{y} \in \Lambda$ are sites of the lattice, d_{bc} is the distance between $\boldsymbol{x}$ and $\boldsymbol{y}$ sites according to Equation (3.50). The constant $\mathscr{C}$ is the normalization constant such that $C_\eta(0) = 1$ while N_r is the number of possible realizations of the distance r on the lattice. Finally, $\overline{p}_d$ is the measured mean concentration of defects for the whole disorder ensemble.

(a) $L = 8$.   **(b)** $L = 32$.   **(c)** $L = 256$.
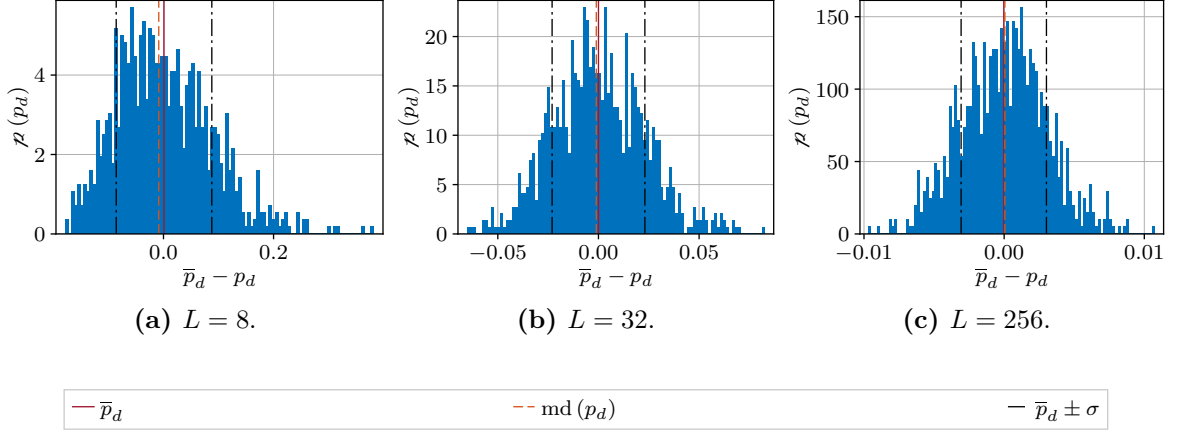
$$-\ \overline{p}_d \qquad\qquad -- \ \mathrm{md}\,(p_d) \qquad\qquad -\ \overline{p}_d \pm \sigma$$

Figure 4.1: Histograms of the concentration of defects for $a = 2.0$, $p_d = 0.2$ and different L. The values are shifted by the imposed p_d to see the deviation between p_d and $\overline{p}_d$. $\mathrm{md}\,(p_d)$ is the median of the ensemble and σ is the standard deviation.

(a) $a = 1.5$.   **(b)** $a = 2.0$.   **(c)** $a = 2.5$.

(d) $a = 3.0$.   **(e)** $a = 3.5$.   **(f)** $a = \infty$.

$$0.05 \qquad\qquad 0.50 \qquad\qquad 1.00$$
$$p_{\mathrm{AD}}$$
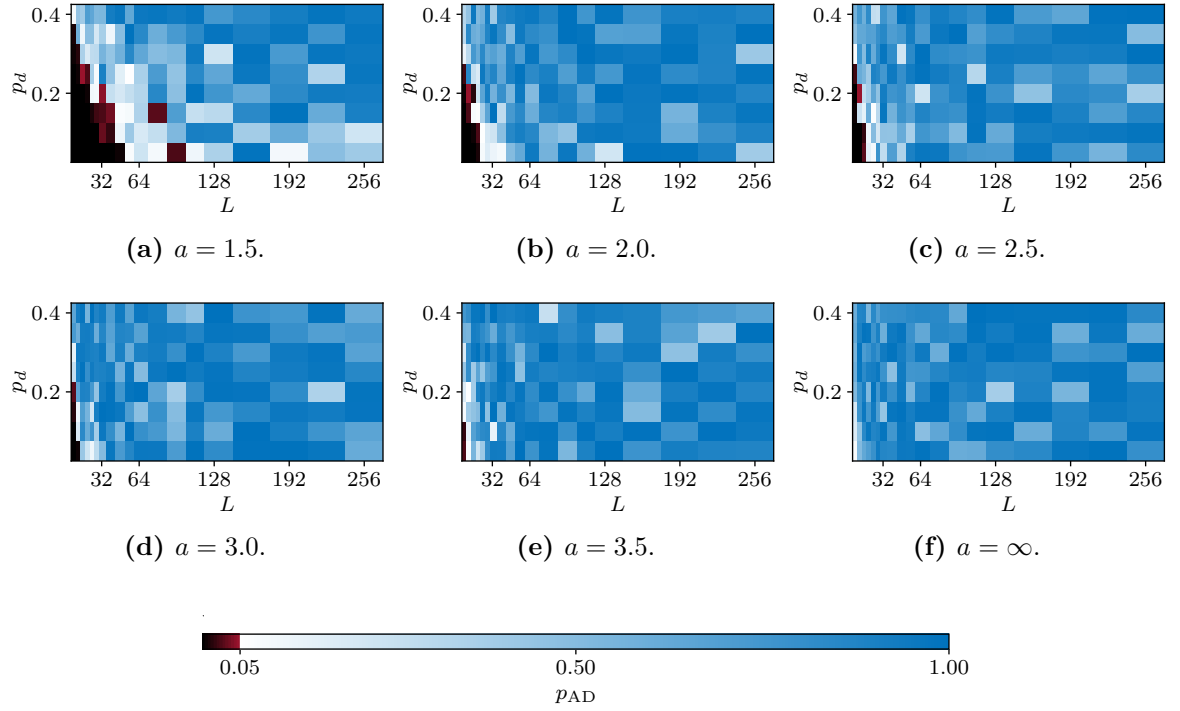
Figure 4.2: Anderson-Darling test results for all parameter tuples (a, p_d, L). The p_{AD} is the probability that the given distribution is normal. For $a \geq 2.0$ and $L \geq 24$ all distributions of the concentrations of defects p_d were identified as normal with 95 % confidence. The white and blue regions identify the distribution as normal while black and red reject the normality assumption.

The normalization constant turns out to be

$$\mathscr{C} = \frac{1}{\overline{p}_d\,(1 - \overline{p}_d)} \ . \tag{4.2}$$

We chose two different directional vectors for the measurement,

$$\hat{\boldsymbol{r}}_1 = (1, 0, 0)^T, \quad \hat{\boldsymbol{r}}_2 = (1, 1, 1)^T, \tag{4.3}$$

and measured the correlation function for all possible distances in each of these two directions. Due to the periodic boundary conditions we have the following numbers of possible realizations of the distances on the lattice,

$$N_r = \begin{cases} V/2 & \text{for } r = L/2 \text{ and } r = \sqrt{3}L/2 \\ V & \text{else} \end{cases}. \tag{4.4}$$

The reduction of the number of realizations from V to $V/2$ for distances which are equal to half of the extension of the lattice along the considered direction is explained in more detail for the example of a one-dimensional lattice in Figure 4.3.

(a) $r = 1 < L/2$.   **(b)** $r = 2 = L/2$.
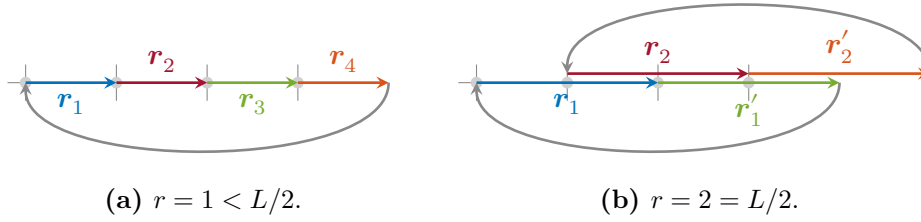
Figure 4.3: Consider a one-dimensional lattice with $L = 4$ and periodic boundary conditions. The total number of sites is $V = 4$. We start with the distance $r = 1$ along the x-axis. This distance can be realized $V = 4$ times as shown in (a). Each distance vector $\boldsymbol{r}_i$ with $i \in \{1, 2, 3, 4\}$ connects a unique pair of sites. Going further to $r = 2 = L/2$ we can again define four vectors as shown in (b). But now $\boldsymbol{r}_1 = -\boldsymbol{r}_1'$ and $\boldsymbol{r}_2 = -\boldsymbol{r}_2'$ which leaves us with only $V/2 = 2$ unique pairs of sites.

To obtain the correlation exponent a we performed a fit to the measured correlation function $C_\eta(r)$ for each parameter tuple (a, p_d, L). We used the linearized ansatz on the logarithmic scale,

$$\ln C_\eta(r) = -a \ln r + B, \tag{4.5}$$

which reflects the imposed power-law behavior of the correlation function $C_\eta(r) \propto r^{-a}$. During the fitting process we had to deal with two problems. On one hand, for short distances the correlation function did not exactly follow the power-law decay as we used a modified function,

$$C_0(r) = \left(1 + r^2\right)^{-a/2} \to r^{-a} \quad \text{for } r \to \infty, \tag{4.6}$$

for the disorder generation. On the other hand, for large distances we had noisy signal due to limited statistics. Therefore, we introduced two threshold distances, $r_{\min}$ and $r_{\max}$. Only distances in the range $r_{\min} \leq r \leq r_{\max}$ were included into the fits. For the minimum distance $r_{\min}$ we used the smallest distance for which the relative deviation between the modified correlation function C_0 and the power-law function $C(r) = r^{-a}$ was lower than a chosen threshold of $\epsilon_C = 0.05$,

$$\frac{C(r_{\min}) - C_0(r_{\min})}{C(r_{\min})} = \frac{r_{\min}^{-a} - (1 + r_{\min}^2)^{-a/2}}{r_{\min}^{-a}} \leq \epsilon_C = 0.05, \tag{4.7}$$

After some algebra we get the minimum distance in dependence of the correlation exponent a,

$$r_{\min}(a) \geq \left((1 - \epsilon_C)^{-2/a} - 1\right)^{-1/2}. \tag{4.8}$$

The minimum distances for the considered correlation exponents a are between $r_{\min} \approx 3.8$ for $a = 1.5$ and $r_{\min} \approx 5.8$ for $a = 3.5$. They do not depend on the lattice size and the estimation does not involve the measured correlation function $C_\eta(r)$.

Furthermore, we had to find a maximum distance $r_{\max}$ after which the correlation function became too noisy to be used in the fits. To estimate the maximum distance $r_{\max}$, we looked at the measured values $C_\eta(r)$ and the distance where its absolute values crossed a low threshold value of $C_{\min} = 10^{-5}$ for the first time,

$$\left| C_\eta(r_{\max}) \right| \leq C_{\min} = 10^{-5} . \tag{4.9}$$

In principle, we were now equipped with $r_{\min}$ and $r_{\max}$ and could proceed to the fitting procedure. However, in some cases, especially for very small lattice sizes $L \leq 20$ and weak correlations $a \geq 2.5$, the minimum and the maximum distances were too close together or even the case that $r_{\min} > r_{\max}$ appeared. In such cases we decreased $r_{\min}$ until we reached four degrees of freedom in the fit. The minimum and maximum distances for all parameter tuples (a, p_d, L) are presented in Figure 4.4. One can see, that for $a = 1.5$ we can use the whole range of measured distances while with increasing a the maximum used distance $r_{\max}$ becomes shorter. This is of course a consequence of the faster correlation decay which leads to the fact that the noise becomes dominant at shorter distances. For the weakest correlation with $a = 3.5$ we can go up to $r_{\max} \approx 20$ only. On the other hand, as one would expect, the concentration of defects p_d only marginally influences the chosen distance ranges. Larger concentrations allow for slightly larger $r_{\max}$, though.
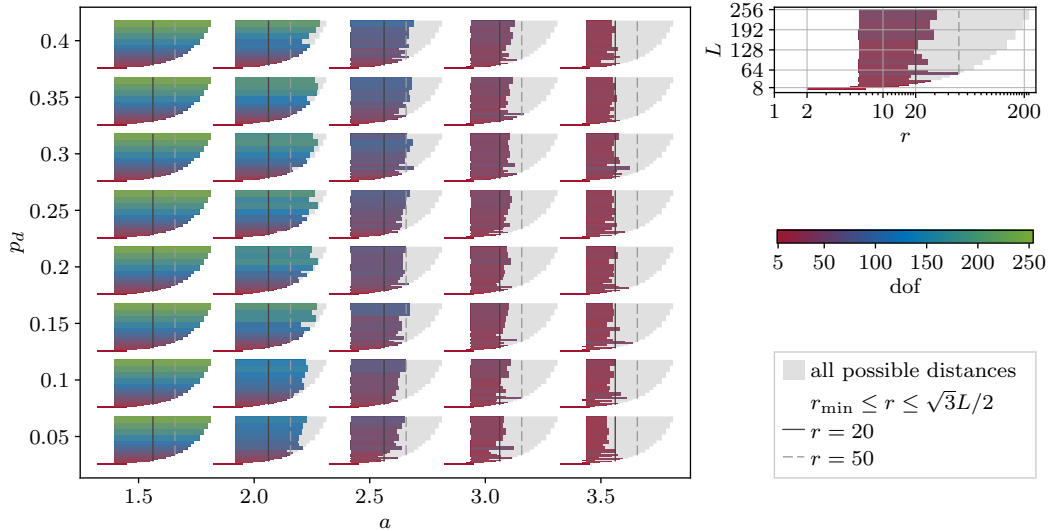
Figure 4.4: The minimum and maximum distances $r_{\min}$ and $r_{\max}$ used for the estimation of $\overline{a}$ for all parameter tuples (a, p_d, L). The plot in the right corner shows a zoomed version of one diagram in order to present the used axes scaling. The x-axis of the distances is shown logarithmically to account for very different lattice sizes. The color is mapped to the number of degrees of freedom (dof) when choosing this particular $r_{\min}$ and $r_{\max}$. For very small lattice sizes sometimes we had to shift the calculated $r_{\min}$ from Equation (4.8) downwards in order to achieve at least four degrees of freedom for the fit. This can be seen in the plots as "spikes" to the left on the bottom of each diagram. Finally, the solid and dashed lines represent the distances $r = 20$ and $r = 50$, respectively, to improve visual comparability.

After we determined the minimum and maximum distances for each parameter tuple (a, p_d, L), we performed the fits to Equation (4.5). Examples of these fits are shown in Figure 4.5. The fitted mean values $\overline{a}(p_d, L)$ are presented in Figure 4.6. For strongest correlations $a \leq 2.5$ we observe a very good agreement of $\overline{a}$ with the imposed values a already for relatively small lattice sizes $L \gtrsim 32$. However, as naturally follows from the determination of $r_{\min}$ and $r_{\max}$, we have fewer degrees of freedom in the fits for larger a. We see larger deviations for $a \geq 3.0$ and the expected a values are reached only for larger lattice sizes $L \gtrsim 128$ where we have better statistics due to larger number of distance realizations per disorder configuration. Our final estimates $\overline{a}$ were means over all p_d and $L \geq L_{\min}$, where $L_{\min}$ was chosen according to the quality of the fits. These values are summarized in Table 4.1. For all correlation exponents $\overline{a}$ we see an underestimation of a. It becomes more pronounced for larger a where it reaches about $5\,\%$. We plotted the relative deviations $(\overline{a} - a)/a$ in Figure 4.7. It can be seen that although the $\overline{a}$ values are underestimated, they more or less always cover the imposed a values with their errors. Note, that the modified correlation function, Equation (4.6) should not be the reason for the inequality $\overline{a} < a$. As already mentioned above, the deviation between the used correlation function and the power-law becomes neglectable very fast (the deviation is less than $5\,\%$ already for $r \geq 6.0$ for all considered a).

Table 4.1: Final estimates of $\overline{a}$ as means over all p_d and $L \geq L_{\min}(a)$. The minimum lattice sizes $L_{\min}(a)$ were chosen according to the quality of the fits. The $\nu = 2/\overline{a}$ are the corresponding critical exponents according to the conjecture by Weinrib and Halperin.

a	$\overline{a}$	$2/\overline{a}$	$L_{\min}$
3.5	3.30(18)	–	112
3.0	2.910(96)	0.687(23)	96
2.5	2.451(26)	0.8159(86)	80
2.0	1.979(18)	1.0105(89)	64
1.5	1.500(30)	1.333(26)	56

As a final test, we compared the estimates $\overline{a}$ for $a = 3.5$ and for different number of disorder realizations to get more clarity on the fact of underestimation. In Figure 4.8 we visualize the $\overline{a}$ and the deviations $(\overline{a} - a)/a$ in dependence of N_c. The results at various p_d and L for different two numbers of realizations are shown in Figure 4.9. We can see that the estimates become considerably better with increasing number of realizations. The underestimation issue remains present even for the largest number of realization $N_c = 5000$ but gets approximately $50\,\%$ smaller. However, for the final estimates of a, we kept the number of disorder realization t $N_c = 1000$ which was the number for which an actual Ising model simulation was run.

Summary. We verified the measured $\overline{a}$ to be in a good agreement with the imposed values a. The $\overline{a}$ values slightly underestimate the a values with a maximum relative deviation of about $5\,\%$. This deviation becomes smaller when the number of considered disorder realizations is increased.

(a) $a = 2.0$, $L = 32$.

(b) $a = 2.0$, $L = 256$.

(c) $a = 3.5$, $L = 32$.

(d) $a = 3.5$, $L = 256$.

○ $C_\eta(r)$ □ $-C_\eta(r)$ — $\ln C_\eta(r) = -a \ln r + B$
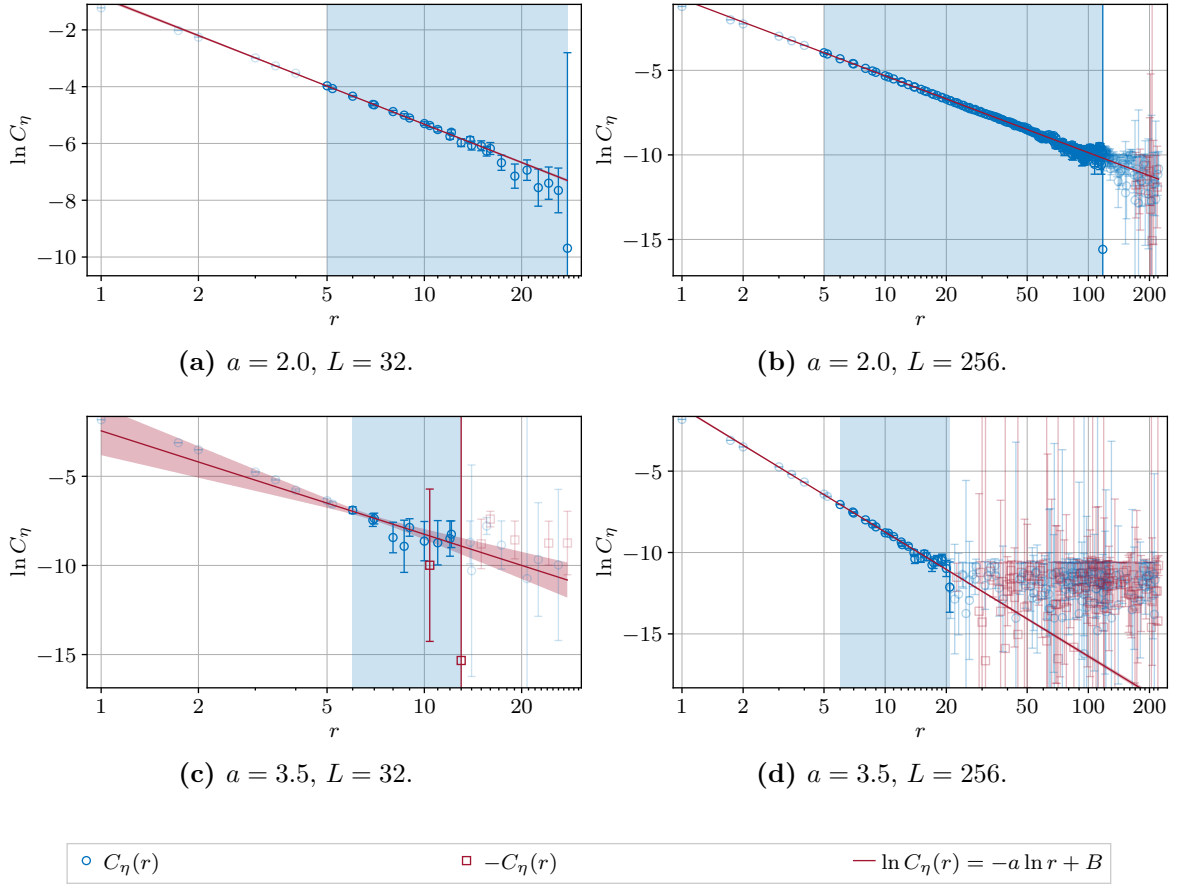
Figure 4.5: Examples of the fits to the ansatz in Equation (4.5) for two different lattice sizes L and correlation exponents a with $p_d = 0.2$. Due to limited statistics, negative values of $C_\eta(r)$ may occur at larger distances. We plot these values with a minus sign. The blue shaded regions show the finally used fitting ranges $r_{\min} \leq r \leq r_{\max}$. Fits to weaker correlations, i.e., larger a, have smaller fitting ranges as the correlation function $C_\eta(r)$ decays faster. The maximum range on the x axis is half the distance along the diagonal $r = \sqrt{3}L/2$.

(a) $a = 1.5$.

(b) $a = 2.0$.

(c) $a = 2.5$.

(d) $a = 3.0$.

(e) $a = 3.5$.
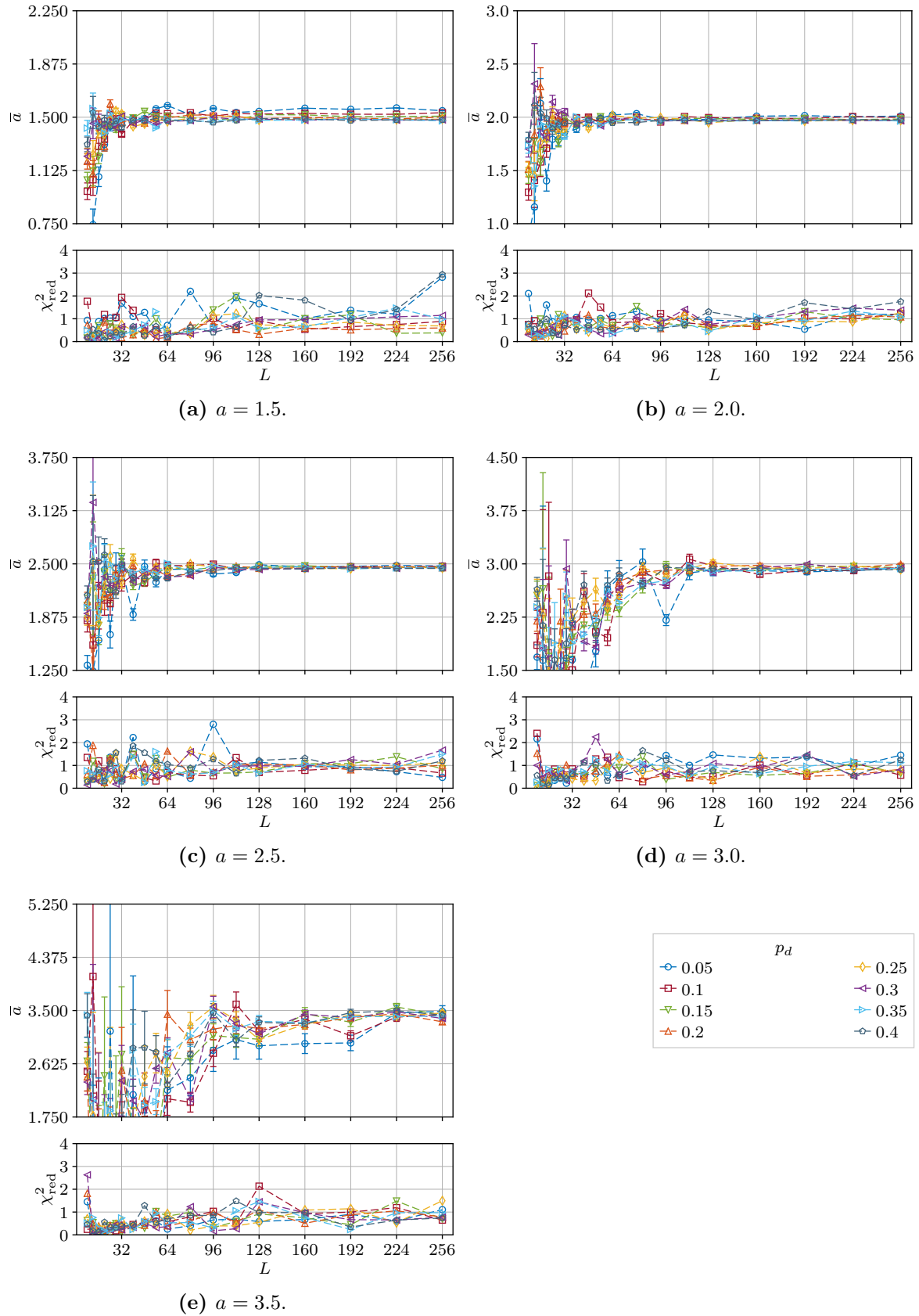
Figure 4.6: Measured correlation exponents $\overline{a}$ and the corresponding χ^2_{red} values of the fits for all parameter tuples (a, p_d, L). Larger lattice sizes have more possibilities of realizing a certain distance which leads to larger statistics and consequently to smaller errors. On the other hand, for weaker correlations, i.e., larger a, we have smaller fitting ranges $r_{\mathrm{min}} \leq r \leq r_{\mathrm{max}}$ as the correlation function $C_\eta(r)$ decays faster. The scaling on the y-axis of the $\overline{a}$ plots is chosen to be $\frac{1}{2}a \leq \overline{a} \leq \frac{3}{2}a$ for better comparability.
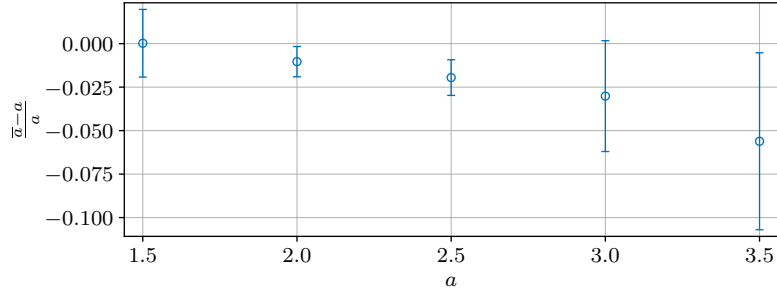
Figure 4.7: Relative deviations between the measured correlation exponents $\overline{a}$ and the corresponding imposed values a. The errors $\epsilon(\overline{a})$ were scaled to $\epsilon(\overline{a})/a$. We can observe a systematic underestimation of the imposed values which increses with increasing a.

(a) $\overline{a}$.

(b) $(\overline{a} - a)/a$.
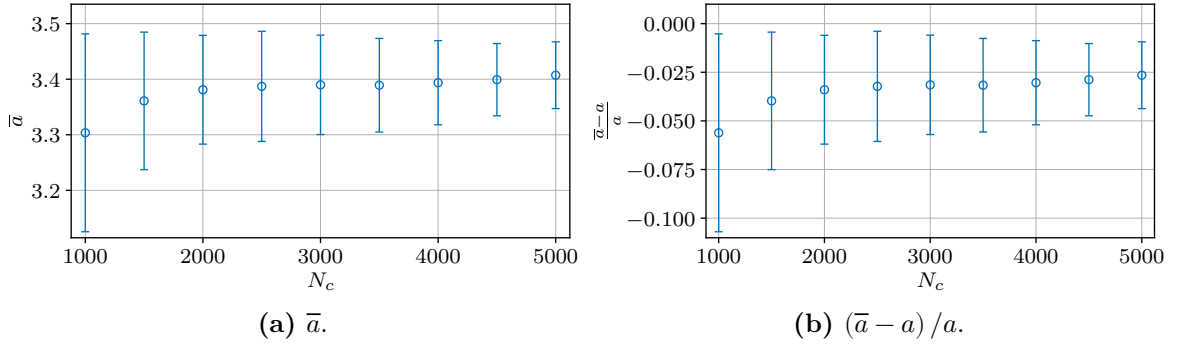
Figure 4.8: Comparison of the estimated values $\overline{a}$ and the deviations $(\overline{a} - a)/a$ for $a = 3.5$ and different number of disorder realizations N_c. The minimum lattice size included into the mean was chosen to be the same as for the case with $N_c = 1000$ disorder realizations, $L_{\min} = 112$.

(a) $N_c = 1000$.

(b) $N_c = 5000$.

p_d

| $\circ$ 0.05 | $\square$ 0.1 | $\triangledown$ 0.15 | $\triangle$ 0.2 | $\diamond$ 0.25 | $\triangleleft$ 0.3 | $\triangleright$ 0.35 | $\circ$ 0.4 |
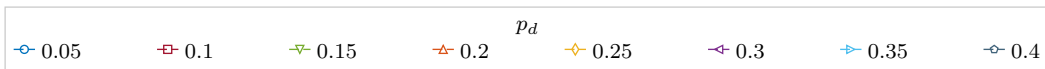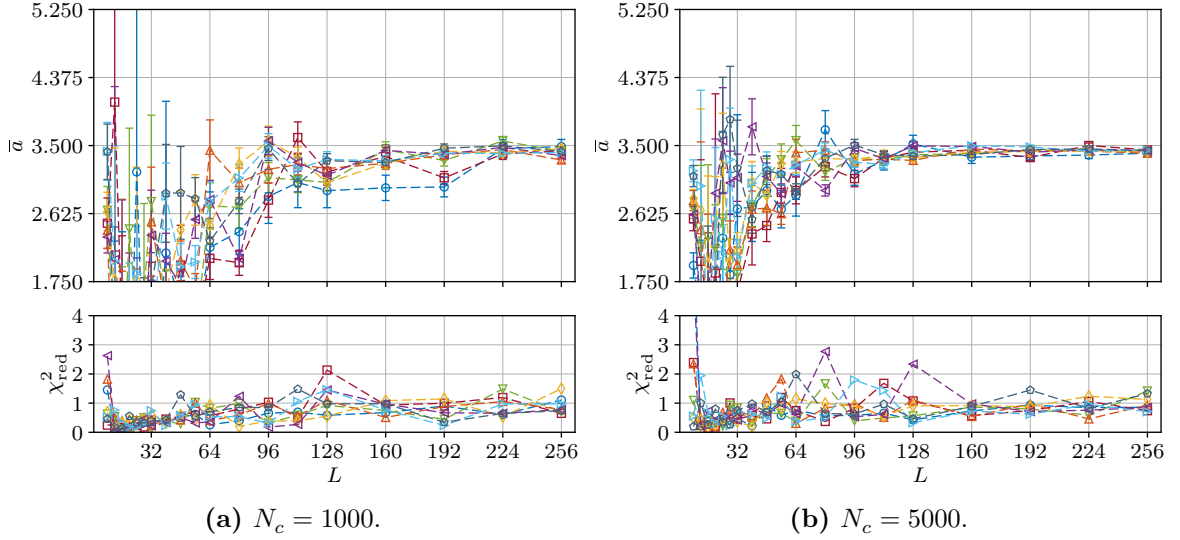
Figure 4.9: Comparison between the $\overline{a}(p_d, L)$ for $a = 3.5$ for different number of disorder realizations N_c. With larger N_c the statistics becomes better and the imposed a is reached already for smaller L.

4.3 Calculation of observables

In this section we will give a more detailed view of the calculation of the observables which were already introduced in Section 2.2.3. It includes the definition of the disorder averaging process and the extraction of observables at their corresponding finite-size critical temperatures (temperature of the peak for a finite L) through histogram reweighting. This section incorporates and extends larger parts the explanations given in the appendix of Ref. [KJ20].

4.3.1 Composed observables and disorder averaging

After we performed our simulations on N_c disorder realizations and made N measurements on each of them, we effectively have two-dimensional arrays of directly measurable observables for each parameter tuple (a, p_d, L) at each simulated temperature β_{sim}. All the directly measured observables were presented in Section 4.1. Let us first concentrate on the total energies E_i^c and total magnetizations M_i^c because these two observables are the building blocks for almost all observables which we studied in this work. Here, i is the thermal (time) index in the range $i \in 1, \dots, N$ and c is the disorder index in the rage $c \in 1, \dots, N_c$. We can derive observables $\mathcal{O}$ of the form of a product of powers of E and M,

$$\mathcal{O}_i^c = (E_i^c)^k (M_i^c)^l \,. \tag{4.10}$$

Note, that $\mathcal{O}_i^c$ is still a two-dimensional array with values for each i and each c. Taking the thermal average denoted by $\langle \cdot \rangle$, we get averaged observables for each disorder realization c,

$$\mathcal{O}^c = \langle \mathcal{O} \rangle = \frac{1}{N} \sum_{i=1}^{N} \mathcal{O}_i^c \,. \tag{4.11}$$

Finally, taking the disorder average denoted by $[\![\cdot]\!]$, we obtain

$$\mathcal{O} = [\![\langle \mathcal{O} \rangle]\!] = [\![\mathcal{O}^c]\!] = \frac{1}{N_c} \sum_{c=1}^{N_c} \mathcal{O}^c \,. \tag{4.12}$$

In Equations (4.11) and (4.12) we introduced clear notation without using the average brackets $\langle \cdot \rangle$ and $[\![\cdot]\!]$ for better readability. Please remember, that until stated otherwise, even $\mathcal{O}$ denotes a statistical average and not a true (theoretical) value.

Not every observable used in this work has the form presented in Equation (4.10). In particular, there are many observables like the susceptibility and specific heat, which are defined in terms of thermal averages in the first place. Let $\mathscr{P}$ denote a composite observable of the following general form

$$\mathscr{P}^c = f(\mathcal{O}_{(1)}^c, \mathcal{O}_{(2)}^c, \dots) \,, \tag{4.13}$$

where each individual $\mathcal{O}_{(k)}^c$ is a thermal average calculated with Equation (4.11) for one particular disorder realization c and the corresponding individual entries $\mathcal{O}_{(k)_i}^c$ fulfill the form of Equation (4.10). In this case, we have two different choices of placing the disorder average. The first possibility is to take the disorder average for each $\mathcal{O}_{(k)}^c$ separately, and plug everything into the compositing function f afterwards. In our notation this choice corresponds to

$$\boxed{\mathscr{P} = f\left([\![\mathcal{O}_{(1)}^c]\!], [\![\mathcal{O}_{(2)}^c]\!], \dots \right) \,,} \tag{4.14}$$

This definition was used in many works, e.g., Refs. [Bal+98a; BP99; Cha02; Cha14; Cha17; Iva+08; Pru+05], as mentioned in Section 2.2.3. It will also be the choice in the present work. However, there exist a second possibility which is to take the disorder average after applying f which corresponds to

$$\mathscr{P}^{\text{out}} = \left[\!\!\left[f\left(\mathscr{O}_{(1)}^c, \mathscr{O}_{(2)}^c, \dots \right) \right]\!\!\right] , \tag{4.15}$$

where the superscript "out" reminds us that the disorder average was taken outside the function f. This approach was favored in the following works: Refs. [Has+07; Vas+15; Wan+19], as mentioned in Section 2.2.3. We performed a short analysis of the differences between using Equation (4.14) and Equation (4.15) and can tell at this point: the difference between this two averaging processes is neglectable compared to the final error sizes in our study. Please note, that Equation (4.14) and Equation (4.15) can be equal if f is composed entirely of summations and multiplications of the individual $\mathscr{O}_{(k)}^c$ but in general, e.g., for ratios, they are not equal. As was already mentioned in Section 2.2.3, for the observables of interest in this work, the decision between the two disorder averaging placements were either unimportant due to their equality, e.g., χ, or arrived naturally from the definition of the observable, e.g., $\partial_\beta(\ln|m|)$.

4.3.2 Estimation of the errors through resampling

The final formula for getting an estimate of a composed observable out of directly measured quantities is Equation (4.14). However, it does not come with an error estimation a priori because all the measured E_i^c, M_i^c (and all other directly measurable observables) sum up to one and only final value $\mathscr{P}$. A way out of this problem is to us a resampling technique. We have already introduced the jackknife resampling in Section 3.4.1. Here, we would like to adopt it to our two-dimensional arrays of observables, e.g., E_i^c and M_i^c and explain our procedure of getting the final error estimates $\epsilon(\mathscr{P})$.

We will perform the resampling in two directions, the thermal direction (index j) and in disorder direction (index k). For each jackknife resampling step j in the thermal direction we leave out a block $J^j \subset \{1, \dots, N\}$ of measurements for each disorder realization c so that the thermal average defined through Equation (4.11) becomes

$$\langle \mathscr{O}^c \rangle^j = \frac{1}{N - |J^j|} \sum_{\substack{i=1 \\ i \notin J^j}}^{N} \mathscr{O}_i^c , \tag{4.16}$$

where $|J^j|$ is the number of left-out samples per disorder c. Analogously, for each resampling step k in the disorder direction we leave out a block $J^k \subset \{1, \dots, N_c\}$ of disorder realizations so that the disorder average defined through Equation (4.12) becomes

$$[\!\![\langle \mathscr{O} \rangle]\!\!]^k = \frac{1}{N_c - |J^k|} \sum_{\substack{c=1 \\ c \notin J^k}}^{N_c} \mathscr{O}^c . \tag{4.17}$$

where $|J^k|$ is the number of left-out realizations. We assume, that the left-out blocks J^j and J^k are chosen according to the general jackknife prescription discussed in Section 3.4.1. This implies the correct multiplicity to be able to divide the total length, N and N_c, into B parts without rejecting elements. A visualization of the blocks for both directions can be seen in Figure 4.10.
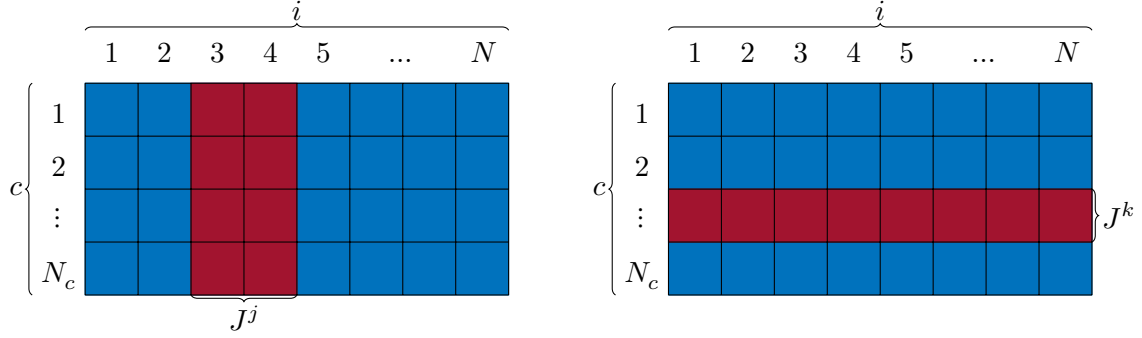
(a) Time direction jackknife resampling blocks. **(b)** Disorder direction jackknife resampling blocks.

Figure 4.10: Left-out jackknife blocks for a two-dimensional observable array $\mathcal{O}_i^c$. Each square represents one measured value at simulation time i for a disorder realization c. The blue region is taken into account while the red region is left out. Using the same number of blocks along the thermal direction i and disorder directions c ensures the same total sizes of the red regions. This is useful in order to compare the sizes of the error estimates for both directions. Adapted from Ref. [Jan08, Fig. 4.7].

Equipped with the modified thermal averages $\langle \mathcal{O}^c \rangle^j$ and disorder averages $[\![\langle \mathcal{O} \rangle]\!]^k$, respectively, we use the desired calculation of the final estimate, e.g., the composed observable estimate given through Equation (4.14), and repeat it for each jackknife block, i.e.,

$$(\mathscr{P})^j = f\left([\![\langle \mathcal{O}_{(1)}^c \rangle^j]\!] , [\![\langle \mathcal{O}_{(2)}^c \rangle^j]\!] , ... \right) , \tag{4.18}$$

$$(\mathscr{P})^k = f\left([\![\langle \mathcal{O}_{(1)}^c \rangle]\!]^k , [\![\langle \mathcal{O}_{(2)}^c \rangle]\!]^k , ... \right) . \tag{4.19}$$

From these two sets of estimates $(\mathscr{P})^j$ and $(\mathscr{P})^k$ we calculate the means and errors according to jackknife formulas provided in Section 3.4.1,

$$\overline{\mathscr{P}}^i = \frac{1}{N_j} \sum_{j=1}^{N_j} (\mathscr{P})^j , \quad \overline{\mathscr{P}}^c = \frac{1}{N_k} \sum_{k=1}^{N_k} (\mathscr{P})^k , \tag{4.20}$$

$$\epsilon(\mathscr{P})^i = \frac{N_j - 1}{N_j} \sum_{j=1}^{N_j} \left((\mathscr{P})^j - \overline{\mathscr{P}}^j \right)^2 , \quad \epsilon(\mathscr{P})^c = \frac{N_k - 1}{N_k} \sum_{k=1}^{N_k} \left((\mathscr{P})^k - \overline{\mathscr{P}}^k \right)^2 . \tag{4.21}$$

Finally, we combine the results to the estimate $\mathscr{P}$ and its error $\epsilon(\mathscr{P})$ in a standard way,

$$\overline{\mathscr{P}} = \frac{1}{2} \left(\overline{\mathscr{P}}^i + \overline{\mathscr{P}}^c \right) , \tag{4.22}$$

$$\epsilon(\mathscr{P}) = \sqrt{(\epsilon(\mathscr{P})^i)^2 + (\epsilon(\mathscr{P})^c)^2} . \tag{4.23}$$

We will compare the errors coming from both resampling directions and also their dependence on the number of jackknife blocks in Section 4.3.3 after we have introduced the critical temperature search procedure.

4.3.3 Calculation of the observables at finite critical temperatures

Histogram reweighting and minimization

So far, we have discussed the estimation of a composed observable $\mathscr{P}$ and its error $\epsilon(\mathscr{P})$. This can be done for any parameter tuple (a, p_d, L) and at any simulated temperature β_{sim}. However, in order to get an estimate of a particular observable at the corresponding finite-

size critical temperature (which is *L*-dependent for each individual observable because of the finite lattice sizes), we would like to use a single histogram reweighting technique. We already introduced it in Section 3.3. Here, we will present the procedure which include the jackknife resampling and analyze our reweighted observables before going to further analyses.

Let us first recall the final result from Section 3.3 which is suitable to reweight $\mathcal{O}^c$ defined through Equation (4.11) for each disorder realization *c*,

$$\text{Rew}(\mathcal{O})^c(\beta) = \frac{\sum_{i=1}^N \mathcal{O}_i^c e^{-(\beta - \beta_{\text{sim}})E_i^c}}{\sum_{i=1}^N e^{-(\beta - \beta_{\text{sim}})E_i^c}} \ . \tag{4.24}$$

We explicitly denote the per-disorder reweighting process with the index *c* in Equation (4.24). The disorder average is taken after the reweighting, analogous to Equation (4.12),

$$\text{Rew}(\mathcal{O})(\beta) = [\![\text{Rew}(\mathcal{O})^c]\!] \ . \tag{4.25}$$

Setting $\beta = \beta_{\text{sim}}$ in Equation (4.25) recovers $\mathcal{O}$ from Equation (4.12). For a composed observable of the form given in Equation (4.13), we proceed in analogy to Equation (4.14) and calculate the finial estimate as

$$\text{Rew}(\mathcal{P})(\beta) = f(\text{Rew}(\mathcal{O}_{(1)})(\beta), \text{Rew}(\mathcal{O}_{(2)})(\beta), \dots) \ , \tag{4.26}$$

where each $\text{Rew}(\mathcal{O}_{(1)})(\beta)$ is calculated through Equation (4.25). Equation (4.26) provides us with a continuous estimate $\mathcal{P}(\beta)$ within a valid reweighting range $\beta_{\text{sim}} - \Delta\beta_{\text{rew}} \leq \beta \leq \beta_{\text{sim}} + \Delta\beta_{\text{rew}}$. This functional form can be used to search for a maximum (minimum) of $\mathcal{P}(\beta)$. Let us assume that the finite-size scaling analysis of $\mathcal{P}(\beta)$ predicts a maximum $\hat{\mathcal{P}}$ at a certain temperature $\hat{\beta}$. Without loss of generality we assume a maximum of $\mathcal{P}(\beta)$, otherwise we transform $\mathcal{P} \to -\mathcal{P}$. In the thermodynamic limit $L \to \infty$ we expect $\hat{\beta} \to \beta_c$. We use an optimization routine from julia package `Optim.jl` [@Opt21] to solve for the pair $(\hat{\beta}, \hat{\mathcal{P}})$ of the minimization problem

$$\hat{\mathcal{P}} = \max_{\beta}(\text{Rew}(\mathcal{P})(\beta)) \ . \tag{4.27}$$

As in the calculation of the estimate $\mathcal{P}$ in Equation (4.14), Equation (4.27) will provide us only one final values $\hat{\mathcal{P}}$. By using the jackknife resampling technique in the same way as it was discussed in Section 4.3.2 (repeating Equation (4.27) for each jackknife block and taking the according averages), we get a final estimate $\overline{\hat{\mathcal{P}}}$ with its error $\epsilon(\hat{\mathcal{P}})$.

In the following, we will return to the symbol $\mathcal{O}$ which will denote a general observable (composed or not) and drop the notation with $\mathcal{P}$. Also note, that the finite-size critical temperature $\beta_c^{\mathcal{O}}$ for a particular observable $\mathcal{O}$ and the peak temperature $\hat{\beta}$ for the same observable are equal, i.e., $\beta_c^{\mathcal{O}} = \hat{\beta}$. We use one or the other notation depending on the context.

Finding the final peaks of observables

Now we are equipped with Equation (4.27), which provides us the maximum $\hat{\mathcal{O}}$ of a chosen observable $\mathcal{O}$ and the corresponding temperature $\hat{\beta}$. This can be done for each parameter tuple (a, p_d, L) and each simulation temperature β_{sim}. However, we still need to find the global maximum. For an infinite statistics, the peak temperatures $\hat{\beta}$ obtained by reweighting

from any β_{sim} would be equal, but in our case each data set from each β_{sim} will result in a different $\hat{\beta}$. In this work we proceeded in the following way. We first selected the three simulation temperatures β_{sim}^i with $i = 1, 2, 3$, for which the considered observable $\mathcal{O}$ calculated at β_{sim}^i was maximal. For this three temperatures we then performed a search according to Equation (4.27), with corresponding jackknife resampling. Out of these three final jackknifed estimates $\hat{\mathcal{O}}^i$ we then have taken the maximal $\hat{\mathcal{O}}^i$ to be our final peak estimate,

$$\hat{\mathcal{O}} = \max_i \hat{\mathcal{O}}^i \,, \tag{4.28}$$

and its corresponding temperature $\hat{\beta}^i$ to be the final critical temperature $\hat{\beta} = \hat{\beta}^i$. We show the process visually for a couple of chosen parameter tuples (a, p_d, L) in Figure 4.11.

Reweighted observables

Let us start to look into the actual observables which were studied in this work. We present the obtained peak values $\partial_\beta \widehat{(\ln|m|)}$, $\widehat{\partial_\beta(|m|)}$ and $\hat{\chi}$ in Figures 4.12 to 4.14, respectively. To overcome the large scale differences, we plotted the logarithm of the observables and rescaled the errors with $\epsilon(\hat{\mathcal{O}}) \to \epsilon(\hat{\mathcal{O}})/|\hat{\mathcal{O}}|$. All three considered observables show a very clear tendency in approaching a particular critical temperature β_c with increasing lattice size L. This will also be compared in more detail in Section 4.5.5. However, for the strongest correlation with $a = 1.5$, $\widehat{\partial_\beta(|m|)}$ and especially $\partial_\beta \widehat{(\ln|m|)}$, the temperature still changes significantly even for the largest lattice sizes. This probably means that such a strong correlation exponent can be analyzed properly only on even larger lattice sizes. Further, we notice that the susceptibility $\hat{\chi}$ shows only very weak dependence on the concentration p_d. Up to the different scaling, different subplots for different a of $\hat{\chi}$ look almost similar. One can see small differences only for small lattice sizes. We will analyze these observables in greater detail when we will come to the finite-size scaling procedure and the extraction of the critical exponents in Section 4.5.

Various comparisons and checks

Reweighting ranges checks   As was mentioned previously, we have to ensure that the found critical temperatures $\hat{\beta}$ for each considered observable $\mathcal{O}$ are close enough to the simulated temperatures. A quantitative measure for the validity of the reweighting procedure, the reweighting range $\Delta\beta_{\text{rew}}$, was introduced in Section 3.3. It is defined as

$$\Delta\beta_{\text{rew}} = \frac{1}{\sqrt{[\![\langle E^2\rangle]\!] - [\![\langle E\rangle^2]\!]}} \,, \tag{4.29}$$

where we now have added the disorder averaging. In order to compare the reweighting ranges for all different parameter tuples (a, p_d, L), we calculated the relative deviation of the found critical temperature $\hat{\beta}$ to the simulated temperature β_{sim} with respect to the reweighting range $\Delta\beta_{\text{rew}}$,

$$\frac{\left|\beta_{\text{sim}} - \hat{\beta}\right|}{\Delta\beta_{\text{rew}}} \,. \tag{4.30}$$

In Figure 4.15 we present the ratios defined in Equation (4.30) for $\partial_\beta(\ln|m|)$, $\partial_\beta(|m|)$ and χ. We see a general tendency of the ratios to become larger for larger lattice sizes and larger concentration of defects p_d as well as for smaller correlation exponents a. The majority of

(a) $\mathcal{O} = \partial_\beta(\ln|m|)$, $a = \infty$, $p_d = 0.2$, $L = 256$.

(b) $\mathcal{O} = \partial_\beta(\ln|m|)$, $a = 2.0$, $p_d = 0.2$, $L = 256$.

(c) $\mathcal{O} = \chi$, $a = \infty$, $p_d = 0.2$, $L = 256$.

(d) $\mathcal{O} = \chi$, $a = 2.0$, $p_d = 0.2$, $L = 256$.
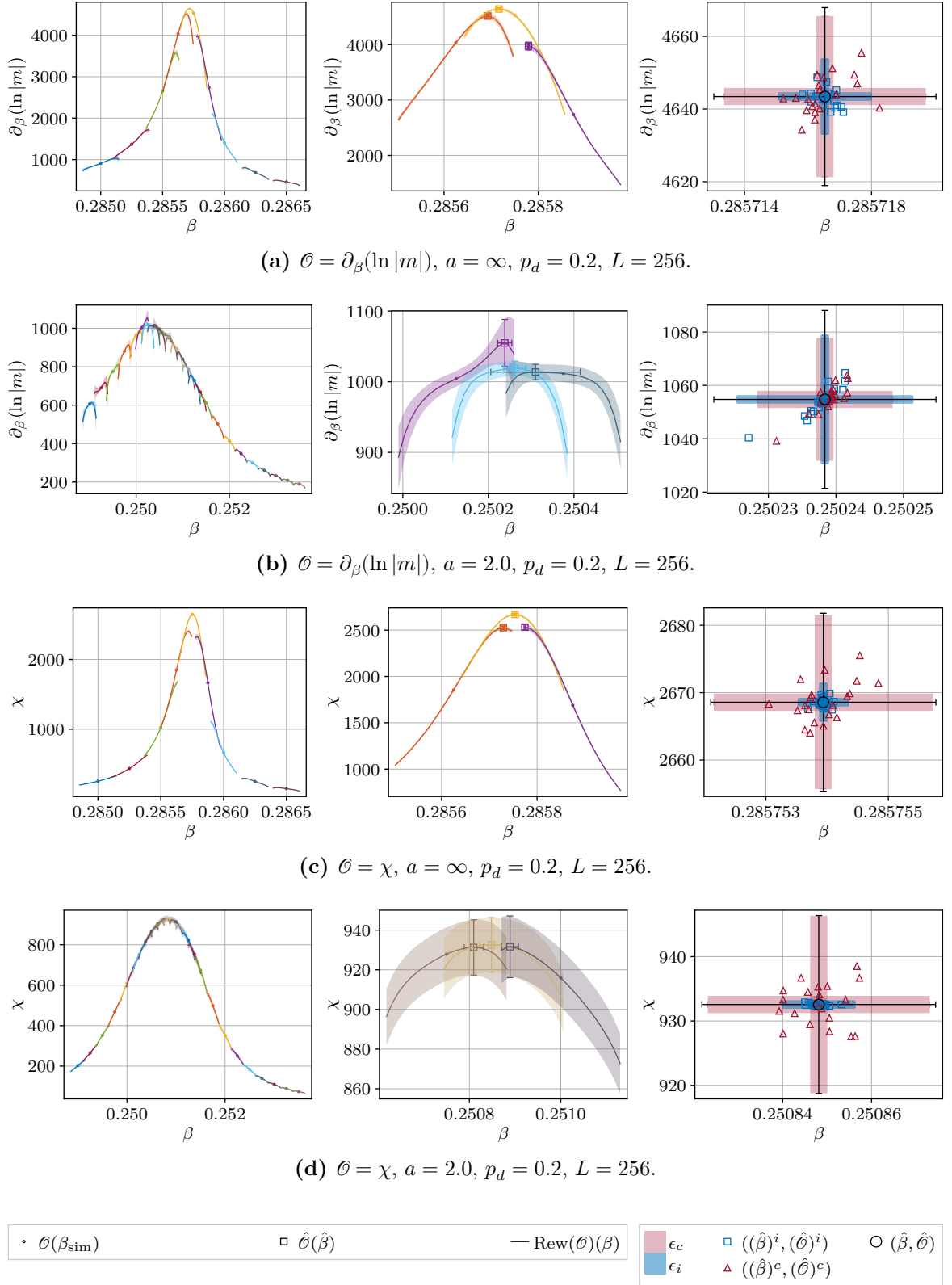
Figure 4.11: Example plots of the histogram reweighting curves and observables peak searches for various parameter tuples (a, p_d, L). The left subplots show the reweighted curves in the range $\beta_{\text{sim}} - 2\Delta\beta_{\text{rew}} \leq \beta \leq \beta_{\text{sim}} + 2\Delta\beta_{\text{rew}}$ for all simulated temperatures β_{sim}. In the middle subplots, the chosen three temperatures and the corresponding reweighting curves as well as the found peaks $(\hat{\beta}, \hat{\mathcal{O}})$ are zoomed in. The right subplots show the individual peaks for each jackknife resampled subset in the thermal and disorder directions for the finally chosen temperature β_{sim}. The ϵ_i and ϵ_c are thermal and disorder errors from the corresponding resampling direction, respectively. The total error is then calculated with Equation (4.23), i.e., $\epsilon = \sqrt{\epsilon_i^2 + \epsilon_c^2}$.

(a) $a = \infty$.

(b) $a = 3.5$.

(c) $a = 3.0$.

(d) $a = 2.5$.

(e) $a = 2.0$.

(f) $a = 1.5$.

	p_d						
⊙ 0.05	⊡ 0.1	▽ 0.15	△ 0.2	◇ 0.25	◁ 0.3	▷ 0.35	⊙ 0.4
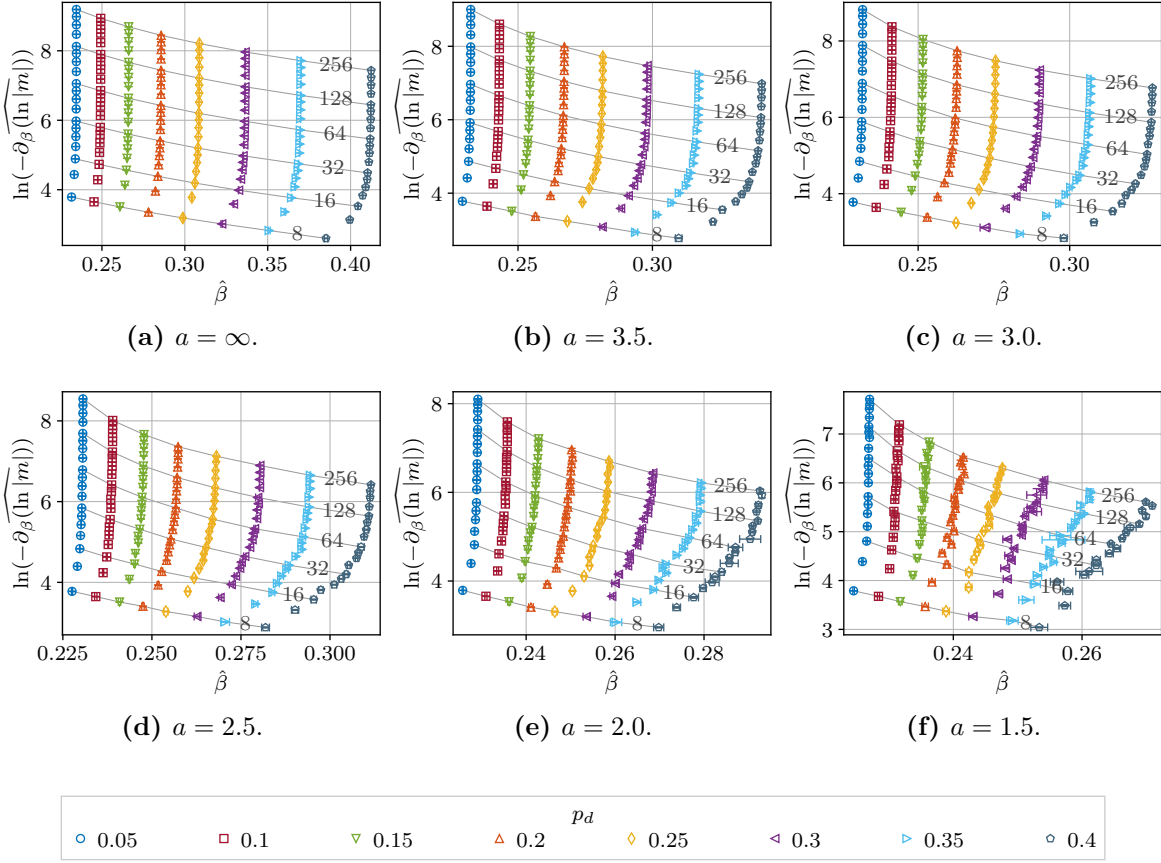
Figure 4.12: Observable peak values $\partial_\beta(\widehat{\ln|m|})$ at its corresponding peak temperatures $\hat{\beta}$ for all considered sizes L. For better readability, we draw connecting and annotated lines for some L between various concentrations of defects p_d. For all data points we plotted the scaled error $\epsilon(\partial_\beta(\widehat{\ln|m|}))/\partial_\beta(\widehat{\ln|m|})$ and as a horizontal error $\epsilon(\hat{\beta})$.

cases lie around and below a value of ≈ 1.0 while nearly all the ratios are smaller than ≈ 1.5. The largest ratios are at a value of ≈ 2.0 for the observable $\partial_\beta(\ln|m|)$. It is noticeable, that there are outliers and jumps in the behavior. This is not surprising as for all L for each particular parameter tuple (a, p_d) we used the same simulation temperatures with the same spacing, and there are lattice sizes for which the chosen simulation temperatures accidentally hit the correct critical temperatures better than for others. The ratio in Equation (4.30) only confirms the applicability of the reweighting technique and does not have a physical meaning. Considering that the rule of where the reweighting technique is valid, $\left|\beta_{\text{sim}} - \hat{\beta}\right| - \Delta\beta_{\text{rew}} \lessapprox 1$, is not rigor but only a "rule of thumb", we can conclude that most of our peaks were found in a valid reweighting range. Additionally, we expect our large thermal measurements number of $N = 10\,000$ to allow for reweighting further away from the simulated temperature without introducing too large systematic errors.

Comparison between the errors from thermal averages and disorder averages
We chose a total number of removed blocks in each direction to be equal $B = 20$. This sets $|J^j| = N/B = 500$ and $|J^k| = N_c/B = 50$ for our data sets. To systematically compare the errors for various parameter tuples (a, p_d, L), we will compare the errors calculated with Equation (4.21) for the thermal direction and the disorder direction as relative errors for
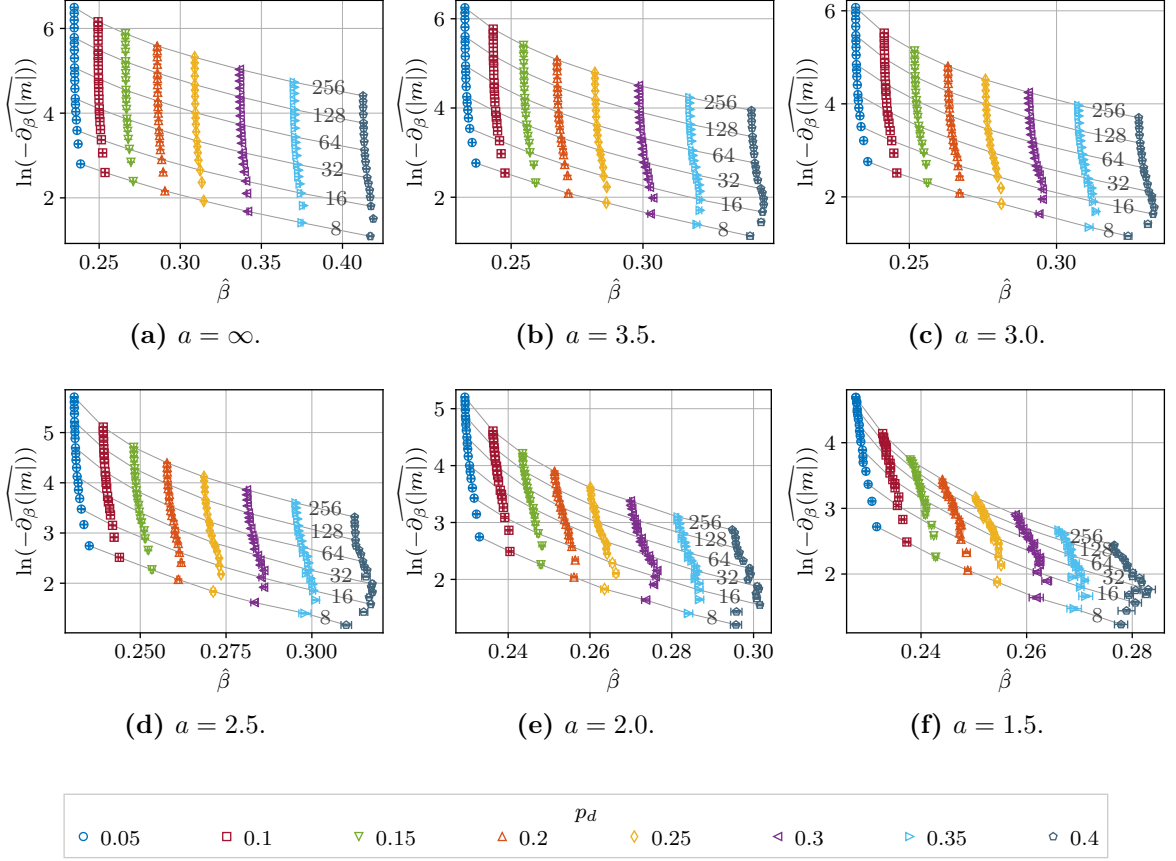
Figure 4.13: Observable peak values $\widehat{\partial_\beta(\widehat{|m|})}$ at its corresponding peak temperatures $\hat{\beta}$ for all considered sizes L. For better readability, we draw connecting and annotated lines for some L between various concentrations of defects p_d. For all data points we plotted the scaled error $\epsilon(\widehat{\partial_\beta(\widehat{|m|})})/\widehat{\partial_\beta(\widehat{|m|})}$ and as a horizontal error $\epsilon(\hat{\beta})$.

selected observables and their peak temperatures,

$$\epsilon_q^{\mathrm{rel}}(\hat{\mathcal{O}}) = \frac{\epsilon(\hat{\mathcal{O}})^q}{\overline{\hat{\mathcal{O}}}^q} , \tag{4.31}$$

$$\epsilon_q^{\mathrm{rel}}(\hat{\beta}) = \frac{\epsilon(\hat{\beta})^q}{\overline{\hat{\beta}}^q} , \tag{4.32}$$

where q is either i for the thermal direction resampling or c for the disorder direction and the means and errors are calculated through Equations (4.20) and (4.21), respectively. Since we also have the simulation temperature as one parameter, but we are mostly interested in the observations close to the critical temperature, we will compare the errors only at observed critical temperatures $\hat{\beta}$ of the corresponding observables for each parameter tuple (a, p_d, L).

We present the errors for $\partial_\beta(\ln|m|)$, $\partial_\beta(|m|)$ and χ in Figure 4.16. At the first glance, we see that the majority of the relative errors is below 0.01. The only exception is χ at $a \leq 2.0$. Further, the thermal average errors are smaller by a factor of ≈ 5 for almost all choices of (a, p_d, L). For the susceptibility χ, the factor is even around 10 or larger. This is not surprising, as we have measured long time series with $N = 10\,000$ compared to the moderate number of disorder realizations $N_c = 1000$. The reason for this choice was the possibility to perform histogram reweighting for each disorder realization separately which needs long-

(a) $a = \infty$.

(b) $a = 3.5$.

(c) $a = 3.0$.

(d) $a = 2.5$.

(e) $a = 2.0$.

(f) $a = 1.5$.
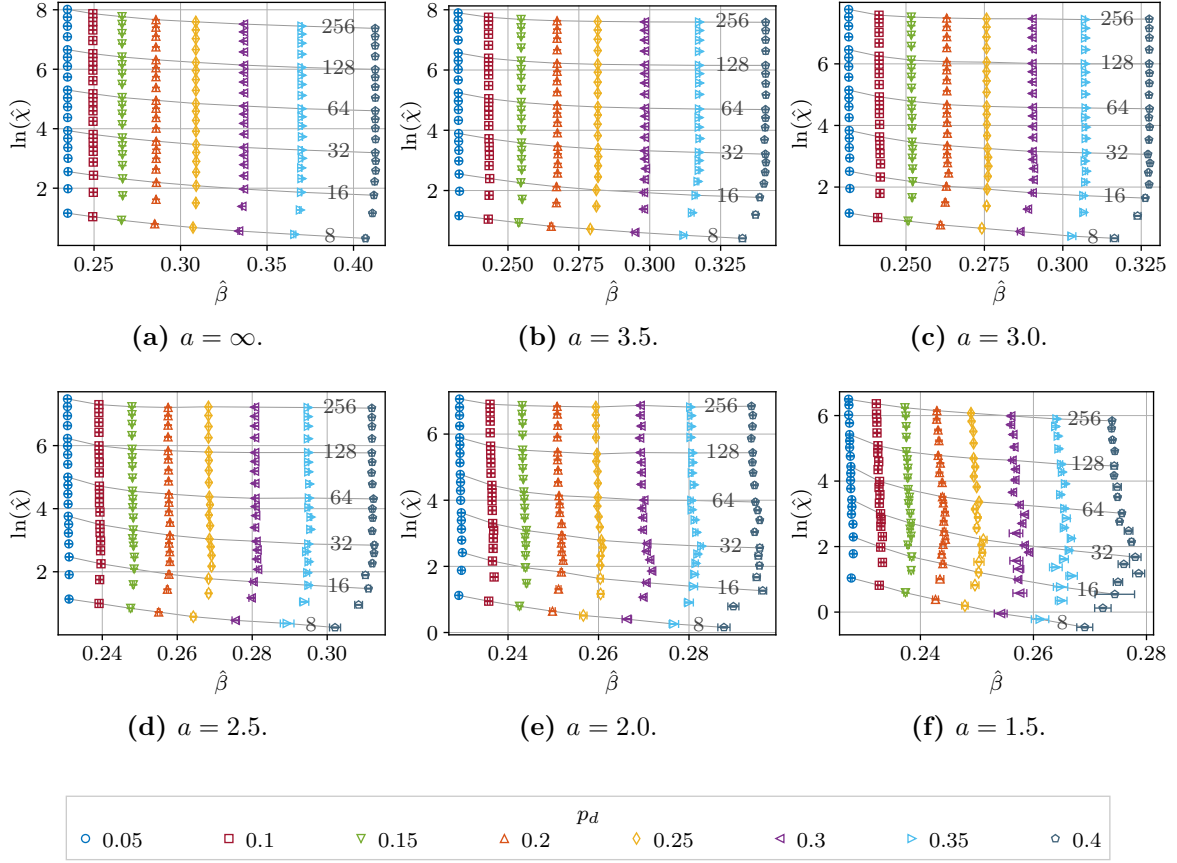
Figure 4.14: Observable peak values $\hat{\chi}$ at its corresponding peak temperatures $\hat{\beta}$ for all considered sizes L. For better readability, we draw connecting and annotated lines for some L between various concentrations of defects p_d. For all data points we plotted the scaled error $\epsilon(\hat{\chi})/\hat{\chi}$ and as a horizontal error $\epsilon(\hat{\beta})$.

enough data series to perform reasonably well. This choice is now reflected in the errors but allowed us to go further away from the simulated temperatures in the reweighting process. If one would omit the reweighting technique and only analyze the observables at simulated temperatures, probably a choice with $N_c \approx N$ would be better in order to equalize the errors from thermal and disorder fluctuations. However, for $\partial_\beta(\ln|m|)$, we see comparable error sizes for $a \leq 2.0$ starting at around $L \approx 128$. Therefore, for this particular strong correlation exponents and large L our choice was already a good compromise with respect to the total computational time.

Let us analyze the dependence of ϵ^{rel} on different parameters. First, there is only a small dependence on the lattice size L for the disorder averages but increasing L generally increases the thermal average errors slightly. Both dependencies are most pronounced for $\partial_\beta(\ln|m|)$. The weak dependence on L for the disorder averages is an indicator for non-self-averaging [LB05, p. 98]. A clear dependence on the correlation exponent a can be observed for all presented observables. Smaller a (stronger correlation) correspond to substantially larger errors, especially for χ. The same applies to the concentration of defects p_d, the errors increase slightly with increasing p_d, mostly pronounced in the case of χ. Both dependencies are not surprising since for larger p_d and for smaller a the variation between each disorder realization increases and therefore in principle one would need larger statistics to compensate

(a) $\mathcal{O} = \partial_\beta(\ln|m|)$.

(b) $\mathcal{O} = \partial_\beta(|m|)$.

(c) $\mathcal{O} = \chi$.
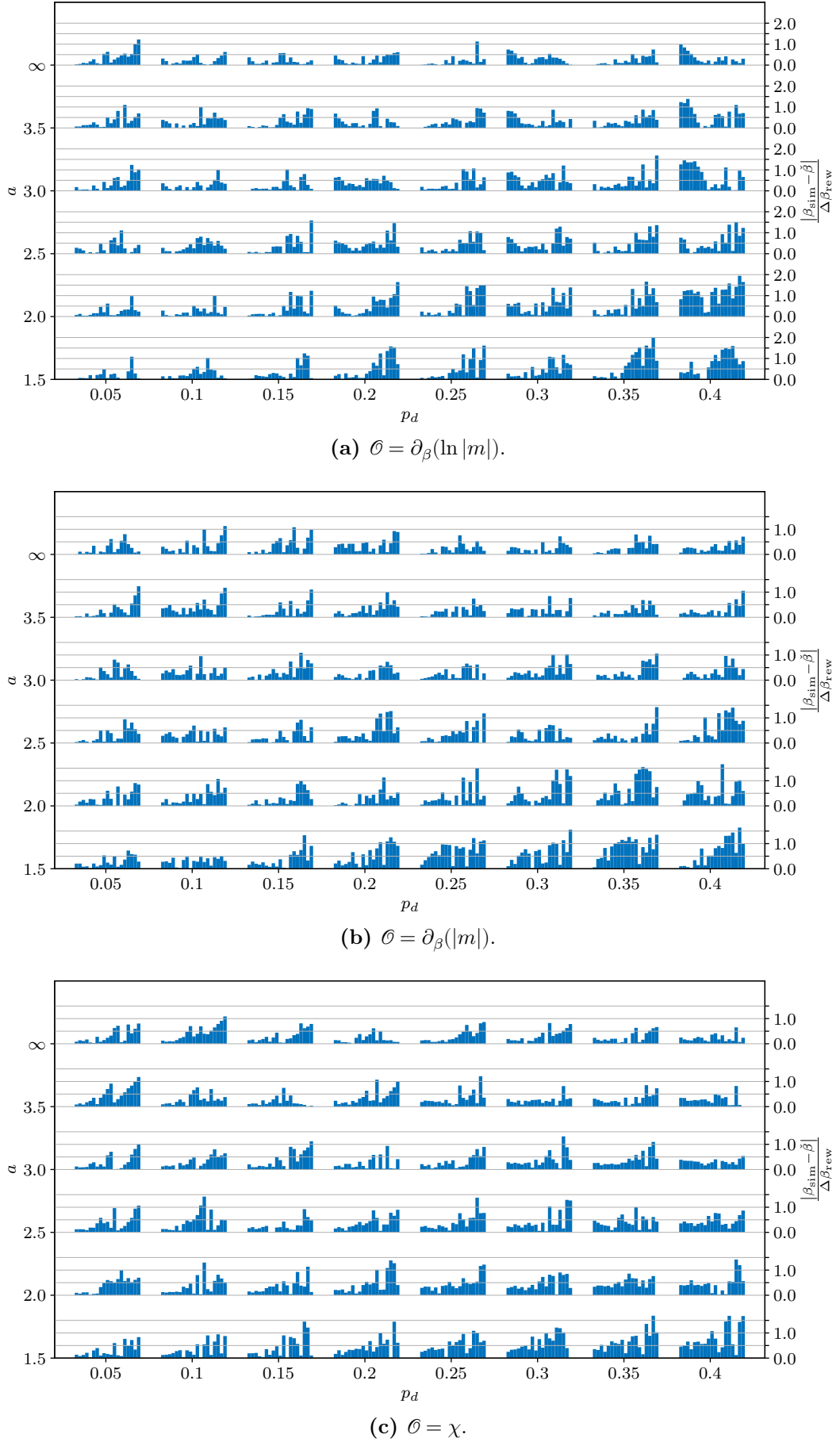
Figure 4.15: Relative ratio of the distance between found peak temperatures $\hat{\beta}$ and the simulated temperature β_{sim} and the reweighting range $\Delta\beta_{\mathrm{rew}}$ as defined in Equation (4.30) for different observables $\mathcal{O}$. For each pictogram, the lattice size increase from left to right from $L = 8$ to $L = 256$.

(a) $\mathcal{O} = \partial_\beta(\ln|m|)$.

(b) $\mathcal{O} = \partial_\beta(|m|)$.

(c) $\mathcal{O} = \chi$.

Legend: ϵ_c^{rel} ϵ_t^{rel} ▲ $\epsilon_c^{\text{rel}} > 0.03$ ▲ $\epsilon_t^{\text{rel}} > 0.03$
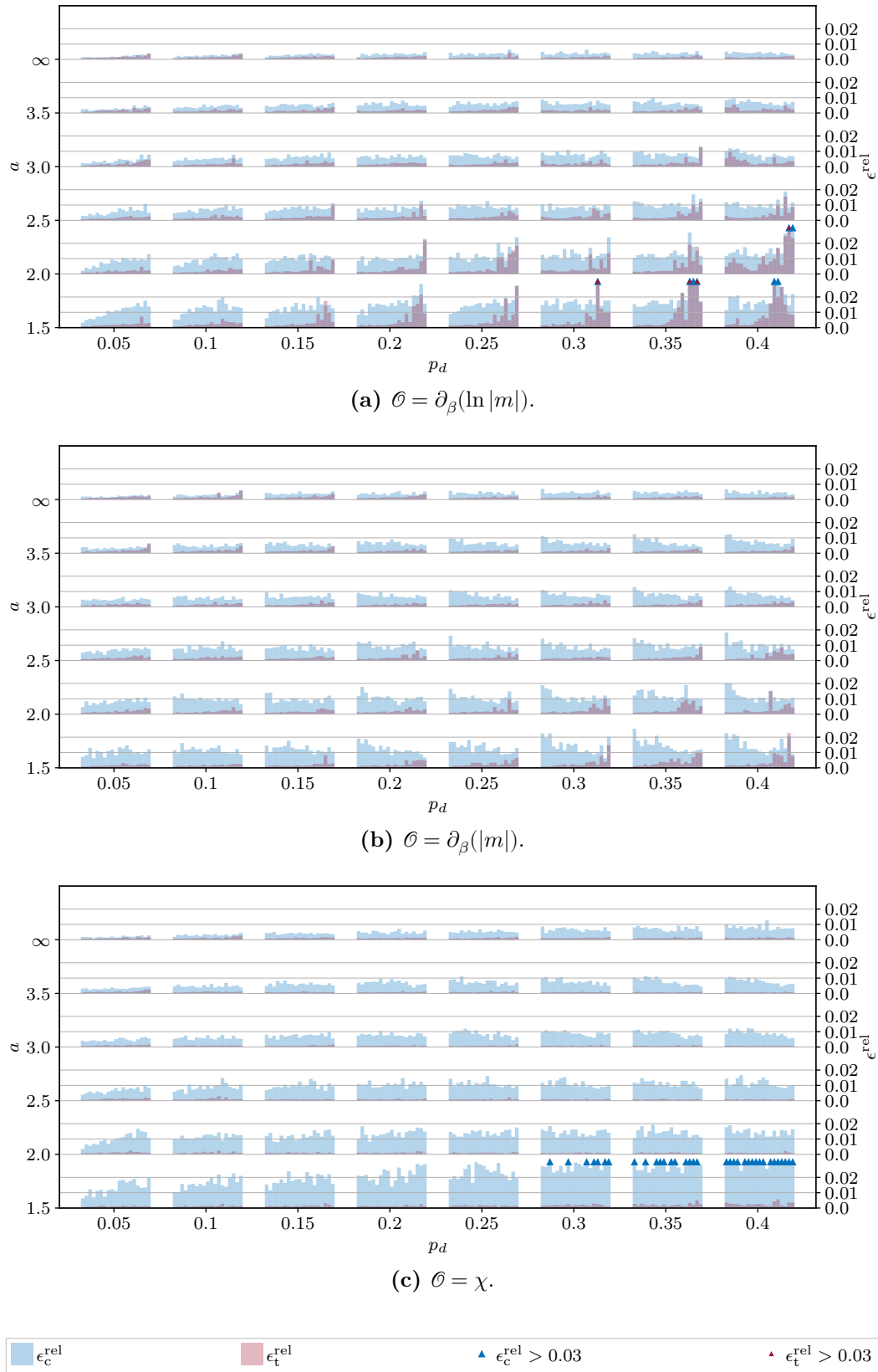
Figure 4.16: Comparison of relative errors coming from resampling in thermal direction, Equation (4.16), and disorder direction, Equation (4.17), for different observables $\mathcal{O}$ reweighted to their corresponding critical temperatures $\hat{\beta}$. For each pictogram, the lattice size increase from left to right from $L = 8$ to $L = 256$.

for this diversity. We have not done this step in this study, but it may improve the results for strong correlation case, e.g., $a = 1.5$, which comes with large errors in our analysis as we will see in Section 4.5.

Having discussed the errors of the observable peaks $\hat{\mathcal{O}}$, we move on to the corresponding peak temperatures $\hat{\beta}$. The thermal and disorder relative errors are shown in Figure 4.17, again for the three observables $\partial_\beta(\ln|m|)$, $\partial_\beta(|m|)$ and χ. Comparing the various plots in Figure 4.17, we can immediately confirm the same tendency with regard to the dependencies on correlation exponent a and concentration of defects p_d. For larger p_d and smaller a the relative errors increase. We also see a similar factor of ≈ 5 between the thermal and the disorder errors. However, the dependence on L is quite different. For small lattice sizes we observe large relative errors while with increasing L the errors decreases significantly and at least visually approach zero. This is a natural consequence of finite lattice sizes. The critical temperature does not increase with V as the corresponding observables do, but varies only slightly with increasing L. On the other hand, the smearing of the critical temperature peaks becomes less and less pronounced for increasing L and by this the relative error defined through Equation (4.32) decreases with increasing L. With maximum error sizes of up to ≈ 0.0003 for very small lattice sizes and $\lesssim 0.0002$ otherwise, we are in a good regime with regard to the relative errors.

Dependence of the errors on jackknife block numbers   In addition to the previous error analysis, we varied the number of jackknife blocks B to see the influence on the error sizes. As was discussed in Section 3.4.1, as long as the blocks along the thermal direction i are not too small, there should be no problems with the autocorrelation of observables and the jackknife technique therefore should give an estimator of the error of the mean correctly. In the direction of the disorder c, the correlation is absent by definition, so it is safe to remove arbitrary numbers of disorder realizations and the jackknife method should work. However, there will always be a dependence on the number of blocks in the estimators for finite data sets. Therefore, we tested whether our choice of $B = 20$ for each direction was sufficient for an accurate estimate. Due to computational efforts and the fact, that leaving larger blocks of data generally increased the chance of failing of the peak search procedure (maximization process, defined in Equation (4.27)), we restricted ourselves to the jackknife resampled observable $\partial_\beta(\ln|m|)$ at simulated temperature β_{sim}. We varied the number of jackknife blocks B and compared the relative deviations of the mean and its error to reference values for a chosen B^r,

$$\frac{\left|\overline{\mathcal{O}}^r - \overline{\mathcal{O}}\right|}{\left|\overline{\mathcal{O}}^r\right|} \quad \text{and} \quad \frac{\left|\epsilon(\mathcal{O})^r - \epsilon(\mathcal{O})\right|}{\left|\overline{\mathcal{O}}^r\right|}, \tag{4.33}$$

respectively. The r denotes estimates calculated for the reference choice of $B^r = 200$, where only five disorder realizations are left out at each jackknife resampling step. The distributions for all parameter tuples (a, p_d, L) for each B are presented in Figure 4.18. We see that the deviations of the means become smaller with larger B, which is not surprising since we approach the reference value B^r. But the relative deviations are small even for the smallest considered B. The choice of $B = 20$ leads to an average relative deviation of the means of $\approx 3.2 \cdot 10^{-5}$. The same tendency can be observed for the deviations of the errors. The average

(a) $\mathcal{O} = \partial_\beta(\ln|m|)$.

(b) $\mathcal{O} = \partial_\beta(|m|)$.

(c) $\mathcal{O} = \chi$.

$\epsilon_c^{\mathrm{rel}}$ $\epsilon_t^{\mathrm{rel}}$ $\blacktriangle$ $\epsilon_c^{\mathrm{rel}} > 0.003$ $\blacktriangle$ $\epsilon_t^{\mathrm{rel}} > 0.003$
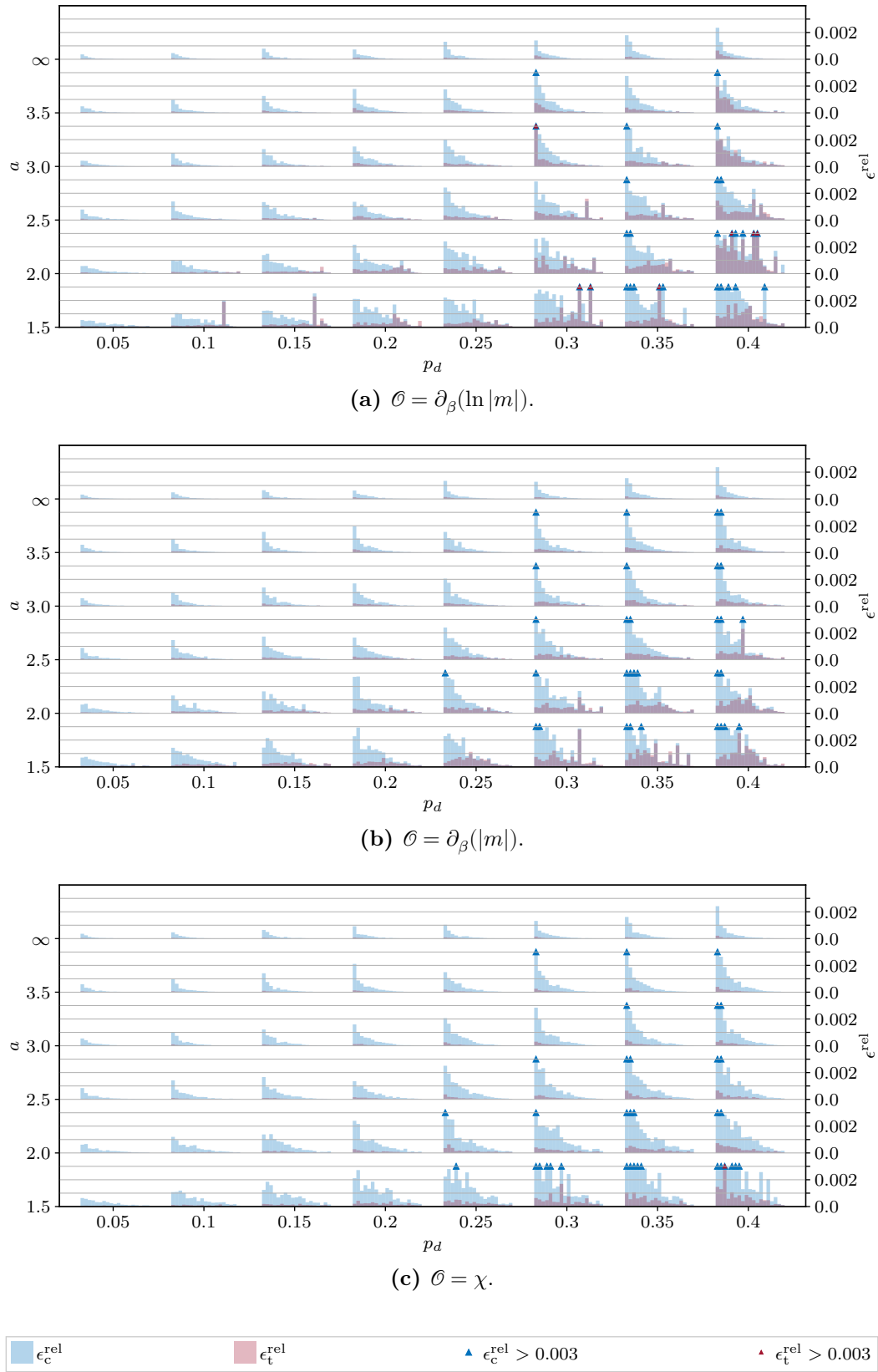
Figure 4.17: Comparison of relative errors coming from resampling in thermal direction, Equation (4.16), and disorder direction, Equation (4.17), for critical temperatures $\hat{\beta}$ for different observables $\mathcal{O}$. For each pictogram, the lattice size increase from left to right from $L = 8$ to $L = 256$.

deviation for $B = 20$ is $\approx 9 \cdot 10^{-4}$. Both relative deviations are very small and justify the choice of $B = 20$ as a sufficient number of blocks to reproduce the results for a much larger $B^r = 500$ quite well. The maximum deviations for the mean and the error estimates are not shown in Figure 4.18, but they lead to the same conclusion.
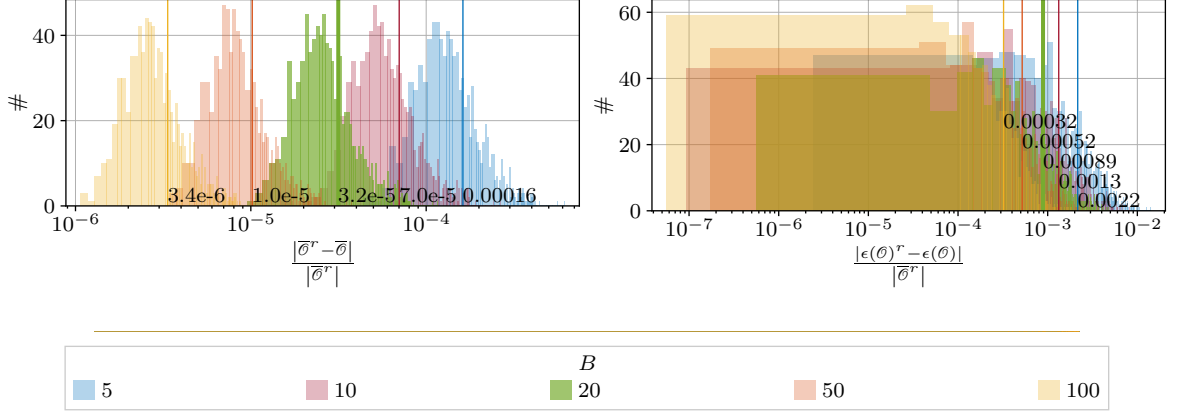
Figure 4.18: The distributions of the relative deviations of the means $\overline{\mathcal{O}}$ (left) and errors $\epsilon(\mathcal{O})$ (right) for all parameter tuples (a, p_d, L) and various jackknife block numbers B. The histograms are unnormalized to keep the heights constant. The x-axis is shown logarithmically, to overcome the large scales compared to the width of the histograms. The lines with numbers are the means for each B case.

Comparison between $\partial_\beta(\ln |m|)$ and $\partial_\beta U_2$ As we will discuss later, we used the derivative of the logarithm of the magnetization $\partial_\beta(\ln |m|)$ for the final estimates of the critical exponent ν. An alternative observable which yields the same critical exponent and can be used for this purpose is the derivative of the binder cumulant $\partial_\beta U_2$ (or $\partial_\beta U_4$), which we have introduced in Section 2.2.3. It was used, e.g., in [HPV99; Iva+08]. Our choice was guided mainly by our analysis strategy. We wanted to be able to reweight from one simulation temperature β_{sim} to other temperatures to be able to find the peaks of observables. But as it turned out, the observable $\partial_\beta(\ln |m|)$ was more stable with respect to the histogram reweighting procedure. This was especially noticeable for weak correlations and the uncorrelated cases. For temperatures further away from β_{sim}, the reweighted curves for $\partial_\beta U_2$ become unreliable much faster than for $\partial_\beta(\ln |m|)$ as can be seen in Figure 4.19. The $\partial_\beta(\ln |m|)$ curves have maximal values for each β_{sim} while the $\partial_\beta U_2$ often does not show a peak at all. This would mean that a manual intervention in the search procedure for the $\partial_\beta U_2$ observables is needed and more simulation temperatures are required, while it can be run automatically with fewer temperatures for $\partial_\beta(\ln |m|)$.

(a) $\mathcal{O} = \partial_\beta(\ln|m|)$, $a = \infty$.

(b) $\mathcal{O} = \partial_\beta(\ln|m|)$, $a = 3.0$.

(c) $\mathcal{O} = \partial_\beta(\ln|m|)$, $a = 2.0$.

(d) $\mathcal{O} = \partial_\beta U_2$, $a = \infty$.

(e) $\mathcal{O} = \partial_\beta U_2$, $a = 3.0$.

(f) $\mathcal{O} = \partial_\beta U_2$, $a = 2.0$.
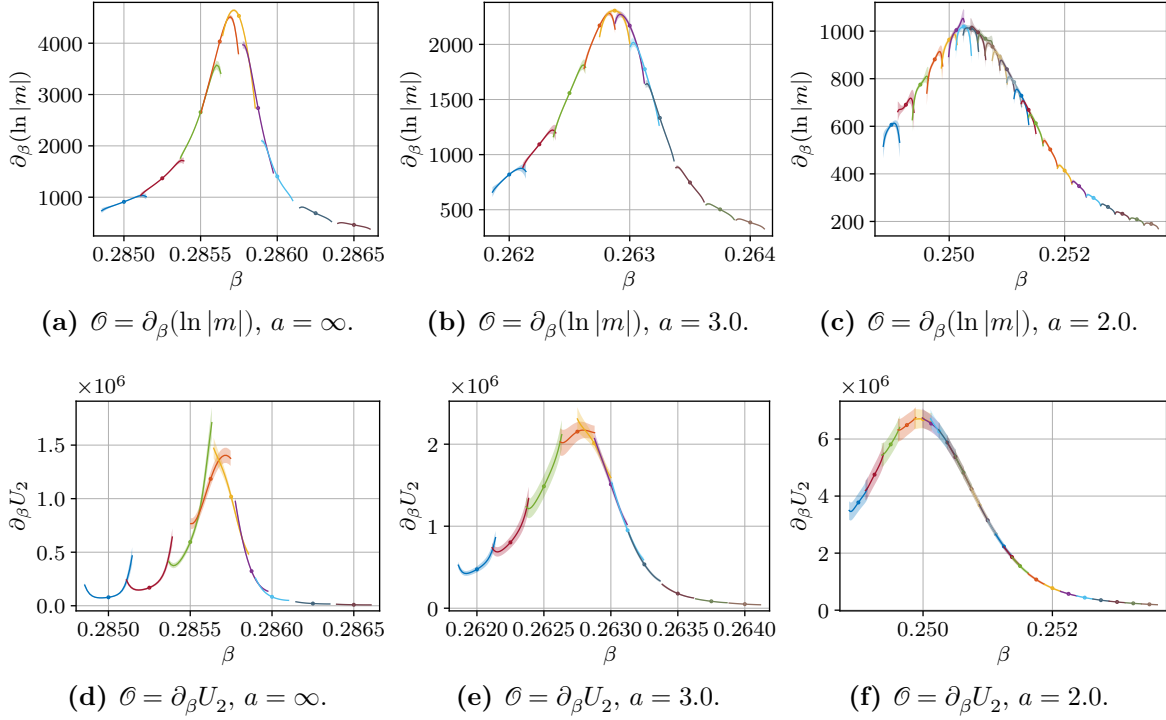
Figure 4.19: Comparison of the histogram reweighted curves for the observables $\partial_\beta(\ln|m|)$ and $\partial_\beta U_2$ for diffrent a and $p_d = 0.2$. One can see a smoother behavior of the curves for the $\partial_\beta(\ln|m|)$ n a wider range around β_{sim}.

4.4 Autocorrelation of observables

4.4.1 Theoretical treatment

In this section we analyze the temporal autocorrelation of observables, i.e., the correlation between an observable measured at different times, near the critical temperature, where the observables become more and more temporally correlated and lead to a smaller effective statistics. This behavior is known as the **critical slowdown** or **critical relaxation** [LB05, pp. 95 sqq.].

The following derivations are done for a measured time series for one disorder realization. At the end we will calculate the disorder averages. Assume we have a sequence of observables $\mathcal{O}_i$ with the total number of N, i.e., $1 \leq i \leq N$. We interpret the discrete number of the observation i as the time at which this observation was done. We define the normalized autocorrelation between two observables at different times i and $i+\Delta$ as [AM05, p. 500]

$$A_\mathcal{O}(\Delta) = \frac{\langle \mathcal{O}_i \mathcal{O}_{i+\Delta} \rangle - \langle \mathcal{O}_i \rangle \langle \mathcal{O}_{i+\Delta} \rangle}{\sigma^2(\mathcal{O})}, \tag{4.34}$$

with $\sigma^2(\mathcal{O}) = \langle \mathcal{O}^2 \rangle - \langle \mathcal{O} \rangle^2$ being the variance of the (uncorrelated) observable $\mathcal{O}$ and consequently with $A(0) = 1$. The Equation (4.34) leads to two definitions of relaxation times, namely the **integrated autocorrelation time** [AM05, p. 500]

$$\tau_{\mathrm{int}}^\mathcal{O} = \frac{1}{2} + \sum_{\Delta=1}^\infty A_\mathcal{O}(\Delta), \tag{4.35}$$

and the **exponential autocorrelation time** [AM05, p. 500]

$$\tau_{\exp}^{\mathscr{O}} = \lim_{\Delta \to \infty} \sup \frac{\Delta}{-\log |A_{\mathscr{O}}(\Delta)|} \,. \tag{4.36}$$

Note, that in the summation in Equation (4.35) the $\Delta = 0$ term is excluded. Hence, the minimum value for the integrated autocorrelation time is $1/2$. The integrated autocorrelation time is responsible for the increase of the errors of estimates obtained during Monte Carlo simulations [AM05, p. 500]. After some algebra it can be shown that the (true) error of an observable $\mathscr{O}$ is [Jan08, p. 103]

$$\epsilon^2(\mathscr{O}) = \left\langle \left(\overline{\mathscr{O}} - \langle \mathscr{O} \rangle \right)^2 \right\rangle \approx \frac{2\tau_{\mathrm{int}}^{\mathscr{O}}}{N} \left(\langle \mathscr{O}^2 \rangle - \langle \mathscr{O} \rangle^2 \right) \,. \tag{4.37}$$

This can be interpreted as an effective number of performed measurements,

$$N_{\mathrm{eff}} = \frac{N}{2\tau_{\mathrm{int}}^{\mathscr{O}}} \leq N \,. \tag{4.38}$$

On the other hand, the exponential autocorrelation time $\tau_{\exp}$ describes the time which is needed for the system to thermalize, i.e., reach an equilibrium state. In the further analysis we will concentrate on the integrated autocorrelation time τ_{int}.

When dealing with finite number of measurements which is always the case for a simulation, we need to be careful with Equation (4.35) since the values of $A(\Delta)$ become very noisy for large Δ. One possible overcome of this issue is to sum only the first $\hat{\Delta} < N$ values of A. This leads to a modified version of Equation (4.35)

$$\tau_{\mathrm{int}}^{\mathscr{O}} = \frac{1}{2} + \sum_{\Delta=1}^{\hat{\Delta}} A_{\mathscr{O}}(\Delta) \,, \tag{4.39}$$

The common way is to choose a self-consistent value $\hat{\Delta}$ such that

$$\hat{\Delta} \approx 6\tau_{\mathrm{int}}^{\mathscr{O}} \,. \tag{4.40}$$

However, we chose a different approach since we wanted to compare τ_{int} values for different a and p_d. First, we looked at the curves $\tau_{\mathrm{int}}^{\mathscr{O}}(\Delta)$ for all a, p_d and L and then chose a value $\hat{\Delta}$ for which a plateau was reached for all curves.

4.4.2 Autocorrelation analysis results

We considered $\mathscr{O} = E$ and $\mathscr{O} = |M|$ as the observables of interest as they were directly measured during the simulations. The absolute value for the magnetization was chosen to match the definitions of composed observables, e.g., Equations (2.39) and (2.44), which use the absolute values of the magnetization in order to overcome the averaging-to-zero for finite lattice sizes. As already mentioned, all presented autocorrelation times $\tau_{\mathrm{int}}^{\mathscr{O}}$ are disorder averages over all $N_c = 1000$ disorder realizations, i.e.,

$$\tau_{\mathrm{int}}^{\mathscr{O}} = [\![(\tau_{\mathrm{int}}^{\mathscr{O}})^c]\!] \,, \tag{4.41}$$

where $(\tau^{\mathcal{O}}_{\text{int}})^c$ is the autocorrelation time measured for one particular disorder realization c. The simulation temperatures for which we calculated the autocorrelation times are the ones which were finally used for the estimation of the peaks of the derivative of the logarithm of the magnetization $\partial_\beta(\ln|m|)$ in Section 4.3.3. Therefore, they are quite close to the critical temperature of the system. The curves $\tau^{\mathcal{O}}_{\text{int}}(\Delta)$ calculated according to Equation (4.39) for all parameter tuples (a, p_d, L) are shown in Figure 4.20. We can clearly see that a plateau value is reached for all cases at a value of $\hat{\Delta} \approx 100$. This will be our fixed value for all following comparisons. The first observation is that the autocorrelation time of the magnetization is slightly smaller than that of the energy. With the mean values taken over all parameter tuples (a, p_d, L), we get the values $\overline{\tau^E_{\text{int}}} = 4.3(22)$ and $\overline{\tau^M_{\text{int}}} = 2.9(19)$. Autocorrelation times which are larger than the mean occur less frequently than times which are smaller than the mean. This is also reflected in the median values which are $\text{md}\left(\tau^E_{\text{int}}\right) = 3.6$ and $\text{md}\left(\tau^M_{\text{int}}\right) = 2.4$ and lie below the corresponding means. At first glance, these numbers are reasonably small, but we will come to the interpretation at the end of this section.

(a) $\mathcal{O} = E$.

(b) $\mathcal{O} = |M|$.
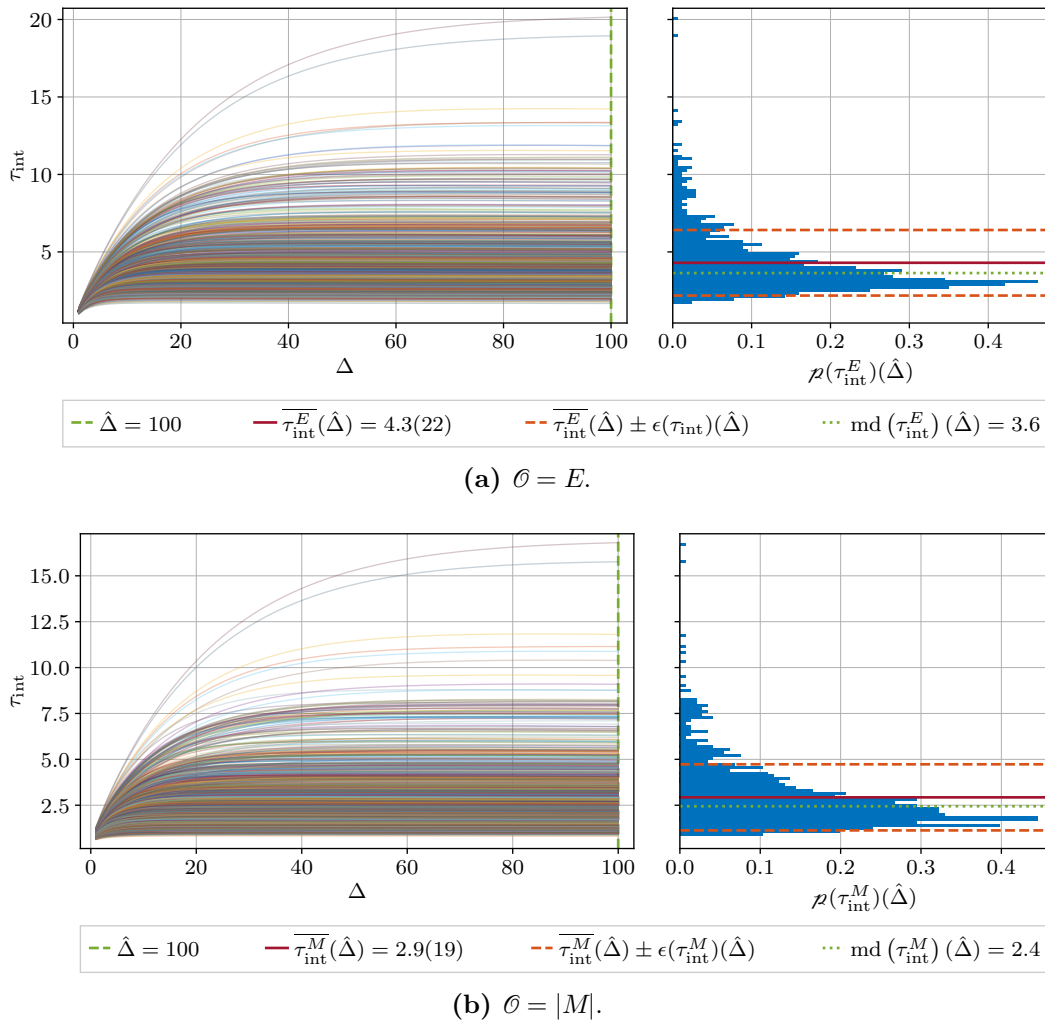
Figure 4.20: Integrated autocorrelation time curves $\tau^{\mathcal{O}}_{\text{int}}(\Delta)$ for the energy E and the magnetization $|M|$ and for all parameter tuples (a, p_d, L). One clerly sees that a plateau value is reached in all cases at $\hat{\Delta} = 100$. The histogram on the right shows the distribution of the times.

Let us take a deeper look into the dependence of $\tau_{\text{int}}^{\mathscr{O}}$ on the different parameters. In Figures 4.21 and 4.22 we present all autocorrelation times for the chosen $\hat{\Delta} = 100$. The following observations will hold for both considered observables, i.e., E and $|M|$, the only difference is that for the magnetization the values are slightly smaller than for the energy, in accordance to the total means. Therefore, we will not distinguish between the observables in the text below. We can analyze the dependence on each parameter separately. Let us start with the correlation exponent a. The general tendency is that for stronger correlations (lower a) we see smaller autocorrelation times. The general dependence on the concentration of defects p_d is very strongly pronounced. With increasing concentration of defects the autocorrelation time decreases. Concerning the lattice size L we observe an increase in the time for larger lattice sizes. The effect can be best seen at $p_d = 0.05$ and $a = \infty$ but persists for all other parameter combinations except for the magnetization at $a \leq 2.0$ and $p_d \leq 0.1$, where the time slightly decreases with increasing lattice size.
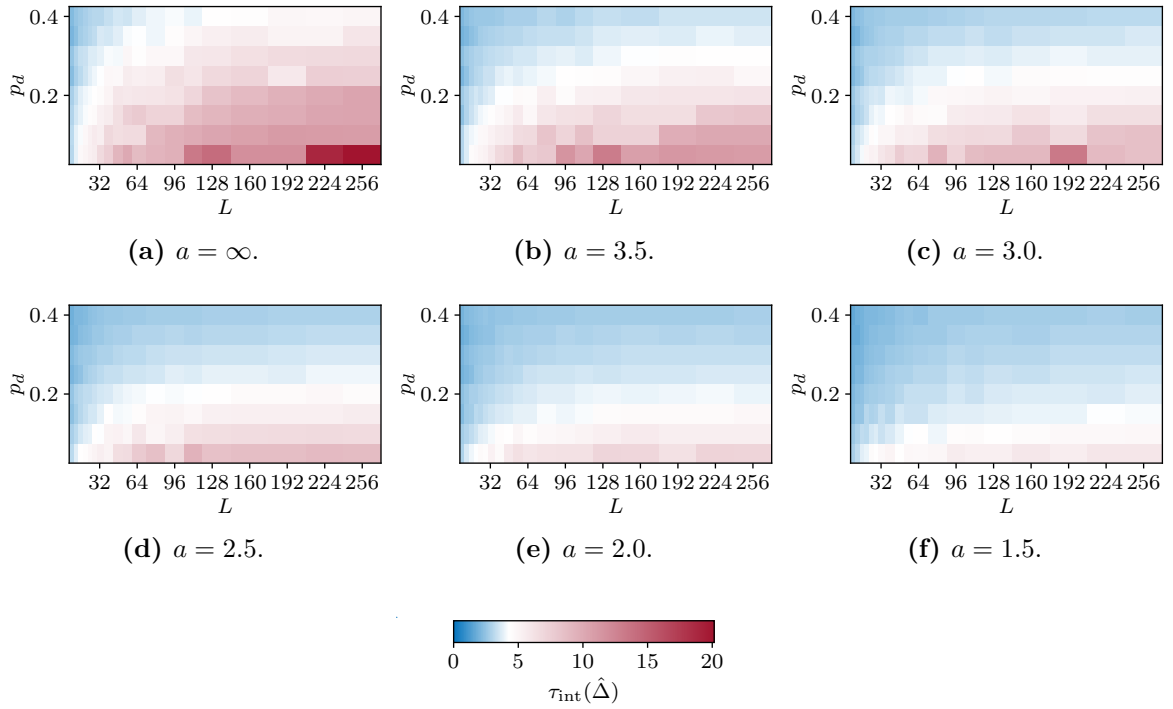
Figure 4.21: Integrated autocorrelation times $\tau_{\text{int}}^E(\hat{\Delta})$ with $\hat{\Delta} = 100$ for all parameter tuples (a, p_d, L). The white color in the colorbar is set to the mean value $\overline{\tau_{\text{int}}^E}$.

Let us follow the worst-case scenario and study the autocorrelation times at $L = 256$ which are mostly the largest for all a and p_d. We show the values in Figure 4.23. For comparison, also the values for the lattice size $L = 64$ are shown. The dependencies on a and p_d can be seen even clearer in these plots. The next observation is that the edge case of $a = \infty$ and $p_d = 0.05$ and $L = 256$ clearly shows spiking values. Excluding this case halves down the maximum autocorrelation time for both considered observables. It is an important fact since we mostly excluded the lowest concentration of $p_d = 0.05$ anyway due to the crossover regime with the pure Ising model.
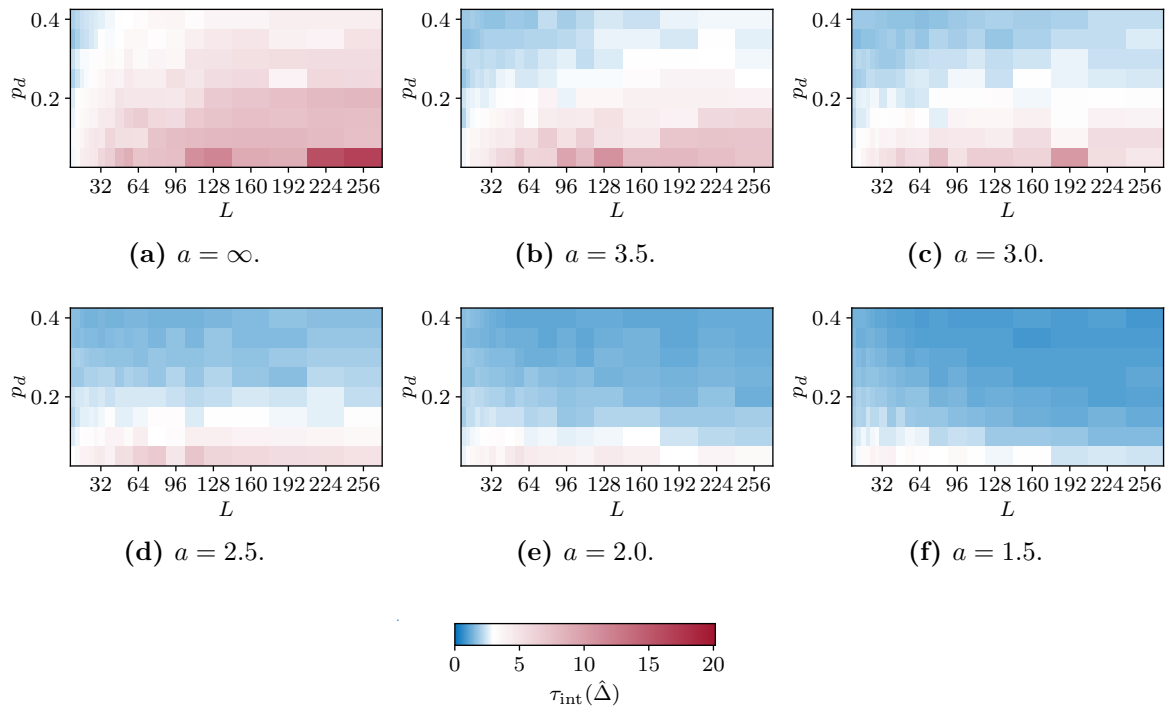
Figure 4.22: Integrated autocorrelation times $\tau_{\mathrm{int}}^M(\hat{\Delta})$ with $\hat{\Delta} = 100$ for all parameter tuples (a, p_d, L). The white color in the colorbar is set to the mean value $\overline{\tau_{\mathrm{int}}^M}$.

Finally, we also took a look on the temperature dependence of the autocorrelation times. We present the curves in Figure 4.24. To achieve better comparability, we plotted the times not against the simulated temperature β_{sim}, but against the reduced temperature $t = (1 - \beta_c/\beta_{\mathrm{sim}})$ with critical temperatures which we will discuss in Section 4.5.5. We have chosen two different cases, $a = \infty$ and $a = 2.0$ and the lattice size $L = 256$. First of all, in the uncorrelated case the maximum of the autocorrelation time is very close to $t = 0$, as expected. We see a very fast decrease in the times when going away from $t = 0$ in both directions. Contrarily, the autocorrelation time does not show a clear peak for the case of $a = 2.0$ and going to the region $t > 0$ tends to further increase the autocorrelation times. The reason for this dependence remains unclear to us. Possibly, it is due to larger spread in the critical temperatures of the individual disorder realizations which causes such averaged autocorrelation times to appear.

We would like to discuss the consequences of the results presented above. As can be seen in Equation (4.38), theoretically the autocorrelation time reduces the effective number of performed measurements. However, the factor of $2\tau_{\mathrm{int}}^{\mathcal{O}}$ depends on the considered observable. Since we mostly studied observables which were composed of various M and E combinations, we expect their autocorrelation times to be smaller than that of the pure observables. Additionally, the errors coming from disorder averaging were approximately 5–10 times larger than the thermal fluctuation errors which are effected by the autocorrelation time presented here. See Figure 4.16 for the comparison of the errors. Finally, we mainly used the histogram reweighted observables to find their maximum values and used the jackknife resampling tech-

p_d	$a=\infty$	3.5	3.0	2.5	2.0	1.5
0.4	3.8	2.9	2.8	2.7	2.6	2.5
	4.3	3.2	3.1	3.0	2.9	2.7
0.3	4.5	3.6	3.5	3.2	3.0	2.9
	5.4	4.0	4.0	3.5	3.4	3.1
0.2	6.0	4.6	4.1	4.1	3.7	3.4
	7.9	4.9	4.7	4.5	3.9	3.5
0.1	6.7	6.8	5.6	5.9	4.5	4.4
	8.8	7.6	7.2	7.9	6.1	4.8

(a) $L = 64$, $\mathcal{O} = E$.

p_d	$a=\infty$	3.5	3.0	2.5	2.0	1.5
0.4	5.0	3.5	3.2	2.9	2.9	2.8
	6.1	3.8	3.6	3.2	3.1	3.0
0.3	6.9	4.4	3.9	3.6	3.3	3.3
	7.5	4.9	4.4	4.1	3.7	3.6
0.2	10.0	6.2	5.3	4.6	4.0	3.8
	10.0	8.3	6.5	5.7	4.8	4.2
0.1	11.0	10.0	8.5	6.7	5.5	4.9
	20.0	11.0	8.5	8.8	7.2	6.1

(b) $L = 256$, $\mathcal{O} = E$.

p_d	$a=\infty$	3.5	3.0	2.5	2.0	1.5
0.4	3.3	1.8	1.7	1.4	1.1	0.92
	3.5	2.1	1.8	1.6	1.3	1.0
0.3	3.4	2.3	2.2	1.6	1.3	1.2
	4.3	2.5	2.5	1.9	1.7	1.4
0.2	4.8	3.1	2.5	2.5	1.9	1.7
	6.6	3.3	3.0	2.8	2.1	1.8
0.1	5.2	5.2	4.0	4.3	2.7	2.7
	7.2	6.1	5.6	6.3	4.5	3.2

(c) $L = 64$, $\mathcal{O} = |M|$.

p_d	$a=\infty$	3.5	3.0	2.5	2.0	1.5
0.4	4.2	2.8	2.3	1.6	1.2	0.84
	5.1	2.7	2.5	1.8	1.2	0.88
0.3	5.5	2.8	2.3	1.9	1.3	0.98
	5.6	3.0	2.5	2.0	1.4	1.1
0.2	8.2	4.0	3.1	2.2	1.3	1.1
	7.7	6.0	3.8	3.1	1.9	1.2
0.1	7.6	7.2	5.5	3.5	2.1	1.6
	17.0	7.3	4.7	5.1	3.4	2.4

(d) $L = 256$, $\mathcal{O} = |M|$.

$$0 \quad 5 \quad 10 \quad 15 \quad 20$$
$$\tau_{\text{int}}(\hat{\Delta})$$

Figure 4.23: Integrated autocorrelation time $\tau_{\text{int}}^{\mathcal{O}}$ for lattice sizes $L = 64$ and $L = 256$ for the energy E and the magnetization $|M|$. The errors of the times arising from the disorder averageing are much lower than the precision shown here.

nique to estimate the fluctuations. This should further decrease the autocorrelation time. These three facts let us assume that we can neglect the autocorrelation times in our further analyses without dramatic issues.

Summary. We presented the steps to calculate the integrated autocorrelation time for a series of observables measured during a simulation process. The autocorrelation times were obtained for all parameter tuples (a, p_d, L), and we studied their dependence on each of the parameters. Finally, we argued that from the performed analysis we may conclude that the autocorrelation between the observables can be neglected in our further analyses.

(a) $a = \infty$, $\mathcal{O} = E$.

(b) $a = 2.0$, $\mathcal{O} = E$.

(c) $a = \infty$, $\mathcal{O} = |M|$.

(d) $a = 2.0$, $\mathcal{O} = |M|$.

p_d

○ 0.05   ⊟ 0.1   ▽ 0.15   △ 0.2   ◇ 0.25   ◁ 0.3   ▷ 0.35   ○ 0.4
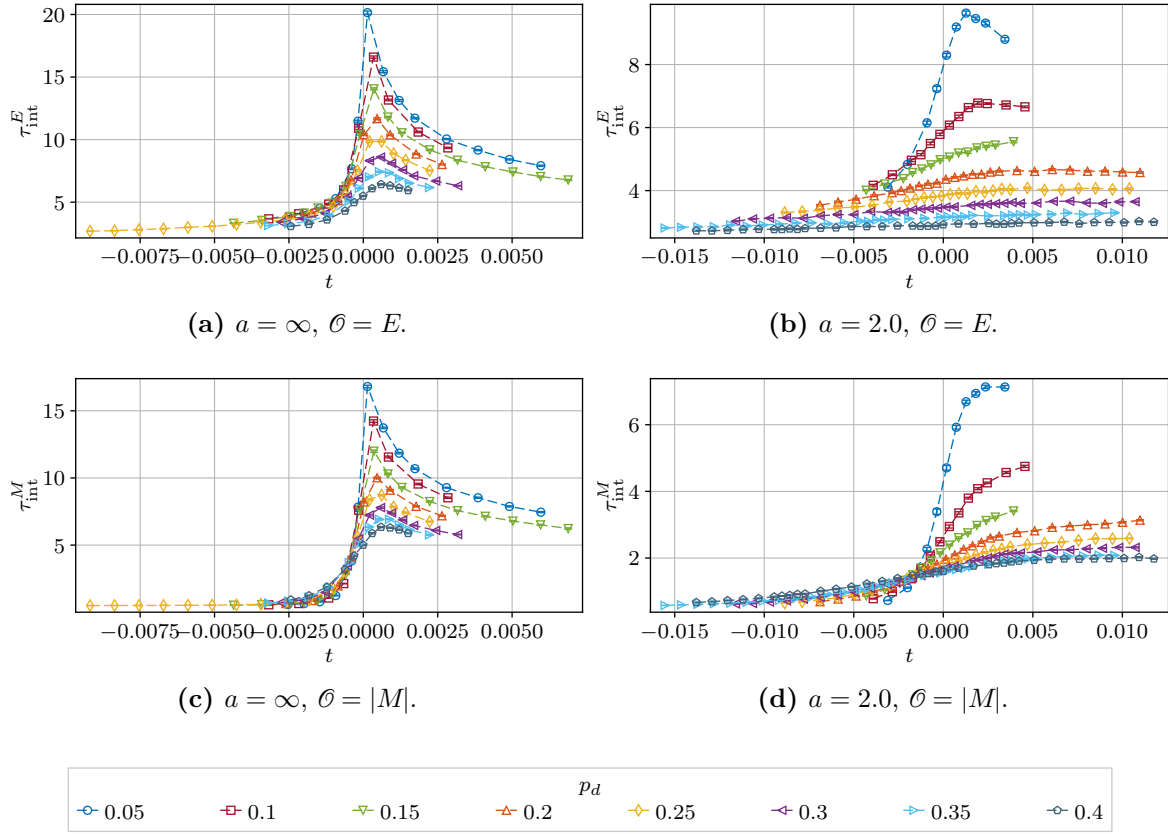
Figure 4.24: The dependence of the integrated autocorrelation time $\tau_{\text{int}}^{\mathcal{O}}$ on the reduced temperature t for chosen correlation exponents a and $L = 256$ for the energy E and the magnetization $|M|$. A clear peak at $t = 0$ can be observed for the uncoreated case with $a = \infty$ but for the coreated case with $a = 2.0$ the region $t > 0$ still shows larger times.

4.5 Finite-size scaling analysis

4.5.1 Confluent correction exponent ω

Quotient method

For the determination of the confluent correction exponent ω we used the **Quotient Method** [Car+95]. It was successfully used in various works, e.g., Refs. [Bal+98a; Bal+98b; FM16] and is described in detail in [AM05, p. 475]. Its main idea consists of canceling out the leading order terms in the finite-size scaling relation of an observable $\mathcal{O}$ by taking a ratio of $\mathcal{O}$ at different lattice sizes. We begin by defining a quotient $Q_{\mathcal{O}}$ of an observable $\mathcal{O}$ at two different lattice sizes L and sL where s is an arbitrary positive (integer) factor,

$$Q_{\mathcal{O}}(L) = \frac{\mathcal{O}(sL, \beta_c^{\mathcal{O}}(sL))}{\mathcal{O}(L, \beta_c^{\mathcal{O}}(L))} \ . \tag{4.42}$$

Each observable is taken at its finite-size critical temperature $\beta_c^{\mathcal{O}}(L)$ and $\beta_c^{\mathcal{O}}(sL)$, respectively. If the observable $\mathcal{O}$ is expected to have a peak at the critical temperature, then $\beta_c^{\mathcal{O}}(L)$ and $\beta_c^{\mathcal{O}}(sL)$ are the finite temperatures where these peaks will occur. Assume, that the finite-size behavior of $\mathcal{O}$ up to the first-order corrections is given by,

$$\mathcal{O}(L) = AL^{x_{\mathcal{O}}/\nu}(1 + BL^{-\omega} + ...) \ , \tag{4.43}$$

where $x_{\mathcal{O}}$ is the critical exponent of $\mathcal{O}$. Inserting Equation (4.43) into Equation (4.42) we immediately see the finite-size behavior of Q [AM05, p. 477],

$$
\begin{aligned}
Q_{\mathcal{O}}(L) &= \frac{A(sL)^{x_{\mathcal{O}}/\nu}\left(1 + B(sL)^{-\omega} + ...\right)}{AL^{x_{\mathcal{O}}/\nu}\left(1 + BL^{-\omega} + ...\right)} \\
&= s^{x_{\mathcal{O}}/\nu} + B'L^{-\omega} + ... ,
\end{aligned}
\tag{4.44}
$$

where in the last step we have omitted all higher order terms in $L^{-\omega}$ and combined the coefficients to a constant B'. Note, that the amplitudes A and B are equal for $\mathcal{O}(L)$ and $\mathcal{O}(sL)$ since we are at critical temperatures for each of the lattice sizes. With the help of Equation (4.44) we can determine the correction exponent ω independently of $x_{\mathcal{O}}$, since

$$
C = s^{x_{\mathcal{O}}/\nu} ,
\tag{4.45}
$$

is constant with respect to L.

Analysis

In our work we chose the derivative of the logarithm of the magnetization $\partial_{\beta}(\ln|m|)$ to calculate the ratios. It was defined in Equation (2.44). In Section 4.3.3 we calculated the peaks of this observable $\partial_{\beta}\widehat{(\ln|m|)}$ for all parameter tuples (a, p_d, L). We will use these values to get the quotients $Q_{\partial_{\beta}(\ln|m|)}(L)$. Since the critical exponents are independent of the concentration of defects p_d in the thermodynamic limit, we can use a global fit procedure and include all p_d for every considered correlation strength a into one fit. A fit for each p_d and a corresponding averaging were not reliable in this case, since the ratios with their errors were only moderately precise. Moreover, we expect the global fit to be favorable over a weighted mean of results from individual fits. See Appendix A.2 for a detailed description of the global fit method and comparison to the weighted mean case. The fit ansatz is then a slightly modified Equation (4.44),

$$
Q_{\partial_{\beta}(\ln|m|)}(L, p_d) = C + A_{p_d}L^{-\omega} ,
\tag{4.46}
$$

where we explicitly denote the dependence of the factors A_{p_d} on the concentration of defects with the index p_d. For our data sets we were able to use $s = 4$ and get eight ratios per concentration without reusing the same lattice size twice, i.e., as a small lattice size L and a large lattice size sL. The fits for all correlation exponents a are shown in Figure 4.25.

To study the stability and the quality of the fits we varied the smallest lattice size $L_{\min}$ included in to the fits as well as the minimum and maximum concentration of defects $p_d^{\min}$ and $p_d^{\max}$, respectively. These dependencies are summarized in Figure 4.26. As one can see, there is only a weak dependence on the maximum concentration of defects $p_d^{\max}$ so that we can stick with $p_d^{\max} = 0.4$ for all correlation exponents a. The same applies for the minimum lattice size $L_{\min}$. We chose $L_{\min} = 20$ for all fits. Note, that since we combine the lattice sizes L and sL into one ratio Q, the minimum lattice size cannot be chosen as large as in the later analyses where all lattice sizes enter the fitting ansatz separately. The dependence of the finial estimates of ω and the qualities of the fits χ^2_{red} on the minimum concentration of defects $p_d^{\min}$ for all correlation exponents a is shown in Figure 4.27. For most correlated cases, $a \neq \infty$, the fits were in a good region of $\chi^2_{\text{red}} \approx 1$ when we excluded the smallest concentration

(a) $a = \infty$.

(b) $a = 3.5$.

(c) $a = 3.0$.

(d) $a = 2.5$.

(e) $a = 2.0$.

(f) $a = 1.5$.

p_d

$\circ$ 0.05 $\square$ 0.1 $\triangledown$ 0.15 $\triangle$ 0.2 $\diamond$ 0.25 $\triangleleft$ 0.3 $\triangleright$ 0.35 $\varhexagon$ 0.4
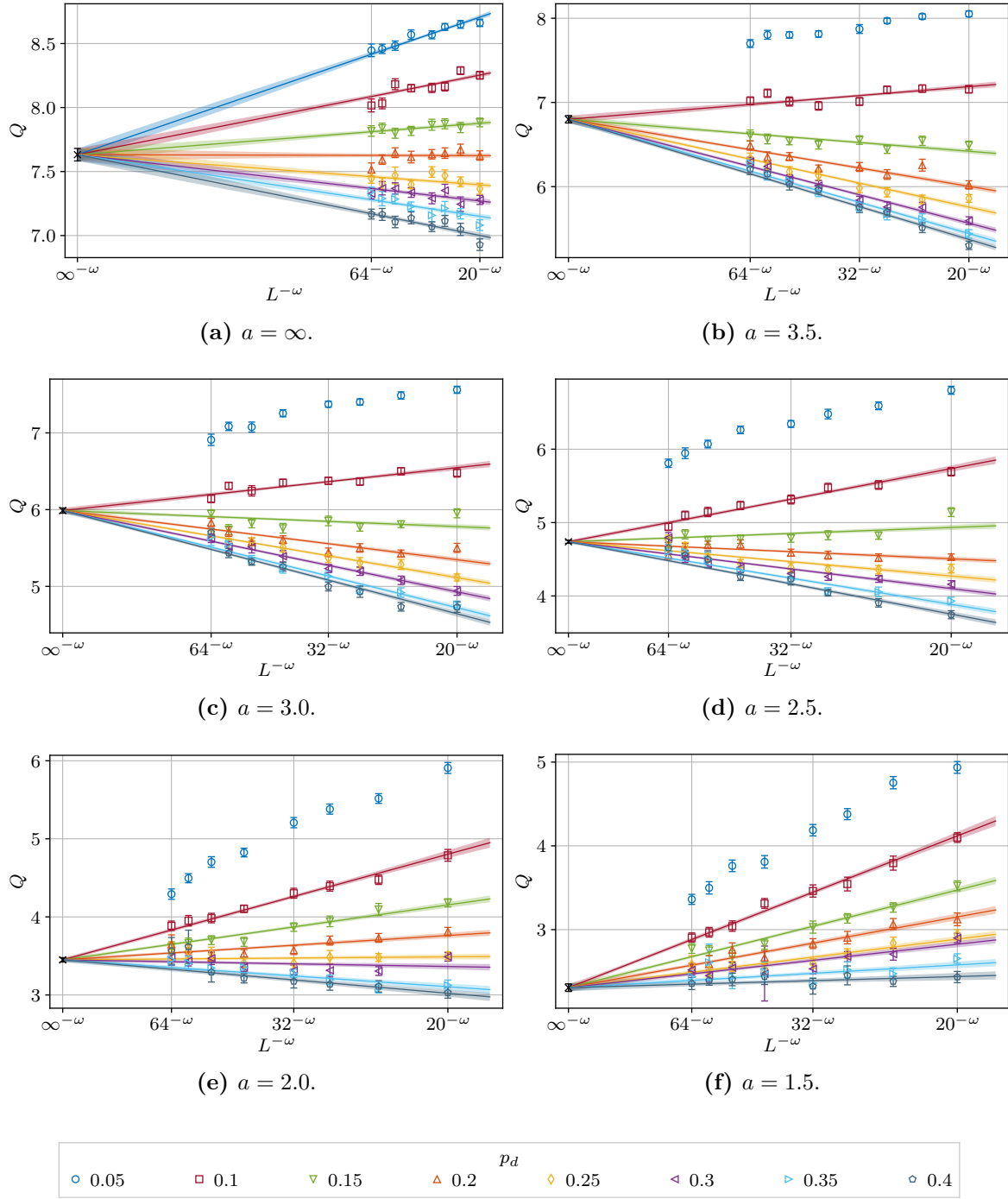
Figure 4.25: Fits of the quotients $Q_{\partial_\beta(\ln|m|)}$ at different lattice sizes L to the ansatz from Equation (4.46) for all considered correlation exponents a. The correlated cases were fitted including the concentrations of defects $0.1 \leq p_d \leq 0.4$. For the uncorrelated case the range was $0.05 \leq p_d \leq 0.4$. For better comparability the plots are shown scaled to $L^{-\omega}$ on the x-axis and therefore the appear linear.

and set $p_d^{\min} = 0.1$. The uncorrelated case with $a = \infty$ was good for all choices of $p_d^{\min}$, so we set $p_d^{\min} = 0.05$ in this case. The final estimates of the correction exponents ω together with the corresponding choice of $p_d^{\min}$ and the quality of the fits χ^2_{red} are summarized in Table 4.2. A comparison with estimates found in the literature can be found in Table 2.3.
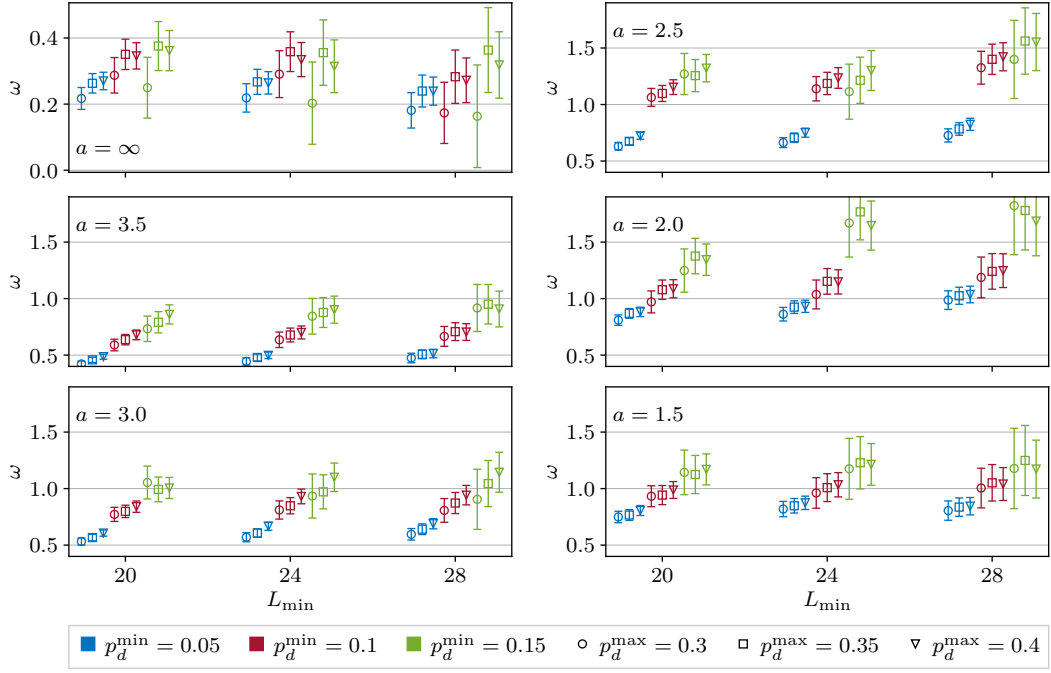
Figure 4.26: Summary of all correction exponents ω for each considered correlation exponent a obtained from a global fit to the ansatz given in Equation (4.46). All tested restriction parameters $L_{\min}$, $p_d^{\min}$ and $p_d^{\max}$ are shown. The dependence on the minimum included lattice size $L_{\min}$ and the maximum included concentration of defects $p_d^{\max}$ is small compared to the dependence on the minimum concentration of defects $p_d^{\min}$. For better comparability we keep the same y-axis scale for all correlated cases and cut some errorbars on one of the ends.

Table 4.2: Final confluent correction exponents ω and constants C from the fits of the quotients $Q_{\partial_\beta(\ln|m|)}$ to the ansatz in Equation (4.46) for all considered correlation exponents a. The minimum lattice size included into the fits was $L_{\min} = 20$ and the maximum included concentration of defects was $p_d^{\max} = 0.4$. We calculated the critical exponents ν from the fitting constant C which follow from the relation in Equation (4.45) with $s = 4$. They agree with our final estimates when using a smaller $L_{\min}$.

a	ω	C	$\nu = \frac{\ln s}{\ln C}$	$p_d^{\min}$	$\chi^2_{\rm red}$
∞	0.346(40)	7.590(42)	0.684(2)	0.1	0.885
3.5	0.679(44)	6.800(45)	0.723(3)	0.1	1.247
3.0	0.840(50)	5.988(35)	0.775(3)	0.1	1.835
2.5	1.154(66)	4.739(22)	0.891(3)	0.1	1.763
2.0	1.087(81)	3.450(29)	1.120(8)	0.1	0.917
1.5	0.988(75)	2.307(46)	1.66(4)	0.1	0.766

From Table 4.2 and Figure 4.27 we see a distinction between the correlated cases $a \neq \infty$ and the uncorrelated case $a = \infty$. Let us first discuss the uncorrelated case. Our estimated value $\omega = 0.346(40)$ is in very good agreement with the result $\omega = 0.37(6)$ found by Ballesteros et al. [Bal+98a]. It is also consistent with $\omega = 0.33(3)$ (for $p_d = 0.2$) obtained by Hasenbusch et al. [Has+07]. However, in Ref. [Cal+03] the authors do not get the exponent $\omega \approx 0.4$ but instead $\omega \approx 0.8$ for $p_d = 0.2$ which they claim is a next-to-leading order correction exponent.
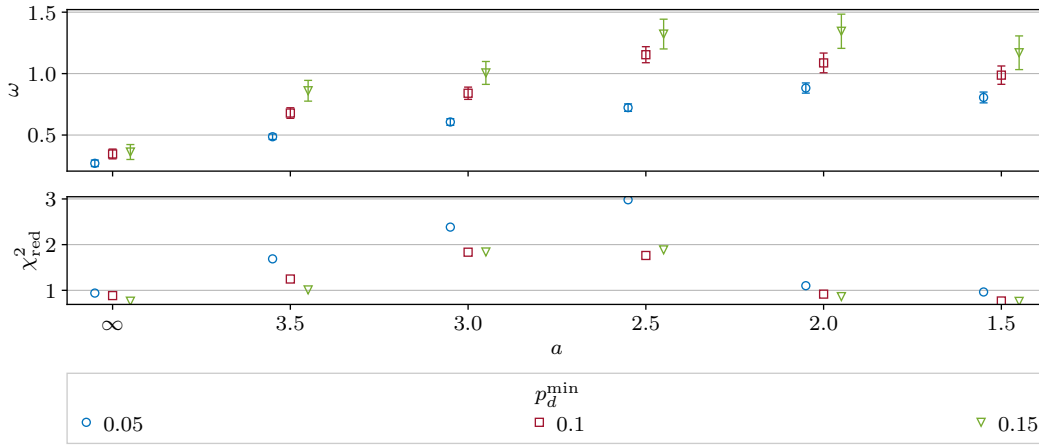
Figure 4.27: Confluent correction exponents ω from the fits of the quotients to the ansatz defined in Equation (4.46) for all considered correlation exponents a and three different minimum concentrations $p_d^{\min}$. The minimum lattice size included into the fits was $L_{\min} = 20$ and the maximum included concentration of defects was $p_d^{\max} = 0.4$. The difference between the correlated cases and the uncorrelated case is clearly visible for all $p_d^{\min}$. For $p_d^{\min} = 0.05$ however, the crossover to the uncorrelated cases begins already at around $a \approx 3.0$ whereas if $p_d^{\min} > 0.05$ is used, no crossover region is observed in our data.

Considering the larger lattice sizes in our study and the good quality of the global fit of the quotients we disagree with this claim and support the $\omega \approx 0.4$ case independently of the concentration of defects.

The correlated case for $a = 2.0$ yields a correction exponent $\omega = 1.087(81)$. This is in very good agreement with the values of $\omega = 1.01(13)$ obtained by Ballesteros and Parisi [BP99] for concentrations $p_d = 0.2$ and $p_d = 0.35$. A theoretical prediction from a Renormalization Group calculation is $\omega = 0.8$ [BFH01]. This prediction does not lie within the error range of our estimate but is not too far away either. We also can partially reproduce the qualitative behavior of $\omega(a)$ from [BFH01] in that it shows a maximum value at a certain a value and decreases when going to stronger (smaller a) or weaker (larger a) correlation exponents. However, our peak is not as pronounced as in Ref. [BFH01]. The comparison is presented in Figure 4.28. The Renormalization Group results in [BFH01] do not provide any error estimation. Therefore, we cannot compare the deviations quantitatively.
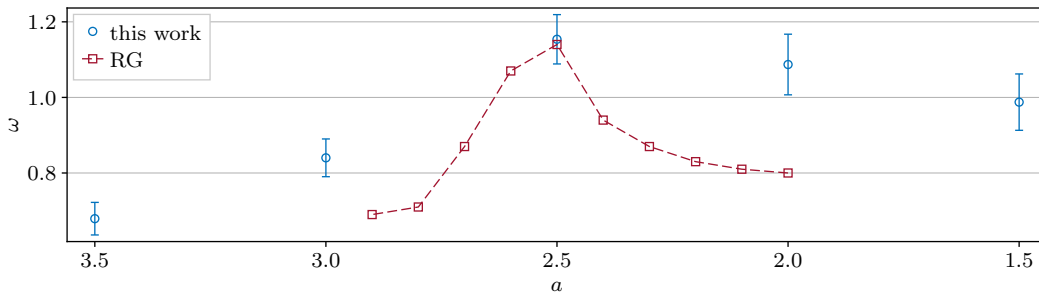
Figure 4.28: Comparison of the correction exponents ω to the values obtained with Renormalization Group techniques in RG: Blavats'ka, Ferber, and Holovatch [BFH01]. Our errorbars cover a substantial portion of the curve from RG making it hard to confirm or reject this behavior even for the simulated values of $a = 2.0$, $a = 2.5$ and $a = 3.0$.

Remark. As pointed in [AM05] we could have been used Equation (4.45) to estimate the critical exponent ratio $x_\mathcal{O}/\nu$, or in case of $x_\mathcal{O} = 1$, e.g., for $\partial_\beta(\ln|m|)$, even the critical exponent ν itself. We present the estimated critical exponents ν in Table 4.2. However, the errors are larger than using other methods (compare to Table 4.5), so we finally used the quotient method only for the extraction of ω.

Summary. With the help of the quotient method and the derivative of the logarithm of the magnetization observable $\partial_\beta(\ln|m|)$ we obtained the confluent correction exponents ω for the uncorrelated case $a = \infty$ with $\omega = 0.346(40)$ and for the correlated cases with $a \leq 3.0$ values in the range with $0.83 < \omega < 1.16$. The case with $a = 3.5$ seems to be a crossover between the uncorrelated and the correlated cases.

4.5.2 Critical exponent ν

One of the key quantities which was obtained in this work is the critical exponent of the correlation length ν. As was described in Section 3.2, this critical exponent enters the finite-size behavior of most observables in the form of a ratio $x_\mathcal{O}/\nu$ where $x_\mathcal{O}$ is the critical exponent of the corresponding observable $\mathcal{O}$. Especially for the correlated disorder Ising model it is the most studied critical exponent for which also theoretical predictions exist. Therefore, we took a great care in estimating the critical exponent ν. In the following we will discuss three different fitting methods which we used in order to get ν and compare them with each other as well as with the Monte Carlo and Renormalization Group predictions in form of Renormalization Group calculations known from literature.

As already mentioned in Section 4.3, we used the derivative with respect to β of the logarithm of the magnetization $\partial_\beta(\ln|m|)$ as our primary observable in the analysis process. Its definition in terms of thermal and disorder averages was given in Equation (2.44). The finite-size scaling behavior was discussed in Section 3.2 and reads in the next-to-leading order

$$\partial_\beta\widehat{(\ln|m|)}(L) = AL^r \left(1 + BL^{-\omega}\right) , \tag{4.47}$$

where $\partial_\beta\widehat{(\ln|m|)}(L)$ are the maximum values of $\partial_\beta(\ln|m|)(\beta)$ at different L, and ω is the confluent correction exponent which was obtained in Section 4.5.1. The exponent r in the ansatz relates to the critical exponent ν by

$$\nu = \frac{1}{r} , \quad \epsilon(\nu) = \frac{\epsilon(r)}{r^2} . \tag{4.48}$$

We used r in Equation (4.47) because this will be the actual fit parameter in the fit ansatzes. Starting with the ansatz from Equation (4.43), we analyzed three different fitting methods. In the first and most simple procedure, we analyzed each parameter pair (a, p_d) separately and used a linear fit ansatz excluding the correction term ($B = 0$). Next, we introduced the correction term but still performed individual fits for each concentration of defects p_d. Finally, we combined all concentrations of defects p_d for each considered correlation exponent a into one corrected global fit. This was possible, because ν and ω are independent of p_d in the thermodynamic limit. In the following we will first go through all of these methods and afterwards compare the results.

Uncorrected individual fits

The most straight forward method is to analyze each parameter pair (a, p_d) separately. The finite-size scaling ansatz for $\partial_\beta(\ln|m|)$ from Equation (4.47) with $B = 0$ reads

$$\partial_\beta \widehat{(\ln|m|)}(L) = A' L^r. \tag{4.49}$$

This ansatz can be transformed to the logarithmic scale and results in a linear fit,

$$\ln\left(\partial_\beta\widehat{(\ln|m|)}\right)(\ln L) = rL + A, \tag{4.50}$$

where $A = \ln A'$. We will denote the obtained estimates for the critical exponent ν by $\overline{\nu}^1_{\mathrm{lin}}$ where 1 indicates that the fits were performed for each concentration of defects p_d separately and "lin" denotes the linear (on log-log-scale) fit ansatz without correction terms. We performed fits for each parameter parameter tuple (a, p_d) varying the minimum included lattice size in the range $8 \le L_{\mathrm{min}} \le 128$. This allowed us to examine the asymptotic behavior for increasing L_{min} and the convergence of $\overline{\nu}^1_{\mathrm{lin}}$ for different concentrations of defects p_d. All resulting values $\overline{\nu}^1_{\mathrm{lin}}(p_d, L_{\mathrm{min}})$ are summarized in Figure 4.29. We clearly see a convergence to one final parameter for increasing L_{min} and different p_d. The smallest concentrations $p_d \le 0.1$ approaches the final value from below, while the largest concentrations $p_d \ge 0.3$ approach it from above. The moderate concentrations in the range $0.15 \le p_d \le 0.25$ show the smallest dependence on L_{min}. However, note that the qualities of the fits χ^2_{red} reach the region of $\chi^2_{\mathrm{red}} \approx 1$ only for large $L_{\mathrm{min}} \gtrsim 64$. This is an indication that at smaller lattice sizes the corrections to scaling involving the correction exponent ω are present and non-neglectable.

To provide a final estimate $\overline{\nu}^w_{\mathrm{lin}}$ for each a, we took the weighted mean over all concentrations in a chosen range $p_d^{\mathrm{min}} \le p_d \le p_d^{\mathrm{max}}$ and at a specific L_{min}. The weighted mean was taken over the fit parameters $r = 1/\nu$ as these were the actual fitting parameters while the estimates ν and their corresponding errors $\epsilon(\nu)$ were derived from them through Equation (4.48). The definitions of the weighted mean and its error are

$$r = \frac{1}{\sum_{p_d=p_d^{\mathrm{min}}}^{p_d^{\mathrm{max}}} \epsilon(r(p_d))^{-2}} \sum_{p_d=p_d^{\mathrm{min}}}^{p_d^{\mathrm{max}}} \epsilon(r(p_d))^{-2} r(p_d), \tag{4.51}$$

$$\epsilon(r) = \sqrt{\frac{1}{\sum_{p_d=p_d^{\mathrm{min}}}^{p_d^{\mathrm{max}}} \epsilon(r(p_d))^{-2}}}. \tag{4.52}$$

In principle one could vary the smallest included lattice size L_{min} for each p_d individually. However, we have not found a reasonable system on how to choose these values $L_{\mathrm{min}}(p_d)$. Instead, we looked into the weighted means in dependence of one common L_{min} for all concentrations. In Figure 4.31 we show the dependence of $\overline{r}^w_{\mathrm{lin}}$ and the resulting $\overline{\nu}^w_{\mathrm{lin}}$ on the chosen p_d^{min} and L_{min}. Note, that we label the weighted mean results with the label w in order to distinguish these results from the results for different ansatzes which will come later. A clear dependence on the choice of L_{min} as well as on the p_d^{min} can be seen for all considered correlation exponents a. To find a reasonable choice for the final estimates of the critical exponent ν, we studied the overlap of the estimates $\overline{r}^w_{\mathrm{lin}}(p_d)$ obtained with different p_d^{min} choices in dependence of the minimum lattice size L_{min}. The main idea was the following: use as many data points as possible while ensure that the dependence on the concentration p_d^{min} is
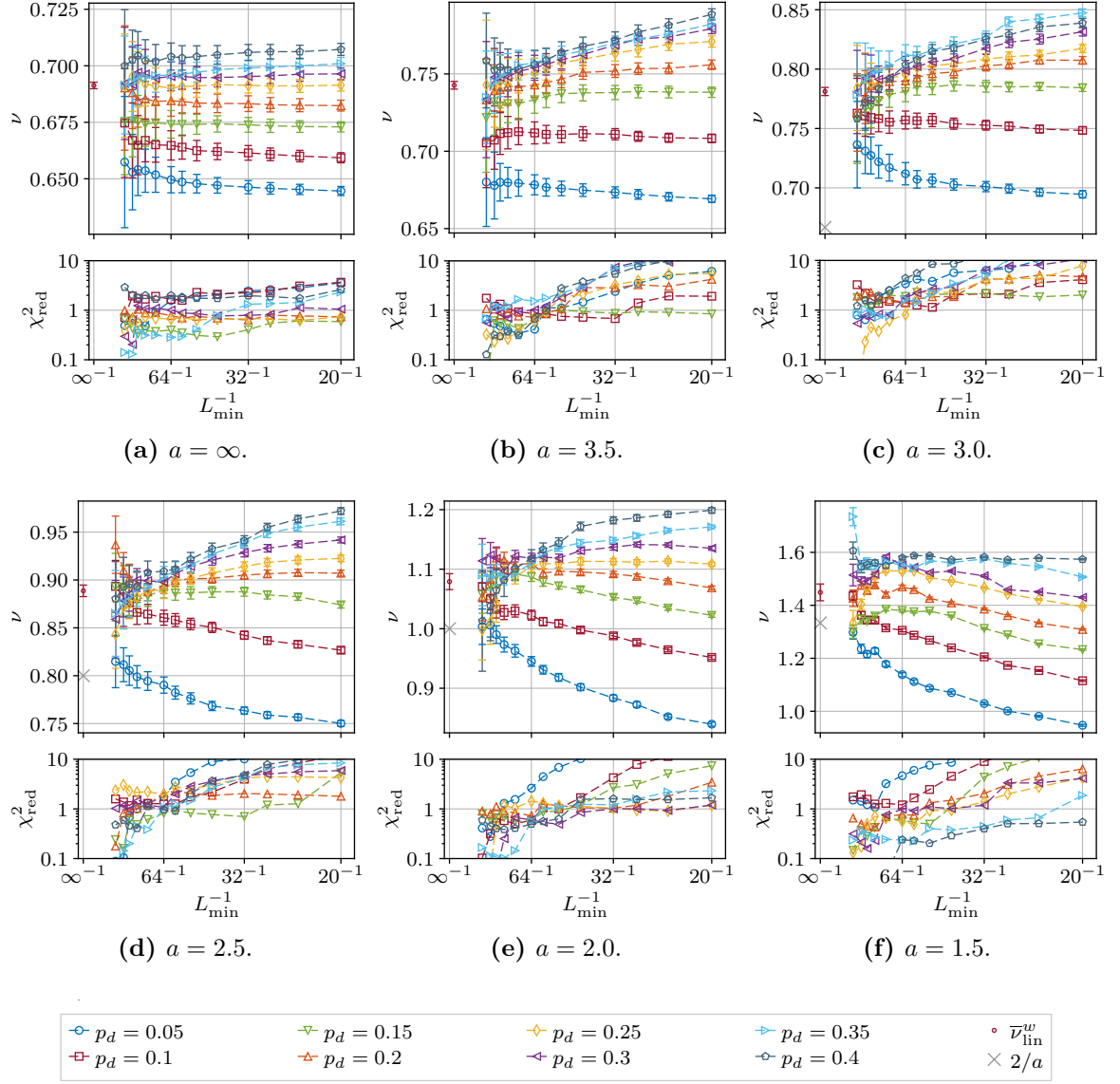
Figure 4.29: Critical exponents $\overline{\nu}_{\mathrm{lin}}^{1}(p_d, L_{\min})$ from fits to the uncorrected individual ansatz given in Equation (4.50), with varying $L_{\min}$ for all correlation exponents a. For the a values where the conjecture by Weinrib and Halperin is assumed to be valid the predicted $2/a$ values were plotted as an orientation. The corresponding qualities of fits χ^2_{red} are shown in the lower plots. χ^2_{red} reaches reasonable values for $L_{\min} \gtrapprox 64$.

mainly covered through the errors of the estimates. To quantify the overlap of the estimates $\overline{r}_{\mathrm{lin}}^{w}$ we assumed that the values $\overline{r}_{\mathrm{lin}}^{w}$ and their errors $\epsilon(r_{\mathrm{lin}}^{w})$ can be represented by a normal distribution and calculated the area covered by these distributions for different minimum concentrations of defects $p_d^{\min}$. More precise, the following formula defines the **overlapping index** $\mathscr{A}$ for a set of distributions p_i [IJ89],

$$\mathscr{A} = \int_{-\infty}^{\infty} \mathrm{d}x \, \min_{i} \left[p_i(x) \right]. \tag{4.53}$$

The index $\mathscr{A}$ would be equal to 1 if only one distribution would be used. Otherwise, it follows the lowest of all distribution densities along x and by this the integral calculates the area which is covered by all the distributions simultaneously. The overlapping index $\mathscr{A}$ is a measure of agreement between several distributions [IJ89]. It not as involved as an ANOVA

analysis or a set of hypothesis tests but is meaningful enough for our purpose. Setting $\rho_i = \mathcal{N}(\overline{r}_{\text{lin}}^w(p_d^{\min}), \epsilon(r_{\text{lin}}^w)^2(p_d^{\min}))$ gives the specific formula for the desired estimates,

$$\mathscr{A}(r) = \int_{-\infty}^{\infty} \mathrm{d}x \min_{\tilde{p}_d^{\min} \leq p_d^{\min} \leq 0.2} \left[\mathcal{N}\big(r(p_d^{\min}), \epsilon(r)^2(p_d^{\min})\big)(x) \right], \tag{4.54}$$

where $\tilde{p}_d^{\min}$ is the smallest $p_d^{\min}$ included into the overlapping index calculation, and the parameter r in the case of uncorrected individual fits is $r = \overline{r}_{\text{lin}}^w$. Visually the overlapping index for different $\tilde{p}_d^{\min}$ is presented in Figure 4.30. The values $\mathscr{A}(\overline{r}_{\text{lin}}^w)$ for all $p_d^{\min}$ and $L_{\min}$ can be found in Figure 4.31.

(a) $\tilde{p}_d^{\min} = 0.05$.   **(b)** $\tilde{p}_d^{\min} = 0.1$.   **(c)** $\tilde{p}_d^{\min} = 0.15$.   **(d)** $\tilde{p}_d^{\min} = 0.2$.
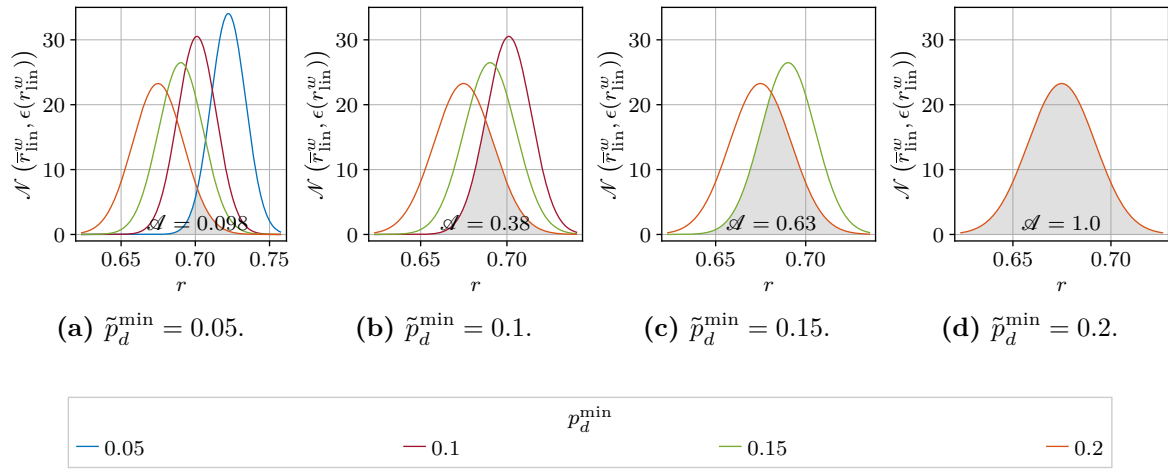
Figure 4.30: The overlapping index $\mathscr{A}(\overline{r}_{\text{lin}}^w)$ calculated with Equation (4.54) at $a = 1.5$ and $L_{\min} = 128$ for different $\tilde{p}_d^{\min}$. The shaded areas represent the area covered by all distributions $\mathcal{N}(\overline{r}_{\text{lin}}^w, \epsilon(r_{\text{lin}}^w)^2)$ calculated from all weighted means $\overline{r}_{\text{lin}}^w(p_d^{\min})$ for the minimum concentrations of defects in the range $\tilde{p}_d^{\min} \leq p_d^{\min} \leq 0.2$.

Due to the finite sizes of our lattices and the finite statistics of the observables we do not expect $\mathscr{A} \approx 1$ but just use $\mathscr{A}$ to quantify our decision for the final $p_d^{\min}$ and $L_{\min}$ settings. Our general rule was to take the lowest $L_{\min}$ where the criterion $\mathscr{A} \gtrsim 0.75$ was fulfilled for smallest possible $\tilde{p}_d^{\min}$. Including $p_d^{\min} = 0.05$ or $p_d^{\min} = 0.1$ into the overlapping index $\mathscr{A}$ resulted in low values for all $L_{\min}$. On the other hand, the results for $p_d^{\min} = 0.15$ or $p_d^{\min} = 0.2$ were in reasonable agreement for high enough lattice size $L_{\min} \gtrsim 128$. Therefore, for later comparison with other methods which will be described below, we constantly chose $L_{\min} = 128$ and $p_d^{\min} = 0.15$ for all correlation exponents a. The final results for $\overline{\nu}_{\text{lin}}^w$ are summarized in Table 4.3. As we can see, the high $L_{\min}$ value indicates that corrections to scaling are important on the considered lattice sizes scale and the linear ansatz needs to reject a lot of data points to fit properly. Therefore, we have not used the results from this analysis as our final results. However, we will discuss them and, most importantly, compare them to the estimates obtained from different methods.

(a) $a = \infty$.

(b) $a = 3.5$.

(c) $a = 3.0$.

(d) $a = 2.5$.

(e) $a = 2.0$.

(f) $a = 1.5$.

$p_d^{\min} \, / \, \tilde{p}_d^{\min}$ for $\mathscr{A}$-plots

○ 0.05   ⊡ 0.1   ▽ 0.15   △ 0.2
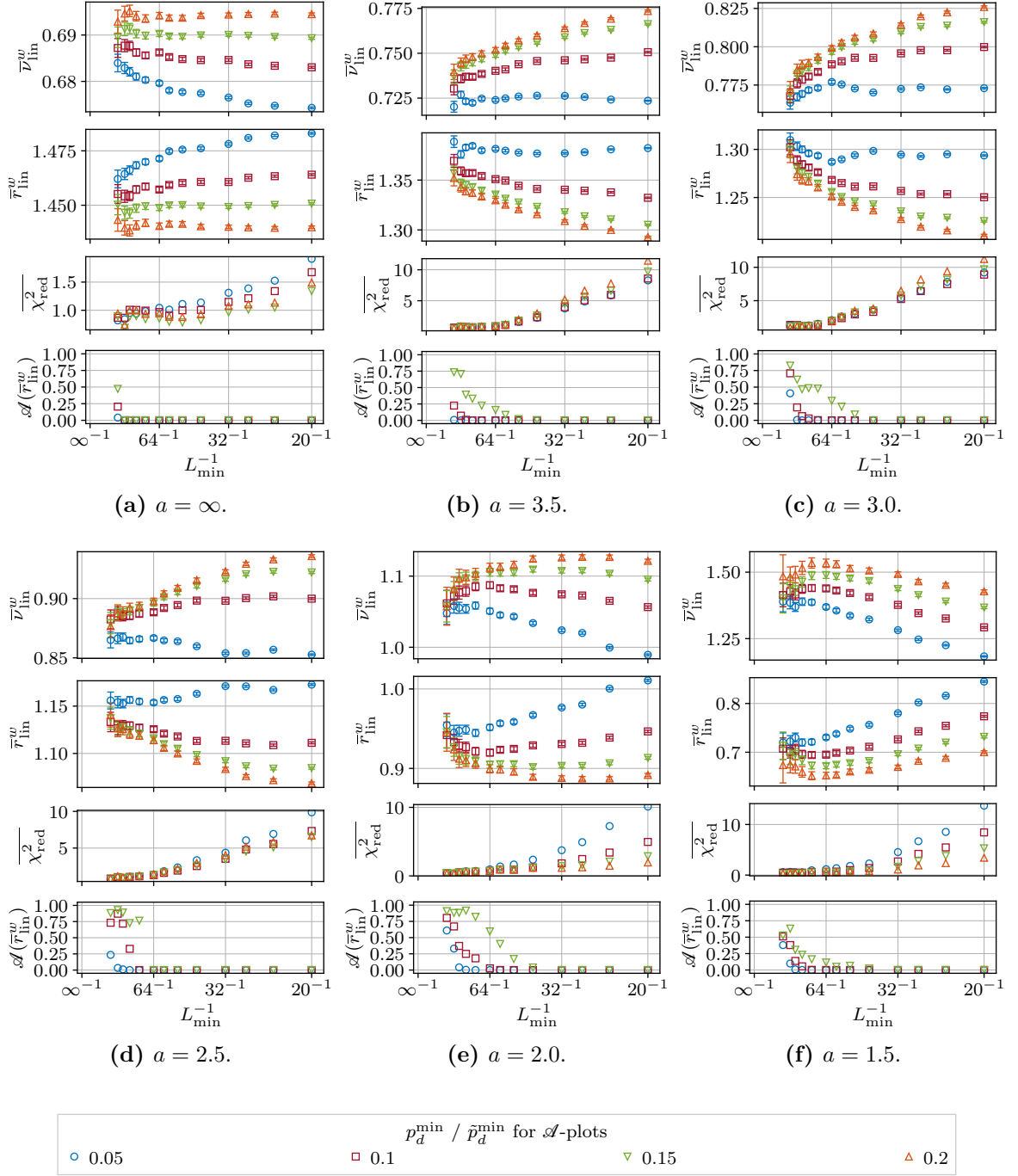
Figure 4.31: Fit parameters $\overline{r}_{\mathrm{lin}}^{w}(L_{\min})$ and the corresponding critical exponents $\overline{\nu}_{\mathrm{lin}}^{w}(L_{\min})$ obtained as a weighted mean over all $p_d^{\min} \leq p_d \leq 0.4$ from the fit parameters $\overline{r}_{\mathrm{lin}}^{1}$ to the uncorrected individual ansatz given in Equation (4.50), with varying $L_{\min}$ and $p_d^{\min}$. Third plots show the mean of the fit qualities $\chi_{\mathrm{red}}^{2}(p_d, L_{\min})$. The lower plots show the overlapping index $\mathscr{A}$ calculated for all parameters $\overline{r}_{\mathrm{lin}}^{w}(p^{\min})$ with the minimum concentration of defects in the range $\tilde{p}_d^{\min} \leq p_d^{\min} \leq 0.2$. $\mathscr{A}$ for $\tilde{p}_d^{\min} = 0.2$ is not plotted, since it is always equal to one.

Table 4.3: Final estimates $\overline{\nu}_{\text{lin}}^w$ obtained as a weighted mean over uncorrected individual fits for concentrations of defects in the range $0.15 \leq p_d \leq 0.4$ taken at the minimum included lattice size $L_{\min} = 128$. For a quantitative description of the final quality of the estimates the mean and the maximum of $\chi_{\text{red}}^2(p_d)$ are listed as well.

a	$\overline{\nu}_{\text{lin}}^w$	$\overline{\chi_{\text{red}}^2}$	$\max(\chi_{\text{red}}^2)$
∞	0.6913(15)	0.689	2.03
3.5	0.7427(25)	0.773	1.26
3.0	0.7812(35)	1.2	2.17
2.5	0.8887(61)	0.988	3.03
2.0	1.079(14)	0.343	0.797
1.5	1.449(32)	0.279	0.497

Corrected individual fits

The next possibility is to use individual fits for each concentration of defects p_d but include the correction term in the finite-size scaling ansatz as defined in Equation (4.47) which we repeat here for clarity,

$$\partial_\beta \widehat{(\ln |m|)}(L) = AL^r \left(1 + BL^{-\omega}\right) . \tag{4.55}$$

Contrarily to the case without corrections discussed previously, we cannot linearize the ansatz but have to deal with the nonlinear form given in Equation (4.55). However, fitting with both exponents, r and ω, as free parameters turned out to be unreliably unstable. Therefore, we took the previously obtained ω estimates from Table 4.2 as fixed parameters in the ansatz from Equation (4.55). The free parameters were r and the amplitudes A and B. We repeated the same procedure as in the uncorrected case and varied the minimum included lattice size $L_{\min}$ in the fits. The resulting critical exponent estimates for all p_d and $L_{\min}$ are shown in Figure 4.32.

As in the case with the uncorrected fits, we see a clear dependence on the minimum included lattice size $L_{\min}$. However, for large enough $L_{\min} \gtrapprox 32$ the curves for different $p_d^{\min}$ mostly overlap within their error bars. The qualities of the fits become reasonable for $L_{\min} \gtrapprox 32$ for all correlated cases as well. The uncorrelated case has good χ_{red}^2 already at $L_{\min} \gtrapprox 20$. We calculated the weighted means $\overline{\nu}^w$ for each a using Equations (4.51) and (4.52) at different $L_{\min}$ and $p_d^{\min}$. The results are presented in Figure 4.33 together with the overlapping index $\mathscr{A}$. The overlapping index $\mathscr{A}$ is defined by Equation (4.54) again. The only minimum concentration for which the overlapping index is not sufficiently large for almost all $L_{\min}$ is $p_d^{\min} = 0.05$. So we chose $p_d^{\min} = 0.1$ for all parameters a. The minimum lattice size was set to $L_{\min} = 32$ for the uncorrelated case, $L_{\min} = 48$ for all correlated cases with $a \geq 3.0$ and $L_{\min} = 64$ for the strongest correlations with $a \leq 2.5$. These decisions were made on the rule of $\mathscr{A} \gtrapprox 0.75$ as in the uncorrected case. All results are summarized in Table 4.4.

The discussion of the final results will be postponed to the end of this section where we will compare different methods and also take into account results from literature and theoretical predictions. At this point we only want to note that we have not used the corrected individual fits method as our first choice since we found an issue which comes along with taking a weighted mean over several fit results. This issue is discussed in Appendix A.2. The main
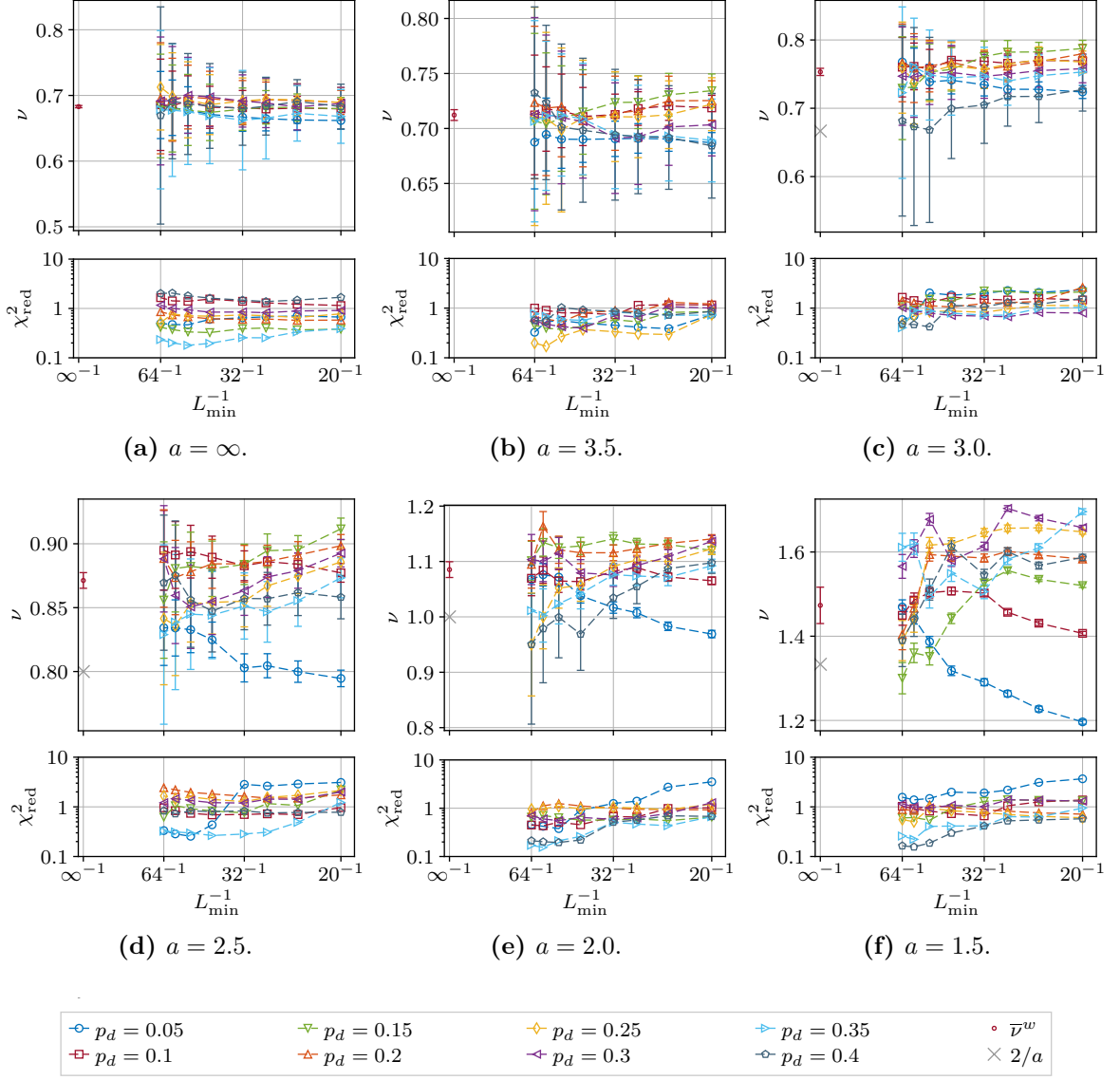
Figure 4.32: Critical exponents $\overline{\nu}^1(p_d, L_{\min})$ from fits to the corrected individual ansatz given in Equation (4.55), with varying $L_{\min}$. For the a values where the conjecture by Weinrib and Halperin is assumed to be valid the predicted $2/a$ values were plotted as an orientation. The corresponding qualities of fits χ^2_{red} are shown in the lower plots.

problem is that the errors of the fit parameters are correlated with the parameters themselves which makes the weighted mean systematically prefer results which deviates from the true parameter in one direction over those deviating in the other direction. The solution to this problem and also a more reliable method with regard to the stability of the fitting procedure was the global fit method which will be discussed below.

Corrected global fits

The most advanced fitting method which was used in this work is the corrected global fit ansatz. The uncorrected (linearizable) global fit ansatz was checked by us, but it can be shown that in the linear case the global fit and individual fits with a weighted mean afterwards give the same results. See Appendix A.2 for a detailed discussion of the global fit method in

(a) $a = \infty$.

(b) $a = 3.5$.

(c) $a = 3.0$.

(d) $a = 2.5$.

(e) $a = 2.0$.

(f) $a = 1.5$.

$p_d^{\min}$ / $\tilde{p}_d^{\min}$ for $\mathscr{A}$-plots

○ 0.05   □ 0.1   ▽ 0.15   △ 0.2
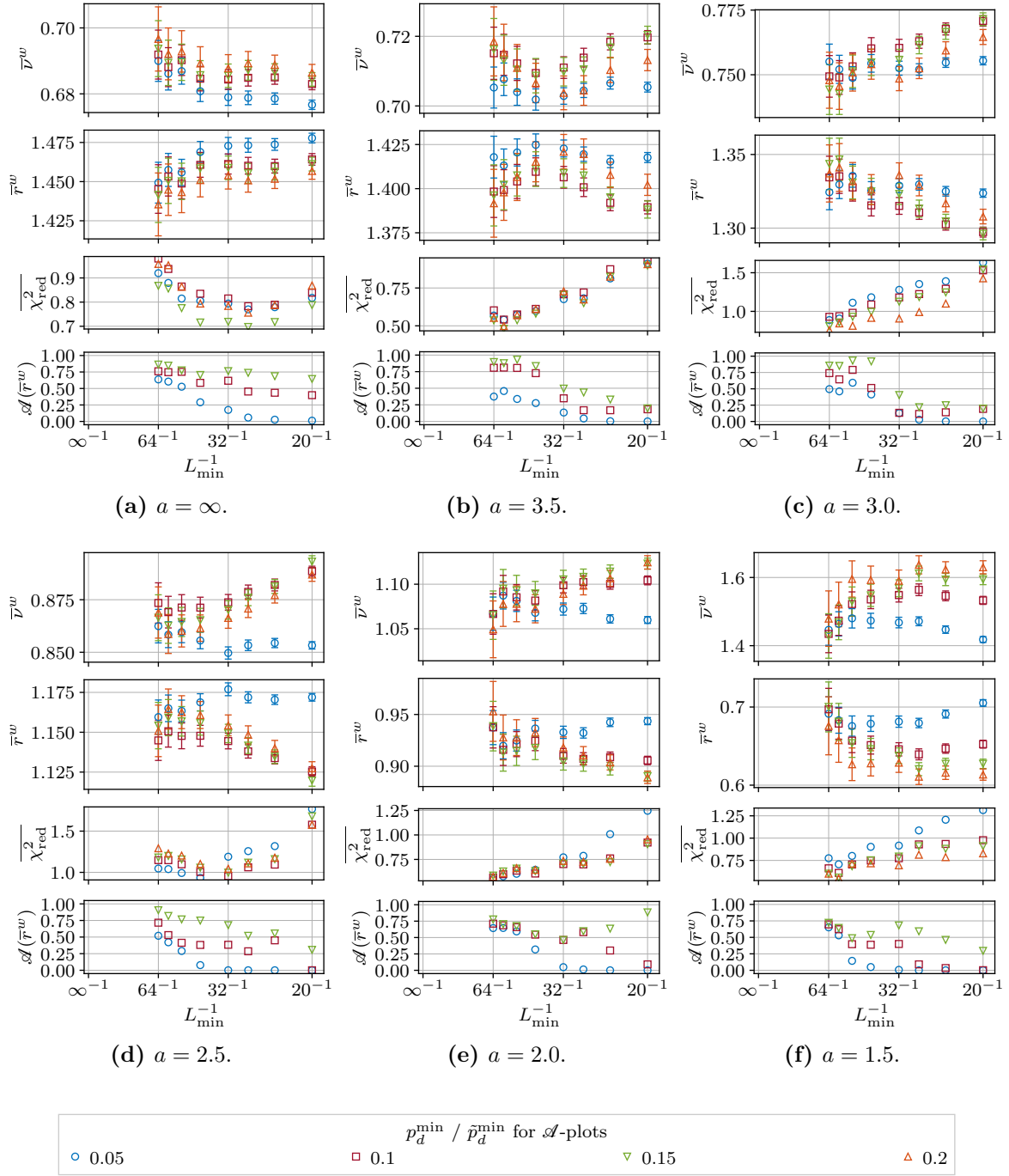
Figure 4.33: Fit parameters $\overline{r}^w(L_{\min})$ and the corresponding critical exponents $\overline{\nu}^w(L_{\min})$ obtained as a weighted mean over all $p_d^{\min} \leq p_d \leq 0.4$ from the fit parameters $\overline{r}^1$ to the corrected individual ansatz given in Equation (4.55), with varying $L_{\min}$ and $p_d^{\min}$. Third plots show the mean of the fit qualities $\chi^2_{\text{red}}(p_d, L_{\min})$. The lower plots show the overlapping index $\mathscr{A}$ calculated for all parameters $\overline{r}^w(p_d^{\min})$ with the minimum concentration of defects in the range $\tilde{p}_d^{\min} \leq p_d^{\min} \leq 0.2$. $\mathscr{A}$ for $\tilde{p}_d^{\min} = 0.2$ is not plotted, since it is always equal to one.

general and its equivalence to the weighted mean in the linear case. The corrected global ansatz for $\partial_\beta(\ln|m|)$ is given by

$$\partial_\beta\widehat{(\ln|m|)}(L, p_d) = A_{p_d} L^r \left(1 + B_{p_d} L^{-\omega}\right), \tag{4.56}$$

Table 4.4: Final estimates $\overline{\nu}^w$ obtained as a weighted mean over individual corrected fits for each concentration of defects $0.1 \leq p_d \leq 0.4$ taken at the minimum included lattice sizes $L_{\min}$. For a quantitative description of the final quality of the estimates the mean and the maximum of $\chi^2_{\mathrm{red}}(p_d)$ are listed as well.

a	$\overline{\nu}^w$	$\overline{\chi^2_{\mathrm{red}}}$	$\max(\chi^2_{\mathrm{red}})$	$L_{\min}$
∞	0.6843(31)	0.815	1.48	32
3.5	0.7122(49)	0.575	1.03	48
3.0	0.7532(53)	0.982	1.52	48
2.5	0.8735(96)	1.15	2.43	64
2.0	1.067(23)	0.566	0.955	64
1.5	1.435(56)	0.662	1.15	64

where we denote the p_d-dependence of the coefficients A_{p_d} and B_{p_d} with the index p_d. The confluent correction exponent was a fixed parameter taken from Table 4.2 for each correlation exponent a.

We analyzed the dependence of the corrected global fits on three parameters: the minimum included lattice size $L_{\min}$ and the minimum and maximum included concentrations of defects $p_d^{\min}$ and $p_d^{\max}$, respectively. It turned out that the maximum concentration of defects $p_d^{\max}$ only marginally modified the fit results compared to the other two parameters. So we set $p_d^{\max} = 0.4$ for all correlation exponents a. In Figure 4.36 we compare the obtained fit parameter results r^g for various $p_d^{\min}$ and $L_{\min}$ for each correlation exponent a. The label g indicates that the results are coming from a global fit ansatz. Figure 4.36 also contains the qualities of the fits χ^2_{red} and the overlapping index in dependence of $\tilde{p}_d^{\min}$ which we used as an indicator to find a suitable $L_{\min}$ and $p_d^{\min}$ as in the previous cases. Excluding the smallest concentration $p_d = 0.05$ produced good χ^2_{red} values from all parameters a and almost all $L_{\min}$. So we set $p_d^{\min} = 0.1$ in all considered cases. The fit parameters $r^g(p_d^{\min}, L_{\min})$ are very close to that of the weighted means over corrected individual fits presented in Figure 4.33. The overlapping indices $\mathscr{A}$ are also in a very good agreement. For better comparability we therefore chose the same $L_{\min}$ parameters: $L_{\min} = 32$ for the uncorrelated case, $L_{\min} = 48$ for all correlated cases with $a \geq 3.0$ and $L_{\min} = 64$ for the cases with $a \leq 2.5$. The fits for the finally selected $L_{\min}$ and $p_d^{\min}$ are shown in Figure 4.34. Looking at Figure 4.34, especially into the lower plots which are divided by $L^{1/\nu}$ to cancel out the leading order behavior, we realize that the corrections to scaling coming from the terms B_{p_d} in Equation (4.56) are minimal for $p_d \approx 0.2$ for all correlation exponents a. This is in agreement with the theoretical prediction from Renormalization Group calculations for the uncorrelated case in Ref. [PV02]. Below and above of $p_d \approx 0.2$, the corrections become more pronounced and tend to bend the curve towards $p_d = 0.2$ at smaller lattice sizes. Except for the strongest correlation ($a = 1.5$), the corrections become neglectable at lattice sizes of $L \gtrsim 128$. At the end of this section we will compare the corrected global fit ansatz with the other two methods discussed previously. As it will turn out, we will use the corrected global fit ansatz as our final choice and therefore we will perform some further analysis before finally compare the results from different methods and known results from other works. We will also drop the index g and just write ν for the estimates obtained through the corrected global fit ansatz from Equation (4.56) whenever it is not confusing.

(a) $a = \infty$, $L_{\min} = 32$.

(b) $a = 3.5$, $L_{\min} = 48$.

(c) $a = 3.0$, $L_{\min} = 48$.

(d) $a = 2.5$, $L_{\min} = 64$.

(e) $a = 2.0$, $L_{\min} = 64$.

(f) $a = 1.5$, $L_{\min} = 64$.

p_d							
○ 0.05	□ 0.1	▽ 0.15	△ 0.2	◇ 0.25	◁ 0.3	▷ 0.35	⬡ 0.4
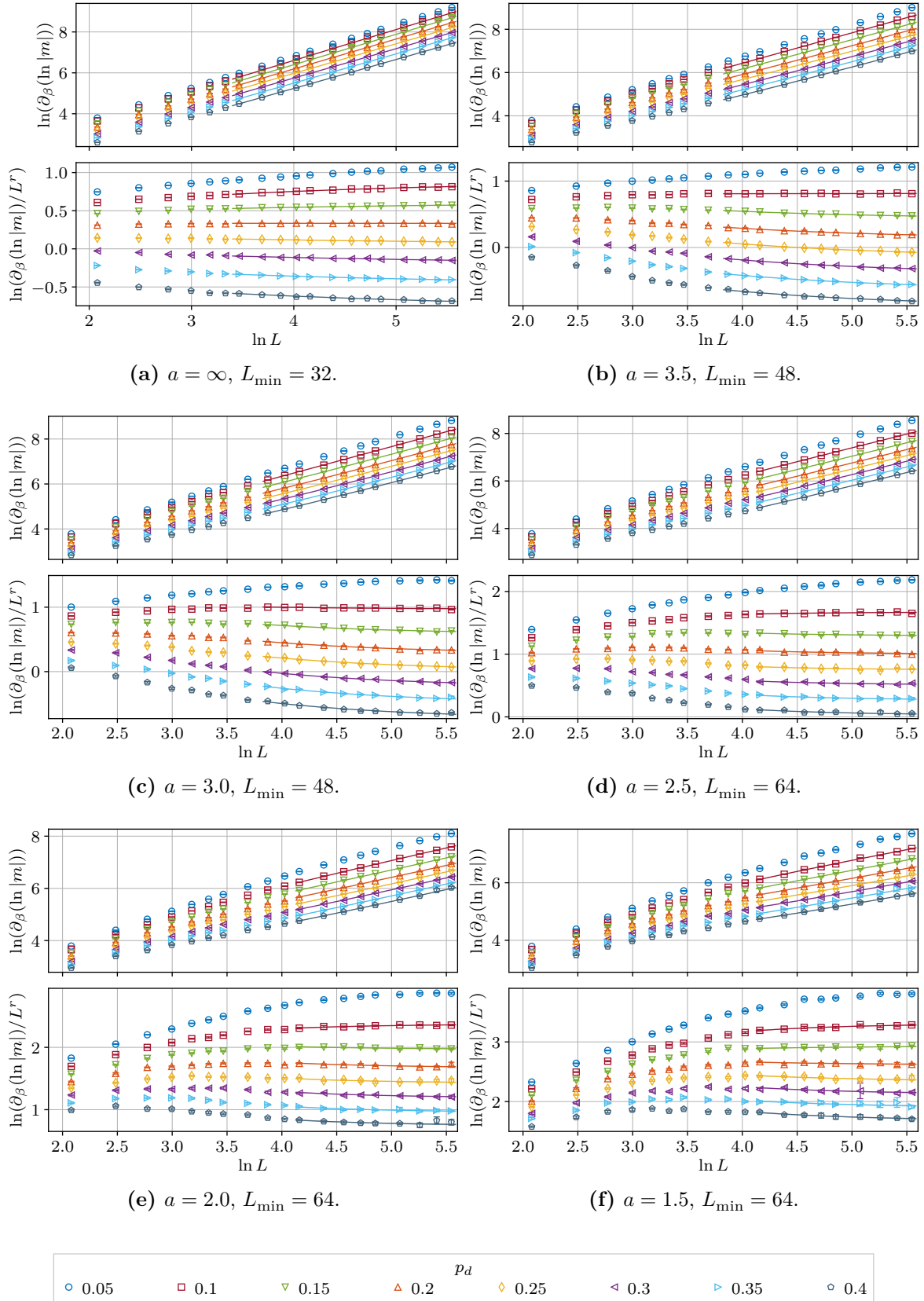
Figure 4.34: Examples of the corrected global fits to the ansatz in Equation (4.56) for all correlation exponents a. The minimum included concentration of defects was $p_d^{\min} = 0.1$ and the maximum included concentration of defects was $p_d^{\max} = 0.4$. The upper plots show the fitted observables $\partial_\beta \widehat{(\ln|m|)}(L, p_d)$ against L on a logarithmic scale. In the lower plots, the observables are divided by $L^{1/\nu}$. This form allows us to better visualize the deviations from the leading behavior $L^{1/\nu}$ through the correction terms with the amplitudes B_{p_d}.

Table 4.5: Final estimates of the critical exponents ν^g obtained through the corrected global fit ansatz given in Equation (4.56). For all case the maximum included concentration of defects was set to $p_d^{\max} = 0.4$ and the minimum concentration of defects was set to $p_d^{\min} = 0.1$. The listed confluent correction exponents ω were taken from Table 4.2. For all cases where the conjecture by Weinrib and Halperin is expected to be valid we show the $2/\overline{a}$ values for comparison. The measured values $\overline{a}$ can be found in Table 4.1.

a	ν^g	$2/\overline{a}$	χ^2_{red}	$L_{\min}$
∞	0.6831(30)	$-$	0.834	32
3.5	0.7117(49)	$-$	0.547	48
3.0	0.7484(52)	0.687(23)	1.18	48
2.5	0.8719(96)	0.8159(86)	1.12	64
2.0	1.060(23)	1.0105(89)	0.6	64
1.5	1.421(55)	1.333(26)	0.639	64

Amplitudes

Let us take a look at the amplitudes which were obtained in the corrected global fit ansatz from Equation (4.56) with the finally chosen $p_d^{\min}$ and different $L_{\min}$. The amplitudes are presented in Figure 4.37. The first observation is that the global amplitudes A_{p_d} are in a relatively small range between 0 and 3 for effectively uncorrelated cases with $a \leq 3.0$. For stronger correlations the upper limit increases fast and reaches ≈ 40 for $a = 1.5$. Therefore, the qualitative difference between the correlated case and uncorrelated case can be seen even on the level of the amplitudes. On the other hand, visually the relative spacings between the amplitudes for different p_d remain the same. Finally, there is only very weak dependence of the global amplitudes A_{p_d} on the minimum chosen lattice size $L_{\min}$. Only for the strongest correlation with $a = 1.5$ larger changes can be observed for increasing $L_{\min}$. The correction amplitudes B_{p_d} are settled around zero for the uncorrelated case with being closest to zero for $p_d \approx 0.2$. This is in agreement with statements in Refs. [Bal+98a; Iva+08] according to which this concentration has the smallest corrections to scaling. However, this argument does not apply anymore to the correlated cases with $a \leq 2.5$. For $a = 2.5$ the zero moves towards $p_d \approx 0.1$ and for the strongest correction with $a = 1.5$ it shifts towards $p_d = 0.4$. For later case, additionally, a strong dependence on $L_{\min}$ is present. Unfortunately, we cannot go to larger $L_{\min}$ with our available data and hence cannot study the region where the amplitude settles down. Therefore, we cannot exclude the possibility that the case with $a = 1.5$ needs larger lattice sizes to be analyzed in the region, where $A \approx$ const. and $B \approx$ const..

Dependence on the correction exponent ω

The next step in analyzing the corrected global fits and the corresponding ν^g estimates, was to look at the stability and dependence of the results with respect to the chosen correction exponent ω. We have already seen in Section 4.5.1, that the correction exponent for all correlated cases is of the order $\omega \approx 1$. On the other hand, in Refs. [BP99; Iva+08], a value of $\omega = 0.8$ was found. We used the ansatz in Equation (4.56) and compared the results of the fits with $\omega = 1.0$ and $\omega = 0.8$. The estimates are compared in Figure 4.39. The result is that the dependence on the correction exponent is very weak and the different estimates mostly coincide within their error bars for all correlation exponents $a \neq \infty$. As an additional step,
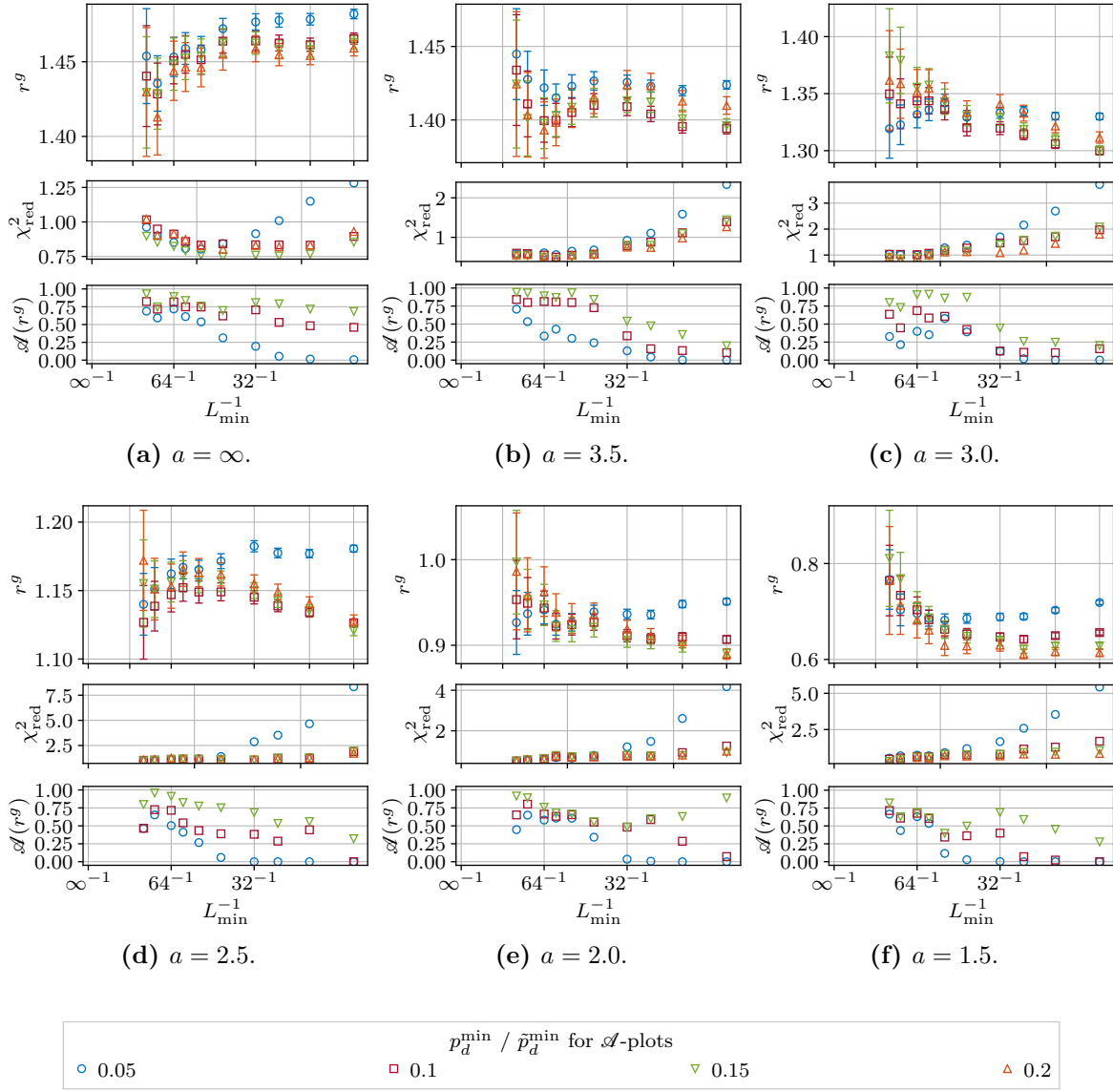
Figure 4.35: Fit parameters $r^g(L_{\min})$ and the corresponding critical exponents $\nu^g(L_{\min})$ obtained as a weighted mean over all $p_d^{\min} \leq p_d \leq 0.4$ from the fit to the corrected global ansatz given in Equation (4.56), with varying $L_{\min}$ and $p_d^{\min}$. Third plots show the fit qualities $\chi^2_{\text{red}}(p_d, L_{\min})$. The lower plots show the overlapping index $\mathscr{A}$ calculated for all parameters $r^g(p_d^{\min})$ with the minimum concentration of defects in the range $\tilde{p}_d^{\min} \leq p_d^{\min} \leq 0.2$. $\mathscr{A}$ for $\tilde{p}_d^{\min} = 0.2$ is not plotted, since it is always equal to one.

we continuously varied the correction exponent ω in a wide range and checked the stability of the resulting $\nu(\omega)$ and the qualities of the fits χ^2_{red}. These dependencies are shown in Figure 4.38. Note, that we do not expect χ^2_{red} to be minimal at the estimated $\overline{\omega}$ parameter as it is a fixed parameter in our fits and the χ^2_{red} minimization does not account for a ω variation. The quality of the fits remain in a reasonable range for a wider range of tested ω values and the final estimates $\nu(\omega)$ lie mostly within the range $\nu \pm \epsilon(\nu)$.

All in all, we expect our final ν estimates to be reasonably correct regardless of the precise values of the correction exponents ω. This is an important observation as the quotient method used for the ω derivation in Section 4.5.1 halves the number of points for the fits and is therefore less accurate than the fits for ν.
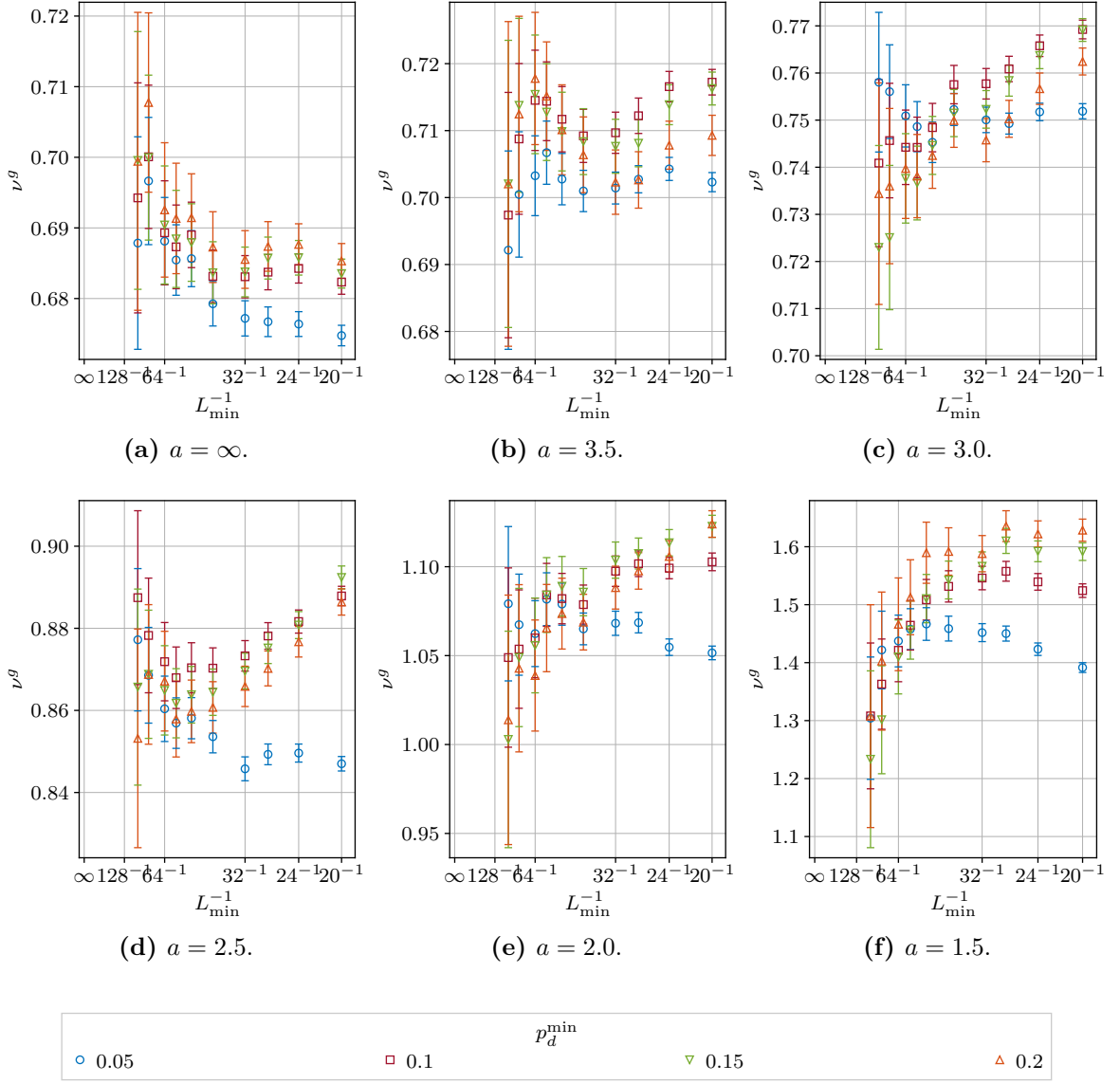
Figure 4.36: Critical exponents ν^g from fits to the corrected global ansatz given in Equation (4.56), with maximum concentration of defects $p_d^{\max} = 0.4$ and varying $p_d^{\min}$ and $L_{\min}$. We used $p_d^{\min} = 0.1$ for all cases and chose the $L_{\min}$ as a minimum lattice size where this overlap was sufficiently large, i.e., $\mathscr{A}(\tilde{p}_d^{\min}) \gtrsim 0.75$.

Final estimates

Let us compare the tree methods for extracting the correlation length critical exponent ν which were discussed previously. The final estimates of the critical exponent ν from each method are summarized in Table 4.6 and Figure 4.40. We clearly see a deviation between the uncorrected case $\overline{\nu}_{\text{lin}}^w$ and the corrected cases $\overline{\nu}^w$ and ν^g. Apart for the cases of $a = 2.0$ and $a = 1.5$, $\overline{\nu}_{\text{lin}}^w$ lie a bit above the other values. The lager deviation may be a consequence of the smaller correction exponents ω for larger a. The discrepancy between $\overline{\nu}^w$ and ν^g is small yet noticeable. In principle every method gives similar results with nearly identical errors. However, as already mentioned, we realized that the weighted mean approach intrinsically
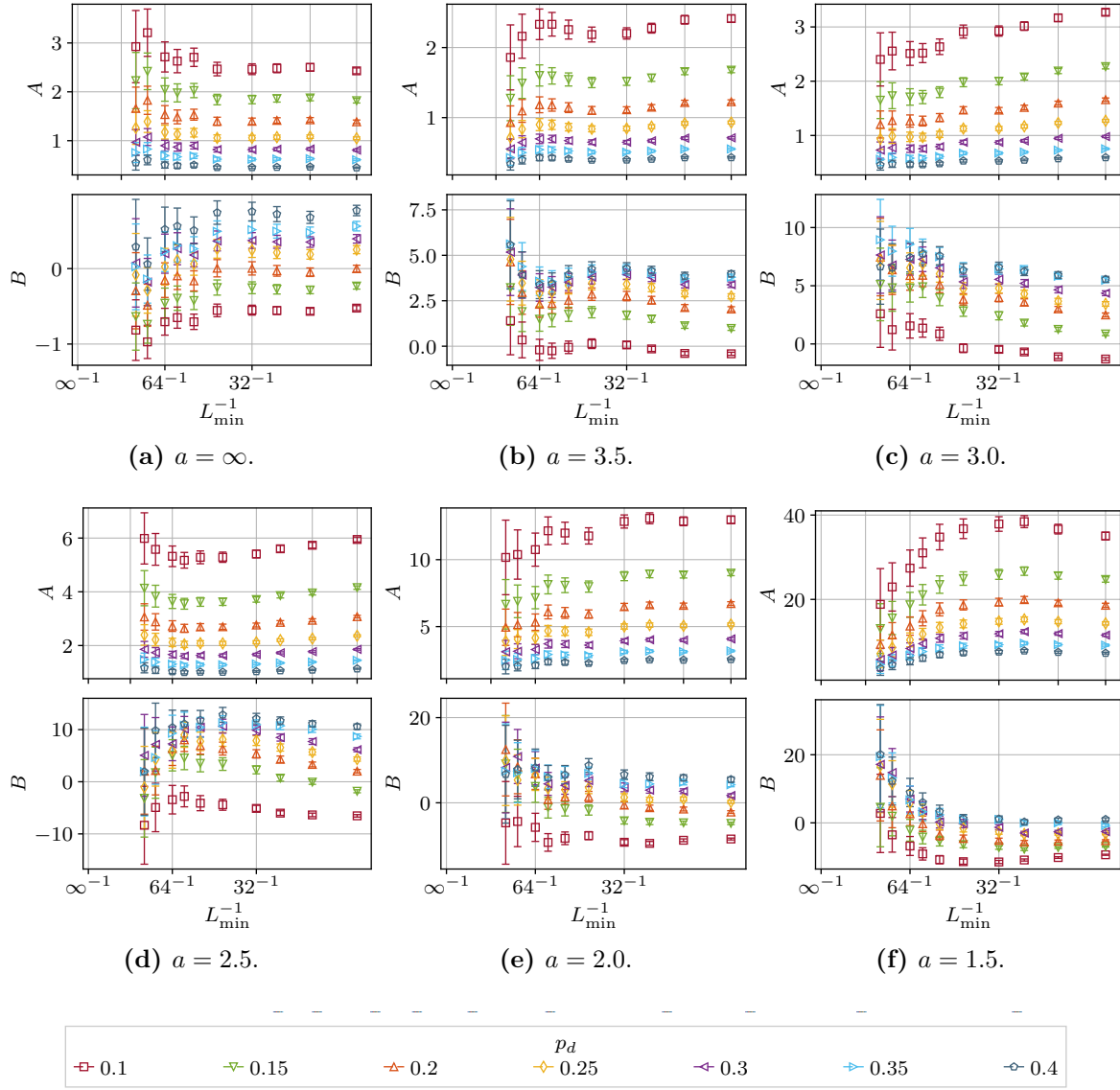
Figure 4.37: Amplitudes A_{p_d} and B_{p_d} for each included concentration of defects $p_d \geq p_d^{\min}$ with $p_d^{\min} = 0.1$ for the corrected global fit ansatz given in Equation (4.56) in dependence of the $L_{\min}$.

produces biased results due to the correlation between the fit parameters and their errors. It is discussed in Appendix A.2. This motivated us to take the corrected global fit ansatz as the final method of choice.

Finally, let us look into our estimates in the context of already published estimates. We summarized our results and results from other works in Table 4.7 and Figure 4.41.

Let us begin with the uncorrelated case with $a = \infty$. Our estimate for the uncorrelated case is $\nu = 0.6831(30)$. Comparing this to known results from other works summarized in Table 4.7 (including our result), it lies slightly above most of the other estimates but fits perfectly within the errorbars as is depicted in the zoomed view in Figure 4.41. We conclude that our estimated ν is in very good agreement with the literature. This is an important observation which statistically proves our ν estimation process and allows us to assume that the same procedure will be correct in the correlated cases as well. Considering our estimated error $\epsilon(\nu) = 0.0030$ we have a small error comparing to other works listed in Table 4.7.
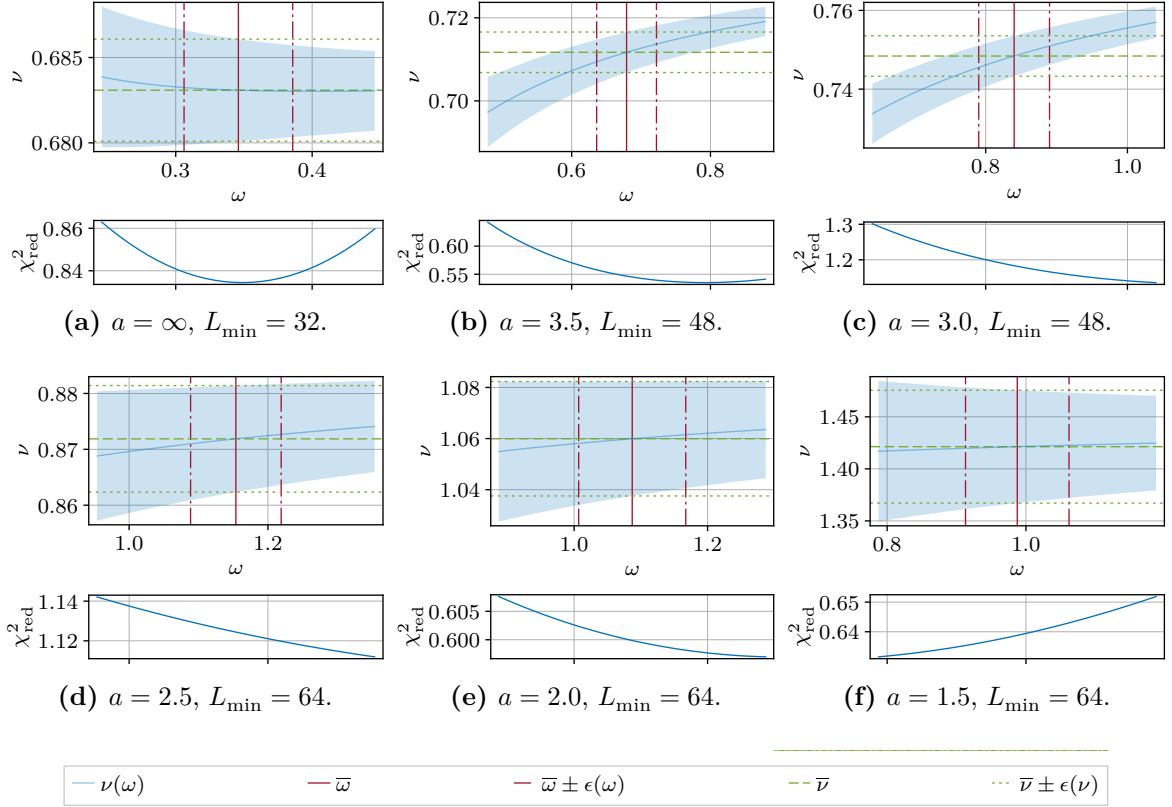
Figure 4.38: The dependence of the corrected global fit results according to Equation (4.56) on the correction exponent ω. The lower plots show the qualities of the fit χ^2_{red}. For a wider range of different ω values, the fits remain stable and reasonably good. The estimates $\nu(\omega)$ are mostly covered through the ranges $\bar{\nu} \pm \epsilon(\nu)$. The values $\bar{\nu}$ are the final estimates from Table 4.5. The bar is added to distinguish between the free parameter ν and the fixed values $\bar{\nu}$.

Table 4.6: Comparison of the final estimates of ν from different fitting methods. The values are also compared in Figure 4.40. The corrected fits estimates $\bar{\nu}^w$ and ν^g are very close together for all a.

a	$\bar{\nu}^w_{\mathrm{lin}}$	$\bar{\nu}^w$	ν^g
∞	0.6913(15)	0.6843(31)	0.6831(30)
3.5	0.7427(25)	0.7122(49)	0.7117(49)
3.0	0.7812(35)	0.7532(53)	0.7484(52)
2.5	0.8887(61)	0.8735(96)	0.8719(96)
2.0	1.079(14)	1.067(23)	1.060(23)
1.5	1.449(32)	1.435(56)	1.421(55)

However, this has to be taken with some care since, as explained previously, the choice of final $p_d^{\min}$ and $L_{\min}$ is not a solid decision but rather an interplay between error size, fit quality and $L_{\min}$-dependence.

Let us move to the correlated cases. In this case we have two separate things to compare: the conjecture by Weinrib and Halperin, $\nu = 2/a$, and the results obtained by other groups. When comparing our results for the correlated cases, we cannot reproduce the Weinrib and Halperin prediction (compare the $2/a$ curve in Figure 4.41 with the corresponding estimates ν). Nevertheless, we see the qualitative behavior $\nu \propto 1/a$ and a deviation from $\nu = 2/a$ by
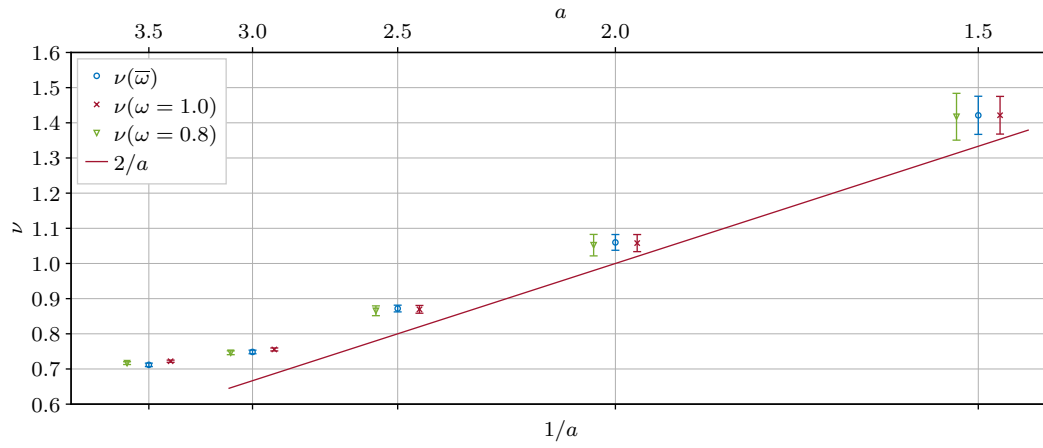
Figure 4.39: Comparison of the corrected global fit results according to Equation (4.56) for the chosen $\overline{\omega}$ as given in Table 4.5 to the choices $\omega = 1.0$ and $\omega = 0.8$ for all correlation exponents $a \neq \infty$. The estimates for $\omega = 1.0$ and $\omega = 8.0$ are shifted left and right from the corresponding a to increase readability. They are meant to lie exactly one over the other for every single considered a. The results are in a prefect agreement within their error bars.
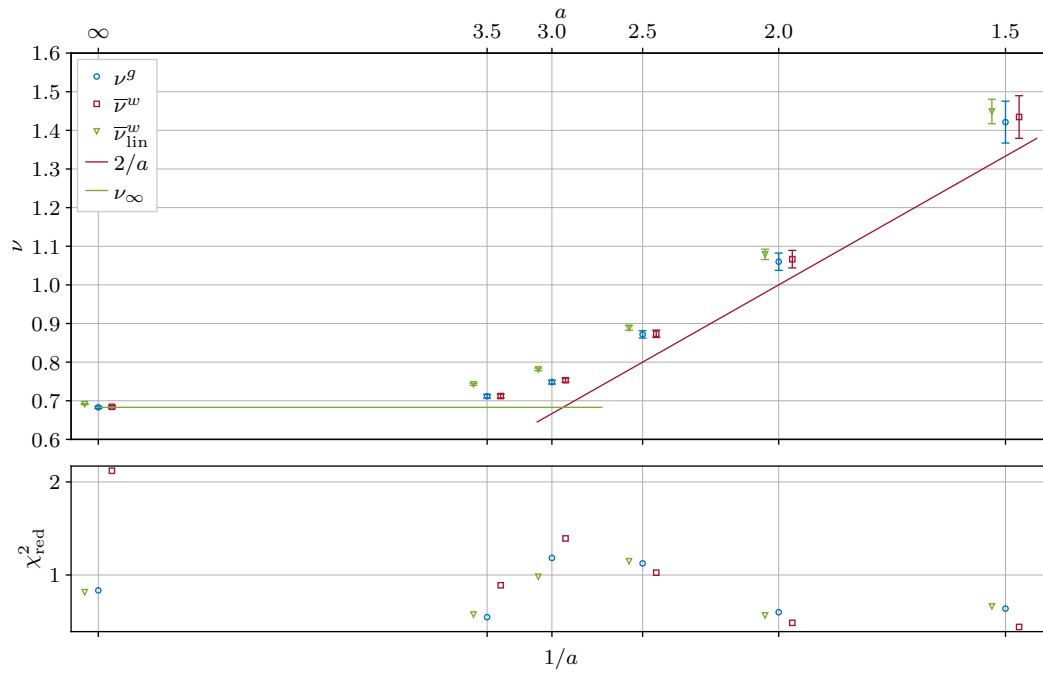
Figure 4.40: Comparison of the final estimates of ν from different fitting methods. The values are also reported in Table 4.6. For each a the points are slightly shifted for better visibility. The uncorrelated disorder case critical exponent was set to $\nu_\infty = 0.683$ as an average value from other works listed in Table 4.7 (only Monte Carlo results).

about $10\,\%$. The estimated errors, which do not cover the $2/a$, suggest that these deviations are not a consequence of the uncertainties coming from our estimation procedure. We completely disagree with the Renormalization Group results by Prudnikov et al. [PPF00] and their Monte Carlo results for $a = 2.0$ in Ref. [Pru+05]. The reason for such a completely different behavior of the critical exponent ν which is obtained in Ref. [PPF00] remains unclear to us. Moving to the Monte Carlo results by Ballesteros et al. [BP99] and Ivaneyko

Table 4.7: Critical exponent ν comparison to the literature. For a more detailed comparison of various works see Table 2.3. Legend: $*$ — averaged over various p_d by us (weighted mean), $\bullet$ — not measured (fixed value or the one which gives best fits), MC — Monte Carlo simulations, RG — Renormalization Group calculations.

Type	Reference	a	ν	ω
	Uncorrelated disorder			
MC	Ballesteros et al. [Bal+98a]	∞	0.6837(53)	0.37(6)
	Calabrese et al. [Cal+03]	∞	0.683(3)	—
	Berche et al. [Ber+04]	∞	0.68(2)	—
	Murtazaev et al. [MKB04]	∞	0.678(6)*	—
	Hasenbusch et al. [Has+07]	∞	0.683(2)	0.33(3)
RG	Pakhnin et al. [PS00]	∞	0.671(5)	0.32(6)
	Pelissetto et al. [PV00]	∞	0.678(10)	0.25(10)
	Kompaniets et al. [KKS21]	∞	0.675(19)	0.15(10)
	This work	∞	0.6831(30)	0.346(40)
	Correlated disorder			
MC	Ballesteros et al. [BP99]	2.0	1.012(16)	1.01(13)
	Prudnikov et al. [Pru+05]	2.0	0.71(1)	0.76(5)$^\bullet$
	Ivaneyko et al. [Iva+08]	2.0	0.958(4)	0.8$^\bullet$
RG	Weinrib et al. [WH83]	$a < d$	2/a	—
	Prudnikov et al. [PPF00]	3.0	0.6715	—
		2.5	0.7046	—
		2.0	0.715	—
	This work	3.5	0.7117(49)	0.679(44)
		3.0	0.7484(52)	0.840(50)
		2.5	0.8719(96)	1.154(66)
		2.0	1.060(23)	1.087(81)
		1.5	1.421(55)	0.988(75)

et al. [Iva+08], we cannot agree on them according to the errorbars. However, both results are close to the prediction $2/a = 1$ in the case of $a = 2.0$, which also supports the qualitative behavior $\nu \propto 1/a$.

Taking a closer look at the dependence of the critical exponent ν on the correlation exponent a, we can see that the deviation from the $2/a$ behavior is biggest at $a \approx 3.0$. This could be an indication of a crossover regime where the system switches from the (effectively) uncorrelated disorder to the correlated disorder case.

Summary. We used three different finite-size scaling ansatzes to get the critical exponent ν. Finally, the corrected global ansatz was chosen, and we studied various aspects of the fits. We analyzed the amplitudes, the dependence on the correction exponent ω and compared the results from different ansatzes with each other as well as with other works. Our results for the uncorrelated case is in a very good agreement with other groups. For the corrected cases, we cannot reproduce the prediction of Weinrib and Halperin $\nu = 2/a$ quantitatively. However, we observe a qualitative behavior proportional to $1/a$.
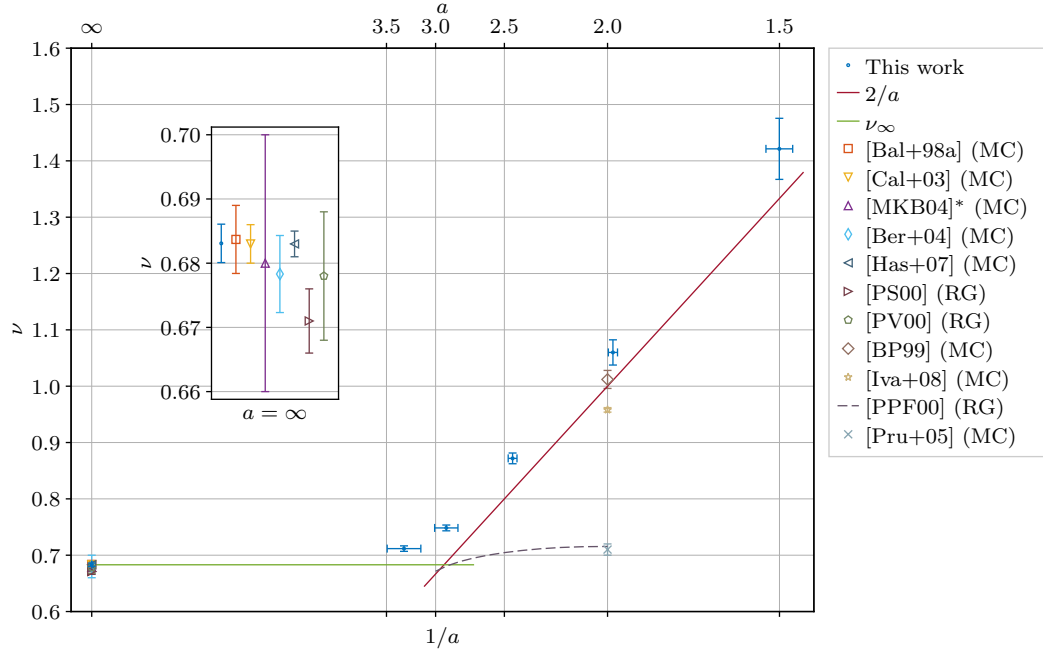
Figure 4.41: Final results of the critical exponents ν compared to the known results from the literature and the conjecture by Weinrib and Halperin, $\nu = 2/a$. The horizontal errorbars come from the true measured $\overline{a}$ values from Table 4.1. The uncorrelated disorder case critical exponent was set to $\nu_\infty = 0.683$ as an average value from other works listed in Table 4.7. The inset shows a zoom to the uncorrelated case $a = \infty$. The results of this work lie about 10 % above the conjecture $\nu = 2/a$.

4.5.3 Critical exponent γ

The next critical exponent which we obtained in this work is the critical exponent of the susceptibility γ. We repeat the definition from Equation (2.39) of the susceptibility,

$$\chi = \beta V \left([\![\langle m^2 \rangle]\!] - [\![\langle |m| \rangle^2]\!] \right) . \tag{4.57}$$

Note, that we used the definition which shows a peak at the critical temperature in contrast to the definition of $\tilde{\chi}$ from Equation (2.41), which is valid only in the high temperature phase and does not show a peak. A peak $\hat{\chi}$ allowed us to proceed in the same way as in the case with the critical exponent ν. We restricted our analysis to the corrected global fit ansatz, which follows from Equation (3.23) and reads

$$\hat{\chi}(L, p_d) = A_{p_d} L^r \left(1 + B_{p_d} L^{-\omega} \right) , \tag{4.58}$$

where the $\hat{\chi}$ values are the previously obtained peaks of the susceptibility. The exponent $r = \gamma/\nu$ was the global fit parameter for all concentrations of defects p_d. By using our estimate for ν, we then get

$$\gamma = r\nu, \quad \epsilon(\gamma) = \sqrt{(r\epsilon(\nu))^2 + (\nu\epsilon(r))^2} . \tag{4.59}$$

As in the case of the critical exponent ν, we took the estimates of the correction exponents ω from Table 4.2 and fixed them in Equation (4.58). We varied the minimum lattice $L_{\min}$ and the minimum concentration of defects $p_d^{\min}$ to study the thermodynamic limit. Results of the

ratios r are shown in Figure 4.42 together with the quality of fits χ^2_{red} and the overlapping index $\mathscr{A}(r)$ which was introduced in Equation (4.53) and basically quantitatively shows the compatibility of r estimates for different p_d^{min} choices.

Let us first discuss the choice of final L_{min} and p_d^{min}. For all considered correlated cases $a \neq \infty$, the quality of fits was bad when $p_d = 0.05$ was included into the global fit. Further, any choice with $p_d^{\mathrm{min}} \geq 0.1$ barely had an influence on the χ^2_{red} values at each L_{min}. However, in order to have a consistent p_d^{min}-independent result with $\mathscr{A}(r) \gtrapprox 0.75$, we had to exclude the $p_d = 0.1$ as well. This was also true for the uncorrelated case with $a = \infty$. Finally, we set $p_d^{\mathrm{min}} = 0.15$ for all considered cases. Concerning L_{min}, we have then used the lowest possible L_{min} which was consistent with a good χ^2_{red} and the $\mathscr{A}(r) \gtrapprox 0.75$ condition. This setup yielded us $L_{\mathrm{min}} = 20$ for the uncorrected case, $L_{\mathrm{min}} = 64$ for all correlated cases except for $a = 1.5$, where we chose $L_{\mathrm{min}} = 80$. The final estimates $r = \gamma/\nu$ as well as the calculated γ and η with the chosen L_{min} and the resulting χ^2_{red} are summarized near the end of this section in Table 4.8.

For the chosen p_d^{min} we have studied the fits more detailed. Let us first provide the data $\hat{\chi}(L, p_d)$ and the resulting fits in Figure 4.44 and the amplitudes A_{p_d} and B_{p_d} of the fits in Figure 4.45. We will start with the uncorrelated case $a = \infty$. We clearly see that the correction amplitudes are in the range $-1 \leq B_{p_d} \leq 0$ which suggest a rather small correction influence. This can also be visually verified by looking into Figure 4.44 where we see that the curves scaled by L^r (lower plots) are indeed quite parallel and horizontal. The amplitudes are also stable with respect to the chosen L_{min}. This stability is also given for the amplitudes A_{p_d}. Contrarily, the amplitudes for A_{p_d} and B_{p_d} do depend on the L_{min} for all correlated cases. The total amplitudes A_{p_d} increase with increasing L_{min} while the correction amplitudes B_{p_d} decrease. The total amplitudes A_{p_d} are a bit smaller than for the uncorrelated case but are compatible. On the other hand, the correction amplitudes B_{p_d} are positive and their value strongly depend on the chosen a. For the strongest correlation exponent $a = 1.5$ they go up to $B_{p_d} \approx 50$. Also, one clearly sees that the smallest amplitudes ≈ 0 are reached for lager concentrations p_d and larger L_{min}. For the strongest correlation exponent $a = 1.5$ the zero is not reached at all. When we look at the correlated cases in Figure 4.44, we can see the reason for the large correction amplitudes. The curves $\hat{\chi}(L)$ have very strong curvature for smaller L. On the other hand, interestingly, the values $\hat{\chi}$ seem to approach a constant value for larger L or at least they come very close together for all different concentrations p_d. To incorporate the strong corrections for the small L, we tried to use an ansatz with second order corrections ($\propto L^{-2\omega\gamma/\nu}$). However, the fit results were not satisfying, and we finally dropped this approach and returned to the simpler ansatz given in Equation (4.58) and used a higher L_{min} at the end.

Next, we checked the dependence of the resulting exponents γ on the choice of the correction exponent ω. The dependence is shown for each a for the chosen L_{min} and p_d^{min} in Figure 4.46. Because the error $\epsilon(\gamma)$ is quite large due to the contribution coming from the critical exponent ν, Equation (4.59), we see that the dependence on ω in the range $\omega \pm \epsilon(\omega)$ is completely covered by the error $\epsilon(\gamma)$ in all cases. To get an impression on how large the contribution of the error of the exponent ν affects the resulting γ compared to the fit error ($\epsilon(r)$), we compared the individual contributions in Table 4.8. It is worth to note that except for the uncorrelated

(a) $a = \infty$.

(b) $a = 3.5$.

(c) $a = 3.0$.

(d) $a = 2.5$.

(e) $a = 2.0$.

(f) $a = 1.5$.

$p_d^{\min}$ / $\tilde{p}_d^{\min}$ for $\mathscr{A}$-plots

○ 0.05   □ 0.1   ▽ 0.15   △ 0.2
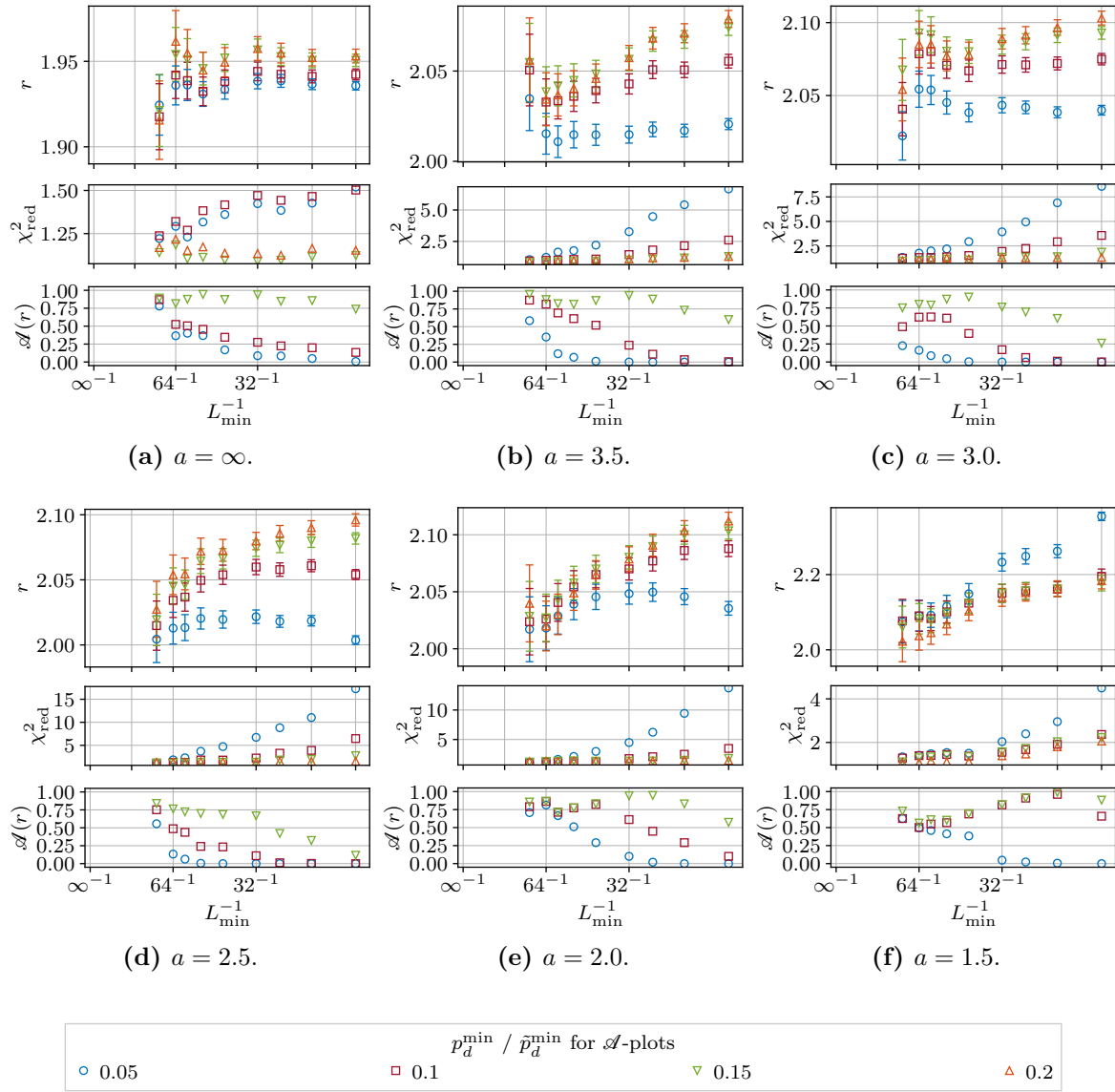
Figure 4.42: Observed fit parameters $r = \gamma/\nu$ to the corrected global fit ansatz given in Equation (4.58) for various $L_{\min}$, $p_d^{\min}$ and all considered correlation exponents a. The quality of the fits χ^2_{red} is given in the middle plots while the overlapping index is presented in the lower plots. The overlapping index $\mathscr{A}(r)$ tells how well the estimates for different minimum concentration of defects $p_d^{\min}$ in the range $\tilde{p}_d^{\min} \leq p_d^{\min} \leq 0.2$ match each other. $\mathscr{A}$ for $\tilde{p}_d^{\min} = 0.2$ is not plotted, since it is always equal to one.

case, the contributions to the total error $\epsilon(\gamma)$, i.e., the terms $r\epsilon(\nu)$ and $\nu\epsilon(r)$ are very similar. A possible reason for this correlation is of course the usage of the same data sets for the estimates r and ν, respectively.

Having discussed some aspects related to the fits themselves, let us turn to the comparison of our final estimates to the results from literature. We present our results with some additional information like the minimum lattice size $L_{\min}$ and quality of the fits χ^2_{red} in Table 4.8. In Figure 4.47 we present the ratios $r = \gamma/\nu$ in dependence of correlation exponent a. Finally, the results are put into context with other works in Figure 4.48 and Table 4.9.
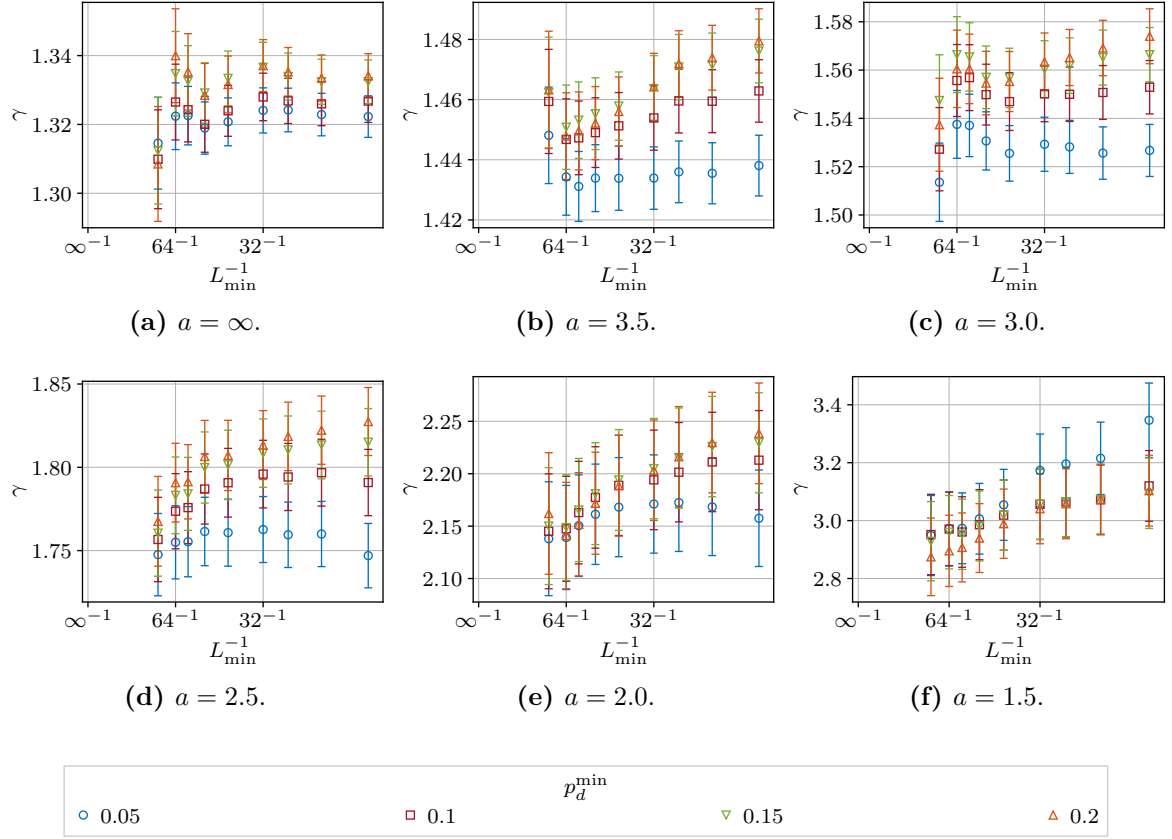
Figure 4.43: Estimates of the critical exponent γ from the fit parameters r to the corrected global fit ansatz given in Equation (4.58) for various $L_{\min}$, $p_d^{\min}$ and all considered correlation exponents a. See Figure 4.42 for the ratios themselves.

Table 4.8: Final estimates of the critical exponent γ. The minimum concentration of defects $p_d^{\min} = 0.15$ was used in all cases. For convenience, the results for ν and ω from Tables 4.2 and 4.5 are also shown, respectively. The terms $r\epsilon(\nu)$ and $\nu\epsilon(r)$ are the contributions to the total error $\epsilon(\gamma)$ according to Equation (4.59).

a	ν	r	$\gamma = r\nu$	$\eta = 2 - r$	$\nu\epsilon(r)$	$r\epsilon(\nu)$	χ^2_{red}	$L_{\min}$	ω
∞	0.6831(30)	1.9506(36)	1.3324(64)	0.0494(36)	0.00245	0.00584	1.12	20	0.346(40)
3.5	0.7117(49)	2.039(14)	1.451(15)	$-0.039(14)$	0.00987	0.00994	0.871	64	0.679(44)
3.0	0.7484(52)	2.093(16)	1.566(16)	$-0.093(16)$	0.0115	0.0108	0.989	64	0.840(50)
2.5	0.8719(96)	2.045(14)	1.783(24)	$-0.045(14)$	0.0122	0.0195	1.16	64	1.154(66)
2.0	1.060(23)	2.027(21)	2.149(51)	$-0.027(21)$	0.022	0.0454	1.29	64	1.087(81)
1.5	1.421(55)	2.061(56)	2.93(14)	$-0.061(56)$	0.0789	0.112	1.11	80	0.988(75)

Let us discuss the uncorrelated case with $a = \infty$. Comparing to other Monte Carlo results our estimate is a bit lower but in a reasonable agreement. On the other hand, it lies slightly above the predictions from the Renormalization Group (RG) calculations. Since we used more different concentrations p_d than any other Monte Carlo simulation results, and the RG results are p_d-independent by definition, we can argue that the deviation to other Monte Carlo results in the direction to the RG estimates could be and improvement in this case. However, the only solid statement we can provide here is the consistency of the results within the error ranges.

(a) $a = \infty$, $L_{\min} = 20$.

(b) $a = 3.5$, $L_{\min} = 64$.

(c) $a = 3.0$, $L_{\min} = 64$.

(d) $a = 2.5$, $L_{\min} = 64$.

(e) $a = 2.0$, $L_{\min} = 64$.

(f) $a = 1.5$, $L_{\min} = 80$.

p_d							
○ 0.05	□ 0.1	▽ 0.15	△ 0.2	◇ 0.25	◁ 0.3	▷ 0.35	⬠ 0.4
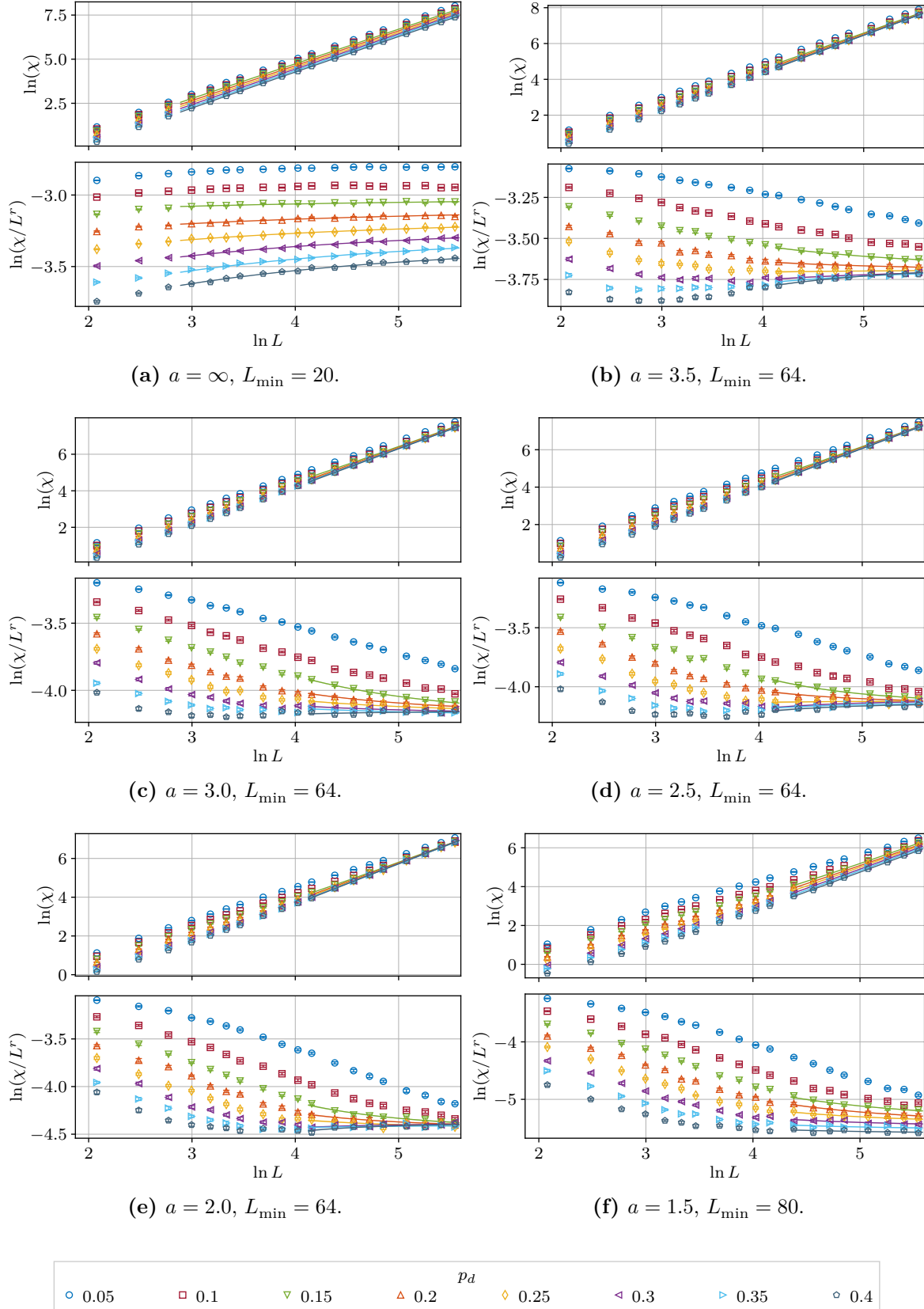
Figure 4.44: Examples of the corrected global fits to the ansatz in Equation (4.58) for all correlation exponents a. The minimum included concentration of defects was $p_d^{\min} = 0.15$ and the maximum included concentration of defects was $p_d^{\max} = 0.4$. The upper plots show the fitted observables $\hat{\chi}(L, p_d)$ versus L on a logarithmic scale. In the lower plots, the observables are divided by L^r where $r = \gamma/\nu$. This form allows us to better visualize the deviations from the leading behavior L^r through the correction terms with the amplitudes B_{p_d}.
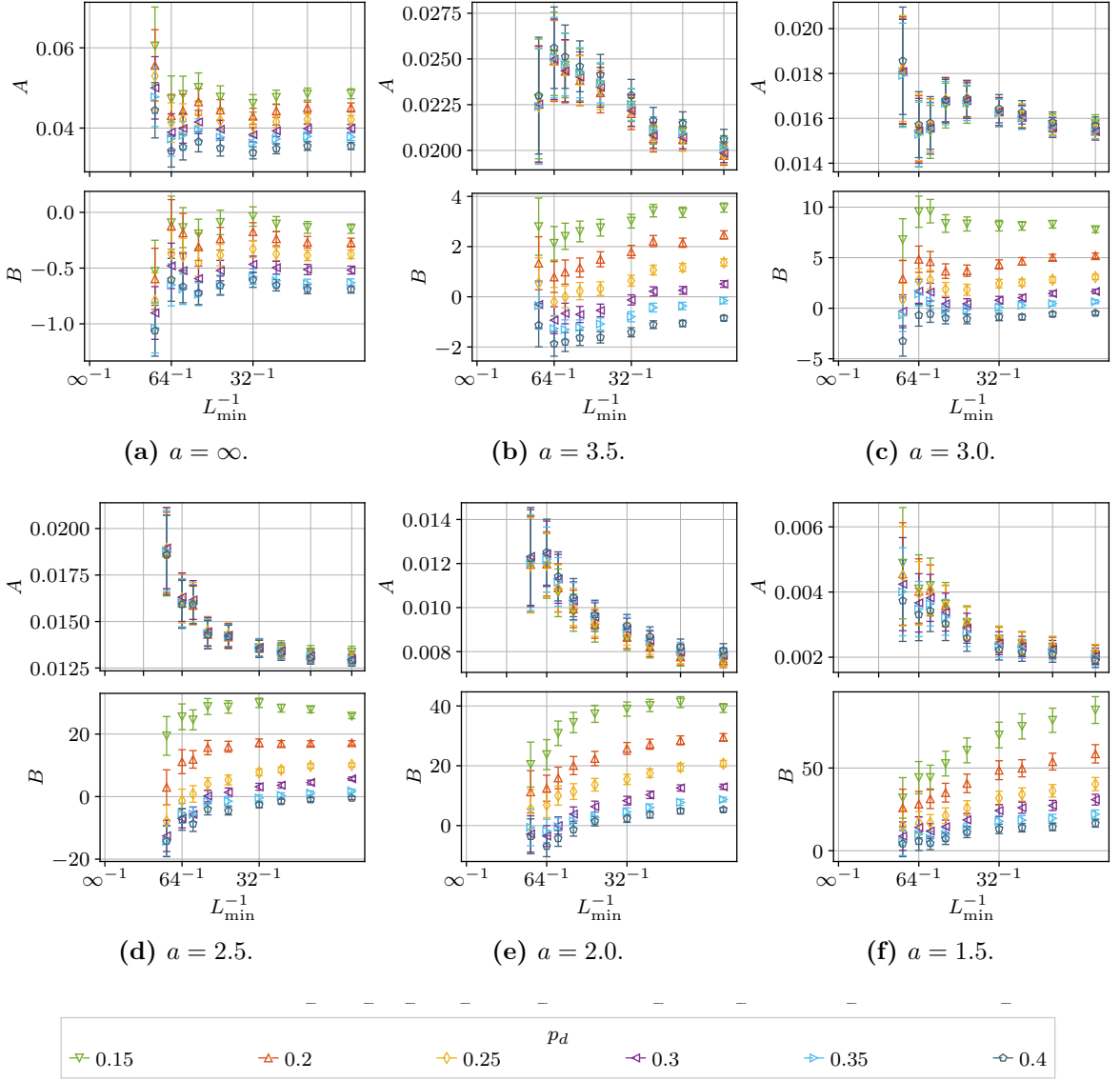
Figure 4.45: Amplitudes A_{p_d} and B_{p_d} for each included concentration of defects $p_d \geq p_d^{\min}$ with $p_d^{\min} = 0.15$ for the corrected global fit ansatz given in Equation (4.58) in dependence of the $L_{\min}$. Consistent ordering can be seen for all cases in the correction amplitudes B_{p_d} while for the global amplitudes A_{p_d} the values mostly overlap except for the uncorrelated case.

Let us move to the correlated cases. But before going to the actual values γ, we first would like to take a closer look at the ratios r. We show the ratios r in Figure 4.47. We observe a negative value of η for all correlation exponents a, since the ratio r is greater than two and from Equation (2.65) it follows, that $\eta = 2 - r$. A negative η was also observed in Refs. [PPF00; Pru+05] for the three-dimensional Ising model. However, due to the differences in the ν estimates, their γ estimate does not coincide with our result. All other works we compared our work to, show a positive η. On the other hand, even for the uncorrelated case, the p_d-dependent values γ/ν can have values larger than 2 [Heu93; WD98][1]. Heuer [Heu93] explains the negative η values as being an artifact of a crossover regime in the uncorrelated

---

[1] We omitted these references in the comparison in Tables 2.3 and 4.9 and the plot Figure 4.48 since they estimated only the ratios γ/ν and β/ν and not the exponents themselves.
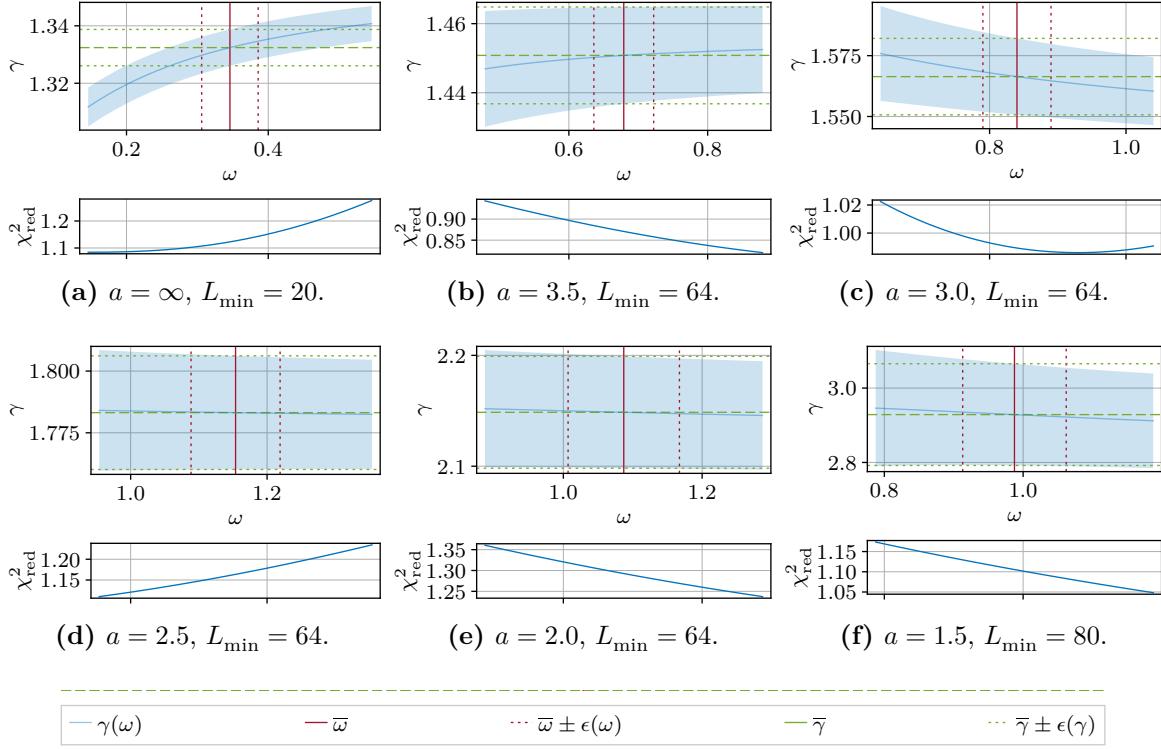
Figure 4.46: The dependence of the corrected global fit results γ on the correction exponent ω. The lower plots show the qualities of the fit χ^2_{red}. For a wider range of different ω values, the fits remain stable and reasonably good. The estimates $\gamma(\omega)$ are mostly covered through the error ranges $\overline{\gamma} \pm \epsilon(\gamma)$. The values $\overline{\gamma}$ are the final estimates from Table 4.8. The bar is added to distinguish between the free parameter γ and the fixed values $\overline{\gamma}$.
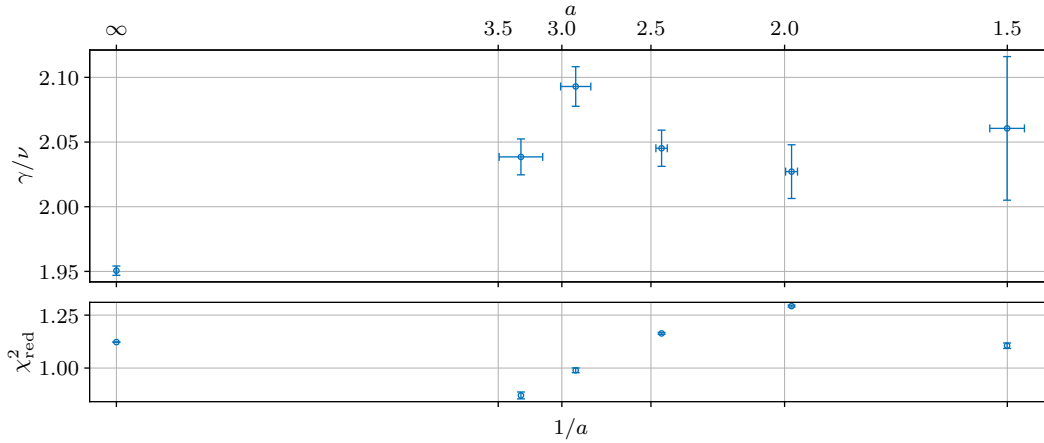
Figure 4.47: Ratios $r = \gamma/\nu$ for the finally chosen $L_{\min}$ and $p_d^{\min}$ parameters for each correlation exponent a. A prominent, approximately constant value can be observed for all correlated cases.

case. Also, we do not observe negative η in the uncorrelated case, we still can imagine that there is a crossover regime at around $a \approx 3.0$ in the correlated cases. Such a crossover regime could explain the negative values at correlation exponents $3.5 \leq a \leq 2.5$. On the other side, for the strongest correlations $a = 2.0$ and $a = 1.5$ we see, that the ratio fitted to the ansatz in Equation (4.58) does not reach a constant value even for the largest $L_{\min}$ choices,

Table 4.9: Critical exponent γ comparison to the literature. For a more detailed comparison of various works see Table 2.3. Legend: † — calculated from other exponents through scaling relations, ∗ — averaged over various p_d by us (weighted mean), ? — result is stated in the paper as an expression for the case where the dimension of the order parameter is $m > 1$, MC — Monte Carlo simulations, RG — Renormalization Group calculations.

Type	Reference	a	ν	η	γ
	Uncorrelated disorder				
MC	Ballesteros et al. [Bal+98a]	∞	0.6837(53)	0.0374(45)	$1.342(10)^\dagger$
	Calabrese et al. [Cal+03]	∞	0.683(3)	0.035(2)	$1.342(6)^\dagger$
	Berche et al. [Ber+04]	∞	0.68(2)	$0.029(60)^\dagger$	1.34(1)
	Murtazaev et al. [MKB04]	∞	$0.678(6)^*$	$0.045(19)^{*,\dagger}$	$1.3258(40)^*$
	Hasenbusch et al. [Has+07]	∞	0.683(2)	0.036(1)	$1.341(4)^\dagger$
RG	Pakhnin et al. [PS00]	∞	0.671(5)	0.025(10)	$1.325(3)^\dagger$
	Pelissetto et al. [PV00]	∞	0.678(10)	0.030(3)	1.330(17)
	Kompaniets et al. [KKS21]	∞	0.675(19)	$0.024(79)^\dagger$	1.334(38)
	This work	∞	0.6831(30)	$0.0494(36)^\dagger$	1.3324(64)
	Correlated disorder				
MC	Ballesteros et al. [BP99]	2.0	1.012(16)	0.043(4)	$1.980(33)^\dagger$
	Prudnikov et al. [Pru+05]	2.0	0.71(1)	$-0.030(36)^\dagger$	1.441(15)
	Ivaneyko et al. [Iva+08]	2.0	0.958(4)	$0.191(18)^\dagger$	1.733(11)
RG	Weinrib et al. [WH83]	$a < d$	$2/a$	$0^?$	$4/a^?$
	Prudnikov et al. [PPF00]	3.0	0.6715	0.0327	$1.321^\dagger$
		2.0	0.715	-0.0205	$1.4456^\dagger$
		2.5	0.7046	0.0118	$1.4008^\dagger$
	This work	3.5	0.7117(49)	$-0.039(14)^\dagger$	1.451(15)
		3.0	0.7484(52)	$-0.093(16)^\dagger$	1.566(16)
		2.5	0.8704(62)	$-0.045(14)^\dagger$	1.780(18)
		2.0	1.082(15)	$-0.027(21)^\dagger$	2.193(37)
		1.5	1.465(43)	$-0.061(56)^\dagger$	3.02(12)

see Figure 4.42. Therefore, chances are that for larger lattice sizes the ratios will go below 2 and the exponent η will become positive again. Since we have not found a rigor argument for a restriction $\eta \geq 0$ (and in fact it is negative in some cases, e.g., in three-dimensional percolation [Adl+90; JS98] or the three-dimensional cubic model [BRR85]), we can accept the negative sign in this work. It would be great, if preciser measurements and/or analytic results could provide us with more clarity in the future. From our data we further can assume that possibly the ratio is constant and independent of a,

$$r = \frac{\gamma}{\nu} \approx 2.05(3) \, . \tag{4.60}$$

In the correlated case, all works with Monte Carlo simulations which we can use to compare our work to have studied the case of $a = 2.0$. We cannot reproduce the values from other groups even in the range of $\pm 4\epsilon(\gamma)$. Additionally, the results between other groups diverge as well. As in the case of the critical exponent ν, we completely disagree with the results from works by Prudnikov et al., Refs. [PPF00; Pru+05], quantitatively and qualitatively. This is not surprising, since the calculation of the exponent γ relies on the exponent ν (at least in the case of a finite-size scaling analysis). The dependence on ν also clearly shows up in the overall
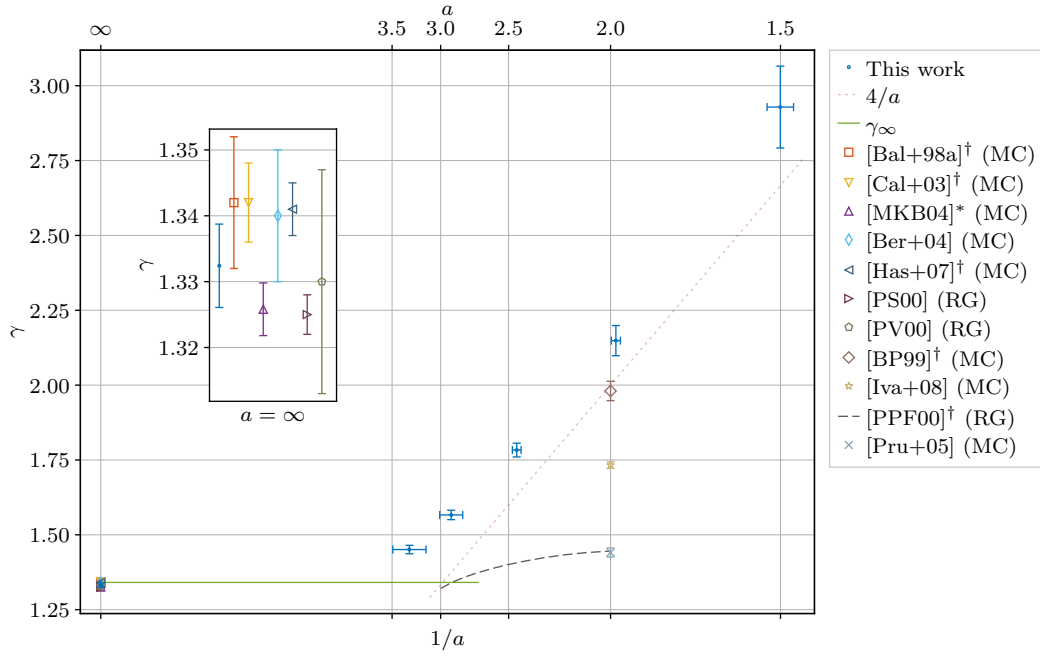
Figure 4.48: Final results of the critical exponent γ compared to the known results from the literature. The horizontal errorbars come from the true measured $\overline{a}$ values from Table 4.1. The value $\gamma_\infty = 1.338$ is the mean value from various groups (only (MC)) for the uncorrelated case and is used as orientation. The line $4/a$ is shown to qualitatively compare the proportionality to $1/a$. Results from Monte Carlo simulations are marked with (MC) while results from Renormalization Group calculations are labeled with (RG). For the works marked with $*$, we calculated the values by ourselves as a weighted mean over different concentrations. In works marked with $\dagger$, the exponent γ was calculated from η and ν.

qualitative behavior of $\gamma(a)$. We observe a proportional behavior $\gamma \propto 1/a$ with a line which is slightly above $4/a$. This is in agreement with the conjecture by Weinrib and Halperin [WH83] for a model with dimension of the order parameter $m > 1$, $\gamma = 4/a$. However, there is no prediction made for $m = 1$ in Ref. [WH83]. The crossover region between the correlated and the (effectively) uncorrelated cases can be seen at $a \approx 3.0$. As in the case with the critical exponent ν, we have a quite large error for the smallest $a = 1.5$. Concerning the quality of the fits, we have good values of $\chi^2_{\mathrm{red}} \leq 1.29$ for all cases which indicates that the fits match the data well.

Summary. We obtained the critical exponent γ in reasonable agreement with other works for the uncorrelated cases. Our value is inbetween the predictions from the Renormalization Group calculations and Monte Carlo simulations. For the correlated cases, we see a constant ratio of $\gamma/\nu \approx 2.05(3)$ and hence observe a negative $\eta \approx -0.05(3)$. We disagree with other works for the correlated for case with $a = 2.0$. Our estimates show a $\propto 1/a$ and lie slightly above $4/a$.

4.5.4 Critical exponent β

After the critical exponents ν and the γ were estimated, im principle all other exponents can be derived by using the scaling relations Equations (2.62) to (2.65), as was discussed in Section 2.3.3. However, in order to get a more consistent picture of the model, we studied the

critical exponent of the magnetization β separately. We will closely follow the steps of the estimation of the critical exponent γ. Let us recall that the derivative of the magnetization $\partial_\beta(|m|)$ has the following definition, Equation (2.43),

$$\partial_\beta(|m|) = V([\![\langle|m|\rangle]\!]\,[\![\langle e\rangle]\!] - [\![\langle|m|\,e\rangle]\!]) \,, \tag{4.61}$$

and its finite-size scaling presented in Equation (3.25) leads to the corrected global fit ansatz

$$\widehat{\partial_\beta(|m|)}(L, p_d) = A_{p_d} L^r \left(1 + B_{p_d} L^{-\omega}\right) \,, \tag{4.62}$$

where the exponent is $r = (1 - \beta)/\nu$ and $\widehat{\partial_\beta(|m|)}$ are the peaks found as described in Section 4.3.3. The ratio r leads to the critical exponent β,

$$\beta = 1 - r\nu, \quad \epsilon(\beta) = \sqrt{(\nu\epsilon(r))^2 + (r\epsilon(\nu))^2} \,. \tag{4.63}$$

We performed fits to the ansatz in Equation (4.62) and varied the minimum included lattice size $L_{\min}$ and the minimum concentration of defects $p_d^{\min}$. The results of the ratios r are summarized in Figure 4.49. The quality of the fits χ_{red}^2 and the overlapping index $\mathscr{A}(r)$, calculated again with Equation (4.54), which shows the consistency between the estimates obtained with different $p_d^{\min}$ in the range $\tilde{p}_d^{\min} \leq p_d^{\min} \leq 0.2$, are also provided. Additionally, we show the resulting critical exponents β in dependence of $L_{\min}$ and $p_d^{\min}$ in Figure 4.50. As in the case with γ, we selected the final $L_{\min}$ and $p_d^{\min}$ according to the qualities of the fits the condition that $\mathscr{A}(r) \gtrsim 0.75$. Excluding the two smallest concentrations and setting $p_d^{\min} = 0.15$ together with $L_{\min} = 32$ gave us satisfying results for all correlation exponents a. Interestingly, the dependence on the $L_{\min}$ is mostly pronounced in the case of $a = 3.0$ and not for the uncorrelated case or the most strongly correlated case $a = 1.5$. On the other hand, for the uncorrelated case, the results for $p_d^{\min} = 0.05$ are clearly separated from all results with larger $p_d^{\min}$ while in all correlated cases we see a larger overlap between the estimates for different $p_d^{\min}$. The fits for the final settings $p_d^{\min} = 0.15$ and $L_{\min} = 32$ are presented in Figure 4.51.

We see very small corrections to scaling in Figure 4.51. This is also reflected in the correction amplitudes B_{p_d} which are shown in Figure 4.52 together with the global amplitudes A_{p_d} for the chosen $p_d^{\min}$ and all $L_{\min}$. The global amplitudes A_{p_d} get their highest values for the uncorrelated and for strongly correlated cases while in the region $2.0 \leq a \leq 3.5$ the maximum values of the amplitudes are smaller. Contrarily, the (absolute) values of the correction amplitudes B_{p_d} are largest in this region. This probably also explains the strongest $L_{\min}$-dependence of the r for the correlation exponent $a = 3.0$, which we mentioned previously. As it was the case for the critical exponent γ, the correction amplitudes B_{p_d} mostly have similar values for different p_d at each $L_{\min}$.

After the discussion of the global fits, let us look at the dependence of the β estimates on the chosen correction exponent ω. For this purpose, we repeated the fitting procedure for various ω in a wide range around the mean values ω. These dependencies are shown in Figure 4.53. Due to the relatively large errors of the β estimates, we see that the variation of ω in the range $\omega \pm \epsilon(\omega)$ is covered by the error $\epsilon(\beta)$ to a great extent.

In the case of the critical exponent γ we had direct access to the ratio γ/ν because this was the actual parameter of the fit. For the critical exponent β, we fitted the exponent $r = (1 - \beta)/\nu$. However, it is still an interesting question, how the ratio β/ν behaves in

(a) $a = \infty$.

(b) $a = 3.5$.

(c) $a = 3.0$.

(d) $a = 2.5$.

(e) $a = 2.0$.

(f) $a = 1.5$.

$p_d^{\min}$ / $\tilde{p}_d^{\min}$ for $\mathscr{A}$-plots

○ 0.05   □ 0.1   ▽ 0.15   △ 0.2
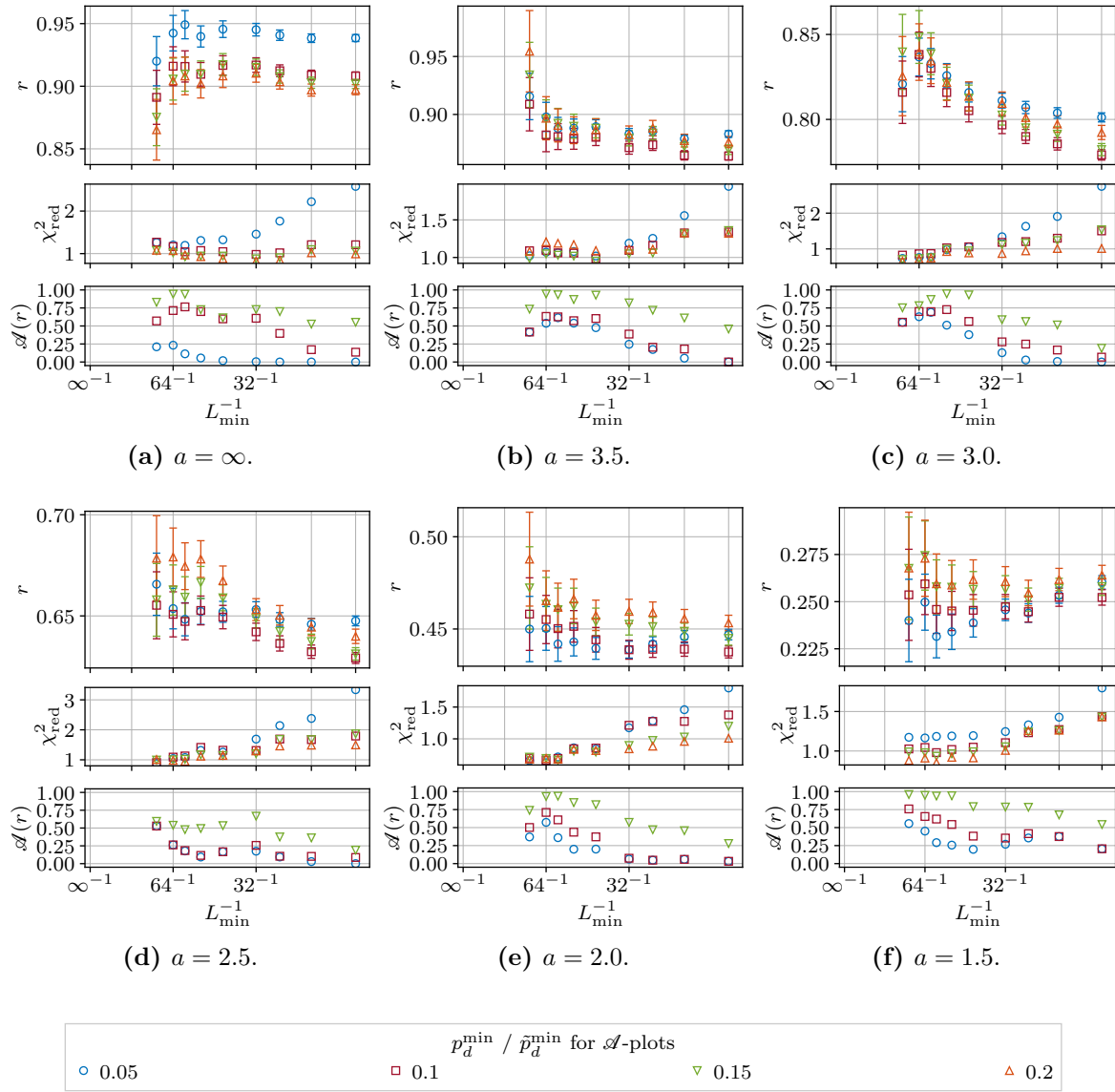
Figure 4.49: Observed fit parameters $r = (1 - \beta)/\nu$ to the corrected global fit ansatz given in Equation (4.62) for various $L_{\min}$, $p_d^{\min}$ and all considered correlation exponents a. The quality of the fits χ_{red}^2 is given in the middle plots while the overlapping index is presented in the lower plots. The overlapping index $\mathscr{A}(r)$ tells how well the estimates for different minimum concentration of defects $p_d^{\min}$ in the range $\tilde{p}_d^{\min} \leq p_d^{\min} \leq 0.2$ match each other. $\mathscr{A}$ for $\tilde{p}_d^{\min} = 0.2$ is not plotted, since it is always equal to one.

dependence of a. We have calculated it with

$$\frac{\beta}{\nu} = \frac{1}{\nu} - r\,, \quad \epsilon\left(\frac{\beta}{\nu}\right) = \sqrt{\left(\frac{\epsilon(\nu)}{\nu^2}\right)^2 + \epsilon(r)^2}\,. \tag{4.64}$$

The estimates are summarized in Table 4.10 and plotted in Figure 4.54. Contrarily to the exponent γ, we do not see a constant value for the correlated cases. Instead, the ratio β/ν falls continuously (except for the $a = 3.5$ case) starting at its largest value for the uncorrelated case.
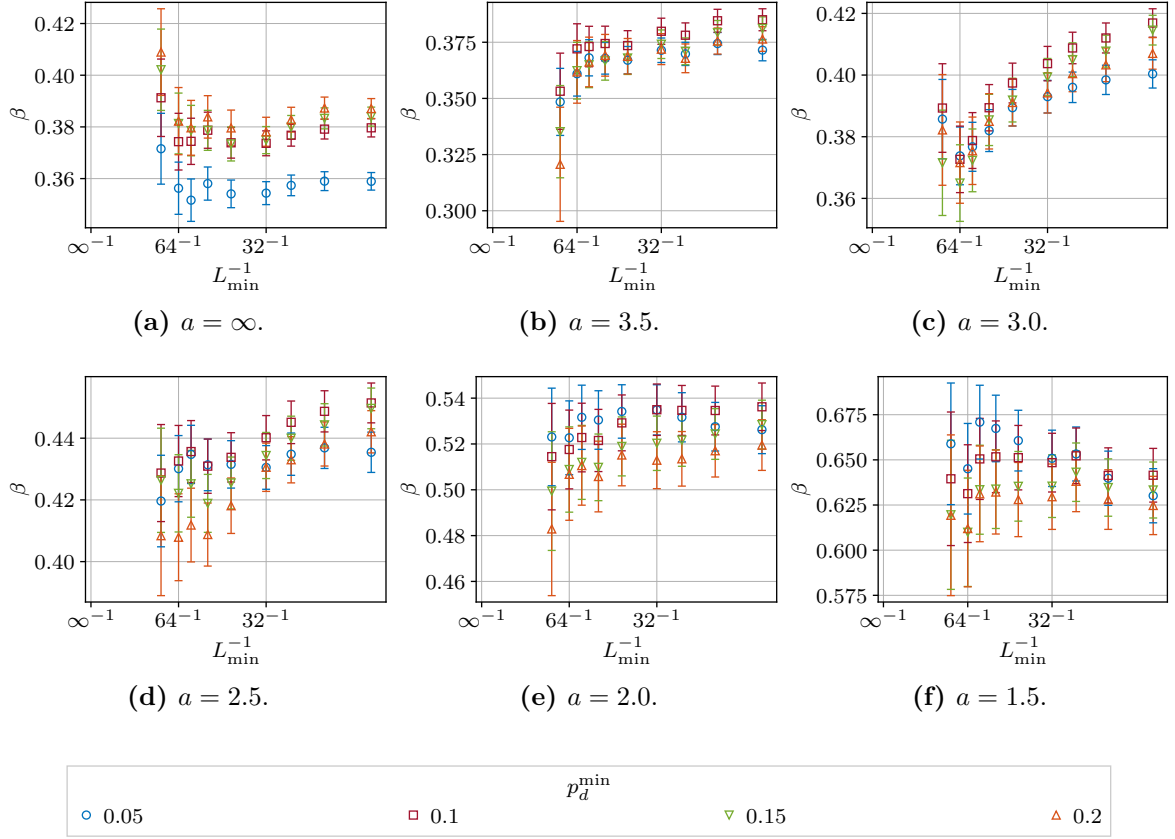
Figure 4.50: Estimates of the critical exponent β from the fit parameters r to the corrected global fit ansatz given in Equation (4.62) for various $L_{\min}$, $p_d^{\min}$ and all considered correlation exponents a. See Figure 4.49 for the ratios themselves.

Our final estimates of the critical exponent β are summarized in Table 4.10. In Figure 4.55 and Table 4.11 we compare the results to other works. Before starting the comparison of our results to the literature, we like to pay attention to the fact that in the most works no separate analysis was done to obtain β. Instead, it was derived from η (or γ) and ν by using the scaling relations. This makes the comparison much less informative than it was for the exponents ν and γ. Nevertheless, we will do the comparison and discuss our results afterwards. We begin our discussion of the results for the uncorrelated case. In Figure 4.55 we clearly see a disagreement of our result with all other works. Our estimate β lies around $2.5 \cdot \epsilon(\beta)$ above all other estimates. Contrarily to the critical exponent γ, in the case of β the RG estimates are even further away from our estimate than the Monte Carlo estimates. If we had been using the result for $p_d^{\min} = 0.05$, we would obtain an estimate β which is much closer to the estimates from other works, compare Figure 4.50. But an unbiased analysis using the quality of fits χ_{red}^2 and the overlapping index $\mathscr{A}$ has shown us, that the change in the estimates by including or excluding the smallest concentrations of defects $p_d = 0.05$ and $p_d = 0.1$ into the fits results in deviations which are not covered by the error of the estimates. This indicates a crossover regime with the pure Ising model and therefore we finally have chosen $p_d^{\min} = 0.15$.

(a) $a = \infty$.

(b) $a = 3.5$.

(c) $a = 3.0$.

(d) $a = 2.5$.

(e) $a = 2.0$.

(f) $a = 1.5$.
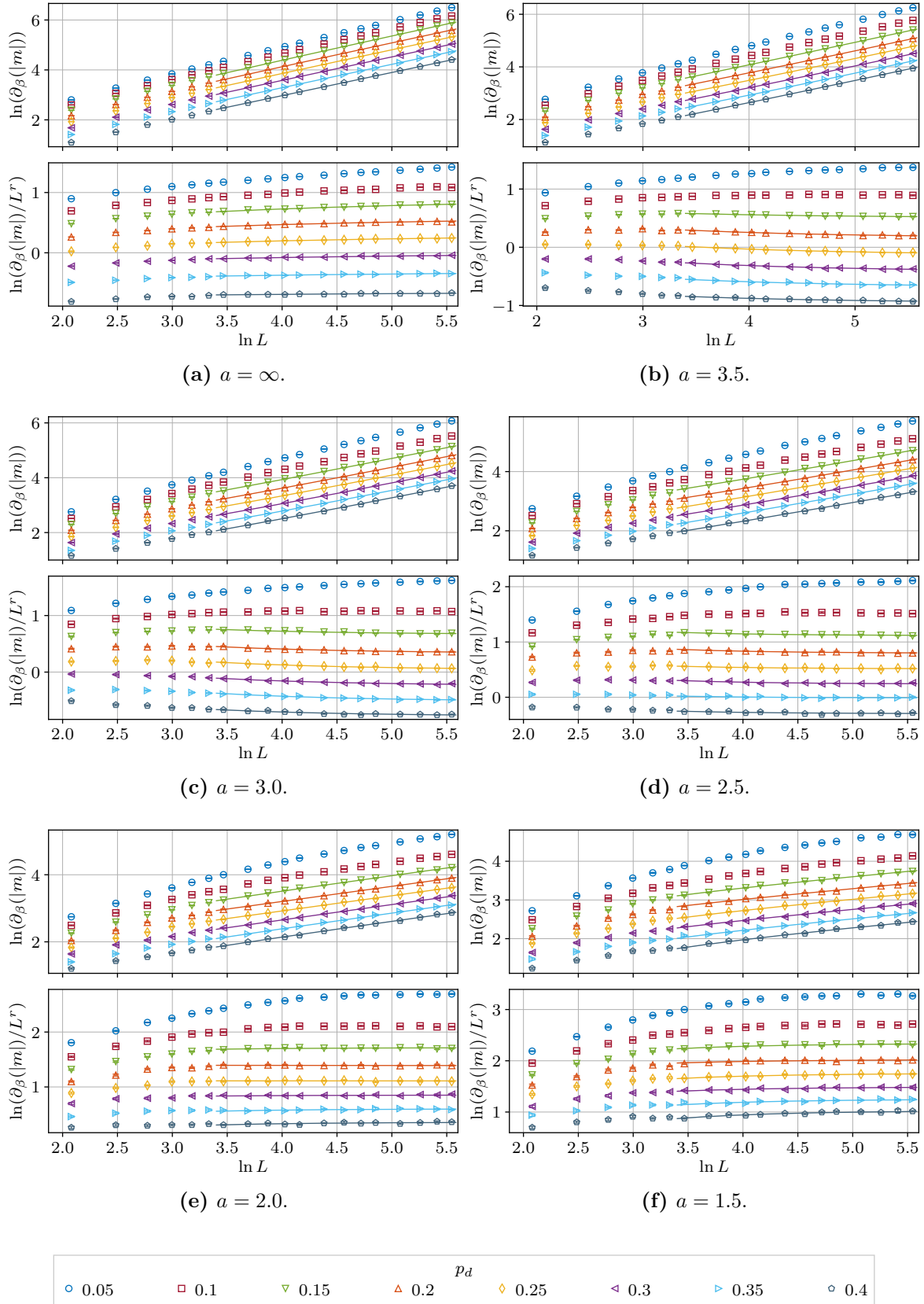
Figure 4.51: Examples of the corrected global fits to the ansatz in Equation (4.62) for all correlation exponents a. The minimum included concentration of defects was $p_d^{\min} = 0.15$ and the maximum included concentration of defects was $p_d^{\max} = 0.4$. The minimum lattice size was chosen to be $L_{\min} = 32$. The upper plots show the fitted observables $\widehat{\partial_\beta(|m|)}(L, p_d)$ versus L on a logarithmic scale. In the lower plots, the observables are divided by L^r where $r = (1 - \beta)/\nu$. This form allows us to better visualize the deviations from the leading behavior L^r through the correction terms with the amplitudes B_{p_d}.
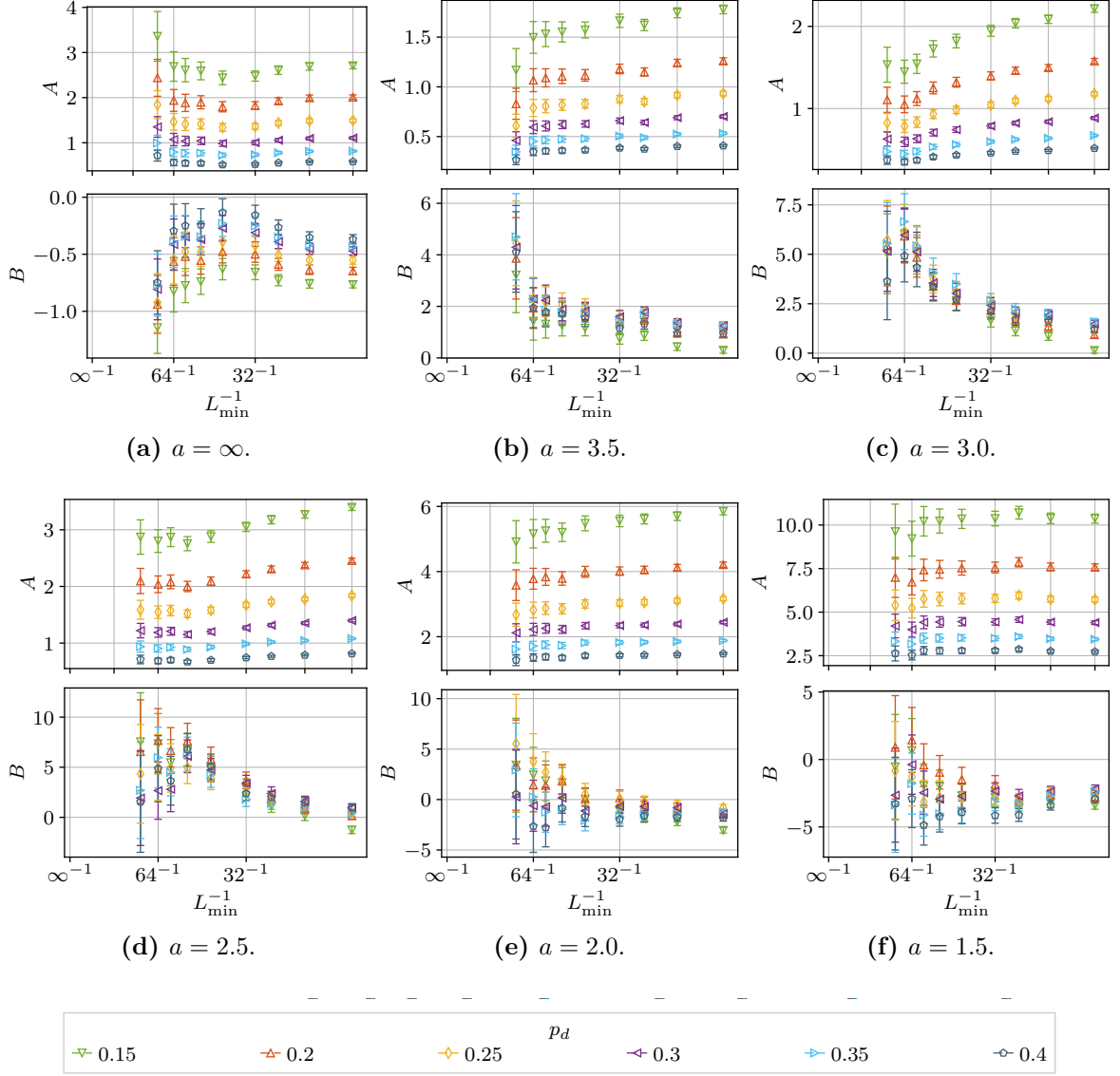
Figure 4.52: Amplitudes A_{p_d} and B_{p_d} for each included concentration of defects $p_d \geq p_d^{\min}$ with $p_d^{\min} = 0.15$ for the corrected global fit ansatz given in Equation (4.62) in dependence of the $L_{\min}$. Consistent ordering can be seen for all cases in the global amplitudes A_{p_d} while for the correction amplitudes B_{p_d} the values mostly overlap except for the uncorrelated case.

For the correlated cases, we observe a compatible result with Ref. [BP99] for the case of $a = 2.0$ within the errorbars. This is surprising, since the estimates for ν and γ did not agree with this reference. The same value as in Ref. [BP99] was obtained in Ref. [Iva+08] but with a considerably smaller error. We do not overlap with it within the errorbars but are close to it. We cannot see any agreement with the results from Refs. [PPF00; Pru+05] as for the previously obtained exponents ν and γ. From the predictions for the critical exponents ν and γ in Ref. [WH83] we can derive the critical exponent β by using scaling relation as $\beta = (d-2)/a$, Equation (2.93). However, as already mentioned, the prediction of γ was stated in Ref. [WH83] only for models with the dimension of the order parameter $m > 1$. Anyway, we only partially can reproduce a behavior of $\beta(a) \propto 1/a$. We see a clear dependence of β on the correlation exponent a but the line is not parallel to $1/a$. Instead, we see values above
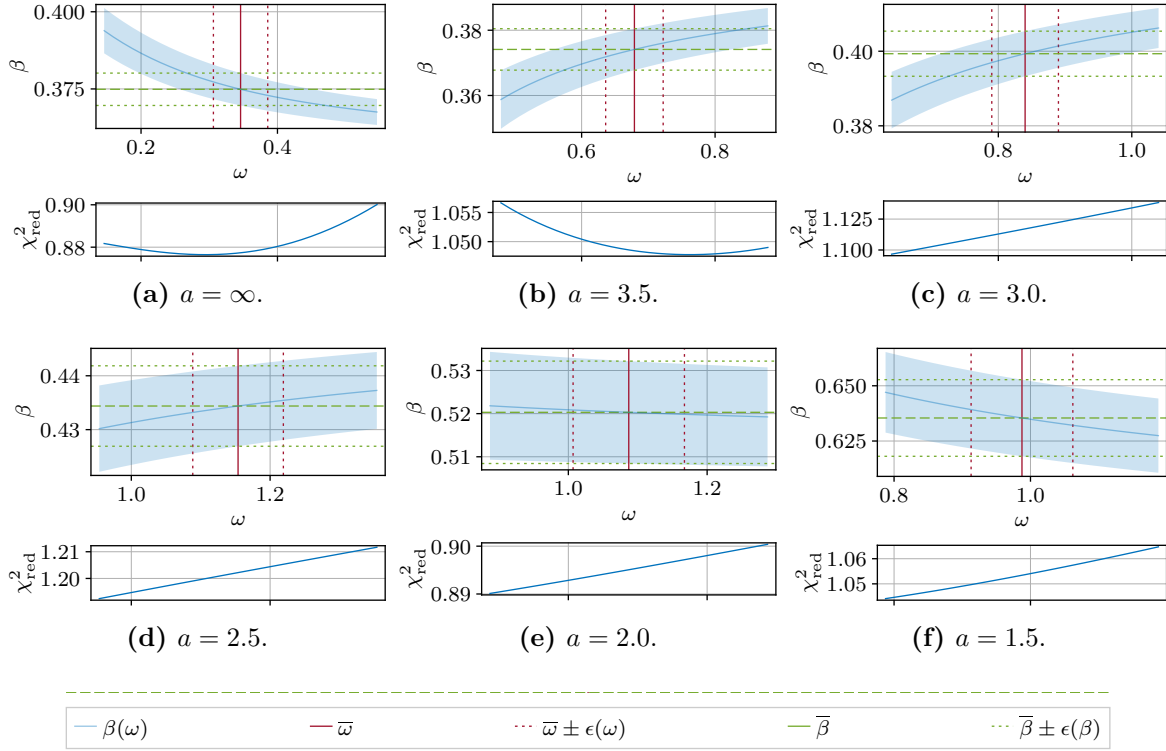
Figure 4.53: The dependence of the corrected global fit results β on the correction exponent ω. The minimum lattice size included into the fits is $L_{\min} = 32$. The lower plots show the qualities of the fit χ^2_{red}. For a wider range of different ω values, the fits remain stable and reasonably good. The estimates $\beta(\omega)$ are mostly covered through the ranges $\overline{\beta} \pm \epsilon(\beta)$. The values $\overline{\beta}$ are the final estimates from Table 4.10. The bar is added to distinguish between the free parameter β and the fixed values $\overline{\beta}$.
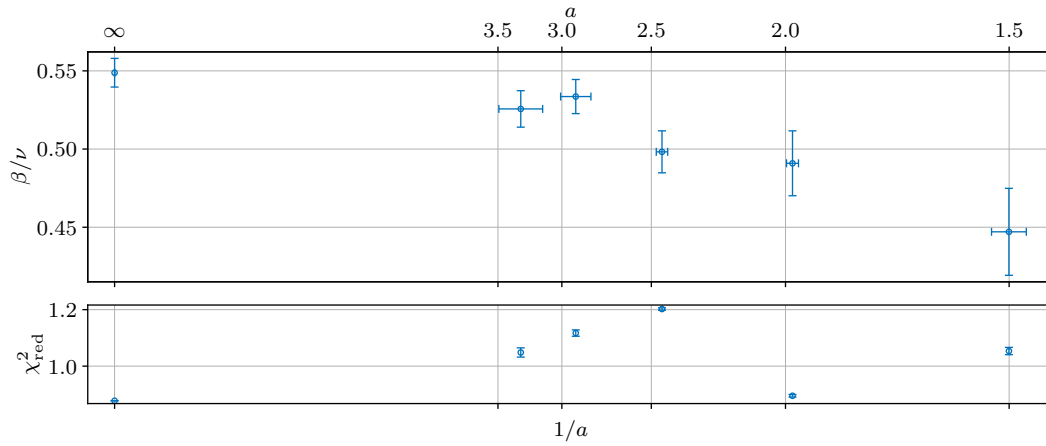
Figure 4.54: Ratios $\beta/\nu = 1/\nu - r$ for the finally chosen $L_{\min}$ and $p_d^{\min}$ parameters for each correlation exponent a.

the line for $a \approx 3.0$, a value which is compatible with $1/a$ for $a = 2.0$ and a value under $1/a$ from $a = 1.5$. The fact that it is not proportional to $1/a$ is already reflected in the ratios β/ν which are not constant, as we mentioned before and shown in Figure 4.54. We cannot find an easy explanation for this discrepancy since our fits are quite good when looking at χ^2_{red} and also the corrections to scaling are smaller compared to the previous case of exponent γ.

Table 4.10: Final results of the critical exponent β. The minimum concentration of defects $p_d^{\min} = 0.15$ and minimum lattice size $L_{\min} = 32$ were used in all cases. For convenience, the results for ν and ω from Tables 4.2 and 4.5 are shown, respectively. Additionally, we provide the estimates of the ratios β/ν for comparison. The terms $r\epsilon(\nu)$ and $\nu\epsilon(r)$ are the contributions to the total error $\epsilon(\beta)$ according to Equation (4.63).

a	ν	r	$\frac{\beta}{\nu} = \frac{1}{\nu} - r$	$\beta = 1 - r\nu$	$\nu\epsilon(r)$	$r\epsilon(\nu)$	χ^2_{red}	ω
∞	0.6831(30)	0.9151(66)	0.5488(92)	0.3749(53)	0.00447	0.00274	0.877	0.346(40)
3.5	0.7117(49)	0.8794(66)	0.526(12)	0.3741(64)	0.00469	0.00429	1.05	0.679(44)
3.0	0.7484(52)	0.8026(60)	0.534(11)	0.3993(61)	0.00442	0.00412	1.12	0.840(50)
2.5	0.8719(96)	0.6487(48)	0.498(14)	0.4344(75)	0.00418	0.00619	1.2	1.154(66)
2.0	1.060(23)	0.4526(59)	0.491(21)	0.520(12)	0.00618	0.0101	0.895	1.087(81)
1.5	1.421(55)	0.2565(73)	0.447(28)	0.635(18)	0.0103	0.0139	1.05	0.988(75)
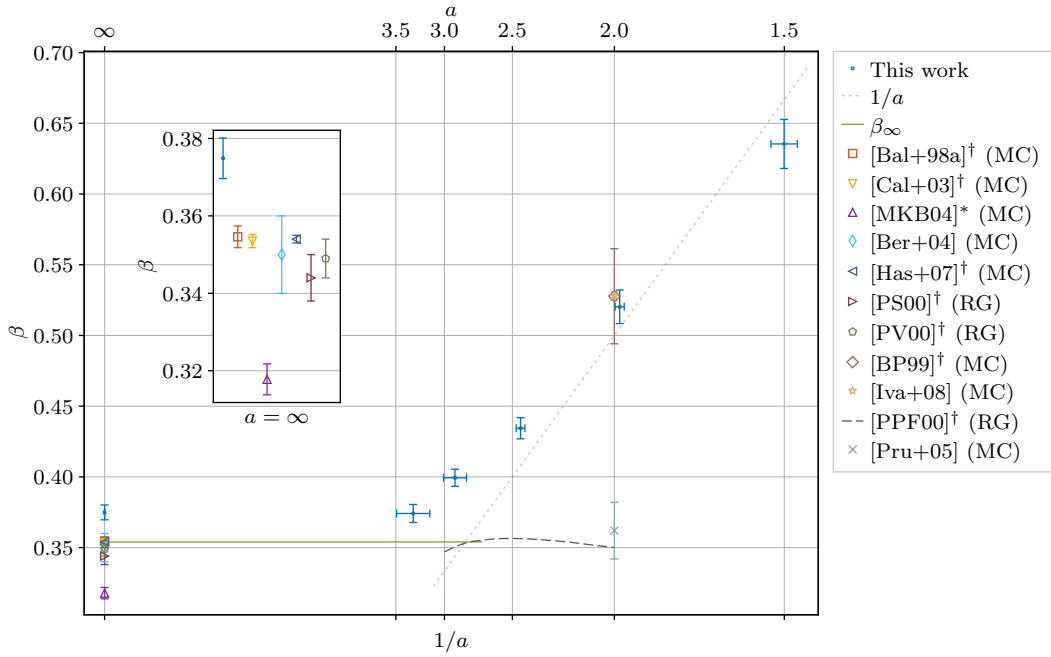
Figure 4.55: Final results of the critical exponent β compared to the known results from the literature. The horizontal errorbars come from the true measured $\overline{a}$ values from Table 4.1. The value $\beta_\infty = 0.354$ is the mean value from various groups (only (MC)) for the uncorrelated case and is used as orientation. The line $1/a$ is shown to qualitatively compare the proportionality to $1/a$. Results from Monte Carlo simulations are marked with (MC) while results from Renormalization Group calculations are labeled with (RG). For the works marked with $*$, we calculated the values by ourselves as a weighted mean over different concentrations. In works marked with $\dagger$, the exponent β was calculated from η (or γ) and ν.

Summary. We derived the critical exponents β from the derivative of the magnetization $\partial_\beta(\widehat{|m|})$ peaks. The case of the uncorrelated disorder yields an estimate which is above the results from other groups. However, most of these results are in fact calculations of β through scaling relations. For the correlated case, we see a dependence on a but cannot see a clear evidence for a proportionality $\propto 1/a$. We partially agree with the estimates of β from other works for the correlated case with $a = 2.0$.

Table 4.11: Critical exponent β comparison to the literature. For a more detailed comparison of various works see Table 2.3. Legend: † — calculated from other exponents through scaling relations, ∗ — averaged over various p_d by us (weighted mean), ? — result is calculated by using scaling relations from expressions which are stated in the paper as expressions for the case where the dimension of the order parameter is $m > 1$, MC — Monte Carlo simulations, RG — Renormalization Group calculations.

Type	Reference	a	ν	β
	Uncorrelated disorder			
MC	Ballesteros et al. [Bal+98a]	∞	0.6837(53)	$0.3546(28)^\dagger$
	Calabrese et al. [Cal+03]	∞	0.683(3)	$0.3535(17)^\dagger$
	Berche et al. [Ber+04]	∞	0.68(2)	0.35(1)
	Murtazaev et al. [MKB04]	∞	$0.678(6)^*$	$0.3178(40)^*$
	Hasenbusch et al. [Has+07]	∞	0.683(2)	$0.354(1)^\dagger$
RG	Pakhnin et al. [PS00]	∞	0.671(5)	$0.344(6)^\dagger$
	Pelissetto et al. [PV00]	∞	0.678(10)	$0.349(5)^\dagger$
	Kompaniets et al. [KKS21]	∞	0.675(19)	$0.346(34)^\dagger$
	This work	∞	0.6831(30)	0.3749(53)
	Correlated disorder			
MC	Ballesteros et al. [BP99]	2.0	1.012(16)	$0.528(34)^\dagger$
	Prudnikov et al. [Pru+05]	2.0	0.71(1)	0.362(20)
	Ivaneyko et al. [Iva+08]	2.0	0.958(4)	0.528(3)
RG	Weinrib et al. [WH83]	$a < d$	$2/a$	$(d-2)/a^{?,\dagger}$
	Prudnikov et al. [PPF00]	3.0	0.6715	$0.347^\dagger$
		2.5	0.7046	$0.3565^\dagger$
		2.0	0.715	$0.34^\dagger$
	This work	3.5	0.7117(49)	0.3741(64)
		3.0	0.7484(52)	0.3993(61)
		2.5	0.8704(62)	0.4353(58)
		2.0	1.082(15)	0.5103(90)
		1.5	1.465(43)	0.624(16)

4.5.5 Critical temperatures

As already presented in Section 4.3.3, together with the peaks of the observables $\hat{\mathcal{O}}$, we also obtained the corresponding temperatures $\hat{\beta}$. These temperatures can be used to estimate the critical temperature β_c in the thermodynamic limit $L \to \infty$. The relation for this estimation was presented in Equation (3.27) and reads

$$\hat{\beta}_{\mathcal{O}}(L) = \beta_c^{\mathcal{O}} + A_{\mathcal{O}} L^{1/\nu}, \tag{4.65}$$

for any observable with peaks at $\hat{\beta}(L)$. Note, that in Equation (4.65) we have added the index $\mathcal{O}$ to the critical temperature $\beta_c^{\mathcal{O}}$. Ideally, $\beta_c = \beta_c^{\mathcal{O}}$ for all $\mathcal{O}$ should be true. But to distinguish between the fit parameters for different $\mathcal{O}$, we will keep the index for the moment. Contrary to the case of the critical exponents discussed in the previous sections, we cannot use a global ansatz here since the critical temperature depends on the concentration of defects p_d. This fact was the main reason for using an ansatz without correction terms, since including further corrections would reduce the number of degrees of freedom too drastically. Hence, we performed fits to the ansatz in Equation (4.65) for all correlation exponents a

and concentration of defects p_d separately for each of the following three observables: the derivative of the logarithm of the magnetization $\partial_\beta(\ln|m|)$, the derivative of the magnetization $\partial_\beta(|m|)$ and the susceptibility χ. It is obvious that we used all observables for which we derived the peaks in Section 4.3.3.

In order to account for the error of the critical exponent ν which enters the ansatz as a parameter, we used the Bootstrap technique which was discussed in Section 3.4.2. We randomly generated a normally distributed ν_b with the distribution

$$\nu_b \sim \mathcal{N}\left(\nu, \epsilon(\nu)^2\right) , \tag{4.66}$$

and repeated the fits for $N_b = 1000$ times. After that, the mean of $\beta_c^{\mathcal{O}}$ and $A_{\mathcal{O}}$ were calculated out of these bootstrapped results. For the critical temperature $\beta_c^{\mathcal{O}}$ this resulted in

$$\beta_c^{\mathcal{O}} = \frac{1}{N_b} \sum_b (\beta_c^{\mathcal{O}})_b , \tag{4.67}$$

$$\epsilon(\beta_c^{\mathcal{O}}) = \sqrt{\overline{\epsilon(\beta_c^{\mathcal{O}})_b}^2 + \sigma((\beta_c^{\mathcal{O}})_b)^2} , \tag{4.68}$$

with the error contributions being

$$\overline{\epsilon(\beta_c^{\mathcal{O}})_b} = \frac{1}{N_b} \sum_b \epsilon(\beta_c^{\mathcal{O}})_b , \tag{4.69}$$

$$\sigma((\beta_c^{\mathcal{O}})_b) = \sqrt{\frac{N_b}{N_b - 1} \sum_b \left((\beta_c^{\mathcal{O}})_b - \overline{(\beta_c^{\mathcal{O}})_b}\right)^2} , \tag{4.70}$$

and $(\beta_c^{\mathcal{O}})_b$ and $\epsilon(\beta_c^{\mathcal{O}})_b$ being the estimated fit parameter and its error obtained for one bootstrapped value ν_b, respectively. In easy words, the total error calculated in Equation (4.68) is the combination of the mean of the fitted errors and the error of the bootstrapped mean.

As usual, we varied the minimum included lattice size $L_{\min}$ to get a feeling of the finite-size contributions. We present the fit curves for all three studied observables for two different correlation exponents a at $p_d = 0.2$ in Figure 4.56. The dependence on the $L_{\min}$ is shown in Figure 4.57 for the same parameters. The overall observation is that contrary to the peak values $\hat{\mathcal{O}}$, the $\hat{\beta}$ values suffer from much larger deviations and relative errors. Possibly, the reason for this is that the critical temperature varies with p_d and each disorder configuration consequentially had its own (finite lattice) temperature. Using more disorder configurations would most likely increase the precision of the $\hat{\beta}$ estimates. The dependence on $L_{\min}$ was usually covered by the size of the errors $\epsilon(\beta_c)$ for $\partial_\beta(\ln|m|)$ and $\partial_\beta(|m|)$ but was slightly more pronounced for χ. However, at the end of the day, these dependencies were neglectable altogether due to much larger deviations between the estimates $\beta_c^{\mathcal{O}}$ for different observables $\mathcal{O}$ which we will discuss next. We used $L_{\min} = 64$ for all a and p_d. We present the qualities of the fits for $L_{\min} = 64$ in Figure 4.58. It can be seen, that for all $a \geq 2.5$ most of the values are in a reasonable range of $\chi_{\mathrm{red}}^2 \lessapprox 3.0$. However, for the strongest correlation cases we observe very large χ_{red}^2 values. This fact again can be understood as a lack of sufficiently many disorder realizations to tackle the critical temperature more precise. Altogether, with a mean of $\overline{\chi_{\mathrm{red}}^2} = 3.61$ and a median of $\mathrm{md}\left(\chi_{\mathrm{red}}^2\right) = 1.75$ we have at least the majority of points for which the fits were acceptable. Also, as bad fits usually also end up in larger errors, and we will use the weighted mean over several observables, bad fits will automatically count less in the final estimates which we will discuss next.

(a) $a = \infty$, $\mathcal{O} = \partial_\beta(\ln|m|)$.

(b) $a = \infty$, $\mathcal{O} = \partial_\beta(|m|)$.

(c) $a = \infty$, $\mathcal{O} = \chi$.

(d) $a = 2.0$, $\mathcal{O} = \partial_\beta(\ln|m|)$.

(e) $a = 2.0$, $\mathcal{O} = \partial_\beta(|m|)$.

(f) $a = 2.0$, $\mathcal{O} = \chi$.

$\circ\ \hat{\beta}$ $\qquad\qquad$ $\circ\ \beta_{c,\mathcal{O}}$
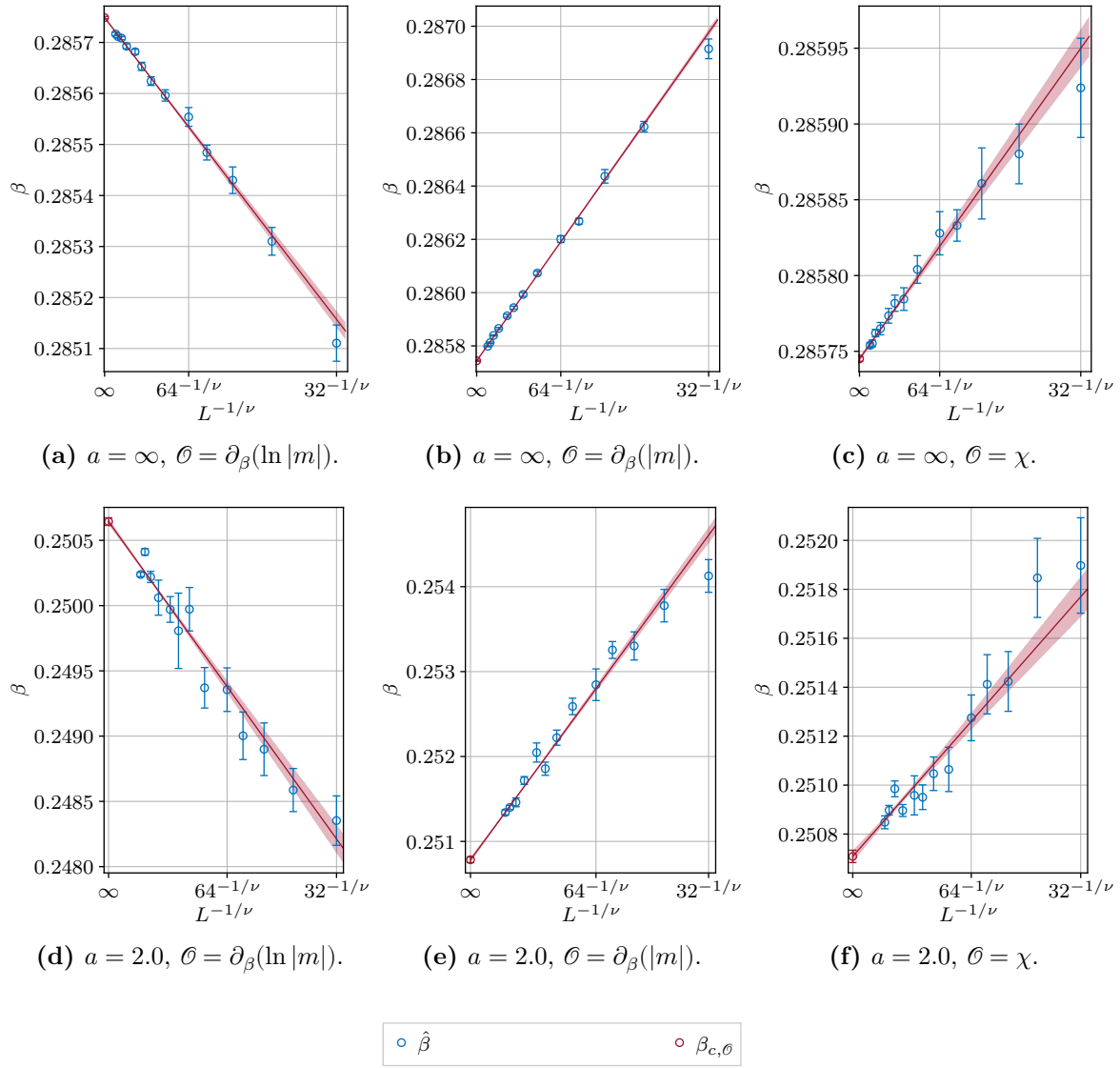
Figure 4.56: Examples of the fits to the ansatz in Equation (4.65) for various observables, $p_d = 0.2$ and $L_{\min} = 32$. It can be seen, that not all estimates $\hat{\beta}_{\mathcal{O}}(L)$ lie on the final fitting line. This is also reflected in the relatively high χ^2_{red} in some cases as reported in Figure 4.58.

After obtaining the $\beta_c^{\mathcal{O}}$ for all considered observables, we calculated the weighted mean as the final estimate

$$\beta_c = \frac{1}{\sum_{\mathcal{O}} \epsilon(\beta_c^{\mathcal{O}})^{-2}} \sum_{\mathcal{O}} \epsilon(\beta_c^{\mathcal{O}})^{-2} \beta_c^{\mathcal{O}}, \tag{4.71}$$

$$\epsilon(\beta_c) = \sqrt{\frac{1}{\sum_{\mathcal{O}} \epsilon(\beta_c^{\mathcal{O}})^{-2}}}. \tag{4.72}$$

Note, that in Equations (4.71) and (4.72) we do not explicitly denote the usage of the weighted mean for the final estimates β_c since we only used one approach for the estimation. To investigate the deviations between the estimates $\beta_c^{\mathcal{O}}$, we calculated their deviations from β_c, i.e., the quantities

$$\Delta\beta_c^{\mathcal{O}} = |\beta_c - \beta_c^{\mathcal{O}}|, \tag{4.73}$$
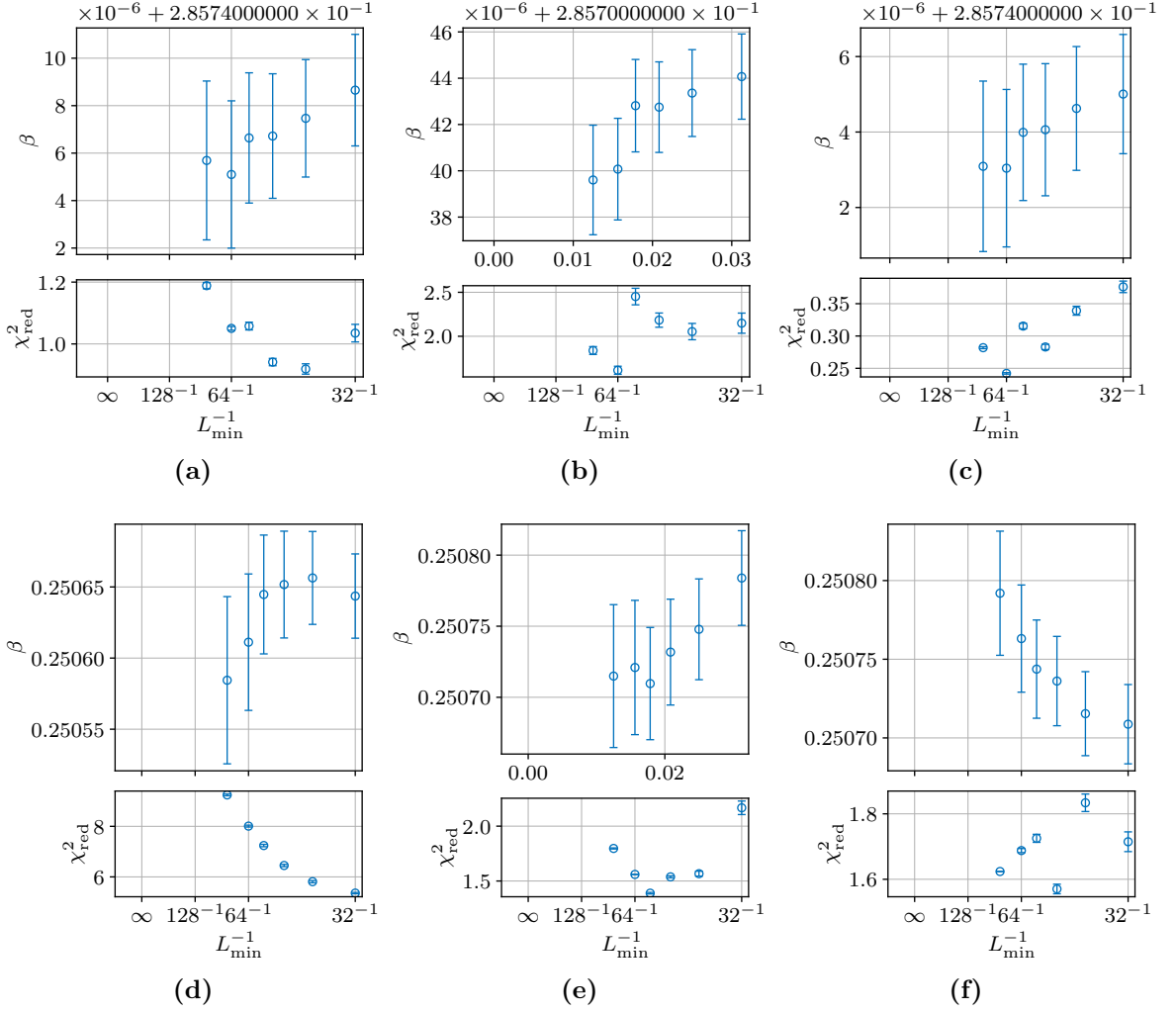
Figure 4.57: The dependence of the resulting $\beta_c^{\mathscr{O}}$ from fits to the ansatz in Equation (4.65) for different observables and $p_d = 0.2$. The dependence is covered to a great extent by the size of the errors in most cases.

and plotted them in Figure 4.59a. First, we notice that the absolute deviations are generally larger for smaller a, i.e., for stronger correlations. There is no particular observable $\mathscr{O}$ which suffers from such deviations the most. This is clear since we have performed simulations only for a few temperatures β_{sim} separated from each other by some fixed spacing. That means, that for each parameter tuple (a, p_d, L) the distance between the simulation temperature β_{sim} and the peak temperature $\hat{\beta}_{\mathscr{O}}$ can be different for different $\mathscr{O}$ and hence the precision can vary significantly (due to the histogram reweighting technique, which gets imprecise as you go further away from the original temperature). The deviations also become larger for larger concentrations p_d. The deviations become as big as $\Delta\beta_c^{\mathscr{O}} \approx 10^{-3}$ for $a = 1.5$ and $p_d = 0.4$.

In the next step we calculated the ratios between the mean of the deviations for all three observables and the weighted error from Equation (4.72), i.e., the quantity

$$\frac{\Delta\beta_c^{\mathscr{O}}}{\epsilon(\beta_c)}. \tag{4.74}$$
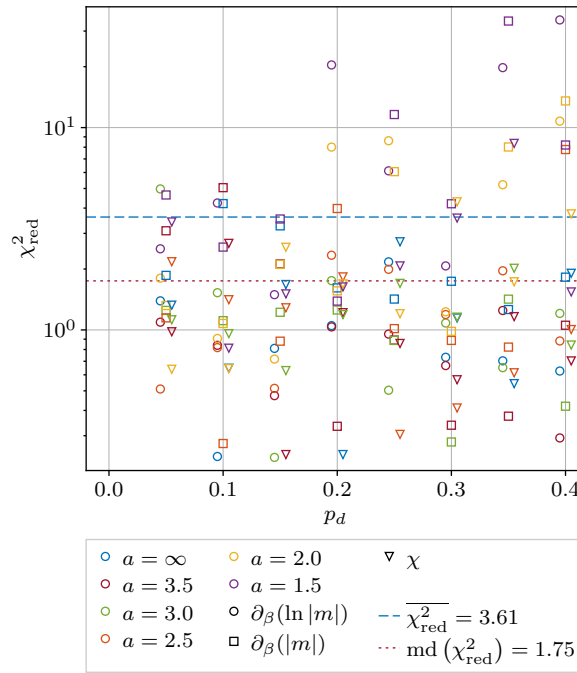
Figure 4.58: The quality of the fits χ^2_{red} to the ansatz in Equation (4.65) for all correlation exponents a and concentration of defects p_d. Some values are rather high but the mean $\overline{\chi^2_{\text{red}}}$ and the median $\text{md}\left(\chi^2_{\text{red}}\right)$ are in a reasonable region. Overall, one sees the problem of large variations between the critical temperature for each disorder realization. For better readability, the values for different observables are slightly shifted horizontally from the considered p_d.

This quantity tells us how much larger (or smaller) the deviation between the individual critical temperatures $\beta_c^{\mathcal{O}}$ and the final estimate β_c is compared to the weighted error $\epsilon(\beta_c)$. These ratios can be found in Figure 4.59b. Comparing the relative deviations with respect to the weighted error $\epsilon(\beta_c)$, we notice that most of the time the deviations from the weighted mean are much larger than $\epsilon(\beta_c)$ with a maximum factor of around 10–15. This large deviation encouraged us to add a second error to the final estimates of β_c, namely the mean of these deviations $\Delta\beta_c^{\mathcal{O}}$ over all observables for each a and p_d,

$$\epsilon(\Delta\beta_c^{\mathcal{O}}) = \overline{\Delta\beta_c^{\mathcal{O}}}. \tag{4.75}$$

These errors are reported together with the weighted errors $\epsilon(\beta_c)$ in Table 4.12 where we summarize our final results for the critical temperatures for all parameter tuples (a, p_d). In Figure 4.60 we present the results visually and the total error is calculated as $\sqrt{\epsilon(\Delta\beta_c^{\mathcal{O}})^2 + \epsilon(\beta_c)^2}$. Here, we additionally extrapolate the curves linearly with the slopes between the temperatures for $p_d = 0.1$ and $p_d 0.05$, to verify the convergence to the pure Ising mode case. This is mostly done for a visual representation because the real $\beta_c(p_d)$ curves generally are not straight lines.

Let us discuss the results in the context of the known values from the literature which are presented in Table 4.13. We clearly see a very good agreement with results for all p_d which have been studied by other groups in the case of site disorder. The accuracy of the agreement is around 4–5 digits of the estimates. Considering the relatively large deviations of our individual results for different observables $\mathcal{O}$, it is a remarkable achievement. As expected, the temperatures for the bond disorder do not coincide with our results since the critical

(a) Deviations $\Delta\beta_c^{\mathcal{O}} = \left|\beta_c - \beta_c^{\mathcal{O}}\right|$.

(b) Ratios $\Delta\beta_c^{\mathcal{O}}/\epsilon(\beta_c)$.
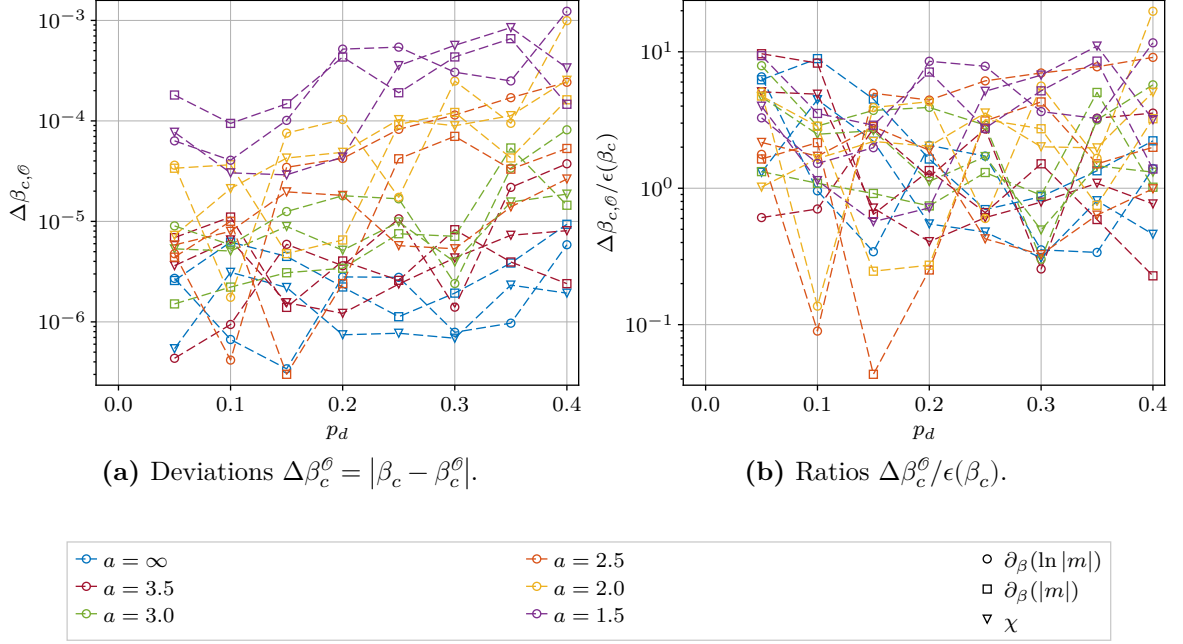
Figure 4.59: Deviations $\Delta\beta_c^{\mathcal{O}} = \left|\beta_c - \beta_c^{\mathcal{O}}\right|$ between the final estimate β_c and the estimates obtained for different observables $\beta_c^{\mathcal{O}}$ and ratios of these deviations and the weighted errors $\Delta\beta_c^{\mathcal{O}}/\epsilon(\beta_c)$.

Table 4.12: Final critical temperatures β_c for all correlation exponents a and concentration of defects p_d. The first error is the mean of the absolute deviations $\epsilon(\Delta\beta_c^{\mathcal{O}})$ calcualted with Equation (4.75), and the second is the weighted mean error calculated with Equation (4.72). Graphically, the values are shown in Figure 4.60.

p_d	$a = \infty$	$a = 3.5$	$a = 3.0$
0.05	0.2345922(20)(5)	0.2324137(40)(8)	0.231696(6)(2)
0.1	0.2492894(40)(7)	0.243131(7)(2)	0.241393(5)(3)
0.15	0.266155(3)(1)	0.254613(3)(3)	0.251679(9)(4)
0.2	0.285742(2)(2)	0.267311(3)(3)	0.262977(9)(5)
0.25	0.308810(2)(2)	0.281646(6)(4)	0.275676(20)(6)
0.3	0.336430(2)(3)	0.298156(5)(6)	0.290212(5)(8)
0.35	0.370175(3)(3)	0.317570(20)(7)	0.30722(4)(2)
0.4	0.412503(6)(5)	0.34088(2)(2)	0.32758(4)(2)

p_d	$a = 2.5$	$a = 2.0$	$a = 1.5$
0.05	0.230677(6)(3)	0.229209(30)(8)	0.22714(20)(2)
0.1	0.239065(7)(5)	0.23592(2)(2)	0.23191(6)(3)
0.15	0.247871(20)(7)	0.24304(5)(2)	0.23694(10)(6)
0.2	0.25753(3)(1)	0.25071(6)(3)	0.24219(40)(7)
0.25	0.26827(5)(2)	0.25928(8)(3)	0.24861(40)(7)
0.3	0.28060(7)(2)	0.26909(20)(5)	0.25590(50)(9)
0.35	0.29482(8)(3)	0.28029(9)(6)	0.26372(60)(8)
0.4	0.31188(20)(3)	0.29400(50)(6)	0.2734(6)(2)

temperature is not only expected to be dependent on the concentration itself but also on the type of the disorder. However, for the case of the correlated site disorder with $a = 2.0$, we cannot reproduce the temperatures from Refs. [BP99; Pru+05]. When looking at the different temperatures from Ref. [BP99] for the case of disorder generated with the Fourier Filter Method (as in our work) and comparing it to the temperature when using lines of defects, we
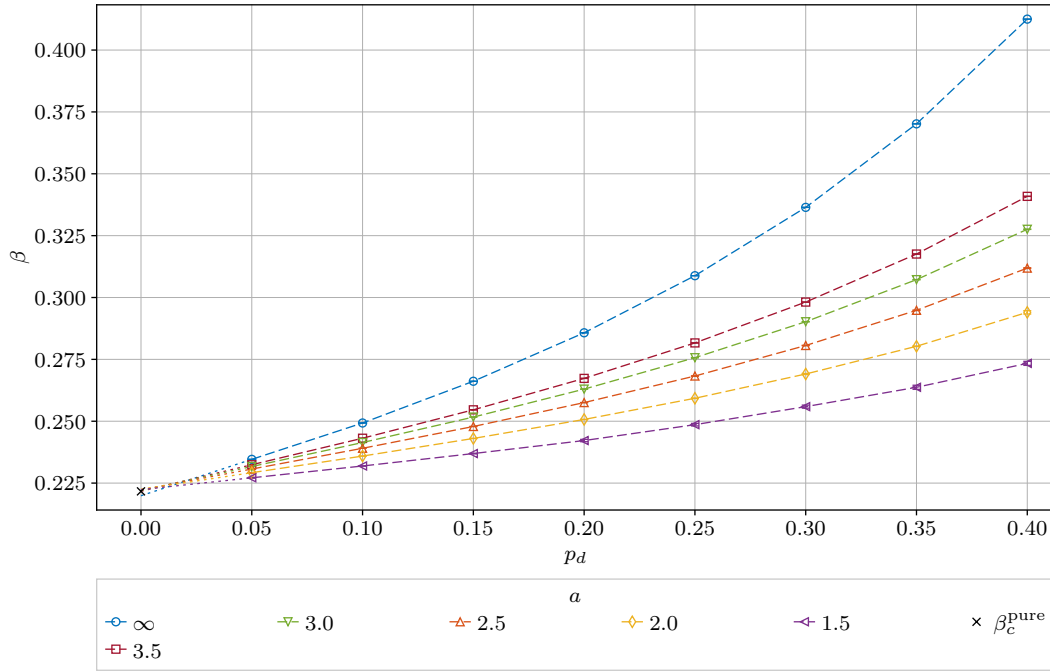
Figure 4.60: Final critical temperatures β_c for all correlation exponents a and concentration of defects p_d. For comparison, the connecting lines for each a between the values for $p_d = 0.1$ and $p_d = 0.05$ are extrapolated to $p_d = 0$ and the value of the pure Ising model reported in Ref. [FXL18] is added. See Table 4.12 for the numerical values.

see that they do not coincide. This is a similar case as for the uncorrelated disorder, i.e., the critical temperature is not universal and depends on the disorder type. Therefore, we expect that our deviations from the literature are due to different (probably subtle) differences in the disorder generation process compared to Ref. [BP99], even though they used the same technique. Another possible reason for this discrepancy could be the deviation between the imposed values for $a = 2.0$ and the true measurable value $\overline{a}$ in Ref. [BP99] which is not reported. Finally, the limited largest lattice size of $L = 128$ could also be a problem for the estimation. Since we cannot check all of these possibilities for correctness, we expect our final results for the critical temperatures in Table 4.12 to be coupled to the site disorder generated with the Fourier Filter Method as described in Section 3.5.

Summary. We estimated critical temperatures for all considered correlation exponents a and concentration of defects p_d by using the peak temperatures $\beta_c^{\mathcal{O}}$. Our estimates are valid for the site disorder and in the correlated case are limited to the disorder generated by the Fourier Filter Method.

Table 4.13: Summary of the critical temperatures of the three-dimensional Ising model with disorder from literature. The temperatures which are missing, were not studied in the corresponding work. The errors for this work were calculated as total errors from Table 4.12. Literature values printed in red do not coincide with our estimates (due to other disorder type or for other reasons). Legend: SD — site disorder, BD — bond disorder, FFM — long-range correlated disorder generated with Fourier Filter Method, DL — long-range correlated disorder reached by using lines of disorder.

Reference	Disorder type	a	p_d							
			0.05	0.1	0.15	0.2	0.25	0.3	0.35	0.4
Uncorrelated disorder										
Ballesteros et al. [Bal+98a]	SD	∞		0.249288(4)		0.285736(5)			0.370156(8)	
Calabrese et al. [Cal+03]	SD	∞				0.285744(2)				
Berche et al. [Ber+04]	BD	∞						0.32670(5)		
Murtazaev et al. [MKB04]	SD	∞	0.23479(3)	0.24951(5)		0.28607(5)				0.41368(10)
Hasenbusch et al. [Has+07]	SD	∞				0.2857429(4)			0.370174(3)	
	BD	∞						0.326707(2)		
This work	SD	∞	0.234592(2)	0.249289(4)	0.266155(3)	0.285742(3)	0.308810(3)	0.336430(3)	0.370175(4)	0.412503(8)
Correlated disorder										
Ballesteros et al. [BP99]	SD, FFM	2.0				0.272722(10)			0.332929(25)	
	SD, DL	2.0				0.257126(14)				
Prudnikov et al. [Pru+05]	SD, DL	2.0				0.2545(2)				
This work	SD, FFM	3.5	0.232414(4)	0.243131(7)	0.254613(4)	0.267311(5)	0.281646(7)	0.298156(8)	0.31757(2)	0.34088(2)
		3.0	0.231696(6)	0.241393(5)	0.251679(9)	0.26298(1)	0.27568(2)	0.29021(1)	0.30722(4)	0.32758(5)
		2.5	0.230677(6)	0.239065(8)	0.24787(2)	0.25753(3)	0.26827(5)	0.28060(7)	0.29482(8)	0.3119(2)
		2.0	0.22921(3)	0.23592(3)	0.24304(5)	0.25071(6)	0.25928(8)	0.2691(2)	0.2803(2)	0.2940(5)
		1.5	0.2271(2)	0.23191(7)	0.2369(2)	0.2422(4)	0.2486(4)	0.2559(5)	0.2637(6)	0.2734(6)

4.5.6 Hyperscaling validation

Before going to the next analysis method, lest us discuss the relation between the obtained estimates ν, γ and β. We know, that knowing two of the critical exponents is enough since we can use scaling relations to calculate all the other. In return, having three critical exponents, allows us to check them against each other for consistency. In particular, we wanted to check the hyper scaling relation Equation (2.62). Let us start with the scaling relations in Equations (2.62) and (2.63) and combine them together to

$$2\beta + \gamma = d\nu\,. \tag{4.76}$$

Since the actual fit parameters were the ratios $1/\nu$, γ/ν and $(1 - \beta)/\nu$ in the first place, we rearrange the terms in Equation (4.76) a bit, use $d = 3$, and define a new variable K,

$$K = -2\left(\frac{1-\beta}{\nu}\right) + 2\left(\frac{1}{\nu}\right) + \left(\frac{\gamma}{\nu}\right) - 3 \overset{?}{=} 0\,. \tag{4.77}$$

To check the validity of the hyperscaling relation, we have to check $K = 0$. Essentially, the value of K is the deviation from the expected dimension $d = 3$. The form of Equation (4.77) allows us to directly use the fitted ratios and therefore the error estimate is also very easily expressed as

$$\epsilon(K) = \sqrt{2^2\epsilon\left(\frac{1-\beta}{\nu}\right)^2 + 2^2\epsilon\left(\frac{1}{\nu}\right)^2 + \epsilon\left(\frac{\gamma}{\nu}\right)^2}\,. \tag{4.78}$$

The K values for all considered correlation exponents a are shown in Figure 4.61. We can see, that for the uncorrelated case, there is a slight deviation from zero. The deviation is not huge but is not covered by the errorbar of K. Considering, how many further uncertainties during the whole calculation process are not reflected in the errors, we would not speak about a violation. Instead, we think that it is an uncertainty in our measurements which causes this discrepancy. Especially the exponent β which was not consistent with other work could be the reason for this discrepancy in the hyperscaling relation. However, a deeper look into this aspect would be of interest. An interesting tendency of K can be seen as a becomes smaller. It has a maximum value at $a = 3.0$ where it reaches a value of $K \approx 0.15$. Starting from $a = 2.5$, all K values decrease with decreasing a and are compatible with $K = 0$ within their errors. This peak at $a = 3.0$ is in accordance with the observations we had for the critical exponents themselves — a crossover region with the largest deviation from the conjecture by Weinrib and Halperin. It is interesting, that here the deviation is not from the conjecture by Weinrib and Halperin but a general deviation from the hyperscaling relation. Therefore, independently of the validity of the conjecture by Weinrib and Halperin, the hyperscaling relation may be violated in the crossover region at $a \approx 3.0$. This final result completes our finite-size scaling analysis section.

Summary. The hyperscaling relation is assumed to be valid in the uncorrelated case, but our data show a minor disagreement with this assumption. However, we can propose that in the crossover regime with $a \approx 3.0$ the hyperscaling relation may be violated. For stronger correlations however, the hyperscaling relation becomes valid again.
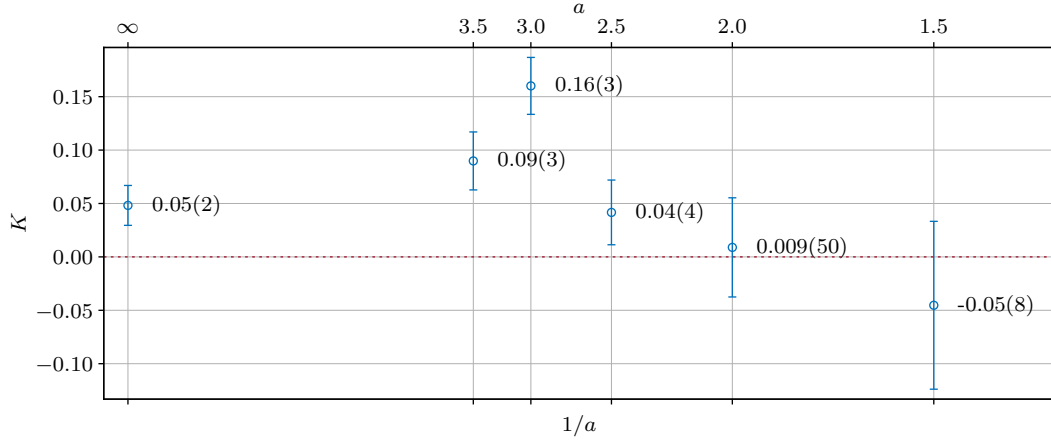
Figure 4.61: Checking the $K = 0$ relation with K which was defined in Equation (4.77). The peak at $a = 3.0$ indicates that the hyperscaling relation may not be valid in the crossver region at $a \approx 3.0$.

4.6 Temperature scaling analysis

In this section we will present the results from the second approach for the derivation of the critical exponents — the temperature scaling (TS). It is based on Equations (2.57) to (2.60) and is widely used ansatz found in literature alongside the finite-size scaling (FSS) ansatz, e.g., in Refs. [Ber+04; Cal+03] it was used for the disordered Ising model and for other models in, e.g., Refs. [HJ93; JH93; MPV02; Vas+15; Wan+19; Wis95]. Contrarily to the FSS ansatz, in general only one lattice size is needed for the TS ansatz. Instead, a wide range of simulated temperatures for this particular lattice is needed. The advantage of the TS ansatz is that the critical exponents can be found directly and not in the form of ratios $x_{\mathcal{O}}/\nu$, as it is the case for the FSS ansatz. The two most important aspects which have to be fulfilled in order for the TS to work are:

1. the lattice size has to be large enough to overcome finite-size corrections (at least further away from T_c),
2. the temperature range should include the critical temperature T_c of the infinite system.

Since the finite-size effects quickly become less pronounced when going away from the critical point, it is a common technique to use different lattice sizes for different temperatures, starting with the largest size at the critical temperature and then decreasing the size as one moves away from that temperature. However, in our case the correlation exponent a was also L-dependent as was discussed in Section 4.2. Therefore, we found it a bad idea to mix different lattice sizes in this analysis. Instead, we used our largest available lattice size of $L = 256$ and performed some additional simulations in order to increase the number of total studied temperatures for all correlation exponents a and concentration of defects p_d. The TS analysis was meant to be a crosscheck of the results obtained through the FSS analysis and to make use of a larger part of the simulated data.

We studied two observables, the second-moment correlation length ξ, calculated as described in Section 2.2.3, and the (high temperature) susceptibility $\tilde{\chi}$, Equation (2.41). These observables provided us the estimates for ν and γ, respectively. We will introduce the analysis

steps for the observable ξ and the exponents ν and discuss the results. For $\tilde{\chi}$ we will mostly only provide the corresponding plots and discuss the results since the analysis steps were identical to the analysis of ξ.

4.6.1 Critical exponent ν

We begin by calculating the observable of interest, i.e., the correlation length ξ for all correlation exponents a and concentrations of defects p_d for the lattice size $L = 256$ and all available temperatures. We used the critical temperatures β_c from Table 4.12 and calculated the reduced temperatures, Equation (2.56),

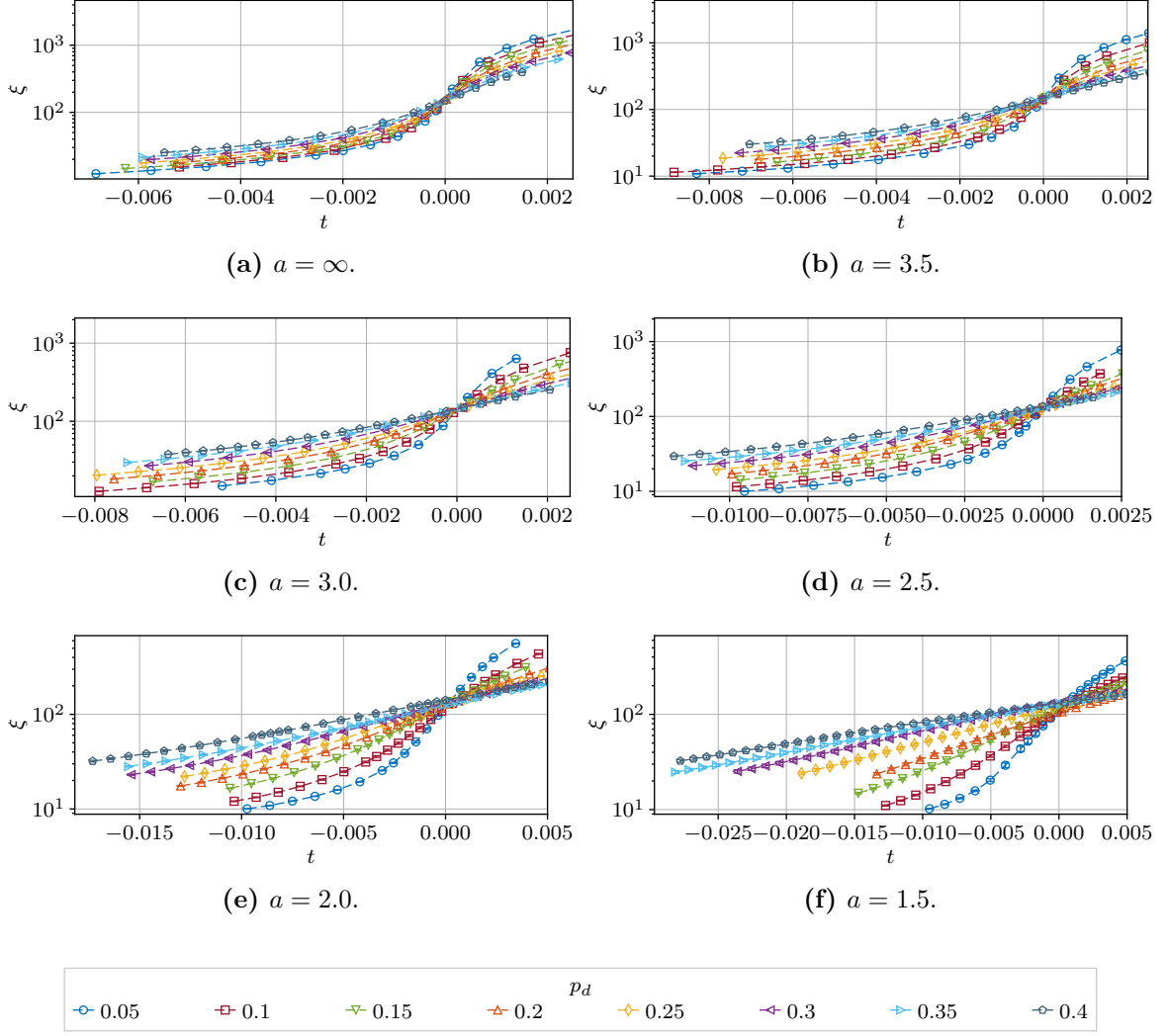$$t = \left(1 - \frac{T}{T_c}\right) = \left(1 - \frac{\beta_c}{\beta_{\mathrm{sim}}}\right) , \tag{4.79}$$

By plotting our $\xi(p_d)$ as a function of t, we visually verified the critical temperature estimates, as can be seen in Figure 4.62. Note, that from Equation (4.79) the negative reduced temperature $t \leq 0$ corresponds to the high temperature phase since $\beta_{\mathrm{sim}} \leq \beta_c$ in this case. The correlation length curves for different p_d all intersect at $t \approx 0$. Only for the strongest correlation exponents $a \leq 2.0$ they visually do not intersect all in one point. Please note, that the plotted ξ is defined only in the high temperature phase, i.e., $t \leq 0$, but we extended it to $t > 0$ in order to see the intersections better.

By using only the high temperature values with $t \leq 0$, we performed individual fits to the ansatz

$$\ln \xi(t) = A - \nu \ln |t| , \tag{4.80}$$

for each concentration of defects p_d and each correlation exponent a. Since the power-law behavior only starts at a certain distance away from $t = 0$, i.e., the region where the finite-size effects become neglectable, we varied the smallest $|t|_{\mathrm{min}}$ included into the fits from its minimum value near $t = 0$ to a maximum value where only three degrees of freedom remained. Examples of the fits are presented in Figure 4.63. In these plots we can see the main problem which we had with this ansatz. We clearly see finite-size effects for each p_d, since the data points follow a curved path, compare, e.g., the plot for $a = 1.5$ where the effect can be seen best. But, since the errors are quite large, a linear fit already provides reasonable χ^2_{red} values. The estimates for all considered $|t|_{\mathrm{min}}$ and each a and p_d are shown in Figure 4.64.

Let us analyze the results shwon in Figure 4.64. We added the final estimates from the FSS analysis from the uncorrected individual fit ansatz and the corrected global fit ansatz to the plots in order to compare them. The estimates from the TS analysis show a clear dependence on the concentration of defects p_d and also on $|t|_{\mathrm{min}}$. They do not reach a plateau value even for the largest $|t|_{\mathrm{min}}$ and the estimates for $p_d \leq 0.1$ are clearly influenced by the crossover to the pure Ising model. Also, as can be seen in Figure 4.62, the correlation length does have the strongest curvature for the smallest concentration of defects p_d. For a quantitative comparison we therefore calculated the weighted mean over all estimates for $p_d \geq 0.15$ where for each p_d we used the largest studied $|t|_{\mathrm{min}}$, which was the one with three degrees of freedom. This was not the best solution but at least it was closer to the possible plateau values than when using the fit results with the lowest possible $|t|_{\mathrm{min}}$ where the condition $\chi^2_{\mathrm{red}} \leq 1.0$ was fulfilled for the first time. These results were way too low and did not represent the

(a) $a = \infty$.

(b) $a = 3.5$.

(c) $a = 3.0$.

(d) $a = 2.5$.

(e) $a = 2.0$.

(f) $a = 1.5$.

p_d

0.05   0.1   0.15   0.2   0.25   0.3   0.35   0.4

Figure 4.62: Correlation length ξ as function of the reduced temperature t for all concentrations of defects p_d and correlation exponents a. The definition of ξ is valid only for the high temperature phase with $t \leq 0$, but we extended the curves in order to see the crossing points better.

asymptotic behavior. As mentioned previously, this was a consequence of the large errors which made the noncorrected fits good, even though the finite-size effects were still present. We summarized the weighted means together with the estimates from the FSS analysis in Table 4.14. Except for the case of $a = 1.5$ the estimates from the TS analysis $\overline{\nu}_{\text{ts}}^{w}$ are closer to the uncorrected estimates $\overline{\nu}_{\text{lin}}^{w}$ than to the corrected estimates ν^g and are slightly larger. The value for $a = 1.5$ is possibly smaller because the estimates for larger p_d show very large errors and hence the smallest concentration result with $p_d = 0.15$ dominates the weighted mean. Due to this huge errors we are very skeptical about the meaningfulness of the estimate for this a. The biggest deviations can be seen for the two correlation exponents $a = 3.0$ and $a = 3.5$ which is exactly the same behavior as for the two FSS estimates, i.e., $\overline{\nu}_{\text{lin}}^{w}$ and ν^g. This fact again indicates the presence of a crossover regime at the transition point of $a \approx 3.0$.

Although we would take the estimates $\overline{\nu}_{\text{ts}}^{w}$ with a great care, we nevertheless can reproduce the same qualitative results in all considered cases. The prediction of Weinrib and Halperin $\nu = 2/a$ is not matched quantitatively and the results lie above this prediction, but the

(a) $a = \infty$.

(b) $a = 3.5$.

(c) $a = 3.0$.

(d) $a = 2.5$.

(e) $a = 2.0$.

(f) $a = 1.5$.
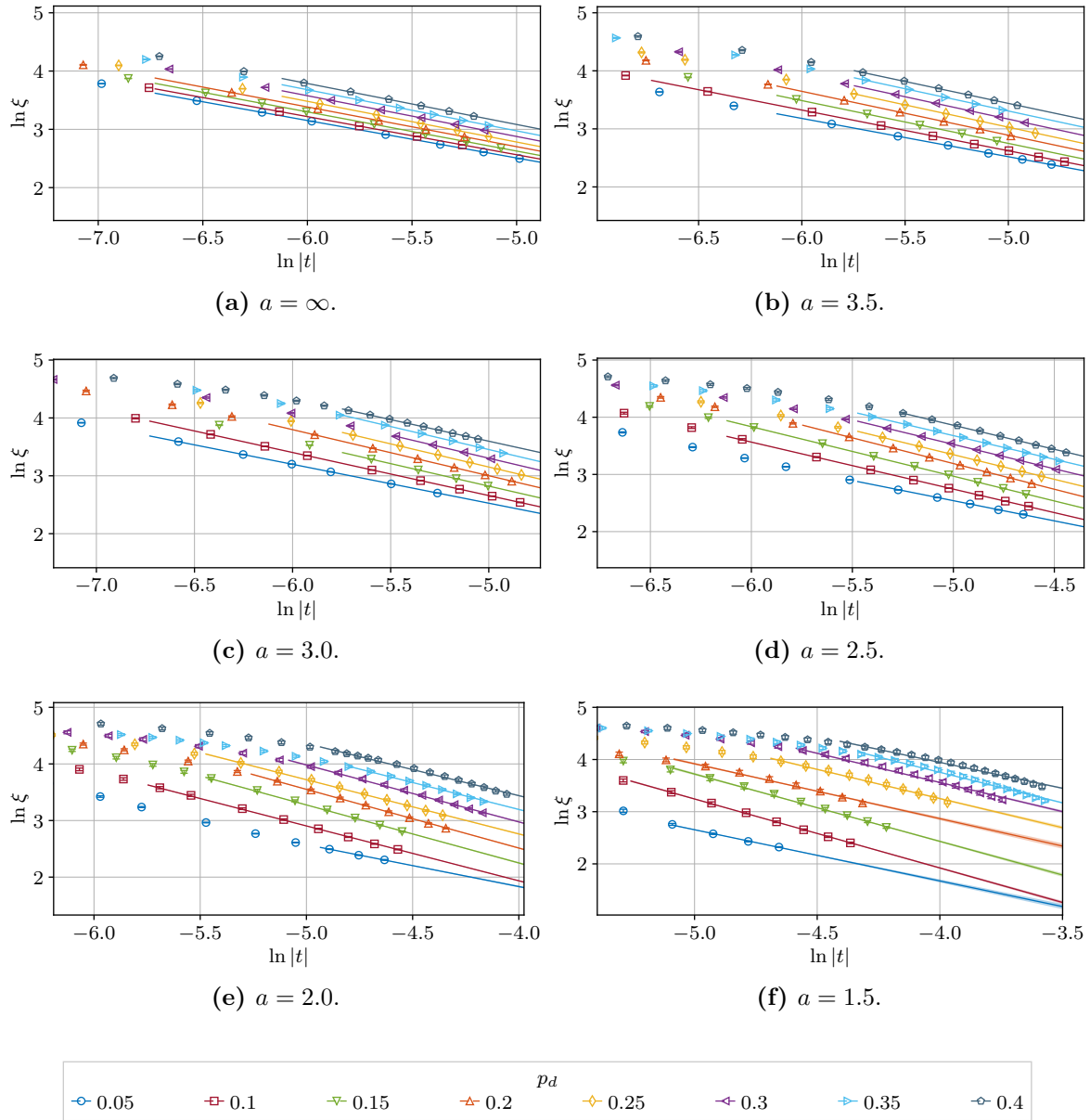
Figure 4.63: Examples of the fits of $\xi(t)$ to the ansatz from Equation (4.80). For each concentration of defects p_d the minimum $|t|_{\min}$ for which $\chi^2_{\mathrm{red}} \leq 1.0$ was true for the first time is used in the plots.

dependence on a is clearly in accordance with the FSS results which have a $\propto 1/a$ behavior. We will discuss the general quality of the performed TS analysis and its validity at the end of the section in the summary, after having presented the results for $\tilde{\chi}$ and the corresponding critical exponent γ. Let us just note, that we also have checked the influence of the error of β_c on the results, but it turned out that it can be neglected due to much larger errors coming from the fits themselves.

4.6.2 Critical exponent γ

As already mentioned, we analyzed the susceptibility $\tilde{\chi}$ in the same way as we have done for the correlation length ξ. We used the ansatz

$$\ln \tilde{\chi}(t) = A - \gamma \ln |t| \, , \tag{4.81}$$

(a) $a = \infty$.

(b) $a = 3.5$.

(c) $a = 3.0$.

(d) $a = 2.5$.

(e) $a = 2.0$.

(f) $a = 1.5$.

Legend: $p_d = 0.05$, $p_d = 0.1$, $p_d = 0.15$, $p_d = 0.2$, $p_d = 0.25$, $p_d = 0.3$, $p_d = 0.35$, $p_d = 0.4$, ν^g, $\overline{\nu}^w_{\mathrm{lin}}$, $\overline{\nu}^w_{\mathrm{ts}}$
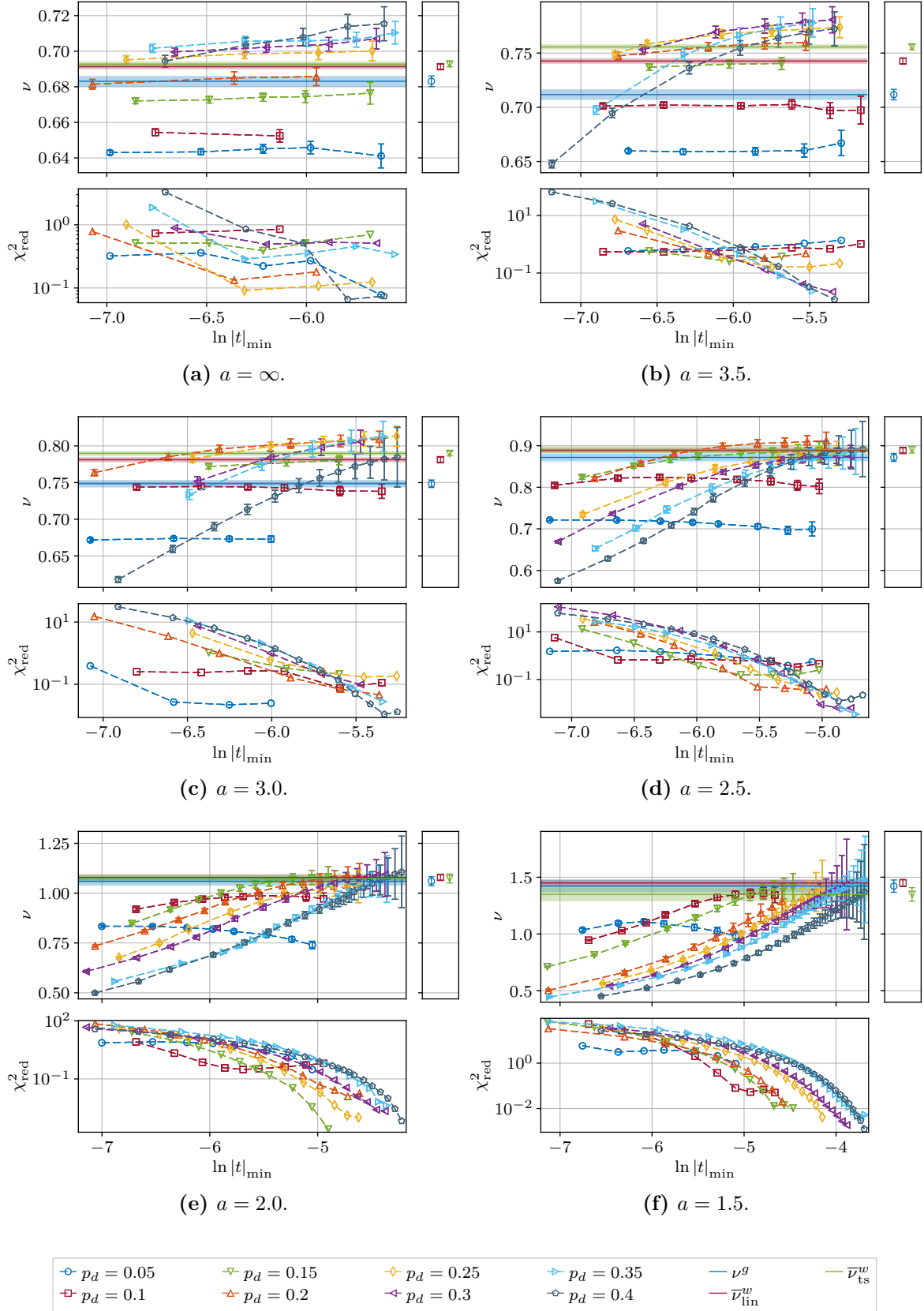
Figure 4.64: Final results of the fits of $\xi(t)$ to the ansatz from Equation (4.80) for different $|t|_{\min}$ and all concentrations of defects p_d. The weighted means $\overline{\nu}^w_{\mathrm{ts}}$ over all concentrations with $p_d \geq 0.15$ and for the largest possible $|t|_{\min}$ are shown together with the results from the FSS analysis ν^g and $\overline{\nu}^w_{\mathrm{lin}}$. The narrow right plots show a separate comparision between the different estimates for ν which are plotted as horizontal lines in the main plots.

Table 4.14: Comparison of the final estimates of the critical exponent ν from the finite-size scaling analysis and the temperature scaling analysis (labeld with "ts"). The values $\overline{\nu}^w_{\mathrm{lin}}$ and ν^g are taken from Table 4.5. The weighted mean over $p_d \geq 0.15$ for the temperature scaling results $\overline{\nu}^w_{\mathrm{ts}}$ were calculated over the estimates with maximum used $|t|_{\mathrm{min}}$ (and hence three degrees of freedom).

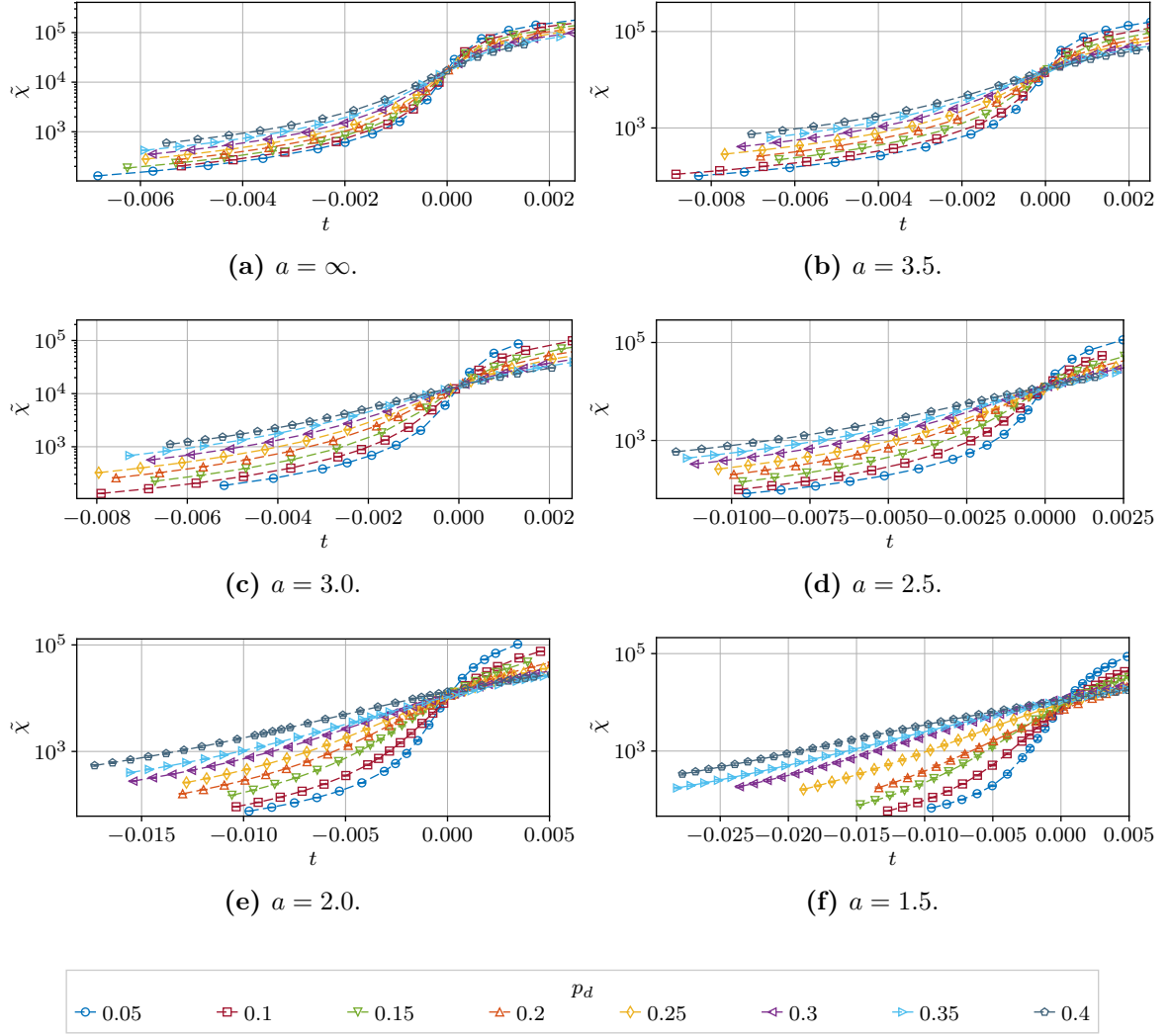| a	$\overline{\nu}^w_{\mathrm{ts}}$	$\overline{\nu}^w_{\mathrm{lin}}$	ν^g
∞	0.6928(17)	0.6913(15)	0.6831(30)
3.5	0.7557(25)	0.7427(25)	0.7117(49)
3.0	0.7898(34)	0.7812(35)	0.7484(52)
2.5	0.8905(82)	0.8887(61)	0.8719(96)
2.0	1.073(23)	1.079(14)	1.060(23)
1.5	1.348(61)	1.449(32)	1.421(55)

and performed individual fits for all concentrations of defects p_d and correlation exponents a. Again, we varied the minimum included $|t|_{\mathrm{min}}$ to see the asymptotic behavior. The susceptibility as function of t is presented in Figure 4.65. It has the same qualitative behavior as the ξ — for different p_d the curves cross each other at $t = 0$. Note, that as in the case with ξ, the definition of $\tilde{\chi}$ is valid only in the high temperature phase, and we extended the values to the low temperatures in order to see the crossing point better. In Figure 4.66 we show examples of the fits for all correlation exponents a. The estimates of the critical exponent γ in dependence of the chosen $|t|_{\mathrm{min}}$ are presented in Figure 4.67. The weighted means for all $p_d \geq 0.15$ and the largest $|t|_{\mathrm{min}}$ are summarized in Table 4.15.

Let us discuss the results of the critical exponent γ. The first observation is the same as in the case of ξ, the smallest concentrations $p_d \leq 0.1$ show a crossover behavior and therefore we excluded them in the weighted mean. Again, the curves do not reach asymptotic values even for the largest $|t|_{\mathrm{min}}$. The final weighted mean estimates $\overline{\gamma}^w_{\mathrm{ts}}$ lie slightly above the global fit estimates γ^g from the FSS analysis except for the case of $a = 1.5$. They match very well for the correlation exponents in the range $3.0 \geq a \geq 2.0$ but do not match in the uncorrelated case, $a = \infty$. The crossover region with $a = 3.5$ shows the largest deviations between $\overline{\gamma}^w_{\mathrm{ts}}$ and γ^g. But in general, the qualitative cross-check supports or estimates from the FSS analysis. Unfortunately, we were not able to compare to the individual uncorrected fits ansatz in the FSS case, since we have not performed it for the critical exponent γ.

Table 4.15: Comparison of the final estimates of the critical exponent γ from the finite-size scaling analysis and the temperature scaling analysis (labeld with "ts"). The values γ^g are taken from Table 4.8. The weighted mean over $p_d \geq 0.15$ for the temperature scaling results $\overline{\gamma}^w_{\mathrm{ts}}$ were calculated over the estimates with maximum used $|t|_{\mathrm{min}}$ (and hence three degrees of freedom).

a	$\overline{\gamma}^w_{\mathrm{ts}}$	γ^g
∞	1.3430(18)	1.3324(64)
3.5	1.4875(33)	1.451(15)
3.0	1.5726(50)	1.566(16)
2.5	1.787(11)	1.783(24)
2.0	2.171(27)	2.149(51)
1.5	2.791(70)	2.93(14)

(a) $a = \infty$.

(b) $a = 3.5$.

(c) $a = 3.0$.

(d) $a = 2.5$.

(e) $a = 2.0$.

(f) $a = 1.5$.

p_d

0.05   0.1   0.15   0.2   0.25   0.3   0.35   0.4

Figure 4.65: Susceptibility $\tilde{\chi}$ as function of the reduced temperature t. The definition of $\tilde{\chi}$ is valid only for the high temperature phase with $t \leq 0$, but we extended the curves in order to see the crossing point better.

Let us summarize the usage of the TS analysis for the estimation of the critical exponents in the context of this work. As mentioned previously, we used the TS ansatz as a supplementary analysis and mostly used the already available data which was produced with the FSS analysis in mind. The available data was not sufficient to perform corrected fits and even the uncorrected fits shown a clear dependence on the used temperature range. Since corrected fits were not possible, also a fit of the specific heat which contains a regular background term was not reliable. Also, we were not able to estimate β since the low temperature side of the available data was too short for most correlation exponents a and concentrations of defects p_d. In order to improve the temperature scaling analysis we would need more simulated temperatures and also change the structure of the whole simulation process by using more disorder realizations instead of longer measurement series for each realization. Concerning this work, we do not include the estimates from TS analysis into our final results but rather see them as a verification of the FSS analysis results.
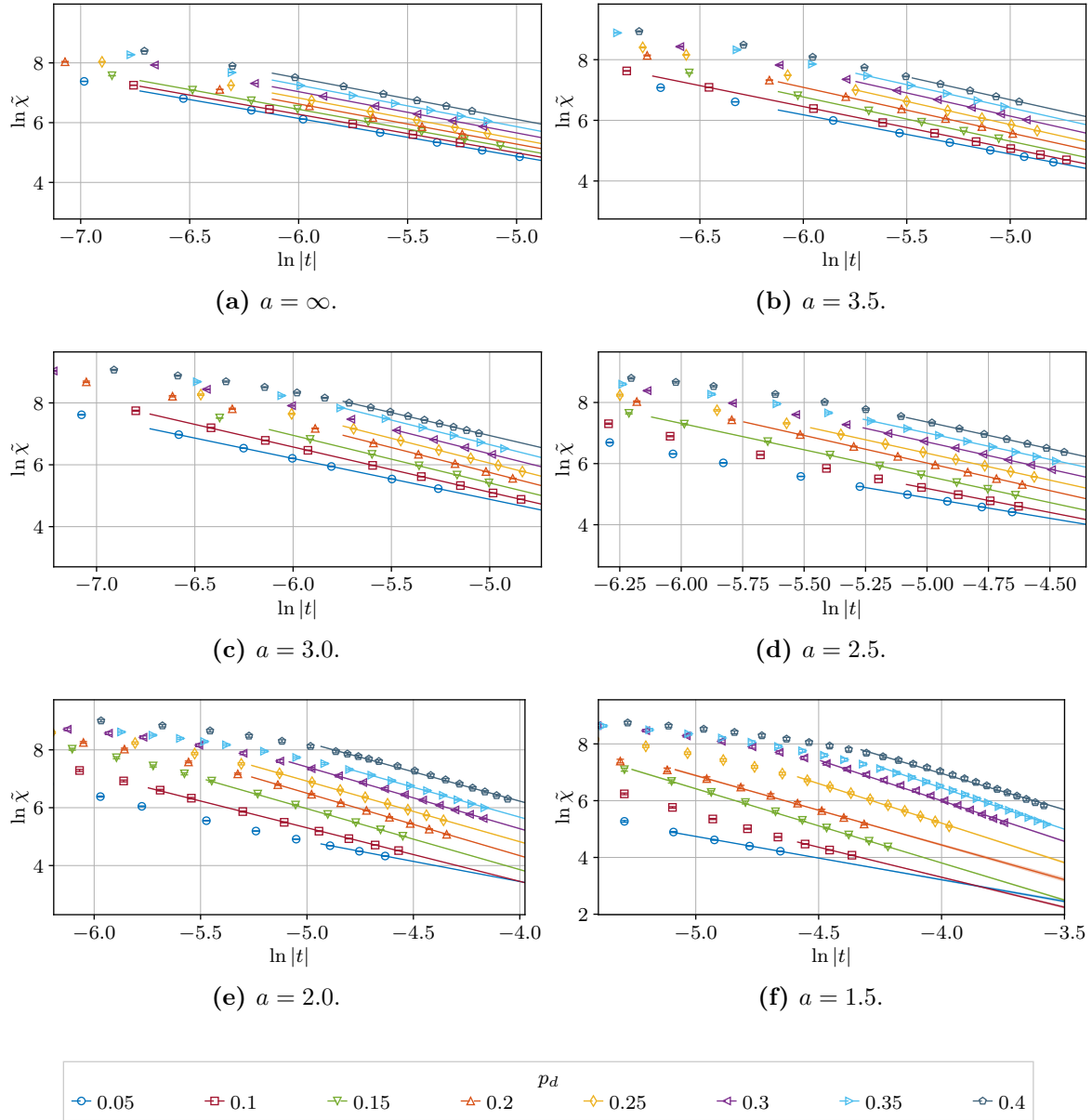
Figure 4.66: Examples of the fits of $\tilde{\chi}(t)$ to the ansatz form Equation (4.81). For each concentration of defects p_d the minimum $|t|_{\mathrm{min}}$ for which $\chi^2_{\mathrm{red}} \leq 1.0$ was true for the first time is used in the plots.

Summary. We successfully used the temperature scaling analysis to validate our finite-size scaling analysis results for the critical exponents ν and γ. Considering that the method used mostly different data in the analysis and also different observables were used, i.e., the correlation length ξ which was not studied in the finite-size scaling case and the high temperature definition of the susceptibility, we can clearly solidify our finite-size scaling results. Additionally, the estimated critical temperatures from the finite-size scaling analysis were proven to be reasonably accurate to be used in the temperature scaling analysis. We do not include the estimates from the temperature scaling in our final results and see them as an additional verification.

(a) $a = \infty$.

(b) $a = 3.5$.

(c) $a = 3.0$.

(d) $a = 2.5$.

(e) $a = 2.0$.

(f) $a = 1.5$.

Legend: $p_d = 0.05$, $p_d = 0.1$, $p_d = 0.15$, $p_d = 0.2$, $p_d = 0.25$, $p_d = 0.3$, $p_d = 0.35$, $p_d = 0.4$, γ^g, $\overline{\gamma}^w_{\mathrm{ts}}$
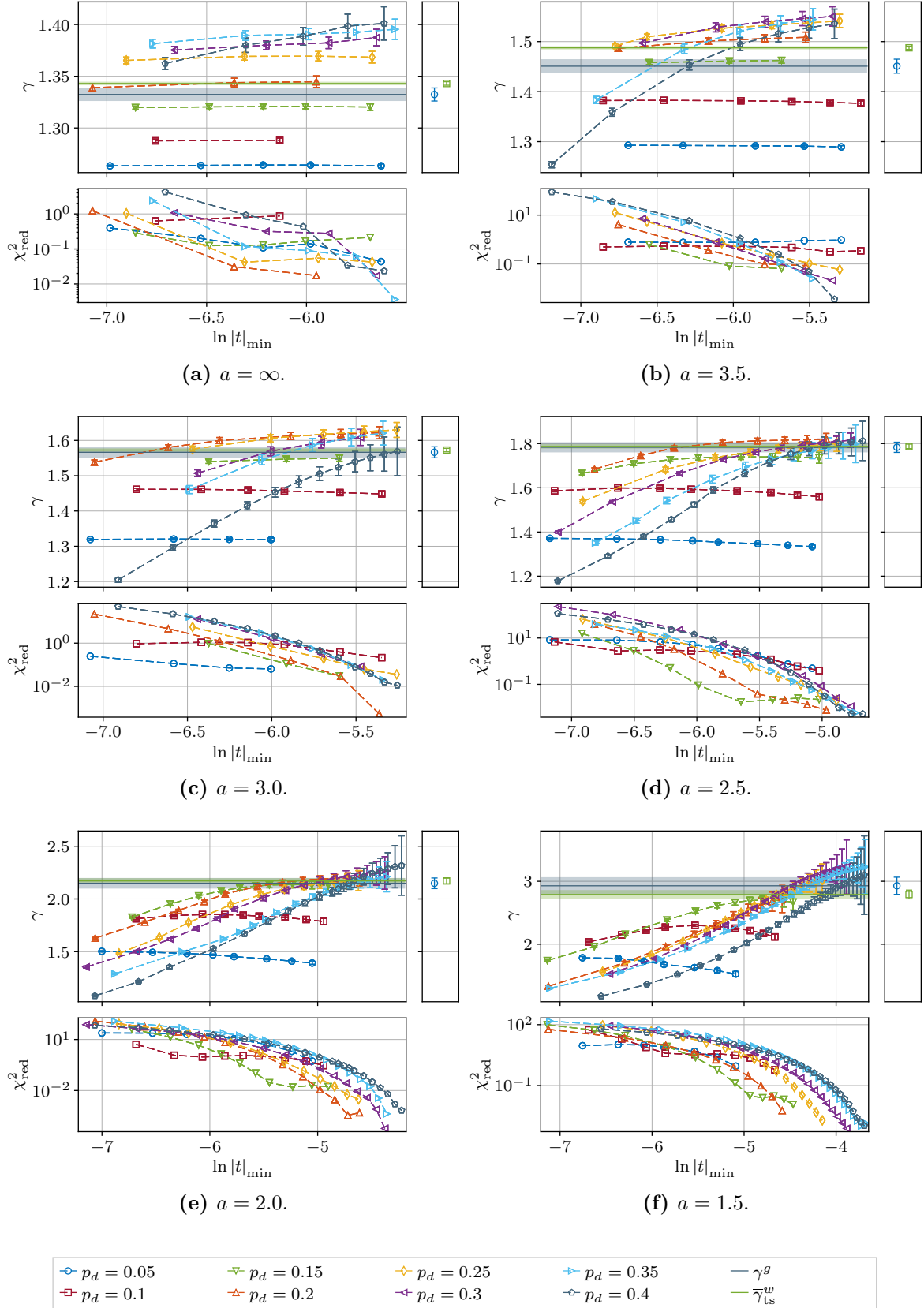
Figure 4.67: Final results of the fits of $\tilde{\chi}(t)$ to the ansatz from Equation (4.81) for different $|t|_{\min}$ and all concentration of defects p_d. The weighted means $\overline{\gamma}^w_{\mathrm{ts}}$ over all concentrations with $p_d \geq 0.15$ and for the largest possible $|t|_{\min}$ are shown together with the result from the FSS analysis γ^g. The narrow right plots show a separate comparision between the different estimates for γ which are plotted as horizontal lines in the main plots.

Conclusions

<div style="text-align: right; font-size: 3em;">**5**</div>

In this work we studied the three-dimensional Ising model on a long-range power-law site disordered lattice with the help of Monte Carlo techniques. We would like to summarize the main results of this work and also give a short outlook for possible further research directions.

Critical exponents

The main results of the present work are the estimates of the critical exponents ν, γ and β in dependence of the correlation exponent a. They were obtained by using the finite-size scaling technique. Additionally, we solidified the results by comparing to the estimates through a temperature scaling analysis. The full set of the obtained critical exponents is summarized in Table 5.1 and Figure 5.1 together with the critical exponents calculated through the scaling relations. For the uncorrelated case our estimates are compatible with estimates known from the literature. We observe a new universality class for the disordered Ising model in accordance with the Harris criterion [Har74] which is characterized by a new set of critical exponents. This is an important proof of the whole analysis process, including the histogram reweighting procedure and the global fit ansatzes. Our estimates of the critical exponents for the correlated cases show a clear dependence on the correlation exponent a in the form of $\propto 1/a$. To our knowledge, it is the first time that a study has derived the critical exponents for a larger number of different correlation exponents a by using simulation techniques. Quantitatively, we cannot reproduce the conjecture of Weinrib and Halperin [WH83] of $\nu = 2/a$ exactly. However, we can suggest that this conjecture is the leading behavior and needs correction terms of some form. This also applies to the other critical exponents for which a dependence on a is given in Ref. [WH83] (but not explicitly sad to be valid for the Ising model) — we see a $\propto 1/a$ behavior, but the estimates do not match the predictions exactly. We clearly see a crossover region at $a \approx 3.0 = d$, in agreement with the extended Harris criterion [WH83]. In this region we observe the largest derivations between our estimates and the predictions from Ref. [WH83]. An interesting observation of this work is the negative exponent η which is more or less constant for all correlated cases. From the present analysis, we cannot exclude a systematic uncertainty in our estimates but a deeper look into this issue could be of importance.

Finally, we checked the estimates ν, γ and β for consistency with the hyperscaling relation. Our results suggest that it may be that the hyperscaling relation is violated in the crossover region around $a \approx 3.0$ while it is valid in the uncorrelated and in strongly correlated cases.
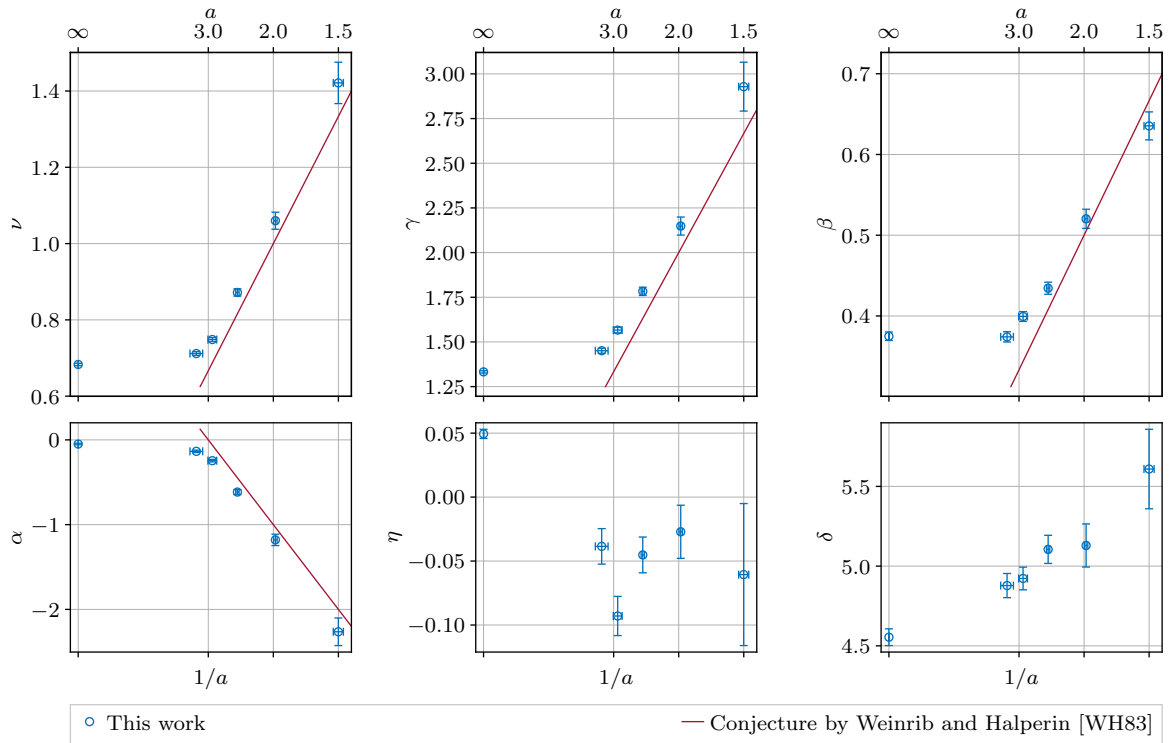
Figure 5.1: Complete set of the critical exponents of the tree-dimensional Ising model with long-range power-law correlated site disorder for various correlation exponents a and for the uncorrected case with $a = \infty$. The exponents in the lower row were calculated by using the scaling relations. The horizontal errors represent the uncertainty in measured correlation exponents $\overline{a}$.

Table 5.1: Complete set of the critical exponents of the tree-dimensional Ising model with long-range power-law correlated site disorder for various correlation exponents a and for the uncorrected case with $a = \infty$. The exponents marked with † were calculated by using the scaling relations. For completeness the measured correlation exponents $\overline{a}$ and the estimated confluent correction exponents ω are added.

a	$\overline{a}$	ν	γ	β	$\alpha^{\dagger}$	$\eta^{\dagger}$	$\delta^{\dagger}$	ω
∞	–	0.6831(30)	1.3324(64)	0.3749(53)	−0.0493(90)	0.0494(36)	4.554(53)	0.346(40)
3.5	3.30(18)	0.7117(49)	1.451(15)	0.3741(64)	−0.135(15)	−0.039(14)	4.878(76)	0.679(44)
3.0	2.910(96)	0.7484(52)	1.566(16)	0.3993(61)	−0.245(16)	−0.093(16)	4.923(72)	0.840(50)
2.5	2.451(26)	0.8719(96)	1.783(24)	0.4344(75)	−0.616(29)	−0.045(14)	5.105(89)	1.154(66)
2.0	1.979(18)	1.060(23)	2.149(51)	0.520(12)	−1.180(68)	−0.027(21)	5.13(14)	1.087(81)
1.5	1.500(30)	1.421(55)	2.93(14)	0.635(18)	−2.26(17)	−0.061(56)	5.61(25)	0.988(75)

Confluent correction exponent

In addition to the critical exponents, we estimated the confluent correction exponent ω. This was achieved by using quotients of an observable at two different lattice sizes which allowed a determination independently of other exponents. The final results are summarized in Table 5.1. We reproduce the values known from other works for the uncorrelated case and partially agree on the values for the correlated case of $a = 2.0$. Altogether, we see an increase in the values of ω when going from $a = \infty$ until $a \approx 2.5$ and after that the exponent ω decreases again. As with the critical exponents, the assumption that this is

a consequence of a crossover regime around $a \approx 3.0$ is appropriate. It is interesting, that the correction exponent ω shows the same qualitative behavior as the deviation from the hyperscaling relation. Probably, both phenomena are connected with each other.

Disorder correlation exponent

Since the critical exponents discussed above are all a-dependent, it was an important step to analyze the underlying long-range power-law correlated site disorder configurations. None of the known works on the long-range correlated disordered Ising model provided a measured correlation exponent a. In our opinion however, it is an important step to map the measured critical exponents to the correlation exponent a conclusively. We measured the correlation exponents $\overline{a}$ and compared them to the imposed values a. These values are listed in Table 5.1 The outcome can be summarized in two main points. The first aspect is that $\overline{a} < a$ is true for all considered cases. The second fact is that the deviations become larger for larger a, i.e., weaker correlations. This behavior becomes less pronounced for larger numbers of disorder realizations N_c. We suppose that both effects are a consequence of the finite-size effects on the lattice and the periodic boundary conditions. They cause the defects on the lattice to be effectively slightly more correlated than if they were placed on an infinite lattice. Note, that we used a slightly modified correlation function $C_0(r) = (1+r)^{-a/2}$ in the disorder generation process since a true power-law function possesses a divergence at $r \to 0$. However, this should not be the reason for the inequality $\overline{a} < a$, since the deviation between the used correlation function and the power-law becomes neglectable very fast (the deviation is less than $5\,\%$ already for $r \geq 6.0$). Independently of the true origin of the fact that $\overline{a} < a$, applied to our work, this inequality implies that the estimated critical exponents have an uncertainty with respect to a to which they belong. In Figure 5.1 it is reflected in the horizontal errorbars.

Critical temperatures

While searching for the peaks of various observables, we also obtained the finite-size critical temperatures and were able to estimate the critical temperatures in the thermodynamic limit for all studied correlation exponents a and concentrations of defects p_d. They are listed in Table 5.2. Since our simulations were not focused on the determination of the critical temperature, the obtained estimates are moderately accurate. Nevertheless, we successfully used them in the temperature scaling ansatz and there they proofed themselves as precise enough. Therefore, we can assume that our temperature estimates can be a good starting point for further analyses and simulations. Note, that besides the dependence on a and p_d, the critical temperatures may also depend on the used boundary conditions, the kind of disorder (bond or site disorder) and also on the disorder generation process, i.e., the disorder distribution and shape.

Other results

Further results obtained in this work are the estimation and analysis of the autocorrelation times of the energy and the magnetization during the Swendsen-Wang multiple-cluster update simulation process. They were found to be moderately low and neglectable in the context of the analyses which were performed in the present work. We analyzed the difference between

Table 5.2: Complete set of the critical temperatures of the tree-dimensional Ising model with long-range power-law correlated site disorder for various correlation exponents a as well as for the uncorrected case with $a = \infty$ and different concentrations of defects p_d.

p_d	a					
	∞	3.5	3.0	2.5	2.0	1.5
0.05	0.234592(2)	0.232414(4)	0.231696(6)	0.230677(6)	0.22921(3)	0.2271(2)
0.1	0.249289(4)	0.243131(7)	0.241393(5)	0.239065(8)	0.23592(3)	0.23191(7)
0.15	0.266155(3)	0.254613(4)	0.251679(9)	0.24787(2)	0.24304(5)	0.2369(2)
0.2	0.285742(3)	0.267311(5)	0.26298(1)	0.25753(3)	0.25071(6)	0.2422(4)
0.25	0.308810(3)	0.281646(7)	0.27568(2)	0.26827(5)	0.25928(8)	0.2486(4)
0.3	0.336430(3)	0.298156(8)	0.29021(1)	0.28060(7)	0.2691(2)	0.2559(5)
0.35	0.370175(4)	0.31757(2)	0.30722(4)	0.29482(8)	0.2803(2)	0.2637(6)
0.4	0.412503(8)	0.34088(2)	0.32758(5)	0.3119(2)	0.2940(5)	0.2734(6)

the usage of global fits compared to a weighted mean over individual fits and found that the global fit ansatz is superior for nonlinear models since the weighted mean estimates is biased. We think that this is a consequence of the correlation between a fit parameter and its error in the nonlinear case.

Outlook

As already mentioned, the results of the critical exponent ν, the confluent correction exponent ω as well as the analysis of the measured correction exponent $\overline{a}$ were already published in Ref. [KJ20]. A second publication Ref. [KJ22] with the critical exponents γ and β followed in 2022. Concerning further possible study directions, following ideas may serve as a starting point:

- analyze the origin of the negative exponent η,
- measure the specific heat exponent α explicitly,
- check the validity of the hyperscaling relation more precise,
- perform appropriate simulations and use the temperature scaling ansatz more expressive,
- study universal amplitude ratios in dependence of a.

There are plenty other possibilities but let us stop at this point. We would like to end our work with these words by Max Planck [Pla36],

> " A scientist is happy, not in resting on his attainments
> but in the steady acquisition of fresh knowledge. "

A

Appendices

A.1 Analysis of the negative spectral density entries

As discussed in Section 3.5, we start the generation process by choosing an appropriate correlation function for the disorder $C_0(\boldsymbol{r})$. In our implementation we used

$$C_0(\boldsymbol{r}) = \left(1 + r^2\right)^{-a/2} \to r^{-a} \quad \text{for } r \to \infty \,, \tag{A.1}$$

where $r = |\boldsymbol{r}|$ is the distance on the lattice adopted to the appropriate boundary conditions. Furthermore, we used the square root of the spectral density $S(\boldsymbol{k})$ of $C_0(\boldsymbol{r})$ in the disorder generation process. As the correlation function is symmetric with respect to $\boldsymbol{r}$, we know that the spectral density will contain only real values. Therefore, we need $S(\boldsymbol{k}) \geq 0$ for all $\boldsymbol{k}$ in order to take the square root of $S(\boldsymbol{k})$. We followed Ref. [Zie+17] and used a modified spectral density $\tilde{S}(\boldsymbol{k})$ defined in Equation (3.82) with a zero-cutoff where we set each negative value of $S(\boldsymbol{k})$ to zero,

$$\tilde{S}(\boldsymbol{k}) = \begin{cases} S(\boldsymbol{k}) & \text{if } S(\boldsymbol{k}) \geq 0 \\ 0 & \text{else} \end{cases} \,.$$

We introduce the abbreviations for the minimum and maximum values of the (unmodified) spectral density $S(\boldsymbol{k})$,

$$\underset{\sim}{S}(\boldsymbol{k}) = \min_{\boldsymbol{k}} S(\boldsymbol{k}) \,, \quad \hat{S}(\boldsymbol{k}) = \max_{\boldsymbol{k}} S(\boldsymbol{k}) \,. \tag{A.2}$$

First, we checked for which correlation exponents a and lattice sizes L analyzed in the present work, negative values of $S(\boldsymbol{k})$ occur. As can be seen in Figure A.1, they only occur for $a = 1.5$ and $L < 24$. Moreover, the ratio between the largest and the smallest value $S(\boldsymbol{k})$ suggest, that the slightly negative values cannot be of great importance for the global picture. In Section 4.5 we have seen, that because of the finite-size effects we excluded such small lattice sizes for $a = 1.5$ in our analyses anyway. This makes the problem of negative $S(\boldsymbol{k})$ completely neglectable in our present study.

Nevertheless, we have analyzed the problem of negative $S(\boldsymbol{k})$ further in order to understand how these values behave in general. Let us first note that on a finite lattice with an even linear dimension L we cannot achieve exact symmetry of $C_0(\boldsymbol{r})$ because we need one center point on the lattice with $\boldsymbol{r} = 0$ which leaves us with an odd number of sites in each direction. Therefore, we analyzed the occurrence of negative $S(\boldsymbol{k})$ values for even and odd L separately. We show the minimum values $\underset{\sim}{S}(\boldsymbol{k})$ and the ratios $\underset{\sim}{S}(\boldsymbol{k})/\hat{S}(\boldsymbol{k})$ for both cases and for different correlation exponents $0.5 \leq a \leq 1.5$ in Figure A.2.
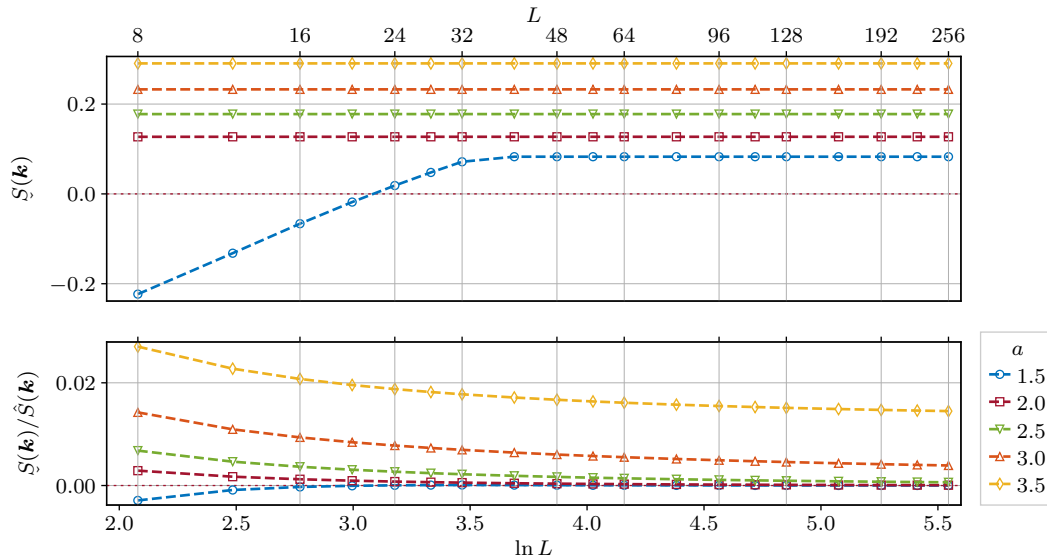
Figure A.1: The smallest values of the spectral density $S(\boldsymbol{k})$ for all a and L parameters used for simulations in this study. Negative values of $S(\boldsymbol{k})$ occur only for $a = 1.5$ and $L < 24$ and therefore the zero-cutoff is considered unproblematic in the present work.

We can differentiate between three different cases. In the first case for correlation exponents $a > 1.0$, negative values of $S(\boldsymbol{k})$ occur only as finite-size effects for even lattice sizes where the symmetry of $C_0(\boldsymbol{r})$ cannot be mapped perfectly. For large enough lattice sizes the minimum values $\undertilde{S}(\boldsymbol{k})$ become positive. This happens faster for larger a. For odd lattice sizes and $a > 1.0$ the minimum values are positive for all L. The ratios between minimum and maximum values $\undertilde{S}(\boldsymbol{k})/\hat{S}(\boldsymbol{k})$ seam to approach zero for both, even and odd lattice sizes. In the second case for stronger correlations with correlation exponents $a < 1.0$, we see negative values which increase as $L \to \infty$ for both, even and odd lattice sizes. However, the ratios between minimum and maximum values $\undertilde{S}(\boldsymbol{k})/\hat{S}(\boldsymbol{k})$ approach negative but constant values. The last case with $a = 1.0$ is a special case. The minimum values stay negative but constant, probably for for $L \to \infty$. As a consequence, the ratio $\undertilde{S}(\boldsymbol{k})/\hat{S}(\boldsymbol{k})$ approach zero from below.

In short, the negative values of $S(\boldsymbol{k})$ occur as finite-size effects for small lattices with even lattice sizes L but otherwise are restricted to $a \leq 1.0$. We have summarized the limit behavior for $\undertilde{S}(\boldsymbol{k})$ and $\undertilde{S}(\boldsymbol{k})/\hat{S}(\boldsymbol{k})$ in Table A.1.

To analyze the quantitative influence of the negative spectral density values, we compared initial $C_0(\boldsymbol{r})$ with the values after a forward and backward Fourier transformation of $C_0(\boldsymbol{r})$ and using the zero-cutoff in-between,

$$C_0(\boldsymbol{r}) \xrightarrow{\text{DFT}} S(\boldsymbol{k}) \xrightarrow{\text{zero-cutoff}} \tilde{S}(\boldsymbol{k}) \xrightarrow{\text{DFT}^{-1}} \tilde{C}_0(\boldsymbol{r}) \,. \tag{A.3}$$

We define the relative deviation between the initial values $C_0(\boldsymbol{r})$ and resulting values $\tilde{C}_0(\boldsymbol{r})$

$$\Delta^r C_0(\boldsymbol{r}) = \frac{C_0(\boldsymbol{r}) - \tilde{C}_0(\boldsymbol{r})}{C_0(\boldsymbol{r})} \,. \tag{A.4}$$

In Figure A.3 we plot the maximum of the absolute values of the deviations $\max\left(|\Delta^r C_0(\boldsymbol{r})|\right)$ for odd and even L and different a, and compare the convergence. We observe the same three cases with separation at $a = 1.0$. For $a \geq 1.0$ the maximal deviations approach zero

(a) Even L.

(b) Odd L.
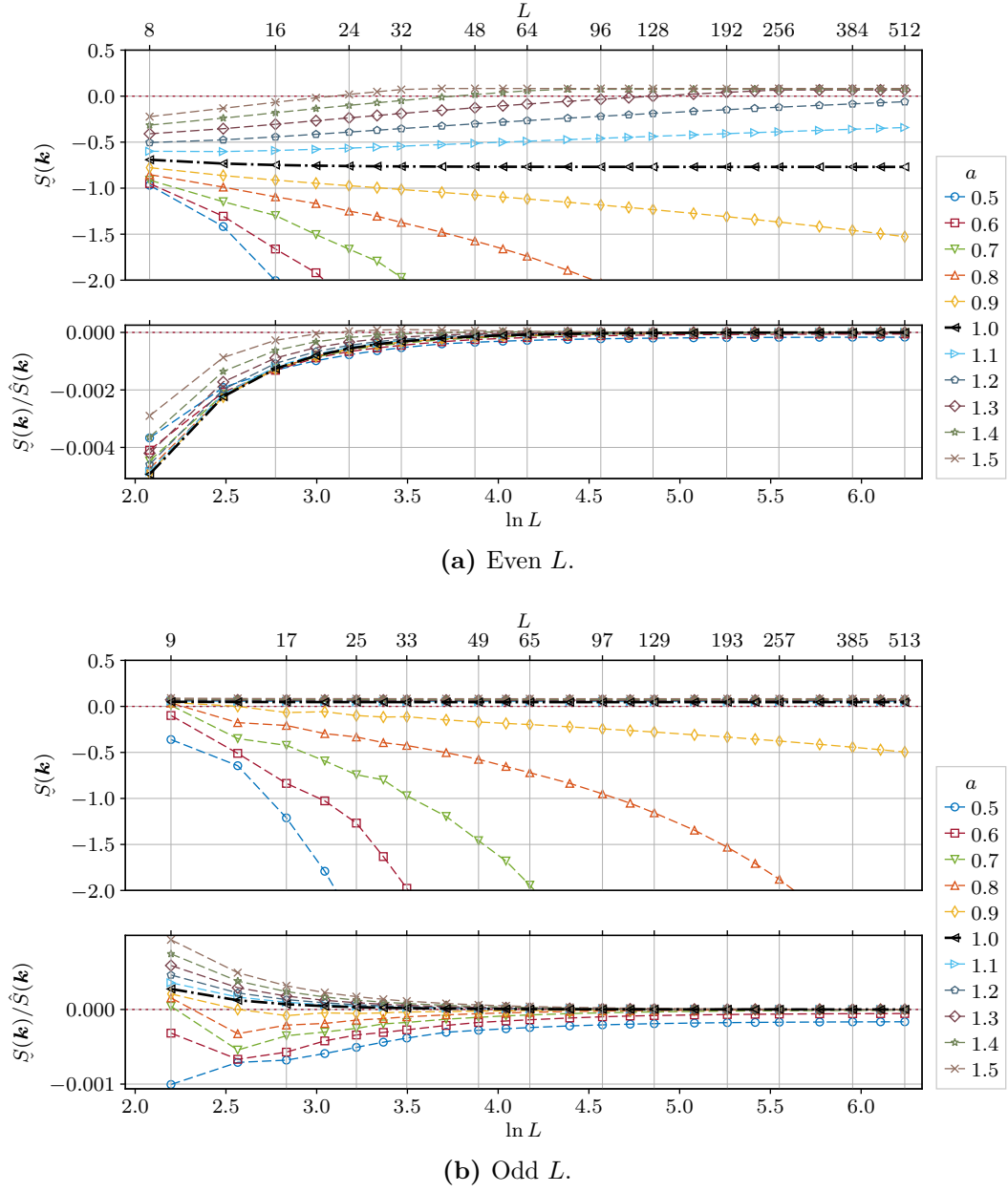
**Figure A.2:** Minimum spectral density values $\underset{\sim}{S}(\boldsymbol{k})$ and ratios $\underset{\sim}{S}(\boldsymbol{k})/\hat{S}(\boldsymbol{k})$ in dependence of the lattice size L and correlation exponent a. Only the case of even L produces negative values for small lattice sizes for $a > 1.0$. On the other hand, for $a < 1.0$, in both even and odd L cases negative values occur and their absolute values increase with increasing L.

as $L \to \infty$. The odd L cases already start at zero for the smallest lattice sizes whereas the even-L curves slowly approach the limit. For $a < 1.0$ a small finite value is approached. Here, the even and odd L curves both have non-zero values throughout the L-range and converge towards each other with increasing L. Altogether, the maximum deviation for all cases with $a \geq 0.5$ lies at $\approx 4\%$ while the limits are at $\approx 1\%$ for $a < 1.0$. We have summarized the limit behavior of $\max\left(|\Delta^r C_0(\boldsymbol{r})|\right)$ in Table A.1. Note, that even if the maximum deviation does not vanish with $L \to \infty$, its influence probably still goes to zero as the lattice size increases.

Summary. This completes our analysis of the negative spectral density values. We checked that the negative spectral density values occur systematically for $a < 1.0$ and lead to a finite maximum deviation between the initial correlation function and the final correlation function after the Fourier transform, applying zero-cutoff on the spectral density and transforming back. However, for $a > 1.0$, the negative spectral density values are finite-size effects which vanish for large enough lattice sizes L.

Table A.1: Expected of $\check{S}(\boldsymbol{k})$, $\check{S}(\boldsymbol{k})/\widehat{S}(\boldsymbol{k})$ and $\max\left(|\Delta^r C_0(\boldsymbol{r})|\right)$ for $L \to \infty$ for different correlation exponent regions. Less or greater than zero is meant to be a finite value below or above zero, respectively.

	$a < 1.0$	$a = 1.0$	$a > 1.0$
$\check{S}(\boldsymbol{k})$	$-\infty$	< 0	> 0
$\check{S}(\boldsymbol{k})/\widehat{S}(\boldsymbol{k})$	< 0	0	0
$\max\left(|\Delta^r C_0(\boldsymbol{r})|\right)$	< 0	0	0
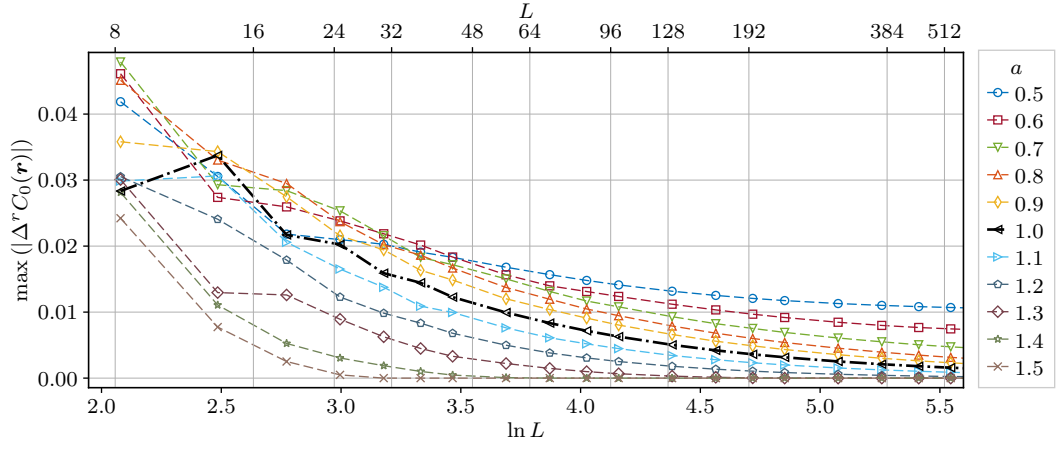
(a) Even L.
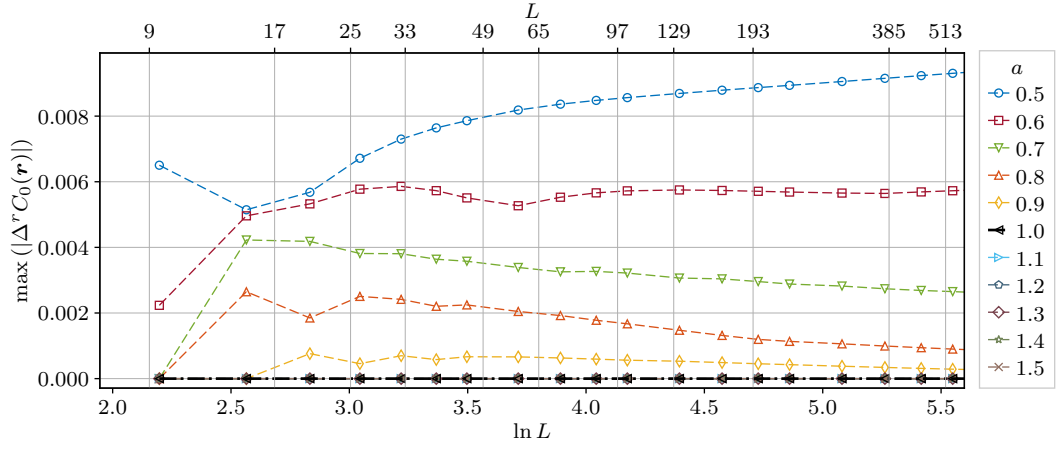
(b) Odd L.
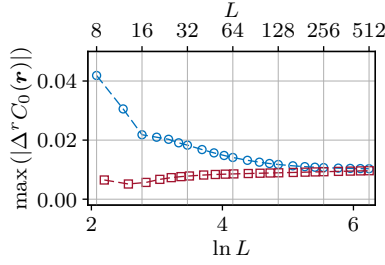
(c) $a = 0.5$.
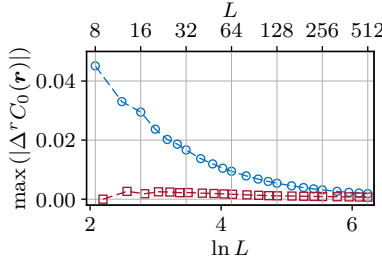
(d) $a = 0.8$.
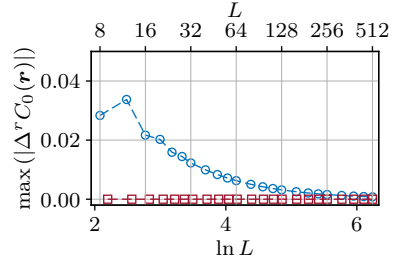
(e) $a = 1.0$.
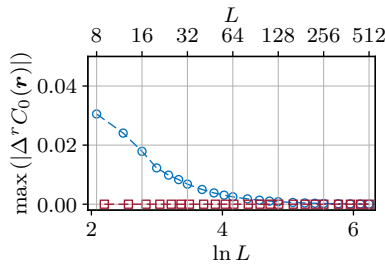
(f) $a = 1.2$.
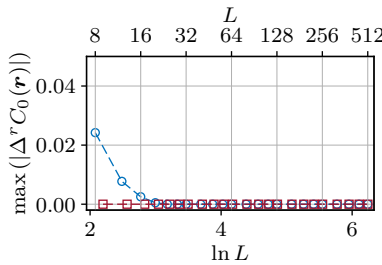
(g) $a = 1.5$.

Figure A.3: Maximum relative deviations $\max(|\Delta^r C_0(\boldsymbol{r})|)$ in dependence of the lattice size L and correlation exponent a. Figures (a) and (b) show the even and odd L cases while in Figures (c)–(g) curves for individual a are plotted. For $a \geq 1.0$, the deviations approach zero for even and odd L cases. For $a < 1.0$, a finite non-zero value is approached.

A.2 Global fits

We would like to present you the concept of a **global fit** which was used at many places throughout this work. Consider a set of N data points of the for $(x^n, y^n, \epsilon(y^n))$ for $n = 1, ..., N$. You expect the data to be described by a model, i.e., a function f. The function f has some parameters which one can get by using least-squares minimization, i.e., perform a fit to the model f. Let A and B be the two parameters of the model. An example is a linear function with

$$f(x; A, B) = Ax + B\,,\tag{A.5}$$

a power-law function

$$f(x; A, B) = B + x^A\,,\tag{A.6}$$

or an exponential function

$$f(x; A, B) = B + e^{-Ax}\,.\tag{A.7}$$

Functions with more parameters can also be used, but we restrict the explanation to functions with only two parameters for simplicity. By using the least-squares minimizer

$$\chi^2 = \sum_{n=1}^{N} \left(\frac{y^n - f(x^n)}{\epsilon(y^n)} \right)^2\,,\tag{A.8}$$

and a technique to minimize it, we finally obtain the estimates $\tilde{A}$ and $\tilde{B}$ for A and B, respectively, and their corresponding errors $\epsilon(\tilde{A})$ and $\epsilon(\tilde{B})$. We do not go into the detail here and refer to, e.g., Refs. [LH95; VV91] for a detailed explanation for the least-square fitting method.

Now, consider that you have similar sets of data, e.g., by repeating the experiment/simulation. Suppose, there are M such sets, $(x_m^n, y_m^n, \epsilon(y_m^n))$ with $m = 1, ..., M$. We can repeat the process of fitting for each set m and get M estimates $\tilde{A}_m$ and $\tilde{B}_m$. But now, **suppose, that we know by theory or assumption that A must be equal for all considered data sets**. Note, that the parameter B can still vary for each data set. We can calculate the weighted mean as a final estimate for the parameter A,

$$A^w = \frac{1}{\sum_{m=1}^{M} \frac{1}{\epsilon(\tilde{A}_m)^2}} \sum_{m=1}^{M} \frac{\tilde{A}_m}{\epsilon(\tilde{A}_m)^2}\,,\tag{A.9}$$

$$\epsilon(A^w) = \sqrt{\frac{1}{\sum_{m=1}^{M} \epsilon(\tilde{A}_m)^{-2}}}\,.\tag{A.10}$$

For comparison reasons we also calculated the standard (unweighted) mean of the individual estimates,

$$A^u = \sum_{m=1}^{M} \tilde{A}_m\,,\tag{A.11}$$

$$\epsilon(A^u) = \sqrt{\frac{1}{M(M-1)} \sum_{m=1}^{M} \left(\tilde{A}_m - A^u \right)^2}\,.\tag{A.12}$$

Using the weighted mean is a usual approach in such situations with individual fits. However, instead of this approach, we can perform one **global fit** which incorporates the data from all M data sets simultaneously and imposes the equality of the parameter A a priori. Let B_m denote the parameter B for the m-th data set and B denote the vector of all B_m. We modify the definition of the model to distinguish between the sets within the function f, i.e., we write, e.g., for the linear case

$$f(x, m; A, B) = Ax + B_m \,, \tag{A.13}$$

and similar for other cases. The only thing that have changed compared to Equation (A.5) is that we have introduced a parameter m which indicates to which of the data sets the provided x belongs and chooses the corresponding B_m parameter. By using a function like the one defined in Equation (A.13), we can write down a modified version of Equation (A.8),

$$\chi^2 = \sum_{n=1}^{N} \sum_{m=1}^{M} \left(\frac{y_m^n - f(x_m^n, m)}{\epsilon(y_m^n)} \right)^2 \,, \tag{A.14}$$

and perform a minimization to get the estimates for the parameters A and B_m with $m = 1, \dots, M$ and their errors. We will call them global fit estimates and write A^g and B_m^g, respectively.

At the first glance both approaches provides very similar estimates, but we wanted to go a bit deeper and see how A^w and A^g are related and how well they hit the true parameter A. We studied three toy examples which were introduced in Equations (A.5) to (A.7). The setup was quite simple. We generated synthetic samples according to each of the models by choosing a fixed value A, using a functional expression for the parameters B_m and random normally distributed errors. We varied the number of data sets M and the number of points in each set N and performed 1000 global and the individual fits (and calculated the weighted mean) for each combination of N and M. To have comparable ranges, we used equally distributed values x from the range $[1, 20]$ for each N. Finally, we calculated the means over the estimates from these 1000 random realizations. i.e., $\overline{A^g}$ and $\overline{A^w}$. Let us first present the settings for each of the cases,

linear case: $\quad A = 1.2 \,, \ B_m = 10 \cdot m \,, \ \epsilon(y_m^n) \sim \mathcal{N}(0, 1^2) \,,$ \hfill (A.15a)

power-law case: $\quad A = 1.2 \,, \ B_m = 10 \cdot m \,, \ \epsilon(y_m^n) \sim \mathcal{N}\left(0, \left(\frac{1}{2} x_m^n\right)^2\right) \,,$ \hfill (A.15b)

exponential case: $A = 0.1 \,, \ B_m = m \,, \qquad \epsilon(y_m^n) \sim \mathcal{N}(0, 0.1^2) \,.$ \hfill (A.15c)

We have tested many different combinations as well but the results for these parameters are presented here as examples. In Figure A.4 we show how the synthetic data sets look like to give a visual impression of what kind of fits we are trying to perform.

Let us start by comparing the qualities of the fits χ^2_{red}. For the global fit ansatz, it is the finally obtained minimum value from Equation (A.14) divided by the total number of the degrees of freedom. For the weighted mean ansatz, we calculated the weighted mean over all $(\chi^2_{\mathrm{red}})_m$ of the individual fits as the final $(\chi^2_{\mathrm{red}})^w$ while using the errors $\epsilon(\tilde{A}_m)$ as weights. Both values and their differences are presented in dependence of N and M in Figure A.5. We see that for all chosen N and M, the qualities are in a good region of $\chi^2_{\mathrm{red}} \approx 0.4$ for the linear case and $\chi^2_{\mathrm{red}} \approx 1.0$ for the non-linear cases. Moreover, they are very comparable

(a) Linear case.   **(b)** Power-law case.   **(c)** Exponential case.
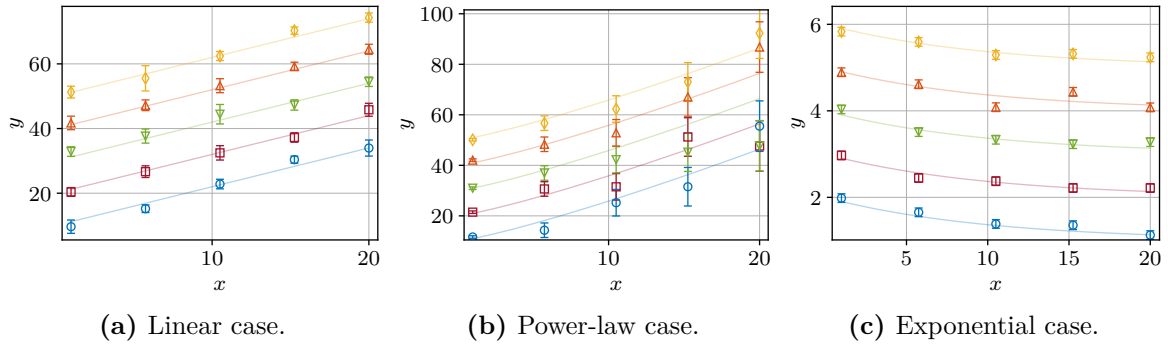
Figure A.4: Examples of the considered data sets with $N = 5$ and $M = 5$ for all three model cases. The solid lines represent the global fit solution.

between the global fit and the weighted mean ansatzes. Comparing the difference, we can see that for the linear case the two cases approach equality for increasing N and increasing M. On the other hand, there is no p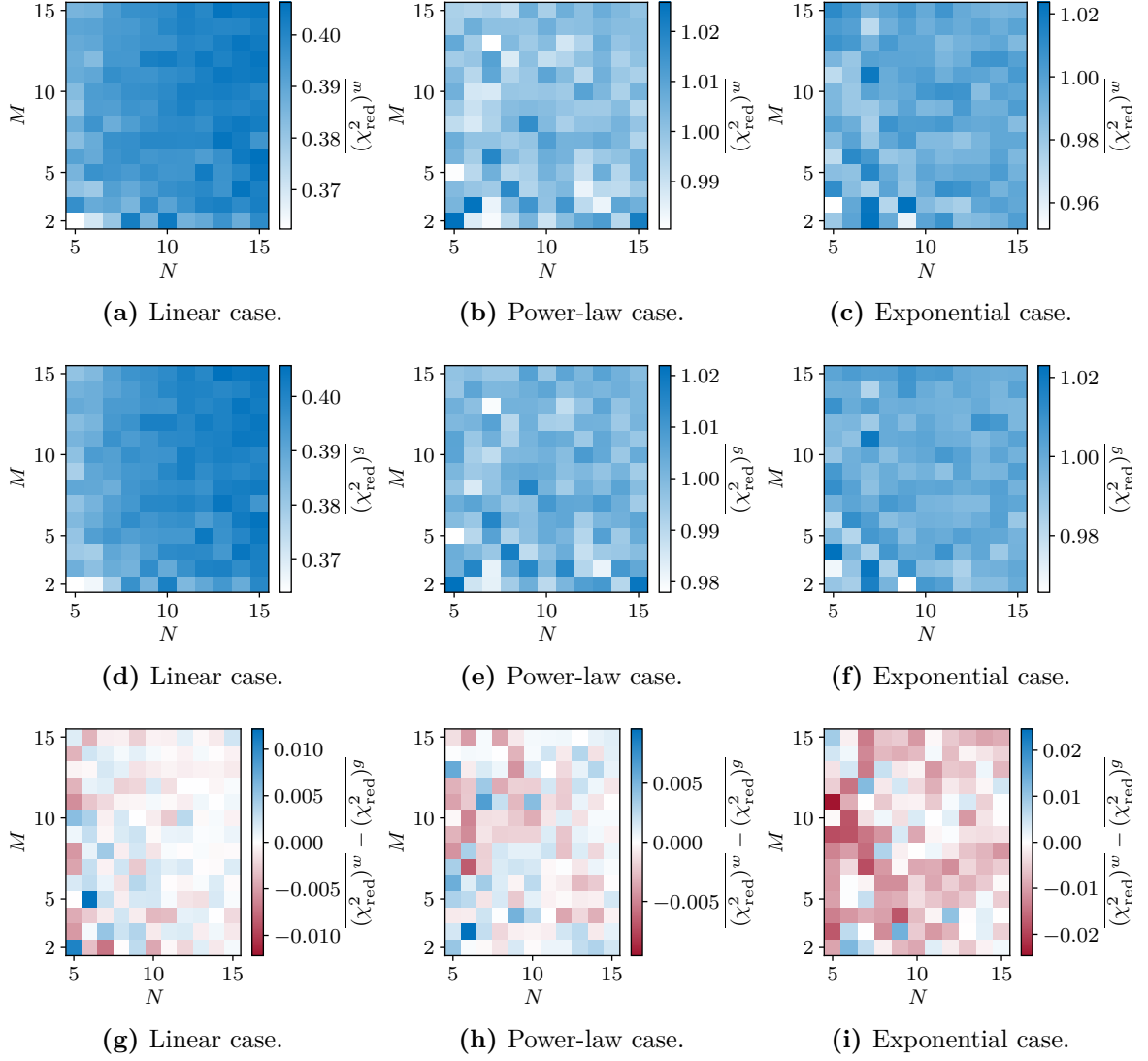ronounced dependence on N and M for the two non-linear cases. In the case of the exponential model, the global fit tends to have slightly larger values than the weighted mean ansatz. But these deviations and fluctuations are probably due to the rather small number of samples. The main outcome is that both ansatzes produce very similar qualities of fit depending on the data.

Let us now discuss the difference between the global fit estimates $\overline{A^g}$, the weighted mean estimates $\overline{A^w}$ and the true parameter A. The differences are presented in Figure A.6. There exists no systematic dependence of the difference between the estimates and the true parameter for the linear case. Moreover, both estimates produce very similar differences with A for each combination N and M. In fact, the difference between the two estimates is in the range of floating number errors with $\left|\overline{A^w} - \overline{A^g}\right| \approx 10^{-10}$. Note, the in the linear case, also the unweighted mean estimate A^u is in a very good agreement with the other two estimates. The errors for both estimates are almost equal and their difference is of order $\left|\overline{\epsilon(A^g)} - \overline{\epsilon(A^w)}\right| \approx 10^{-13}$. The picture changes for the nonlinear models. Here we see a clear deviation between the estimates from the weighted mean ansatz $\overline{A^w}$ and the true parameters A. The interesting thing is that the deviation become larger for increasing M. It means that adding more individual data sets makes the weighted mean worse. On the other hand, for increasing N the deviations become smaller. For the global fit estimates $\overline{A^g}$ we see an approach to A for larger N and M. The global fit estimates therefore become more and more precise with increasing both, the number of points in each data set and the number of total data sets. Comparing the errors, we see that the error $\epsilon(A^g)$ is always larger than $\epsilon(A^w)$. However, the difference is quite small. The error $\epsilon(A^g)$ is expected to have a slightly larger error since there are fewer degrees of freedom in the global fit than in total for all individual fits. If we look at the fourth row in Figure A.6, we see that for the exponential model, the results between $\overline{A^g}$ and $\overline{A^w}$ do not match even within their errorbars and that the estimate $\overline{A^w}$ clearly diverges away from the true value A. The same behavior, but a bit less pronounced is also present for the power-law model. But why does it happen?
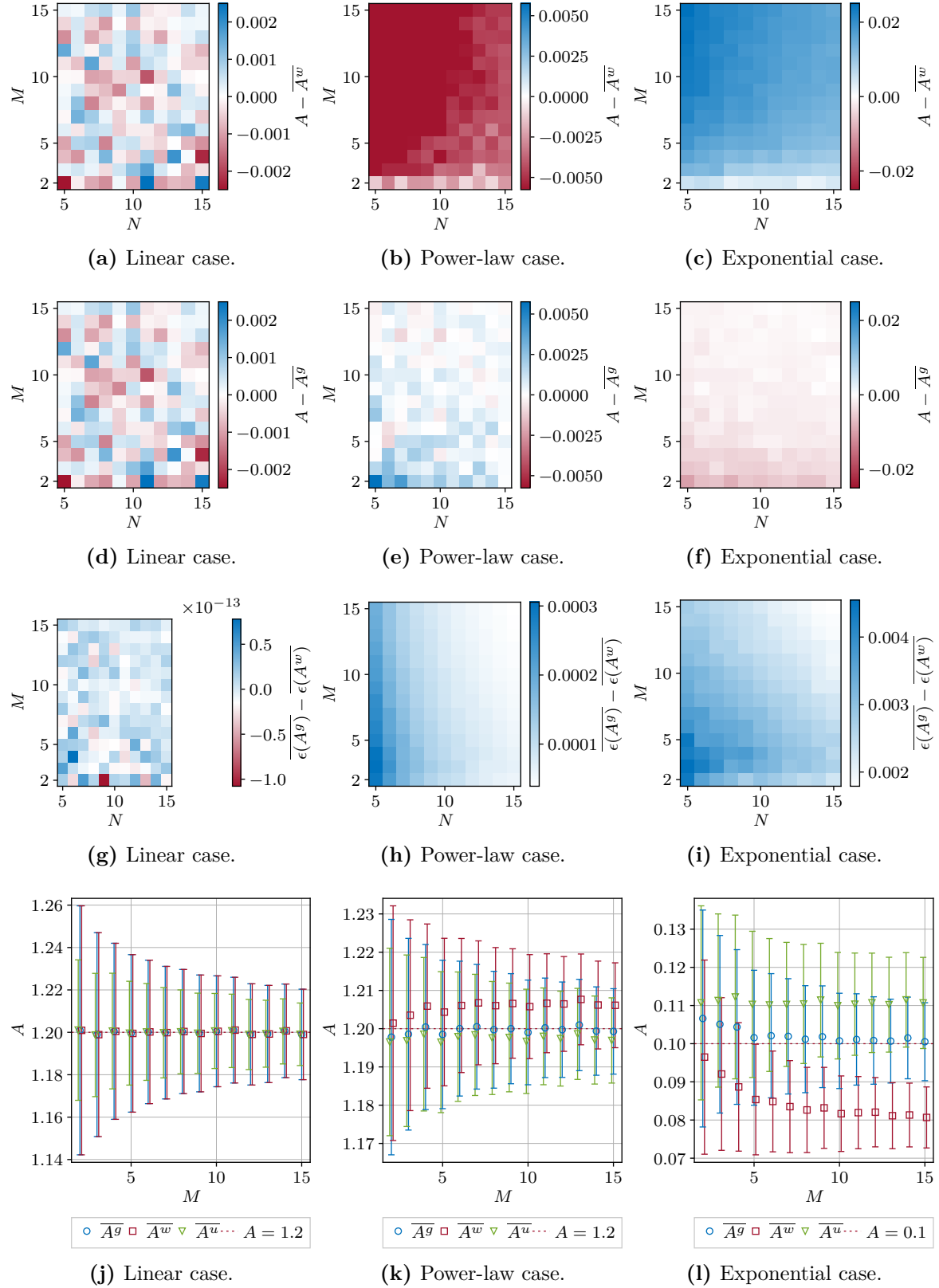
To answer this question, we looked at the dependence between the estimates A^w and their corresponding errors $\epsilon(A^w)$. They are presented in Figure A.7. At this point, everything became clear. It is the correlation between A^w and $\epsilon(A^w)$ which causes the divergence from

(a) Linear case.

(b) Power-law case.

(c) Exponential case.

(d) Linear case.

(e) Power-law case.

(f) Exponential case.

(g) Linear case.

(h) Power-law case.

(i) Exponential case.

Figure A.5: The means of the qualities of fits $\overline{(\chi^2_{\mathrm{red}})^g}$ and $\overline{(\chi^2_{\mathrm{red}})^w}$. First row: qualities of the weighted mean fit ansatz $\overline{(\chi^2_{\mathrm{red}})^g}$, second row: qualities of the global fit ansatz $\overline{(\chi^2_{\mathrm{red}})^g}$, third row: differences $\overline{(\chi^2_{\mathrm{red}})^w} - \overline{(\chi^2_{\mathrm{red}})^g}$.

the true parameter A. In the linear case there is no correlation present and hence $A^g = A^w$ is true. This equality can be derived rigorously, but it would go beyond the scope of an appendix to write the lengthy calculation down. On the other hand, in the case for the nonlinear models, there is a clear dependence between A^w and $\epsilon(A^w)$. Since the errors for the power-law model are smaller for larger A^w, the weighted mean will favor larger values of A and consequently the weighted mean will lie above , $A^w > A$. For the exponential model the opposite is the case and hence $A^w < A$ is true. This can fluctuate from data set to data set, but the general tendency will always remain. The consequence of this correlation between the mean and its error goes even beyond the global fit versus weighted mean comparison. Even by just repeating the same experiment/simulation multiple times and performing the fit to the data with the same nonlinear model each time (even without different parameters B_m), the weighted mean will miss the true value because it will systematically favor one side (above or below A). We have checked that for the very same power-law model but with $B_m = 0$ for all m and the effect remains.

(a) Linear case.

(b) Power-law case.

(c) Exponential case.

(d) Linear case.

(e) Power-law case.

(f) Exponential case.

(g) Linear case.

(h) Power-law case.

(i) Exponential case.

(j) Linear case.

(k) Power-law case.

(l) Exponential case.

Figure A.6: Comparison of the global fit estimates $\overline{A^g}$, the weighted mean estimates $\overline{A^w}$ and the true parameter A for various N and M and for all three considered models. First row: differences $A - \overline{A^g}$, second row: differences $A - \overline{A^w}$, third row: difference between the errors $\overline{\epsilon(A^g)} - \overline{\epsilon(A^w)}$, fourth row: estimates $\overline{A^g}$, $\overline{A^w}$ and $\overline{A^u}$ in dependence of M for $N = 10$ (the small horizontal shifts are added for better visibility).

(a) Linear case.   **(b)** Power-law case.   **(c)** Exponential case.
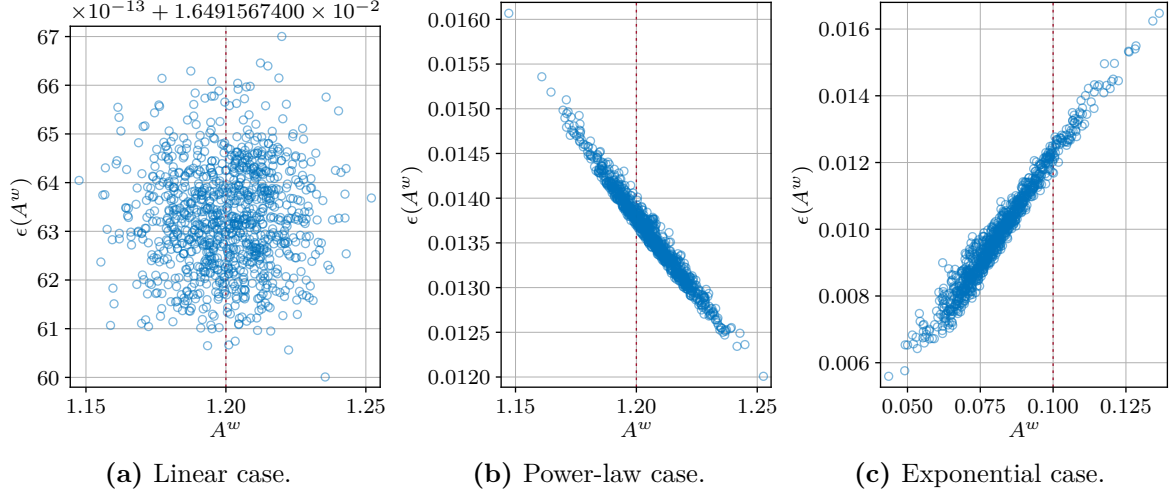
Figure A.7: Dependence between the weighted mean A^w and its error $\epsilon(A^w)$ for each realization and for each of the considered models.

We tested many further considerations and nonlinear models sand all of them shown the same behavior. And, as we already have noticed, this effects becomes worse and worse with increasing number of data sets M. So, let us summarize the outcome.
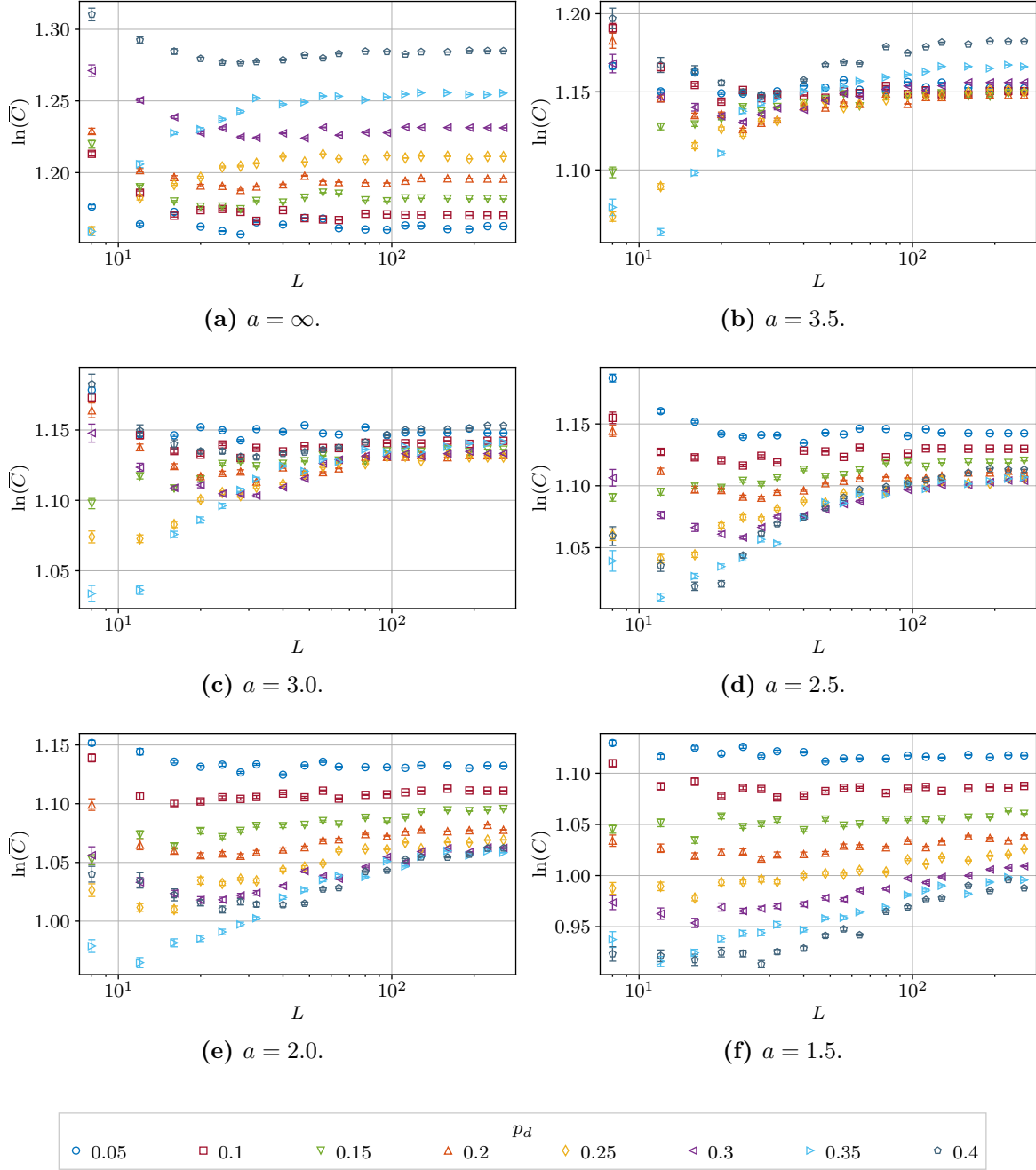
Summary. We presented a global fit ansatz as an alternative to a weighted mean over individual fits. It can be used whenever it is known that several data sets share the same parameter. In fact, we showed that the weighted mean is a biased estimator for a nonlinear fit ansatz because of the correlation between a fit a parameter and its error. In our opinion, whenever possible, it is advisable to use the global fit ansatz which does not suffer from this bias, or more precise, the correlation between A^g and $\epsilon(A^g)$ is still present, but it does not change the estimate A^g itself.

A.3 Stochastic clusters analysis

We have not used the mean $(\overline{C})$ and maximum $(\hat{C})$ Swendsen-Wang stochastic cluster sizes, which we measured during our simulation as described in Section 4.1. Nevertheless, we would like to provide the data which we measured here. We will only present the sizes which were measured at the simulation temperatures for which the final peaks of $\partial_\beta(\ln|m|)$ were found. That means, the presented data points are not exactly at the critical temperature but close to it.

Let us start with the mean cluster sizes $\overline{C}$ which are shown in Figure A.8. One sees, that the values tend to approach a constant value for each p_d with increasing L. Further, the sizes increase with increasing concentration of defects p_d for $a = \infty$ and $a = 3.5$. For the crossover region at $a = 3.0$ we see that the sizes approximately come together to one value for all p_d. Decreasing a further leads to a change in the behavior and the cluster sizes decrease with increasing p_d. Unfortunately, we have no good explanation for this behavior at this point, but it is definitely worth it to look at this phenomenon in more detail.

Contrarily to the nice behavior of $\overline{C}$, we do not see a comprehensive picture in the data points for $\hat{C}$ which are shown in Figure A.9. By dividing the data with $L^{2.5}$ we see a more or less constant behavior for all p_d and a but the spread of the data suggests that any fit procedure would fail here. Probably, this is due to a rather small number if disorder realizations $N_c = 1000$.

(a) $a = \infty$.

(b) $a = 3.5$.

(c) $a = 3.0$.

(d) $a = 2.5$.

(e) $a = 2.0$.

(f) $a = 1.5$.

p_d							
○ 0.05	□ 0.1	▽ 0.15	△ 0.2	◇ 0.25	◁ 0.3	▷ 0.35	⬠ 0.4

Figure A.8: The dependence of the mean stochastic cluster sizes $\overline{C}$ on L for all parameter tuples (a, p_d) near the finite-size critical temperatures of $\partial_\beta(\ln|m|)$.
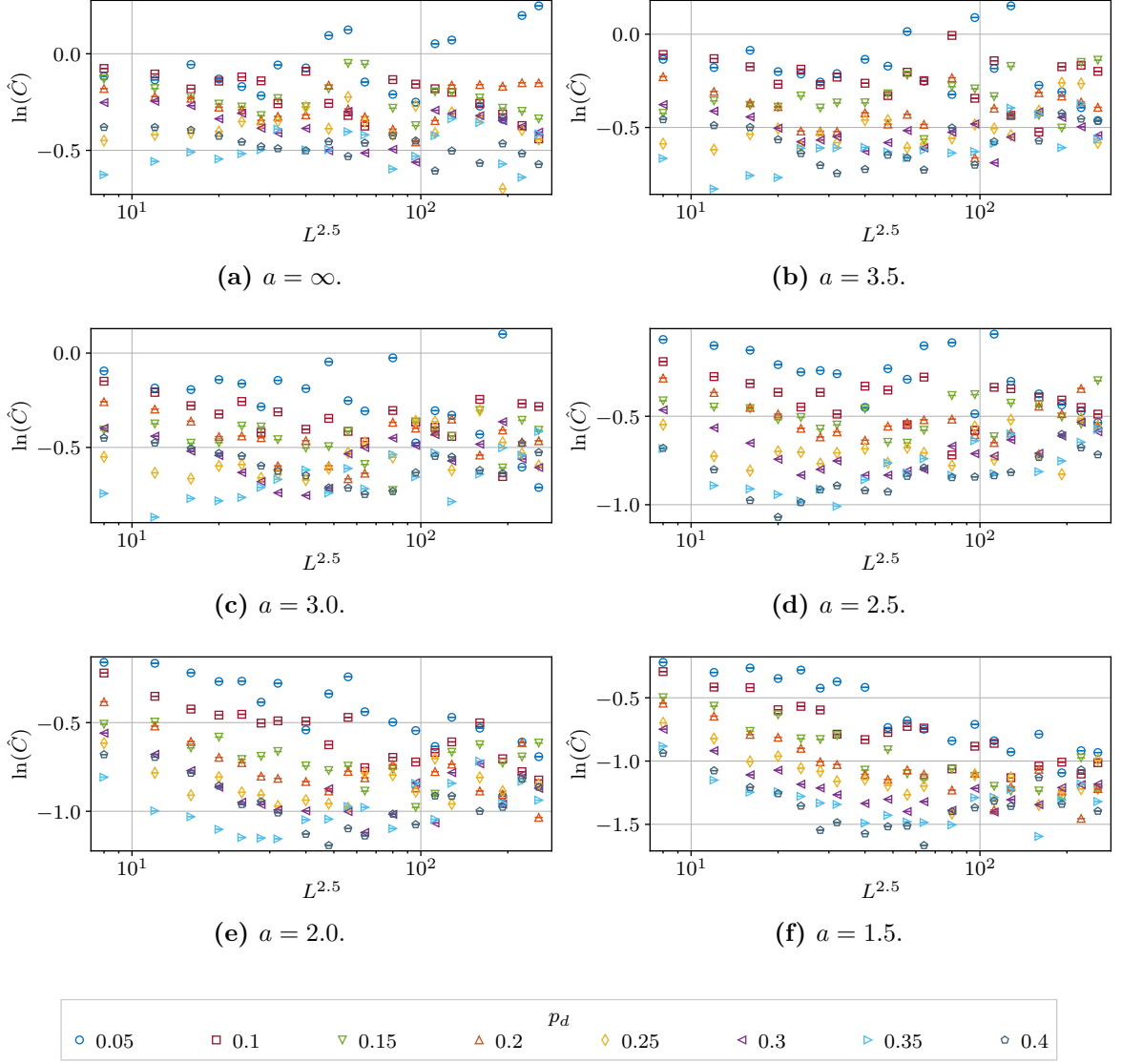
Figure A.9: The dependence of the maximum stochastic cluster sizes $\hat{C}$ on L for all parameter tuples (a, p_d) near the finite-size critical temperatures of $\partial_\beta(\ln|m|)$.

A.4 Implementation details

A.4.1 Simulation details

All simulations for this work were run on the local computing cluster at the Max Planck Institute for Mathematics in the Sciences in Leipzig and at the Max Planck Computing and Data Facility located in Garching. The average CPU frequency from all used CPUs was about 2.4 GHz. With this average speed the total time spend on the simulation process was about 1800 CPU-years. This is a huge number, but after taking into account all considered parameter tuples $(a, p_d, L, \beta_{\mathrm{sim}})$ and the $N_c = 1000$ realizations for each them, the number becomes clear. Putted into other words, we usually had a parallelization of factor 1000 and in this case the "physical" computation time boils down to 1.8 years. In order to get an insight in the distribution of the computing time, we provide the time fractions used for different correlation exponents a, the concentrations of defects p_d and the lattice sizes L in

Figure A.10. We see that the times are more or less equally distributed with respect to the studied concentrations of defects p_d with a minor increase for larger p_d. Nearly half of the time was spent on the two strongest correlation exponents $a = 2.0$ and $a = 1.5$. Both tendencies are not surprising, since we usually used more simulation temperatures for larger concentrations and stronger correlations due to a wider spread in the critical temperatures for the individual disorder realizations. Finally, the three largest lattices sizes $L =$ 192, 224, 256 used more than three quarters of the total time. It is a direct consequence of the computation time being roughly proportional to the volume of the lattice $V = L^d$. Moreover, we added more simulation temperatures for $L = 256$ in order to be able to use the temperature scaling analysis.

All simulated temperatures are summarized in Figure A.11. We omitted the preparation temperatures for which simulations up to $L = 48$ were performed. See Section 4.1 for a full description of the simulation process. The total amount of the simulated data in compressed state is about 6.6 TB. We stored the whole time series for each simulation run to be able to use reweighting techniques and other tools directly on the unprocessed observables.

(a) Parameter a.　　　　**(b)** Parameter p_d.　　　　**(c)** Parameter L.
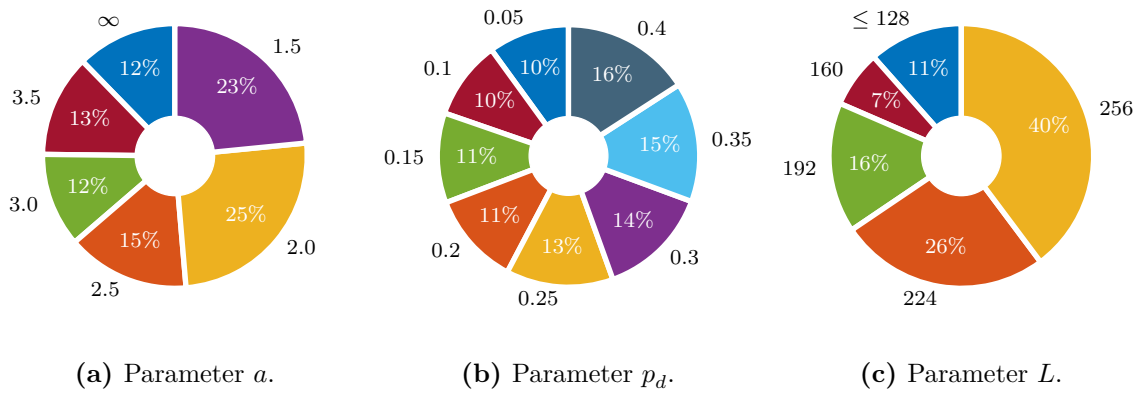
Figure A.10: Total computation time fractions with respect to various parameters. Note, that the number of simulated temperatures is not reflected in these plots.

A.4.2 Code

We would like to provide the julia code which was used for the simulations in this work. It can be found in [@Git21]. Even though the repository can be in a more recent state, the code presented here can be found by checking out the tag `phd_thesis`. The original code was organized in modules but to keep it as simple as possible, the presented code is organized in separate files and does not use any modules. As is common in julia, the implemented functions are preceded with a documentation string. In the syntax highlighting scheme used below they are colored orange. Listings A.1 to A.3 provide the periphery needed for the simulation process. In Listing A.4, the Ising model is defined and finally in Listing A.5 we show an example usage of the presented code.

Our experience with the julia implementation and usage on a large computation cluster was very satisfying. There were some minor difficulties from time to time, but the general case was a fluently and fast working code. A big advantage of the language was the mixing between the simulation code, the analysis code and the plotting code.
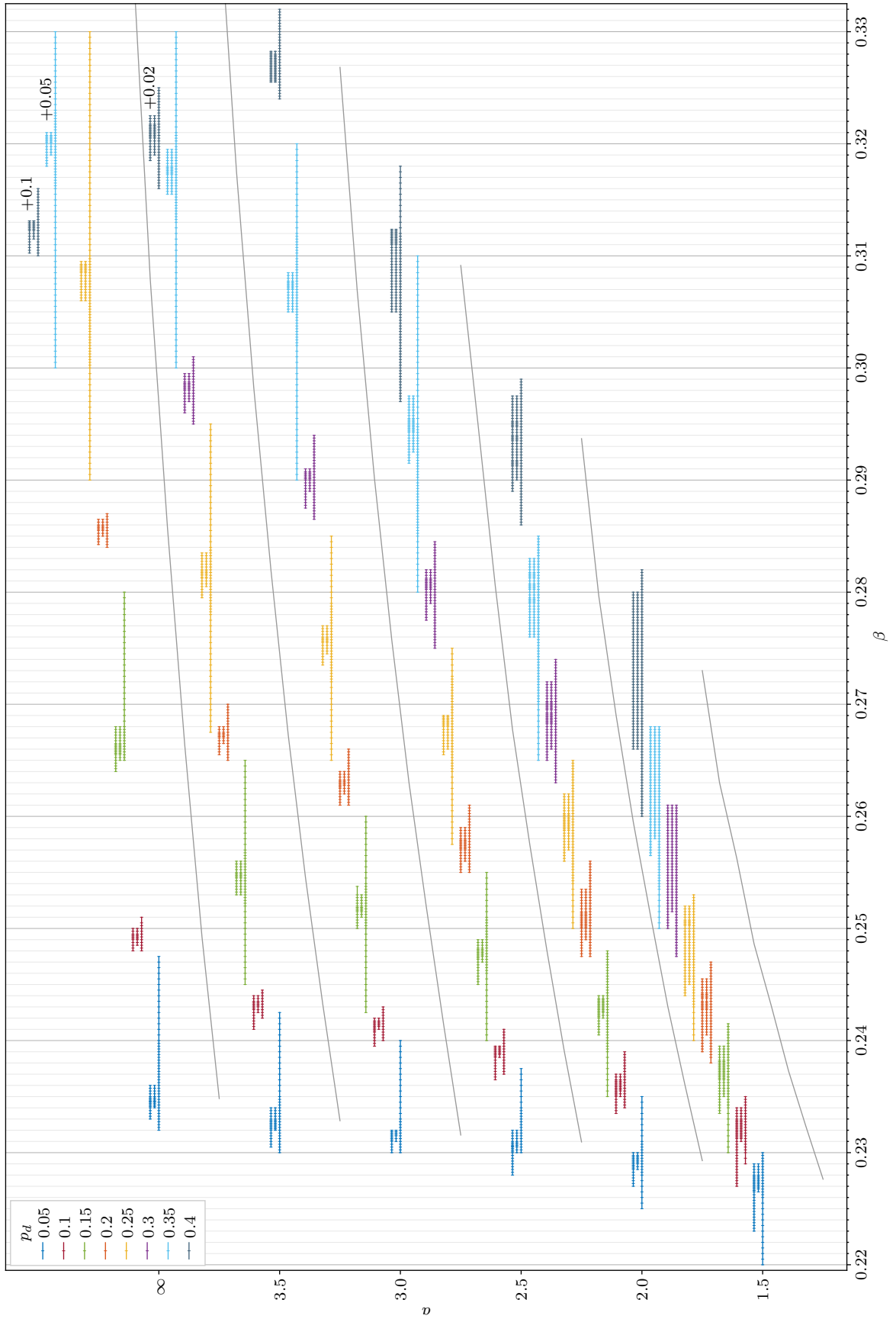
Figure A.11: Simulated temperatures for all parameter tuples (a, p_d, L). For each a and p_d there are three rows of temperatures. The bottom row corresponds to lattice sizes $L \leq 96$, the middle row is for $112 \leq L \leq 224$ and finally the top row is for $L = 256$. For $a = \infty$ and 3.5 the largest concentrations are shifted to the left to fit better into the plot (the amount is annotated). The gray lines separate different a values.

Listing A.1: `lattice_utils.jl` Contains utilities needed and useful for working with lattices. Defines the forward and backward indexing by applying boundary conditions.

```julia
using Colors
using Crayons
using Formatting

abstract type LatticeBC end
abstract type LinearBC <: LatticeBC end

struct PeriodicBC <: LinearBC end
struct APeriodicBC <: LinearBC end
struct FreeBC <: LinearBC end

@inline apply_bc(::PeriodicBC, x) = x
@inline apply_bc(::APeriodicBC, x) = -x
@inline apply_bc(::FreeBC, x) = zero(x)

"""
    display_lattice(Λ::AbstractArray [, prepare]; kwargs...)

Prints a 1, 2 or 3 dimentional array where each diffenret value gets a unique background color.

# Arguments
- `prepare::Function=x->"\$(x)"`: apply on each array element before printing, return something printable
- `title::String=""`: optional title above the array output
- `minwidth::Int = 2`: minimal width (number of characters) for each array element
"""
function display_lattice(Λ::AbstractArray, prepare::Function = x -> "$(x)"; title::String = "", minwidth::Int = 2)
  L = size(Λ)
  width = max(maximum(length.(prepare.(Λ))), minwidth - 1) + 1
  unique_species = sort(unique(prepare.(Λ)))
  colors_raw = distinguishable_colors(length(unique_species);lchoices = range(60; stop = 100, length = 15))

  color_dict = Dict(unique_species[i] => reinterpret(UInt32, convert(RGB24, colors_raw[i])) for i in 1:length(
        ↪ unique_species))
  fmt = "%$(width)s"
  println(typeof(Λ))
  title ≠ "" && println(title)
  if ndims(Λ) == 1
    for i in 1:L[1]
      print(Crayon(background = color_dict[prepare(Λ[i])]), sprintf1(fmt, prepare(Λ[i])))
      print(Crayon(reset = true), "\n")
    end
  elseif ndims(Λ) == 2
    for i in 1:L[1]
      for j in 1:L[2]
        print(Crayon(background = color_dict[prepare(Λ[i,j])]), sprintf1(fmt, prepare(Λ[i,j])))
      end
      print(Crayon(reset = true), "\n")
    end
  elseif ndims(Λ) == 3
    for k in 1:L[1]
      println("level $k")
      for i in 1:L[2]
        for j in 1:L[3]
          print(Crayon(background = color_dict[prepare(Λ[i,j,k])]), sprintf1(fmt, prepare(Λ[i,j,k])))
        end
        print(Crayon(reset = true), "\n")
      end
      print(Crayon(reset = true), "\n")
    end
  else
    println("display_lattice not defined for ndims = $(ndims(Λ))")
  end
  print("\n")
end

"""
unit(dims, dir::Integer)

Returns an Array as a unit vector in direction `dir` in `dims` dimentions.
`dims` can be an `Integer` or an `AbstractArray`
"""
unit(dims::Integer, dir::Integer) = [dir == i ? 1 : 0 for i ∈ 1:dims]
unit(Λ::AbstractArray, dir::Integer) = unit(ndims(Λ), dir)

"""
    neighbor_back(Λ::AbstractArray, i, dir, bc = x -> x)

Returns the next nearest neigbor of site `i` on a lattice `Λ` backward in direction `dir`.
When the element is at boundary, applies `bc` to it.
"""
@generated function neighbor_back(Λ::AbstractArray{T,N}, i, dir, bc = PeriodicBC()) where {T,N}
  quote
    $(Expr(:meta, :inline))
    @inbounds begin
      if i[dir] == 1
        return apply_bc(bc, Λ[Base.Cartesian.@ncall $N CartesianIndex d -> (d ≠ dir ? i[d] : size(Λ, d))])
      else
        return Λ[Base.Cartesian.@ncall $N CartesianIndex d -> (d ≠ dir ? i[d] : i[d] - 1)]
      end
    end
  end
end

"""
    neighbor_for(Λ::AbstractArray, i, dir, bc = x -> x)

Returns the next nearest neigbor of site `i` on a lattice `Λ` forward in direction `dir`.
When the element is at boundary, applies `bc` to it.
"""
@generated function neighbor_for(Λ::AbstractArray{T,N}, i, dir, bc = PeriodicBC()) where {T,N}
  quote
```

```
102        $(Expr(:meta, :inline))
103        @inbounds begin
104          if i[dir] == size(Λ, dir)
105            return apply_bc(bc, Λ[Base.Cartesian.@ncall $N CartesianIndex d -> (d ≠ dir ? i[d] : 1)])
106          else
107            return Λ[Base.Cartesian.@ncall $N CartesianIndex d -> (d ≠ dir ? i[d] : i[d] + 1)]
108          end
109        end
110      end
111    end
112
113    """
114        neighbor_ind_back(Λ::AbstractArray, i, dir)
115
116    Returns the `CartesianIndex` of the next nearest neigbor of site `i` on a lattice `Λ` backward in direction `dir`.
117    """
118    @generated function neighbor_ind_back(Λ::AbstractArray{T,N}, i, dir) where {T,N}
119      quote
120        $(Expr(:meta, :inline))
121        @inbounds begin
122          return Base.Cartesian.@ncall $N CartesianIndex d -> (d ≠ dir ? i[d] : (i[dir] == 1 ? size(Λ, d) : i[d] - 1))
123        end
124      end
125    end
126
127    """
128        neighbor_ind_for(Λ::AbstractArray, i, dir)
129
130    Returns the `CartesianIndex` of the next nearest neigbor of site `i` on a lattice `Λ` forward in direction `dir`.
131    """
132    @generated function neighbor_ind_for(Λ::AbstractArray{T,N}, i, dir) where {T,N}
133      quote
134        $(Expr(:meta, :inline))
135        @inbounds begin
136          return Base.Cartesian.@ncall $N CartesianIndex d -> (d ≠ dir ? i[d] : (i[dir] == size(Λ, d) ? 1 : i[d] + 1))
137        end
138      end
139    end
```

Listing A.2: `hoshen_kopelman_clustering.jl` Implements the Hoshen-Kopelman clustering algorithm [HK76] for arbitrary dimensions and different bond conditions functions.

```julia
"""
    hk_find!(x::Int, labels::Array{Int,1})

Finds the proper label for the culster number `x` in `labels`
"""
@inline function hk_find!(x::Int, labels::Array{Int,1})
  @inbounds while labels[x] ≠ x
    p = labels[x]
    labels[x] = labels[p]
    x = p
  end
  return x
end

"""
    hk_union!(x, y, labels)

Unite cluster labels `x` and `y` in `labels`
"""
hk_union!(x, y, labels) = @inbounds labels[hk_find!(x, labels)] = hk_find!(y, labels)

"""
    hk_cluster!(Λ::Array{T, N}, Γ::Array{Int, N}, labels::Array{Int,1}, bc::NTuple{N, Function}, bond_condition::Function ,
        ↪  empty_site::T = zero(T))

Clusterize the lattice `Λ` and writes the cluster labels to `Γ`, the proper labels to `labels` and the maximum label
        ↪ counter to `max_label`.

`bond_condition` is a function which takes `(x,y,i,d)` as arguments and returns a bool.
`x` and `y` are the values on the neighboring sites,`i` is the index of `x` and `d` is the direction of the bond.
`bc` is a tuple of boundary conditions for each direction.
`empty_site` describes which sites to skip (empty).
"""
@generated function hk_cluster!(Λ::Array{T,N}, Γ::Array{Int,N}, labels::Array{Int,1}, bc::NTuple{N,LinearBC},
        ↪ bond_condition::Function, empty_site::T = zero(T)) where {T,N}
  return quote
    @inbounds begin
      for i ∈ 1:length(Γ)
        Γ[i] = 0
        labels[i] = i
      end
      max_label = 0
      for i ∈ CartesianIndices(size(Γ))
        Λ[i] ≠ empty_site || continue
        Base.Cartesian.@nexprs $N d -> (begin
          nn = neighbor_ind_for(Γ, i, d)
          if Γ[i] == 0
            if bond_condition(Λ[i], (nn[d] == 1 ? apply_bc(bc[d], Λ[nn]) : Λ[nn]), i, d)
              if Γ[nn] == 0
                Γ[i] = Γ[nn] = max_label += 1
              else
                Γ[i] = Γ[nn]
              end
            else
              Γ[i] = max_label += 1
            end
          else
            if bond_condition(Λ[i], (nn[d] == 1 ? apply_bc(bc[d], Λ[nn]) : Λ[nn]), i, d)
              if Γ[nn] == 0
                Γ[nn] = Γ[i]
              else
                hk_union!(Γ[i], Γ[nn], labels)
              end
            end
          end
        end)
      end
      return max_label
    end
  end
end

"""
    hk_relabel!(Γ::Array{T, N}, old_labels::Array{Int}, max_label::Int)

Relabels the cluster lattice `Γ` with subsequent labels and returns the number of clusters.
"""
function hk_relabel!(Γ::Array{T,N}, old_labels::Array{Int}, max_label::Int) where {T,N}
  label = 0
  labels = fill(0, max_label)

  @inbounds for i ∈ 1:length(Γ)
    Γ[i] ≠ 0 || continue
    current = hk_find!(Γ[i], old_labels)
    if labels[current] == 0
      labels[current] = label += 1
    end
    Γ[i] = labels[current]
  end
  return label
end
```

Listing A.3: `disorder_generator.jl` Implements the long-range disorder generation with the Fourier Filter Method [Mak+95; Zie+17]. This implementation was not used in the present work, instead the C++ implementation from Ref. [Zie+17] was used as a shared library.

```julia
using Statistics
using StatsBase
using LinearAlgebra
using FastTransforms
using Distributions
using Random

periodic_dist(x, L) = x ≤ L / 2 ? x : L - x

"""
    generate_corr_matrix(dims::Tuple, C::Function; T::Type = Float64)

Calculate the function `C` for each distance `r` and returns an array where each C(r) is stored.
The distnace `r` is measured from upper left corner and implies periodic boundary conditions.

# Arguments:
- `dims::Tuple`: dimensions of the desired lattice
- `C::Function`: desired correlation function `C(r)`
- `T::Type = Float64`: type of the retured array
"""
function generate_corr_matrix(dims::Tuple, C::Function; T::Type = Float64)
  Λ = Array{T}(undef, dims)
  fill_periodic_distances!(Λ, C)
  return Λ
end

"""
    fill_periodic_distances!(Λ::AbstractArray, C::Function)

Helper function for the `generate_corr_matrix` function.
The type of `Λ` is known on call and therefore can this inner function works faster.

# Arguments:
- `Λ::AbstractArray`: array to save the `C(r)` to
- `C::Function`: desired correlation function `C(r)`
"""
function fill_periodic_distances!(Λ::AbstractArray, C::Function)
  for i ∈ CartesianIndices(Λ)
    r = norm(periodic_dist.(Tuple(i) .- 1, size(Λ)))
    Λ[i] = C(r)
  end
end

"""
    generate_continuous_disorder(dims::Tuple, S::AbstractArray)

Produces an array with dimensions `dims` with correlated disorder where the correlation follows the function `C(r)`

# Arguments:
- `dims::Tuple`: dimensions of the desired lattice
- `C::Function`: desired correlation function `C(r)`
- `RNG = Random.MersenneTwister(1)`: a random number generator for the continuous disorder
"""
function generate_continuous_disorder(dims::Tuple, S::AbstractArray, RNG)
  φq = sqrt.(max.(S, 0)) .* rand.(RNG, Normal(0, √(2 * prod(dims)))) # 2V = 2prod(dims) is used because the random numbers
                                                                     # ↪ are produced only in real space
  φ = real.(ifft(φq))
  return φ
end

"""
    generate_spectral_density(dims::Tuple, C::Function)

Produces a spectral density array with dimensions `dims` of the array with `C(r)` entries

# Arguments:
- `dims::Tuple`: dimensions of the desired lattice
- `C::Function`: desired correlation function `C(r)`
"""
generate_spectral_density(dims::Tuple, C::Function) = real.(fft(generate_corr_matrix(dims, C)))

"""
    transform_to_discrete_disorder(Λ::AbstractArray, p::Number; T = Int8(1), F = Int8(0))

Produces a truncated array similar to `Λ` but only with `T` and `F` values.
The concentration of `T` is given through `p`.

# Arguments:
- `Λ::AbstractArray`: expect an array with continuous correlated numbers
- `p::Number`: concentration of `T` values
- `T = Int8(1)`: values with concentration `p` to fill into the returned array
- `F = Int8(0)`: values with concentration `1 - p` to fill into the returned array
- `RNG = Random.MersenneTwister(1)`: a random number generator for the continuous disorder
"""
transform_to_discrete_disorder(Λ::AbstractArray, p::Number; T = Int8(1), F = Int8(0)) = [i ≤ quantile(Normal(0, 1), p) ? T
        ↪ : F for i ∈ Λ]

function generate_discrete_correlated_disorder(dims::Tuple; p::Number = 0.5, a = 1.0, C = (r, a) -> (1 + r^2)^(-a / 2), T
        ↪ = Int8(1), F = Int8(0), RNG = Random.MersenneTwister(1))
  S = generate_spectral_density(dims, r -> C(r, a))
  Λc = generate_continuous_disorder(dims, S, RNG)
  Λd = transform_to_discrete_disorder(Λc, p; T, F)
  return Λd
end
```

Listing A.4: `ising_model.jl` Implementation of the Ising model and the Swendsen-Wang multiple-cluster update algorithm [SW87]. Additionally, the functions for the calculation of observables, and higher-level functions for generating long-range correlated and uncorrelated disordered lattices for the Ising model and a full simulation run including the saving process are provided.

```julia
using Random
using JLD2
using FileIO
using LinearAlgebra
using StatsBase: counts, weights

include("lattice_utils.jl")
include("hoshen_kopelman_clustering.jl")
include("disorder_generator.jl")

mutable struct IsingModel{T,N,F <: NTuple{N,LinearBC},TJ <: Number,Tβ <: Number}
  Λ::Array{T,N}
  bc::F
  empty_site::T
  Nempty::Int
  V::Int
  J::TJ
  β::Tβ
  Γ::Array{Int,N}
  labels::Array{Int,1}
  max_label::Int
  FT1::Array{Complex{Float64},N}
  RNG::Random.MersenneTwister
end
IsingModel(Λ::Array{T,N}, bc::F, seed::Int = 0) where {T,N,F} = IsingModel(Λ, bc, zero(T), count(i -> i == zero(T), Λ),
      ↪ prod(size(Λ)), 1, 0.1, similar(Λ, Int), Array{Int}(undef, length(Λ)), 1, calc_FT_mode(Λ, unit(Λ, 1)), Random.
      ↪ MersenneTwister(seed))

"""
    sw_update!(M::IsingModel{T}, empty_site::T = zero(T))

Swendsen-Wang update of the model `M`
"""
function sw_update!(M::IsingModel{T}, empty_site::T = zero(T); p_bond = 0.0) where {T}
  M.max_label = hk_cluster!(M.Λ, M.Γ, M.labels, M.bc, (x, y, i, d) -> (x == y && rand(M.RNG) < p_bond), empty_site)
  M.max_label = hk_relabel!(M.Γ, M.labels, M.max_label)
  new_values = rand(M.RNG, Array{T}([-1,1]), M.max_label)

  @inbounds for i ∈ eachindex(M.Λ)
    M.Λ[i] == empty_site || (M.Λ[i] = new_values[M.Γ[i]])
  end
  return nothing
end

"Energy of the Ising Model `M`"
function energy(M::IsingModel)
  s::Int = 0
  @inbounds @simd for i ∈ CartesianIndices(size(M.Λ))
    @inbounds for d ∈ 1:ndims(M.Λ)
      s += M.Λ[i] * neighbor_for(M.Λ, i, d, M.bc[d])
    end
  end
  return -M.J * s
end

"Magnetization of the Ising Model `M`"
function magnetization(M::IsingModel)
  s::Int = 0
  @inbounds @simd for i ∈ eachindex(M.Λ)
    s += M.Λ[i]
  end
  return s
end

"Mean size of the stohastic clusters of the Ising Model `M`"
stohastic_cluster_mean(M::IsingModel) = (M.V - M.Nempty) / M.max_label
"Maximal size of the stohastic clusters of the Ising Model `M`"
stohastic_cluster_max(M::IsingModel) = maximum(counts(M.Γ, 1:M.max_label))

"Maximal size of the geometric clusters of the Ising Model `M`"
function geometric_cluster_max(M::IsingModel)
  M.max_label = hk_cluster!(M.Λ, M.Γ, M.labels, M.bc, (x, y, i, d) -> (x == y), M.empty_site)
  M.max_label = hk_relabel!(M.Γ, M.labels, M.max_label)
  return stohastic_cluster_max(M::IsingModel)
end
### call only AFTER!!! geometric_cluster_max, because the latter generates the clusters
"Mean size of the geometric clusters of the Ising Model `M`"
geometric_cluster_mean(M::IsingModel) = stohastic_cluster_mean(M::IsingModel)

"Precalcultion of the Fourier transformed exponentials with vector `k`"
calc_FT_mode(Λ::AbstractArray, k::Vector) = return reshape([exp(im * dot([Tuple(CartesianIndices(Λ)[i])...] .- 1, k .* (2π
      ↪ ./ size(Λ)))) for i ∈ eachindex(Λ)], size(Λ)...)

"Fourier mode in (1,0,...) direction for the Ising Model `M`"
correlation_FT1_mode(M::IsingModel) = abs(sum(M.Λ .* M.FT1))^2

alias_to_observable = Dict{Symbol,Function}(
:E => energy,
:M => magnetization,
:Csmean => stohastic_cluster_mean,
:Csmax => stohastic_cluster_max,
:Cgmean => geometric_cluster_mean,
:Cgmax => geometric_cluster_max,
:FT1 => correlation_FT1_mode,
)
observable_to_alias = Dict{Function,Symbol}(reverse(p) for p ∈ pairs(alias_to_observable))

"Initialize the `NamedTuple` for the observables given in `aliases` with `Nmeas` number of measurements"
```

```julia
 96  function init_observables(model::IsingModel, aliases::Array{Symbol}, Nmeas::Int)
 97    return NamedTuple{Tuple(aliases)}(Array{typeof(alias_to_observable[i](model))}(undef, Nmeas) for i ∈ aliases)
 98  end
 99
100  "Calculate observables given as Array of `aliases` and store in `D` at row `m`"
101  function calc_observables!(M::IsingModel, D::NamedTuple, m::Int, aliases::Array{Symbol})
102    for a ∈ aliases
103      D[a][m] = alias_to_observable[a](M)
104    end
105  end
106
107  """
108      generate_defected_ising_lattice(L, dim, seed, pd, a;T::Type=Int)
109  Generate a (correlated) defected lattice of size `L^dim` with correlation exponent `a`, defect concentration `pd`,
          ↪ gaussian width `sigma2`. Potentially convert elements to type `T`.
110
111  """
112  function generate_defected_ising_lattice(L, dim, seed, pd, a; T::Type = Int,)
113    RNG = Random.MersenneTwister()
114    if pd == 0.0
115      println("return pure ising lattice")
116      return reshape(convert.(T, rand(RNG, [-1,1], L^dim)), ntuple(d -> L, dim))
117    end
118
119    if a == Inf
120      println("return uncorrelated ising lattice")
121      Λ = reshape(convert.(T, rand(RNG, [-1,1], L^dim)), ntuple(d -> L, dim))
122      for i ∈ eachindex(Λ)
123        rand(RNG) < pd && (Λ[i] = zero(T))
124      end
125      return Λ
126    end
127
128    println("return correlated ising lattice")
129
130    Λ = generate_discrete_correlated_disorder(ntuple(d -> L, dim); p = 1 - pd, a, RNG)
131    for i ∈ eachindex(Λ)
132      if isapprox(Λ[i], 0.0)
133        Λ[i] = 0.0
134      else
135        rand(RNG) > 0.5 ? Λ[i] = 1.0 : Λ[i] = -1.0
136      end
137    end
138    return Λ
139  end
140
141  """
142    run_simulation(ising::IsingModel; kwargs...)
143
144  Performs a series of simulations at each temperature from `β_array`.
145  Start with a prethermalization and thermalized betwwen each temperature.
146
147  The saved result consists of:
148  - `data`: the measured observables as `Array{NamedTuple}`
149  - `ising`: the final state of the model
150  - `config`: the parameters passed to `run_simulation` function
151  - `total_time`: elapsed time
152  A NamedTuple `(;data, config, total_time, cfg_params)` is returned.
153
154  ### Arguments
155  - `β_array = 0.2:0.1:0.5`: the β range for the simulation
156  - `Ntherm::Int = 0`: number of thermalization sweeps before each β
157  - `Nmeas::Int = 1`: number of measurements at each β
158  - `Nbetween::Int = 1`: number of sweeps between two subsequent measurements (1 means measure after each sweep)
159  - `obs_aliases::Array{Symbol} = [:E, :M, :Csmax, :Csmean, :Cgmax, :Cgmean, :FT1]`: observables to measure. Possible
          ↪ aliases are: $(keys(alias_to_observable)). `Cgmax` **must** come before `Cgmean` and is needed for the latter.
160  - `output_dir = "./observables/"`: directory for the output
161  - `name_prefix = "ising_"`: prefix for the generated name
162  - `name_suffix = "_raw_observables"`: suffix for the generated name
163  - `save_data = true`: whether to save the data
164  - `cfg_params = (;)`: parameters of the cfg which was used (provided by the user)
165  - `verbose = 0`: defined the level of verbosity (0-2)
166  """
167  function run_simulation(
168    ising::IsingModel;
169    β_array = 0.2:0.1:0.5,
170    Ntherm::Int = 0,
171    Npretherm::Int = 0,
172    Nmeas::Int = 0,
173    Nbetween::Int = 1,
174    obs_aliases::Array{Symbol} = [:E, :M, :Csmax, :Csmean, :Cgmax, :Cgmean, :FT1],
175    output_dir::String = "./observables/",
176    name_prefix::String = "ising_",
177    name_suffix::String = "_raw_observables",
178    save_data::Bool = true,
179    cfg_params::NamedTuple = NamedTuple(),
180    verbose::Int = 0,
181    compress = true,
182    )
183    ### preparation
184    L = size(ising.Λ, 1)
185    dim = length(size(ising.Λ))
186
187    ## generate names and directories
188    save_data && mkpath(output_dir)
189    result_file = "$(output_dir)/$(name_prefix)d$(dim)_L$(L)$(name_suffix).jld2"
190
191    time1 = time_ns()
192
193    config = (β_array = β_array, Ntherm = Ntherm, Nmeas = Nmeas, Nbetween = Nbetween, Npretherm = Npretherm, obs_aliases =
          ↪ obs_aliases, verbose = verbose)
194
195    ### initialization
196    ising.β = β_array[1]
197    p_bond = 1 - exp(-2 * β_array[1] * ising.J)
198    data = Array{NamedTuple}(undef, 0)
199
```

```julia
200    ### pre-thermalization
201    verbose ≥ 1 && println("start simulations")
202    verbose ≥ 2 && println(" start $Npretherm pre-thermalization sweeps")
203    for sweep ∈ 1:Npretherm; sw_update!(ising; p_bond = p_bond) end
204
205    for β ∈ β_array
206      verbose ≥ 1 && println(" start simulation at β = $β")
207      ising.β = β
208      p_bond = 1 - exp(-2 * β * ising.J)
209
210      data_at_β = init_observables(ising, obs_aliases, Nmeas)
211      ### thermalization
212      verbose ≥ 2 && println(" start $Ntherm thermalization sweeps")
213      for sweep ∈ 1:Ntherm
214        sw_update!(ising; p_bond = p_bond)
215      end
216
217      ### measurements
218      verbose ≥ 2 && println(" start $Nmeas measurements")
219      for meas ∈ 1:Nmeas
220        for sweep ∈ 1:Nbetween
221          sw_update!(ising; p_bond = p_bond)
222        end
223        calc_observables!(ising, data_at_β, meas, obs_aliases)
224      end
225      push!(data, merge((β = β, L = size(ising.Λ)), data_at_β))
226    end
227    verbose ≥ 1 && println("end simulations")
228
229    time2 = time_ns()
230
231    total_time = (meas_time = (time2 - time1) / 1.0e9)
232
233    if save_data
234      verbose ≥ 1 && println("saving data to $(result_file)")
235      jldopen(result_file, true, true, true, IOStream; compress = compress) do file
236        file["data"] = data
237        file["config"] = config
238        file["total_time"] = total_time
239        file["cfg_params"] = cfg_params
240      end
241      verbose ≥ 1 && println("saving data finished")
242    end
243    return (;data, config, total_time, cfg_params)
244  end
```

Listing A.5: `test_runs.jl` Example usage of the Ising model and a comparison of the measured data to exact data for a two-dimensional pure Ising model.

```julia
1    include("ising_model.jl")
2
3    using QuadGK
4
5    ### set parameters
6    dim = 2
7    a = 2.0
8    pd = 0.0
9    L = 32
10   seed = 1
11
12   V = L^dim
13
14   ### temperautre range
15   β_array = 0.4:0.001:0.5
16
17   ### init Ising model and run simulaiton
18   IM = IsingModel(generate_defected_ising_lattice(L, dim, seed, pd, a), ntuple(d -> PeriodicBC(), dim), seed)
19
20   D = run_simulation(IM; β_array = β_array, Npretherm = 1000, Ntherm = 100, Nmeas = 1000, save_data = true, cfg_params = (;
       ↪ L, a, pd, seed, dim), verbose = 1)
21
22   ### calcualte observables
23   e_mean = [mean(d.E) / V for d ∈ D.data]
24   m_mean = [mean(abs.(d.M)) / V for d ∈ D.data]
25   χ_mean = [(mean(d.M.^2) - mean(abs.(d.M)).^2) * d.β / V for d ∈ D.data]
26
27   ### exact results for 2d
28   K(β; J = 1) = 1 / (sinh(2 * β * J) * sinh(2β * J))
29   Intθ(β; J = 1) = quadgk(θ -> 1 / sqrt(1 - 4 * K(β;J = J) * (1 + K(β;J = J))^-2 * sin(θ)^2), 0, π / 2; rtol = 1e-8)[1]
30
31   u∞(β; J = 1) = -J * coth(2β * J) * (1 + 2 / π * (2 * tanh(2β * J)^2 - 1) * Intθ(β; J = J))
32   m∞(β; J = 1) = β > log(1 + √2) / 2 / J ? (1 - sinh(2β * J)^(-4))^(1 / 8) : 0.0
33
34   ### plot results
35   using Plots
36
37   plot(β_array, e_mean, label = "e")
38   plot!(β_array, m_mean, label = "m")
39   plot!(β_array, u∞.(β_array), label = "e exact")
40   plot!(β_array, m∞.(β_array),label = "m exact", xlabel = "β", ylabel = "e, m")
41   plot!(twinx(), β_array, χ_mean, label = "χ", legend = :right, ylabel = "χ")
42
43   ### check correlated disorder
44   IM = IsingModel(generate_defected_ising_lattice(16, 2, 1, 0.2, Inf), ntuple(d -> PeriodicBC(), dim), seed)
45   display_lattice(IM.Λ)
46
47   IM = IsingModel(generate_defected_ising_lattice(16, 2, 1, 0.2, 2.0), ntuple(d -> PeriodicBC(), dim), seed)
48   display_lattice(IM.Λ)
49
50   IM = IsingModel(generate_defected_ising_lattice(16, 2, 1, 0.2, 1.0), ntuple(d -> PeriodicBC(), dim), seed)
51   display_lattice(IM.Λ)
```

References

[AD52]   T. W. Anderson and D. A. Darling. "Asymptotic theory of certain "goodness of fit" criteria based on stochastic processes." In: *Ann. Math. Statist.* 23.2 (1952), pp. 193–212. DOI: 10.1214/aoms/1177729437.

[Adl+90]   J. Adler, Y. Meir, A. Aharony, and A. B. Harris. "Series study of percolation moments in general dimension." In: *Phys. Rev. B* 41.13 (1990), pp. 9183–9206. DOI: 10.1103/PhysRevB.41.9183.

[AM05]   D. J. Amit and V. Martín-Mayor. *Field Theory, the Renormalization Group, and Critical Phenomena: Graphs to Computers.* 3rd ed. World Scientific, 2005. DOI: 10.1142/5715.

[Bal+97]   H. G. Ballesteros, L. A. Fernández, V. Martín-Mayor, A. M. Sudupe, G. Parisi, and J. J. Ruiz-Lorenzo. "Ising exponents in the two-dimensional site-diluted Ising model." In: *J. Phys. A: Math. Gen.* 30.24 (1997), p. 8379. DOI: 10.1088/0305-4470/30/24/006.

[Bal+98a] H. G. Ballesteros, L. A. Fernández, V. Martín-Mayor, A. Muñoz Sudupe, G. Parisi, and J. J. Ruiz-Lorenzo. "Critical exponents of the three-dimensional diluted Ising model." In: *Phys. Rev. B* 58.5 (1998), pp. 2740–2747. DOI: 10.1103/PhysRevB.58.2740.

[Bal+98b] H. G. Ballesteros, L. A. Fernández, V. Martín-Mayor, A. M. Sudupe, G. Parisi, and J. J. Ruiz-Lorenzo. "The four dimensional site-diluted Ising model: a finite-size scaling study." In: *Nucl. Phys. B* 512.3 (1998), pp. 681–701. DOI: 10.1016/S0550-3213(97)00797-9.

[Bel+95]   D. Belanger, J. Wang, Z. Slanič, S.-J. Han, R. Nicklow, M. Lui, C. Ramos, and D. Lederman. "Neutron scattering study of the random field Ising film $Fe_{0.5}Zn_{0.5}F_2$." In: *J. Magn. Magn. Mater.* 140-144 (1995), pp. 1549–1550. DOI: 10.1016/0304-8853(94)01353-5.

[Ber+04]   P. E. Berche, C. Chatelain, B. Berche, and W. Janke. "Bond dilution in the 3D Ising model: a Monte Carlo study." In: *Eur. Phys. J. B* 38.3 (2004), pp. 463–474. DOI: 10.1140/epjb/e2004-00141-x.

[Ber+05]   B. Berche, P.-E. Berche, C. Chatelain, and W. Janke. "Random Ising model in three dimensions: theory, experiment and simulation - a difficult coexistence." In: *Condensed Matter Physics* 8 (2005), pp 47–58.

[BF83]   O. F. d. A. Bonfim and I. P. Fittipaldi. "Bond and site diluted Ising-model systems: A unified treatment." In: *Physics Letters A* 98.4 (1983), pp. 199–202. DOI: 10.1016/0375-9601(83)90583-2.

[BFH01]   V. Blavats'ka, C. von Ferber, and Y. Holovatch. "Polymers in long-range-correlated disorder." In: *Phys. Rev. E* 64.4 (2001), p. 041102. DOI: 10.1103/PhysRevE.64.041102.

[Bir+83]   R. J. Birgeneau, R. A. Cowley, G. Shirane, H. Yoshizawa, D. P. Belanger, A. R. King, and V. Jaccarino. "Critical behavior of a site-diluted three-dimensional Ising magnet." In: *Phys. Rev. B* 27.11 (1983), pp. 6747–6753. DOI: 10.1103/PhysRevB.27.6747.

[Blö+96]   H. W. J. Blöte, J. R. Heringa, A. Hoogland, E. W. Meyer, and T. S. Smit. "Monte Carlo Renormalization of the 3D Ising Model: Analyticity and Convergence." In: *Phys. Rev. Lett.* 76.15 (1996), pp. 2613–2616. DOI: 10.1103/PhysRevLett.76.2613.

[Boc83]   N. Boccara. "Dilute Ising models: A simple theory." In: *Physics Letters A* 94.3 (1983), pp. 185–187. DOI: 10.1016/0375-9601(83)90379-1.

[BP18]   Y. Bar-Yam and S. P. Patil. "Renormalization of Sparse Disorder in the Ising Model." 2018. arXiv: 1805.12556 [cond-mat, physics:hep-th].

[BP99]   H. G. Ballesteros and G. Parisi. "Site-diluted three-dimensional Ising model with long-range correlated disorder." In: *Phys. Rev. B* 60.18 (1999), pp. 12912–12917. DOI: 10.1103/PhysRevB.60.12912.

[BRR85]   R. Badke, P. Reinicke, and V. Rittenberg. "The discrete cubic and chiral cubic spin systems in various dimensions and their large-N limits." In: *J. Phys. A: Math. Gen.* 18.4 (1985), pp. 653–660. DOI: 10.1088/0305-4470/18/4/014.

[Bug96]   E. A. Bugrii. "Solution of the 2D ising model on a triangular lattice by the method of auxiliary q-deformed Grassmann fields." In: *Theor Math Phys* 109.3 (1996), pp. 1590–1607. DOI: 10.1007/BF02073876.

[Cal+03]   P. Calabrese, V. Martín-Mayor, A. Pelissetto, and E. Vicari. "Three-dimensional randomly dilute Ising model: Monte Carlo results." In: *Phys. Rev. E* 68.3 (2003), p. 036136. DOI: 10.1103/PhysRevE.68.036136.

[Car+95]   S. Caracciolo, R. G. Edwards, S. J. Ferreira, A. Pelissetto, and A. D. Sokal. "Extrapolating Monte Carlo Simulations to Infinite Volume: Finite-Size Scaling at $\xi/L \gg 1$." In: *Phys. Rev. Lett.* 74.15 (1995), pp. 2969–2972. DOI: 10.1103/PhysRevLett.74.2969.

[Cha02]   H. Chamati. "Finite-size scaling in disordered systems." In: *Phys. Rev. E* 65.2 (2002). DOI: 10.1103/PhysRevE.65.026129.

[Cha14]   C. Chatelain. "Griffiths phase and critical behavior of the two-dimensional Potts models with long-range correlated disorder." In: *Phys. Rev. E* 89.3 (2014), p. 032105. DOI: 10.1103/PhysRevE.89.032105.

[Cha17]   C. Chatelain. "Infinite disorder and correlation fixed point in the Ising model with correlated disorder." In: *Eur. Phys. J.: Spec. Top.* 226.4 (2017), pp. 805–816. DOI: 10.1140/epjst/e2016-60332-9.

[Chr+20]   H. Christiansen, S. Majumder, M. Henkel, and W. Janke. "Aging in the Long-Range Ising Model." In: *Phys. Rev. Lett.* 125.18 (2020), p. 180601. DOI: `10.1103/PhysRevLett.125.180601`.

[CMO19]   A. Cappelli, L. Maffi, and S. Okuda. "Critical Ising model in varying dimension by conformal bootstrap." In: *J. High Energ. Phys.* 2019.1 (2019), p. 161. DOI: `10.1007/JHEP01(2019)161`.

[DD83]   V. S. Dotsenko and V. S. Dotsenko. "Critical behaviour of the phase transition in the 2D Ising model with impurities." In: *Adv. Phys.* 32.2 (1983), pp. 129–172. DOI: `10.1080/00018738300101541`.

[DM10]   A. Dembo and A. Montanari. "Ising models on locally tree-like graphs." In: *The Annals of Applied Probability* 20.2 (2010), pp. 565–592. DOI: `10.1214/09-AAP627`.

[Dou+18]   R. Douc, E. Moulines, P. Priouret, and P. Soulier. *Markov Chains.* Springer Series in Operations Research and Financial Engineering. Cham: Springer International Publishing, 2018. DOI: `10.1007/978-3-319-97704-1`.

[El+12]   S. El-Showk, M. F. Paulos, D. Poland, S. Rychkov, D. Simmons-Duffin, and A. Vichi. "Solving the 3D Ising model with the conformal bootstrap." In: *Phys. Rev. D* 86.2 (2012), p. 025022. DOI: `10.1103/PhysRevD.86.025022`.

[El+14]   S. El-Showk, M. F. Paulos, D. Poland, S. Rychkov, D. Simmons-Duffin, and A. Vichi. "Solving the 3d Ising Model with the Conformal Bootstrap II. c-Minimization and Precise Critical Exponents." In: *J. Stat. Phys.* 157.4 (2014), pp. 869–914. DOI: `10.1007/s10955-014-1042-7`.

[ET93]   B. Efron and R. Tibshirani. *An Introduction to the Bootstrap.* Monographs on statistics and applied probability 57. New York: Chapman & Hall, 1993. 436 pp. ISBN: 978-0-412-04231-7.

[EV29]   A. Einstein and G. S. Viereck. "What Life means to Albert Einstein." In: *The Saturday Evening Post* (1929), p. 117.

[FHY03]   R. Folk, Y. Holovatch, and T. Yavorskii. "Critical exponents of a three-dimensional weakly diluted quenched Ising model." In: *Phys.-Usp.* 46.2 (2003), p. 169. DOI: `10.1070/PU2003v046n02ABEH001077`.

[Fis69]   M. E. Fisher. "Rigorous Inequalities for Critical-Point Correlation Exponents." In: *Phys. Rev.* 180.2 (1969), pp. 594–600. DOI: `10.1103/PhysRev.180.594`.

[FM13]   N. G. Fytas and V. Martín-Mayor. "Universality in the Three-Dimensional Random-Field Ising Model." In: *Phys. Rev. Lett.* 110.22 (2013), p. 227201. DOI: `10.1103/PhysRevLett.110.227201`.

[FM16]   N. G. Fytas and V. Martín-Mayor. "Efficient numerical methods for the random-field Ising model: Finite-size scaling, reweighting extrapolation, and computation of response functions." In: *Phys. Rev. E* 93.6 (2016), p. 063308. DOI: `10.1103/PhysRevE.93.063308`.

[FS88]   A. M. Ferrenberg and R. H. Swendsen. "New Monte Carlo technique for studying phase transitions." In: *Phys. Rev. Lett.* 61.23 (1988), pp. 2635–2638. DOI: `10.1103/PhysRevLett.61.2635`.

[FT10]   N. G. Fytas and P. E. Theodorakis. "Universality in disordered systems: The case of the three-dimensional random-bond Ising model." In: *Phys. Rev. E* 82.6 (2010), p. 062101. DOI: `10.1103/PhysRevE.82.062101`.

[FV17]   S. Friedli and Y. Velenik. *Statistical mechanics of lattice systems: a concrete mathematical introduction.* Cambridge University Press, 2017. ISBN: 978-1-107-18482-4.

[FXL18]   A. M. Ferrenberg, J. Xu, and D. P. Landau. "Pushing the limits of Monte Carlo simulations for the three-dimensional Ising model." In: *Phys. Rev. E* 97.4 (2018), p. 043301. DOI: `10.1103/PhysRevE.97.043301`.

[Gar95]   C. Garrod. *Statistical Mechanics and Thermodynamics.* Oxford University Press, 1995. 642 pp. ISBN: 978-0-19-508523-5.

[Gri65]   R. B. Griffiths. "Thermodynamic Inequality Near the Critical Point for Ferromagnets and Fluids." In: *Phys. Rev. Lett.* 14.16 (1965), pp. 623–624. DOI: `10.1103/PhysRevLett.14.623`.

[GZ98]   R. Guida and J. Zinn-Justin. "Critical exponents of the N-vector model." In: *J. Phys. A: Math. Gen.* 31.40 (1998), p. 8103. DOI: `10.1088/0305-4470/31/40/006`.

[Har74]   A. B. Harris. "Effect of random defects on the critical behaviour of Ising models." In: *J. Phys. C: Solid State Phys.* 7.9 (1974), pp. 1671–1692. DOI: `10.1088/0022-3719/7/9/009`.

[Has+07] M. Hasenbusch, F. P. Toldin, A. Pelissetto, and E. Vicari. "The universality class of 3D site-diluted and bond-diluted Ising systems." In: *J. Stat. Mech.* 2007.02 (2007), P02016. DOI: `10.1088/1742-5468/2007/02/P02016`.

[Has10a] M. Hasenbusch. "Finite size scaling study of lattice models in the three-dimensional Ising universality class." In: *Phys. Rev. B* 82.17 (2010), p. 174433. DOI: `10.1103/PhysRevB.82.174433`.

[Has10b] M. Hasenbusch. "Universal amplitude ratios in the three-dimensional Ising universality class." In: *Phys. Rev. B* 82.17 (2010), p. 174434. DOI: `10.1103/PhysRevB.82.174434`.

[Hen99]   M. Henkel. *Conformal Invariance and Critical Phenomena.* Springer Berlin Heidelberg, 1999. DOI: `10.1007/978-3-662-03937-3`.

[Heu93]   H.-O. Heuer. "Critical crossover phenomena in disordered Ising systems." In: *J. Phys. A: Math. Gen.* 26.6 (1993), p. L333. DOI: `10.1088/0305-4470/26/6/007`.

[HJ93]   C. Holm and W. Janke. "Critical exponents of the classical three-dimensional Heisenberg model: A single-cluster Monte Carlo study." In: *Phys. Rev. B* 48.2 (1993), pp. 936–950. DOI: `10.1103/PhysRevB.48.936`.

[HK76]   J. Hoshen and R. Kopelman. "Percolation and cluster distribution. I. Cluster multiple labeling technique and critical concentration algorithm." In: *Phys. Rev. B* 14.8 (1976), pp. 3438–3445. DOI: 10.1103/PhysRevB.14.3438.

[HN89]   J. Honkonen and M. Y. Nalimov. "Crossover between field theories with short-range and long-range exchange or correlations." In: *J. Phys. A: Math. Gen.* 22.6 (1989), pp. 751–763. DOI: 10.1088/0305-4470/22/6/024.

[Hol07]   Y. Holovatch. *Order, Disorder and Criticality: Advanced Problems of Phase Transition Theory Volume 2*. World Scientific, 2007. DOI: 10.1142/6482.

[HPV99]   M. Hasenbusch, K. Pinn, and S. Vinti. "Critical exponents of the three-dimensional Ising universality class from finite-size scaling with standard and improved actions." In: *Phys. Rev. B* 59.17 (1999), pp. 11471–11483. DOI: 10.1103/PhysRevB.59.11471.

[HY98]   Y. Holovatch and T. Yavors'kii. "Critical Exponents of the Diluted Ising Model between Dimensions 2 and 4." In: *Journal of Statistical Physics* 92.5 (1998), pp. 785–808. DOI: 10.1023/A:1023032307964.

[IJ89]   H. F. Inman and E. L. B. Jr. "The overlapping coefficient as a measure of agreement between probability distributions and point estimation of the overlap of two normal densities." In: *Communications in Statistics - Theory and Methods* 18.10 (1989), pp. 3851–3874. DOI: 10.1080/03610928908830127.

[Isi25]   E. Ising. "Beitrag zur Theorie des Ferromagnetismus." In: *Z. Physik* 31.1 (1925), pp. 253–258. DOI: 10.1007/BF02980577.

[Iva+08]   D. Ivaneyko, B. Berche, Y. Holovatch, and J. Ilnytskyi. "On the universality class of the 3d Ising model with long-range correlated disorder." In: *Physica A* 387.18 (2008), pp. 4497–4512. DOI: 10.1016/j.physa.2008.03.034.

[Jan08]   W. Janke. "Monte Carlo methods in classical statistical physics." In: *Computational Many-Particle Physics*. Ed. by H. Fehske, R. Schneider, and A. Weiße. Lecture Notes in Physics 739. Berlin, Heidelberg: Springer, 2008, pp. 79–140. ISBN: 978-3-540-74685-0.

[Jan12]   W. Janke. "Monte Carlo simulations in statistical physics – From basic principles to advanced applications." In: *Order, Disorder and Criticality: Advanced Problems of Phase Transition Theory*. Ed. by Y. Holovatch. Singapore: World Scientific, 2012. ISBN: 978-981-4417-89-1.

[JH93]   W. Janke and C. Holm. "Finite-size scaling study of the three-dimensional classical Heisenberg model." In: *Physics Letters A* 173.1 (1993), pp. 8–12. DOI: 10.1016/0375-9601(93)90077-D.

[Jos67a]   B. D. Josephson. "Inequality for the specific heat: I. Derivation." In: *Proc. Phys. Soc.* 92.2 (1967), pp. 269–275. DOI: 10.1088/0370-1328/92/2/301.

[Jos67b]   B. D. Josephson. "Inequality for the specific heat: II. Application to critical phenomena." In: *Proc. Phys. Soc.* 92.2 (1967), pp. 276–284. DOI: 10.1088/0370-1328/92/2/302.

[JS98]   N. Jan and D. Stauffer. "Random site percolation in three dimensions." In: *Int. J. Mod. Phys. C* 09.02 (1998), pp. 341–347. DOI: 10.1142/S0129183198000261.

[Kis+04]   L. F. Kiss, D. Kaptás, J. Balogh, L. Bujdosó, T. Kemény, L. Vincze, and J. Gubicza. "Rigid magnetic foam-like behavior in ball-milled FeAl." In: *Phys. Rev. B* 70.1 (2004), p. 012408. DOI: 10.1103/PhysRevB.70.012408.

[KJ20]   S. Kazmin and W. Janke. "Critical exponent ν of the Ising model in three dimensions with long-range correlated site disorder analyzed with Monte Carlo techniques." In: *Phys. Rev. B* 102.17 (2020), p. 174206. DOI: 10.1103/PhysRevB.102.174206.

[KJ22]   S. Kazmin and W. Janke. "Critical exponents of the Ising model in three dimensions with long-range power-law correlated site disorder: A Monte Carlo study." In: *Phys. Rev. B* 105.21 (2022), p. 214111. DOI: 10.1103/PhysRevB.105.214111.

[KKS21]   M. V. Kompaniets, A. Kudlis, and A. I. Sokolov. "Critical behavior of the weakly disordered Ising model: Six-loop $\sqrt{\epsilon}$ expansion study." In: *Phys. Rev. E* 103.2 (2021), p. 022134. DOI: 10.1103/PhysRevE.103.022134.

[Kos+16]   F. Kos, D. Poland, D. Simmons-Duffin, and A. Vichi. "Precision islands in the Ising and $O(N)$ models." In: *J. High Energy Phys.* 08.2016 (2016), p. 36. DOI: 10.1007/JHEP08(2016)036.

[KP94]   J.-K. Kim and A. Patrascioiu. "Critical behavior of the two-dimensional site-diluted Ising system." In: *Phys. Rev. B* 49.22 (1994), pp. 15764–15770. DOI: 10.1103/PhysRevB.49.15764.

[KR08]   R. Kenna and J. J. Ruiz-Lorenzo. "Scaling analysis of the site-diluted Ising model in two dimensions." In: *Phys. Rev. E* 78.3 (2008), p. 031134. DOI: 10.1103/PhysRevE.78.031134.

[KS21]   O. Klimenkova and L. Shchur. "Algorithm for foam generation in plane." In: *J. Phys.: Conf. Ser.* 1740 (2021), p. 012030. DOI: 10.1088/1742-6596/1740/1/012030.

[Lav15]   D. A. Lavis. *Equilibrium Statistical Mechanics of Lattice Models*. Theoretical and Mathematical Physics. Springer, Dordrecht, 2015. DOI: 10.1007/978-94-017-9430-5_1.

[LB05]   D. P. Landau and K. Binder. *A Guide to Monte Carlo Simulations in Statistical Physics*. 2nd ed. Cambridge: Cambridge University Press, 2005. DOI: 10.1017/CBO9780511614460.

[Leb11]   J.-L. Lebrun. *Scientific writing 2.0: a reader and writer's guide*. World Scientific, 2011. 265 pp. ISBN: 978-981-4350-59-4.

[Len20]   W. Lenz. "Beiträge zum Verständnis der magnetischen Eigenschaften in festen Körpern." In: *Physikalische Zeitschrift* 21 (1920), pp. 613–615.

[LH95]   C. L. Lawson and R. J. Hanson. *Solving Least Squares Problems*. Classics in Applied Mathematics. Society for Industrial and Applied Mathematics, 1995. 351 pp. DOI: 10.1137/1.9781611971217.

[LL02]   D. S. Lemons and P. Langevin. *An introduction to stochastic processes in physics: containing "On the theory of Brownian motion" by Paul Langevin, translated by Anthony Gythiel.* Baltimore: Johns Hopkins University Press, 2002. 110 pp. ISBN: 978-0-8018-6866-5.

[Mak+95]   H. Makse, S. Havlin, H. E. Stanley, and M. Schwartz. "Novel method for generating long-range correlations." In: *Chaos, Solitons & Fractals* 6 (1995), pp. 295–303. DOI: 10.1016/0960-0779(95)80035-F.

[Mak+96]   H. A. Makse, S. Havlin, M. Schwartz, and H. E. Stanley. "Method for generating long-range correlations for large systems." In: *Phys. Rev. E* 53.5 (1996), pp. 5445–5449. DOI: 10.1103/PhysRevE.53.5445.

[Mar09]   M. I. Marqués. "Monte Carlo study of the competition between long-range and short-range correlated disorder in a second-order phase transition." In: *Phys. Rev. E* 79.5 (2009), p. 052103. DOI: 10.1103/PhysRevE.79.052103.

[MBM96]   T. MacFarland, G. T. Barkema, and J. F. Marko. "Equilibrium phase transitions in a porous medium." In: *Phys. Rev. B* 53.1 (1996), pp. 148–158. DOI: 10.1103/PhysRevB.53.148.

[Met+53]   N. Metropolis, A. W. Rosenbluth, M. N. Rosenbluth, A. H. Teller, and E. Teller. "Equation of state calculations by fast computing machines." In: *J. Chem. Phys.* 21.6 (1953), pp. 1087–1092. DOI: 10.1063/1.1699114.

[Mit+86]   P. W. Mitchell, R. A. Cowley, H. Yoshizawa, P. Boni, Y. J. Uemura, and R. J. Birgeneau. "Critical behavior of the three-dimensional site-random Ising magnet: $Mn_xZn_{1-x}F_2$." In: *Phys. Rev. B* 34.7 (1986), pp. 4719–4725. DOI: 10.1103/PhysRevB.34.4719.

[MK99]   G. Mazzeo and R. Kühn. "Critical behavior of the two-dimensional spin-diluted Ising model via the equilibrium ensemble approach." In: *Phys. Rev. E* 60.4 (1999), pp. 3823–3836. DOI: 10.1103/PhysRevE.60.3823.

[MKB04]   A. K. Murtazaev, I. K. Kamilov, and A. B. Babaev. "Critical behavior of a cubic-lattice 3D Ising model for systems with quenched disorder." In: *J. Exp. Theor. Phys* 99.6 (2004), pp. 1201–1206. DOI: 10.1134/1.1854807.

[MP07]   P. H. L. Martins and J. A. Plascak. "Universality class of the two-dimensional site-diluted Ising model." In: *Phys. Rev. E* 76.1 (2007), p. 012102. DOI: 10.1103/PhysRevE.76.012102.

[MPV02]   V. Martín-Mayor, A. Pelissetto, and E. Vicari. "Critical structure factor in Ising systems." In: *Phys. Rev. E* 66.2 (2002), p. 026112. DOI: 10.1103/PhysRevE.66.026112.

[NB99]   M. E. J. Newman and G. T. Barkema. *Monte Carlo Methods in Statistical Physics.* New York: Oxford University Press Inc., 1999. 475 pp. ISBN: 978-0-19-851796-2.

[NO10]   H. Nishimori and G. Ortiz. *Elements of Phase Transitions and Critical Phenomena.* Oxford University Press, 2010. ISBN: 978-0-19-172294-3.

[Nol14]   W. Nolting. *Grundkurs Theoretische Physik 6*. Springer-Lehrbuch. Berlin, Heidelberg: Springer Berlin Heidelberg, 2014. ISBN: 978-3-642-25392-8.

[Ons44]   L. Onsager. "Crystal Statistics. I. A Two-Dimensional Model with an Order-Disorder Transition." In: *Phys. Rev.* 65.3-4 (1944), pp. 117–149. DOI: `10.1103/PhysRev.65.117`.

[Paw+84]   G. S. Pawley, R. H. Swendsen, D. J. Wallace, and K. G. Wilson. "Monte Carlo renormalization-group calculations of critical behavior in the simple-cubic Ising model." In: *Phys. Rev. B* 29.7 (1984), pp. 4030–4040. DOI: `10.1103/PhysRevB.29.4030`.

[Pla36]   M. Planck. *The Philosophy of Physics*. W.W. Norton, Incorporated, 1936. 140 pp.

[PPF00]   V. V. Prudnikov, P. V. Prudnikov, and A. A. Fedorenko. "Field-theory approach to critical behavior of systems with long-range correlated defects." In: *Phys. Rev. B* 62.13 (2000), pp. 8777–8786. DOI: `10.1103/PhysRevB.62.8777`.

[Pru+05]   V. V. Prudnikov, P. V. Prudnikov, S. V. Dorofeev, and V. Y. Kolesnikov. "Monte Carlo studies of critical behaviour of systems with long-range correlated disorder." In: *Condens. Matter Phys.* 8.1 (2005), pp. 213–224. DOI: `DOI:10.5488/CMP.8.1.213`.

[PS00]   D. V. Pakhnin and A. I. Sokolov. "Five-loop renormalization-group expansions for the three-dimensional *n*-vector cubic model and critical exponents for impure Ising systems." In: *Phys. Rev. B* 61.22 (2000), pp. 15130–15135. DOI: `10.1103/PhysRevB.61.15130`.

[PS08]   A. A. Pogorelov and I. M. Suslov. "Estimate of the critical exponents from the field-theoretical renormalization group: mathematical meaning of the "Standard Values"." In: *J. Exp. Theor. Phys.* 106.6 (2008), pp. 1118–1129. DOI: `10.1134/S1063776108060113`.

[PV00]   A. Pelissetto and E. Vicari. "Randomly dilute spin models: A six-loop field-theoretic study." In: *Phys. Rev. B* 62.10 (2000), pp. 6393–6409. DOI: `10.1103/PhysRevB.62.6393`.

[PV02]   A. Pelissetto and E. Vicari. "Critical phenomena and renormalization-group theory." In: *Physics Reports* 368.6 (2002), pp. 549–727. DOI: `10.1016/S0370-1573(02)00219-3`.

[PV06]   R. Paredes and C. Vásquez. "Three-dimensional Ising model confined in low-porosity aerogels: A Monte Carlo study." In: *Phys. Rev. B* 74.5 (2006), p. 054201. DOI: `10.1103/PhysRevB.74.054201`.

[Rui97]   J. J. Ruiz-Lorenzo. "Griffiths singularities in the two-dimensional diluted Ising model." In: *J. Phys. A: Math. Gen.* 30.2 (1997), pp. 485–493. DOI: `10.1088/0305-4470/30/2/014`.

[Rus63]   G. S. Rushbrooke. "On the thermodynamics of the critical region for the Ising problem." In: *J. Chem. Phys.* 39.3 (1963), pp. 842–843. DOI: `10.1063/1.1734338`.

[Sad12]   M. V. Sadovskii. *Statistical Physics.* Berlin, Boston: De Gruyter, 2012. DOI: 10.1515/9783110270372.

[Sau17]   T. Sauer. "A look back at the Ehrenfest classification." In: *Eur. Phys. J. Spec. Top.* 226.4 (2017), pp. 539–549. DOI: 10.1140/epjst/e2016-60344-y.

[SB98]   Z. Slanič and D. P. Belanger. "The random-field specific heat critical behavior at high magnetic concentration: $Fe_{0.93}Zn_{0.07}F_2$." In: *J. Magn. Magn. Mater.* 186.1 (1998), pp. 65–73. DOI: 10.1016/S0304-8853(98)00065-1.

[SBF98]   Z. Slanič, D. Belanger, and J. Fernandez-Baca. "Random-field critical scattering at high-magnetic concentration in the Ising antiferromagnet $Fe_{0.93}Zn_{0.07}F_2$." In: *J. Magn. Magn. Mater.* 177-181 (1998), pp. 171–172. DOI: 10.1016/S0304-8853(97)00333-8.

[Sch02]   F. Schwabl. *Statistical Physics.* Advanced Texts in Physics. Springer Berlin Heidelberg, 2002. DOI: 10.1007/978-3-662-04702-6_1.

[SFN09]   L. F. da Silva, U. L. Fulco, and F. D. Nobre. "The two-dimensional site-diluted Ising model: a short-time-dynamics approach." In: *J. Phys.: Condens. Matter* 21.34 (2009), p. 346005. DOI: 10.1088/0953-8984/21/34/346005.

[Sha87]   R. Shankar. "Exact critical behavior of a random bond two-dimensional Ising model." In: *Phys. Rev. Lett.* 58.23 (1987), pp. 2466–2469. DOI: 10.1103/PhysRevLett.58.2466.

[Sha94]   B. N. Shalaev. "Critical behavior of the two-dimensional Ising model with random bonds." In: *Physics Reports* 237.3 (1994), pp. 129–188. DOI: 10.1016/0370-1573(94)90086-8.

[SM09]   M. Saito and M. Matsumoto. "A PRNG Specialized in Double Precision Floating Point Numbers Using an Affine Transition." In: *Monte Carlo and Quasi-Monte Carlo Methods 2008.* Ed. by P. L' Ecuyer and A. B. Owen. Springer Berlin Heidelberg, 2009, pp. 589–602. DOI: 10.1007/978-3-642-04107-5_38.

[SNH17]   H. Schawe, C. Norrenbrock, and A. K. Hartmann. "Ising Ferromagnets on Proximity Graphs with Varying Disorder of the Node Placement." In: *Scientific Reports* 7.1 (1 2017), p. 8040. DOI: 10.1038/s41598-017-08531-8.

[ST95]   J. Shao and D. Tu. *The Jackknife and Bootstrap.* Springer Series in Statistics. Springer, New York, 1995. DOI: 10.1007/978-1-4612-0795-5.

[Str14]   D. W. Stroock. *An Introduction to Markov Processes.* Vol. 230. Graduate Texts in Mathematics. Springer Berlin Heidelberg, 2014. DOI: 10.1007/978-3-642-40523-5.

[SW87]   R. H. Swendsen and J.-S. Wang. "Nonuniversal critical dynamics in Monte Carlo simulations." In: *Phys. Rev. Lett.* 58.2 (1987), pp. 86–88. DOI: 10.1103/PhysRevLett.58.86.

[TF11]   P. E. Theodorakis and N. G. Fytas. "Wang-Landau study of the 3D Ising model with bond disorder." In: *Eur. Phys. J. B* 81.2 (2011), pp. 245–251. DOI: 10.1140/epjb/e2011-20091-4.

[Tho02]   H. C. Thode. *Testing For Normality*. CRC Press, Boca Raton, 2002. DOI: 10.1201/9780203910894.

[Tim97]   P. N. Timonin. "Griffiths' phase in dilute ferroelectrics." In: *Ferroelectrics* 199.1 (1997), pp. 69–81. DOI: 10.1080/00150199708213429.

[Var00]   K. B. Varnashev. "Stability of a cubic fixed point in three dimensions: Critical exponents for generic N." In: *Phys. Rev. B* 61.21 (2000), pp. 14660–14674. DOI: 10.1103/PhysRevB.61.14660.

[Vas+15]   O. Vasilyev, B. Berche, M. Dudka, and Y. Holovatch. "Monte Carlo study of anisotropic scaling generated by disorder." In: *Phys. Rev. E* 92.4 (2015), p. 042118. DOI: 10.1103/PhysRevE.92.042118.

[VFB10]   R. L. C. Vink, T. Fischer, and K. Binder. "Finite-size scaling in Ising-like systems with quenched random fields: Evidence of hyperscaling violation." In: *Phys. Rev. E* 82.5 (2010), p. 051134. DOI: 10.1103/PhysRevE.82.051134.

[Voj06]   T. Vojta. "Rare region effects at classical, quantum and nonequilibrium phase transitions." In: *J. Phys. A: Math. Gen.* 39.22 (2006), R143. DOI: 10.1088/0305-4470/39/22/R01.

[VV91]   S. Van Huffel and J. Vandewalle. *The Total Least Squares Problem*. Frontiers in Applied Mathematics. Society for Industrial and Applied Mathematics, 1991. 301 pp. DOI: 10.1137/1.9781611971002.

[Wan+13]   J. Wang, Z. Zhou, W. Zhang, T. M. Garoni, and Y. Deng. "Bond and site percolation in three dimensions." In: *Phys. Rev. E* 87.5 (2013), p. 052107. DOI: 10.1103/PhysRevE.87.052107.

[Wan+19]   W. Wang, H. Meier, J. Lidmar, and M. Wallin. "Three-dimensional universality class of the Ising model with power-law correlated critical disorder." In: *Phys. Rev. B* 100.14 (2019), p. 144204. DOI: 10.1103/PhysRevB.100.144204.

[Wan90]   J.-S. Wang. "Critical dynamics of the Swendsen-Wang algorithm in the three-dimensional Ising model." In: *Physica A: Statistical Mechanics and its Applications* 164.2 (1990), pp. 240–244. DOI: 10.1016/0378-4371(90)90197-Z.

[WD98]   S. Wiseman and E. Domany. "Self-averaging, distribution of pseudocritical temperatures, and finite size scaling in critical disordered systems." In: *Phys. Rev. E* 58.3 (1998), pp. 2938–2951. DOI: 10.1103/PhysRevE.58.2938.

[WH83]   A. Weinrib and B. I. Halperin. "Critical phenomena in systems with long-range correlated quenched disorder." In: *Phys. Rev. B* 27.1 (1983), pp. 413–427. DOI: 10.1103/PhysRevB.27.413.

[Wis95]   S. Wiseman. "Critical behavior of the random-bond Ashkin-Teller model: A Monte Carlo study." In: *Phys. Rev. E* 51.4 (1995), pp. 3074–3086. DOI: 10.1103/PhysRevE.51.3074.

[Wol89]   U. Wolff. "Collective Monte Carlo updating for spin systems." In: *Phys. Rev. Lett.* 62.4 (1989), pp. 361–364. DOI: 10.1103/PhysRevLett.62.361.

[Xio+10]   W. Xiong, F. Zhong, W. Yuan, and S. Fan. "Critical behavior of a three-dimensional random-bond Ising model using finite-time scaling with extensive Monte Carlo renormalization-group method." In: *Phys. Rev. E* 81.5 (2010), p. 051132. DOI: `10.1103/PhysRevE.81.051132`.

[Zhi+09]   L. Zhi-Huan, L. Mushtaq, L. Yan, and L. Jian-Rong. "Critical behaviour of the ferromagnetic Ising model on a triangular lattice." In: *Chinese Phys. B* 18.7 (2009), pp. 2696–2702. DOI: `10.1088/1674-1056/18/7/012`.

[Zie+17]   J. Zierenberg, N. Fricke, M. Marenz, F. P. Spitzner, V. Blavatska, and W. Janke. "Percolation thresholds and fractal dimensions for square and cubic lattices with long-range correlated defects." In: *Phys. Rev. E* 96.6 (2017), p. 062125. DOI: `10.1103/PhysRevE.96.062125`.

Web references

[@Fun21]   *TOP500 (the 500 most powerful commercially available computer systems).* 2021. URL: `https://www.top500.org/`.

[@Git21]   S. Kazmin. *long-range_correlated_ising_model*. GitHub. 2021. URL: `https://github.com/stakaz/long-range_correlated_ising_model`.

[@MT06]   *SIMD-oriented Fast Mersenne Twister (SFMT).* 2006. URL: `http://www.math.sci.hiroshima-u.ac.jp/m-mat/MT/SFMT/#dSFMT`.

[@Opt21]   D. Segal (dan@seg.al). *Optim.jl*. Julia Packages. 2021. URL: `https://juliapackages.com/p/optim`.

[@Rng21]   *Random Numbers · The Julia Language.* 2021. URL: `https://docs.julialang.org/en/v1/stdlib/Random/`.

[@Sci]   *ScienceDirect Search Results - Keywords("Ising model").* URL: `https://www.sciencedirect.com/search?qs=%22Ising%20model%22`.

[@Spr]   *Beitrag zur Theorie des Ferromagnetismus | SpringerLink.* URL: `https://link.springer.com/article/10.1007/BF02980577`.

Selbstständigkeitserklärung

Ich versichere hiermit wahrheitsgemäß, die vorliegende Dissertation selbstständig angefertigt, alle benutzten Hilfsmittel vollständig und genau angegeben und alles kenntlich gemacht zu haben, was aus Arbeiten anderer unverändert oder mit Abänderungen entnommen wurde.

Gemeinsame Auswahl und Auswertung der Resultate erfolge ausschließlich mit meinem Betreuer Prof. Dr. Wolfhard Janke, sowie im Rahmen eines zweiwöchentlichen Aufenthaltes am Laboratoire de Physique et Chimie Théoriques an der Université de Lorraine, Frankreich, mit Dr. Christophe Chatelain und Prof. Dr. Malte Henkel. Ich versichere weiterhin, dass keine weiteren Personen bei der geistigen Herstellung der vorliegenden Arbeit beteiligt waren.

Diese Dissertation wurde weder im Ganzen noch in Teilen vorher einer Prüfungsbehörde zum Zwecke einer Promotion oder eines anderen Prüfungsverfahrens vorgelegt und wurde nicht veröffentlicht. Frühere erfolglose Promotionsversuche haben nicht stattgefunden.

M. Sc. Stanislav Kazmin   Leipzig, 12. Mai 2021